The Static and Fatigue Behaviour of Through-Bolt Shear Connectors in Steel-Precast Composite Bridge Girders

by

Kyle Daniel Balkos

A thesis

presented to the University of Waterloo

in fulfilment of the

thesis requirement for the degree of

Master of Applied Science

in

Civil Engineering

Waterloo, Ontario, Canada, 2018

Author's Declaration

I hereby declare that I am the sole author of this thesis. This is a true copy of my thesis, including any required final revisions, as accepted by my examiners.

I understand that my thesis may be made electronically available to the public.

Abstract

Increasing demand for the rapid and economically efficient construction of bridges has encouraged engineers to employ the use of accelerated bridge construction through modular assembly. The replacement of vehicular bridges in highly populated areas using traditional construction methods typically results in significant social and economic impacts as a consequence of lengthy closures of these bridges during construction. Accelerated bridge construction through modular assembly offers an advantageous alternative, as it can drastically reduce the duration for which the bridge is out of service, therefore minimizing the corresponding impacts. Full-depth, precast concrete decks connected to steel girders using mechanical shear connectors is one form of accelerated bridge construction where the major components can be fabricated off-site. Employing modular bridge components takes advantage of improved quality and efficient construction through prefabrication, resulting in easier and more rapid installation on-site. Currently, welded, headed shear studs are the most common type of shear connector used in composite bridge construction. An attractive alternative to this connection type is the use of slip-critical through-bolt shear connectors as they are expected to offer advantages with regards to their reduced installation and disassembly times, as well as their fatigue performance.

Currently, relatively little is known about the true static load-slip and the fatigue behaviour of slip-critical through-bolt shear connectors in composite beams. Therefore, the following research project investigates the static and fatigue performance of these connectors. In order to do this, three large-scale composite beam specimens were fabricated, instrumented, and tested in an experimental program involving both static and fatigue loading. In order to better understand the static load-slip behaviour of this connector type, a mechanistic model was also developed, along with a nonlinear finite element (FE) model of a through-bolt connection. Results of the beam tests were compared with results from a previous study employing a simpler push test configuration, in order to understand the behaviour differences resulting from the choice of test configuration. Comparisons were also made between the experimental results and load-slip predictions made using the developed mechanistic and FE models.

The fatigue testing did not result in the failure of any through-bolt shear connectors for the configurations considered in this experimental program. The fatigue performance of the through-bolt shear connectors far exceeded the predicted fatigue life obtained using the current fatigue design provisions for welded, headed shear studs. The static beam test and the push test resulted in similar peak shear loads prior to the onset of failure of the through-bolts. However, the slopes of the two load-slip curves were quite different, with the through-bolt shear connectors behaving in a much less stiff manner when tested in a beam test relative to a push test. Moreover, the slip required to produce a through-bolt failure is seen to be much

higher in a beam test. The static load-slip behaviour of a through-bolt push test specimen was predicted using a mechanistic model. Comparison of the load-slip curves generated by the mechanistic model with the available push test results revealed that the mechanistic model is capable of accurately predicting the load-slip behaviour of through-bolt shear connectors. A comparison of the load-slip curves generated by the FE analysis revealed that the FE models are also able to predict the load-slip behaviour of through-bolt shear connectors.

The findings in this study suggest that the performance of composite bridges, in terms of fatigue life, could be significantly improved if through-bolts were used in place of traditional headed shear studs. However, further experimental testing is recommended to fully develop this connection concept.

Acknowledgements

I would first like to express my sincere gratitude to my supervisors Dr. Scott Walbridge, P.Eng., and Dr. Jeffrey West, P.Eng., for their guidance, support and mentorship throughout this research project. Their expertise and wealth of knowledge had a significant influence on my successes at the University of Waterloo. I would also like to thank Dr. Wayne Parker, P.Eng., and Dr. Sriram Narasimhan, P.Eng., for their review of this thesis.

I would like to extend my gratitude to the Civil Engineering Structures Laboratory technicians Richard Morrison, Peter Volcic, and Douglas Hirst for their enormous efforts in assisting with the experimental portions of this research project. Their experience and knowledge was essential for the completion of the experimental testing.

Furthermore, I would like to thank my colleagues at the University of Waterloo for their friendship and support throughout my graduate studies: Matthew Sjaarda, Adam Felinczak, Shelley H. Yang, and Stan Fong for their assistance with the fabrication of the specimens and testing frames; Graeme Milligan and Ryan Barrage for their time and commitment to helping me process the experimental data; and Dylan Dowling and Taylor Porter for their advice in the preparation of my thesis.

The funding for this research has been graciously received from the Natural Science and Research Council of Canada and the Ontario Graduate Scholarship. This research project supported a project funded by the Ministry of Transportation of Ontario and the Canadian Institute of Steel Construction.

Dedication

To my mother and father for their unconditional love, guidance and support, and for instilling in me the confidence that I am capable of achieving anything I put my mind to. Thank you for everything.

Table of Contents

List of Figures

List of Tables

1 Introduction

The replacement of vehicular bridges in highly populated areas using traditional construction methods typically results in significant social and economic impacts as a consequence of the lengthy closures of these bridges during construction. Impacts due to such bridge closures may include: increased travel time, increased construction cost for traffic control, increased risk of vehicle collisions on detour routes, increased response times for emergency vehicles, and disruptions for businesses. Accelerated bridge construction through modular assembly offers an advantageous alternative to traditional construction methods as it can drastically reduce the duration for which the bridge is out of service, therefore minimizing the corresponding impacts (Tadros & Baishya, 1998).

Full-depth, precast concrete decks connected to steel girders using mechanical shear connectors is one form of accelerated bridge construction where the major components can be fabricated off-site (Dalehenley, 2009). Employing modular bridge components takes advantage of improved quality and efficient construction through off site prefabrication, resulting in easier and more rapid installation on-site.

1.1 Overview

Currently the welded, headed shear stud connector is the most commonly used mechanical shear connector due to its reliability and ease of installation. However, there are several shortcomings associated with the use of welded shear studs. For instance, specialized equipment is required for the installation of the shear studs and the connection requires the use of grout to be completed, the curing of which increases the overall construction time. Most importantly, the fatigue resistance of shear studs is a particular concern due to the inherently poor fatigue performance of welded connections in comparison to other connection types.

The current research project investigates the use of slip-critical, through-bolt shear connectors as an alternative to welded shear studs for modular bridges. The use of through-bolt shear connectors is hypothesized to have several advantages over welded, headed shear studs. It is theorized that through-bolt shear connectors possess a substantially superior fatigue resistance than welded, headed shear studs due to the absence of weldments. Furthermore, through-bolt shear connectors can be installed rapidly without the need of specialized equipment and do not require grouting, further shortening construction time. Deconstruction for bridge repair or replacement may also be easier with such connections.

The significance of this research stems from the need of a shear connection that presents a structurally efficient and economical design and conforms well to accelerated bridge construction practices. The

proposed connection would eliminate the requirement for grouting and weldments in the installation, thus rendering an efficient shear connection that is inherently less vulnerable to fatigue.

1.2 Research Objectives

The purpose of this research project is to explore the adequacy of slip-critical, through-bolt shear connectors with respect to their static and fatigue performance when used in steel-precast concrete composite bridge girders. This research project extends the previously limited understanding of the behaviour and performance of through-bolt shear connectors, revealing significant advantages over the more popular welded, headed shear stud connectors. The specific objectives of this research project address the gaps in the current knowledge, and can be summarized as follows:

- The current Canadian Highway Bridge Design Code, CSA S6 (CSA S6, 2014) relies upon the implicit assumption that the fatigue performance of through-bolt shear connectors are identical to welded, headed shear stud connectors. A large-scale, composite beam fatigue testing program was designed and implemented to investigate this assumption.
- The current design provisions provided for shear connectors in the CSA S6 (CSA S6, 2014) were formulated from a regression analysis of push tests. Therefore, a testing program featuring large-scale, composite beams was undertaken to critically investigate this practice.
- A finite element (FE) model was prepared, simulating the load-slip behaviour of a through-bolt shear connector. A mechanistic model of the full load-slip behaviour of a through-bolt shear connector was also constructed. Both the FE model and the developed mechanistic model present the opportunity to perform sensitivity analyses on various parameters influencing the load-slip curve of a through-bolt shear connector, revealing possible sources of discrepancy between the results from a push test and a large-scale composite beam test.
- A novel instrumentation technique, designed to monitor and record the stresses experienced by through-bolt shear connectors is proposed and demonstrated.

1.3 Thesis Outline

This thesis consists of seven chapters beginning with the current introductory chapter. The following is a brief description of the contents to be discussed in the remainder of this thesis.

In Chapter 2, a comprehensive review of the current literature in subject areas related to this research project is presented. First, a detailed background of steel-concrete composite members is provided. The concept of accelerated bridge construction is introduced, explaining the potential benefits and motivation for its use. A discussion of the various forms of shear connectors used to achieve composite behaviour is provided, including descriptions of popular testing procedures used to evaluate shear connectors. Next,

the previous research assessing the static and fatigue resistance of shear connectors is presented. The current governing design codes for shear connectors are discussed along with all pertinent design equations. Following this, the previous research regarding the modelling of composite beams is described. Lastly, the significant gaps in the current knowledge pertaining to through-bolt shear connectors are outlined, identifying the research needs that are the focus of this research project.

In Chapter 3, the fabrication and assembly of the specimens tested within the experimental program are described. Construction procedures, specimen geometry, and material properties are presented along with a detailed description of the instrumentation used to monitor the specimen behaviour during testing. Moreover, the loading patterns and data acquisition details are discussed.

In Chapter 4, the experimental results obtained from the static and fatigue tests are presented. The results are presented and discussed in detail, and observed trends are explained.

In Chapter 5, the derivation of the mechanistic model for predicting the static load-slip behaviour of through-bolt shear connectors is presented. Additionally, the formulation of an FE model simulating a push test experiment is described. The specifics pertaining to both the mechanistic model and FE model are described in detail and include material properties, assumed boundary conditions, loading configurations, and contact conditions. Lastly, the mechanistic model and the FE model are validated by comparing model predictions with measurements from the structural tests.

In Chapter 6, conclusions and significant findings of this research project are presented. Moreover, recommendations for future research to further our knowledge of the behaviour of through-bolt shear connectors are made in this chapter.

2 Literature Review

The literature review presented in this Chapter provides a thorough background of the significant research that has been conducted prior to this research project, highlighting gaps in the current knowledge that are addressed in this thesis. Section 2.1 provides an overview of accelerated bridge construction through the implementation of modular assembly. The various types of shear connectors currently used are identified and the concepts of shear connection and shear interaction are differentiated and explained. Moreover, Section 2.1 introduces push-tests and beam tests, outlining the benefits and differences of each. Section 2.2 presents the findings of the existing research pertaining to the static resistance of shear connectors, including the design code requirements. Similarly, Section 2.3 presents the findings of the existing research involving the fatigue resistance of shear connectors in addition to a brief overview of the fatigue of metals and the pertinent design code requirements. Section 2.4 discusses the current research regarding the modelling of composite beams. Lastly, Section 2.5 highlights the discontinuities in the current research which need to be addressed.

2.1 Steel-Concrete Composite Members

Structural elements that are aggregated from multiple materials fastened together are termed composite members. Often, the modular components are constructed from various materials that complement one another in such a way that the strengths of one material will compensate for the weakness of the other. The unification of precast concrete decks and steel girders to form a composite structural element is a common adaptation of composite members. Precast concrete decks connected to steel girders using welded, headed shear studs is a common composite assembly used in modular bridge construction. The amalgamation of these two materials offers several advantages. The large area and moment of inertia contributed by the concrete deck laterally braces the compression flange of the steel girder, preventing lateral torsional buckling in positive bending. When concrete decks and steel girders are integrated to form a composite member, the steel girder resists the tensile loading while the concrete deck typically resists the compression loading. Therefore, the respective strengths of each are utilized to their fullest, rendering a more efficient use of the materials. Lastly, the composite structure exhibits a greater flexural stiffness than each of the individual constituent components, thus reducing deflections.

2.1.1 Accelerated Bridge Construction

Accelerated bridge construction is the employment of innovative construction materials and procedures in an attempt to reduce the on-site construction time, thereby minimizing economic and societal costs. Modular bridge construction is a modern approach to accelerated bridge construction. Accelerated bridge construction through modular assembly offers an advantageous alternative to traditional methods as it can

drastically reduce the duration for which the bridge is out of service for both the construction of new bridges and the rehabilitation of existing bridges. The modular components are traditionally fabricated off-site prior to the intended installation date in a steel fabrication plant or precast concrete plant with favorable conditions such as adequate lighting, supply of skilled labor, improved safety, limited overhead work such as no work from scaffolding and optimal temperatures and relative humidity. Consequently, the consistency and strength of the modular components tend to be higher with fewer imperfections due to the highly controlled environments they were subjected to during their fabrication. Also, production of the modular components is faster as their manufacture is largely independent of weather conditions and other external factors. Once the prefabricated components are complete, they are shipped to the construction site and craned or hoisted into position as needed. An example of a composite bridge is shown in Figure 2–1.

Figure 2–1: Steel-concrete composite bridge

The three primary areas where modular construction offers the possibility for improved construction time, as suggested by Tadros & Baishya (1998), is the demolition of the existing bridge structure, the assembly of the bridge deck and the connection between the bridge deck to the girders. The time required for the decommissioning of existing structures can be dramatically decreased if the modular components were joined using mechanical fasteners such as bolted connections, which can be removed in a non-destructive manner. Following the completion of the service life of the bridge, limiting the amount of sawing or in

some cases explosives, will significantly reduce the cost and time required for the disassembly of the existing bridge as well as improve safety for construction workers. As mentioned above, the modular components are fabricated off-site in a controlled facility. Therefore, the construction time required for the assembly of the bridge deck and other structural members can be significantly reduced since the members have been prepared, cured and inspected for quality control ahead of time. All that remains is the physical installation of the various components. Finally, the construction time required for establishing the connection between the bridge deck and the girders can be reduced through modular assembly by equipping the modular components with the required installation mounts or holes, permitting the rapid assembly of the connectors on-site.

2.1.2 Composite Behaviour

The concrete deck and the steel girder will behave compositely when there is a mechanism by which the longitudinal shear force, or shear flow, is transferred between the concrete deck and the steel girder, thus resisting the two members from slipping relative to one another. When the interfacial slip is resisted, the force resultants in the concrete deck and the steel girder are equal and opposite and a more efficient use of the materials is achieved and lower maximum bending stresses and deflections are observed. Friction alone is insufficient to completely transfer the shear forces between the concrete deck and the steel girder. Indeed, the contribution of friction is often neglected as it is comparatively small to the resistance offered by the provided shear connectors. Composite behaviour is achieved through the use of shear connectors which transfer the longitudinal shear forces and prevent separation between the steel-concrete interface. The magnitude or degree of composite behaviour is directly related to the strength and stiffness of the shear connectors as they limit the longitudinal shear force that may be transferred between the concrete deck and steel girder. When a section behaves compositely, the strength of the composite section is greater than the sum of the individual strengths of the components and the overall deflection is less as the section properties of each component contribute in forming an overall larger, stiffer section. The behaviour of a composite beam is compared to that of a non-composite beam in Figure 2–2.

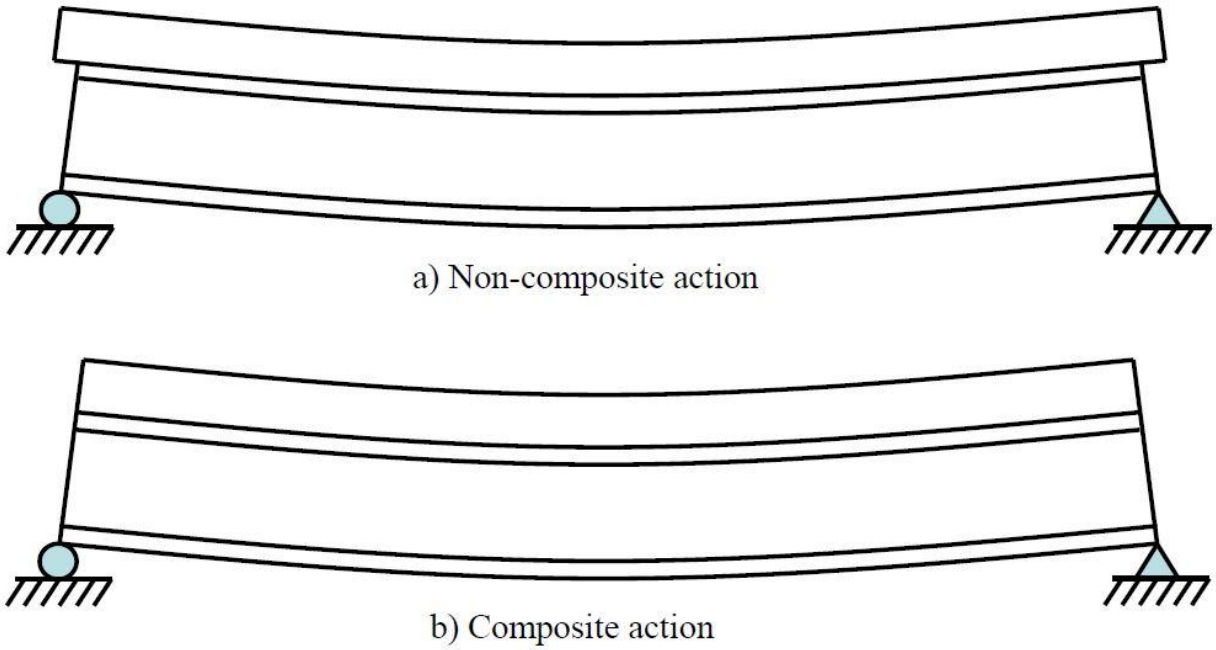

Figure 2–2: (a) Non-composite beam (b) composite beam (Kwon, 2008)

Figure 2–2 illustrates the concept of relative slip between the concrete deck and steel girder interface. When a section behaves fully compositely, there is no relative slip. Conversely, when there is no composite action, the two sections slip relative to one another as there is no transfer of longitudinal shear forces at the interface between the sections.

Composite beams that employ mechanical shear connectors require the occurrence of slip between the concrete deck and steel girder for them to resist the longitudinal shear forces. The ultimate strength of the shear connectors and the presence of slip each influence the overall degree of composite behaviour. Describing the degree of composite behaviour requires the consideration of both the equilibrium of forces and the continuity of the strain profiles. These two components of composite behaviour are termed the degree of shear connection (η) and the degree of interaction (φ) (Oehlers et al., 1997).

The degree of shear connection pertains to the equilibrium of forces between the concrete deck and the steel girder at the ultimate limit state. When subjected to a positive bending moment, at the ultimate limit state, concrete crushing in compression is generally the limiting criterion for failure in all cases except those where the shear connectors fail first. When the strength of the shear connection is greater than the compressive strength of the concrete deck, the strength of the shear connection does not control the flexural capacity and the composite section is said to have a full shear connection, or the degree of shear

connection is equal to one (η = 1). Figure 2–3 (a) illustrates a composite section with a full shear connection.

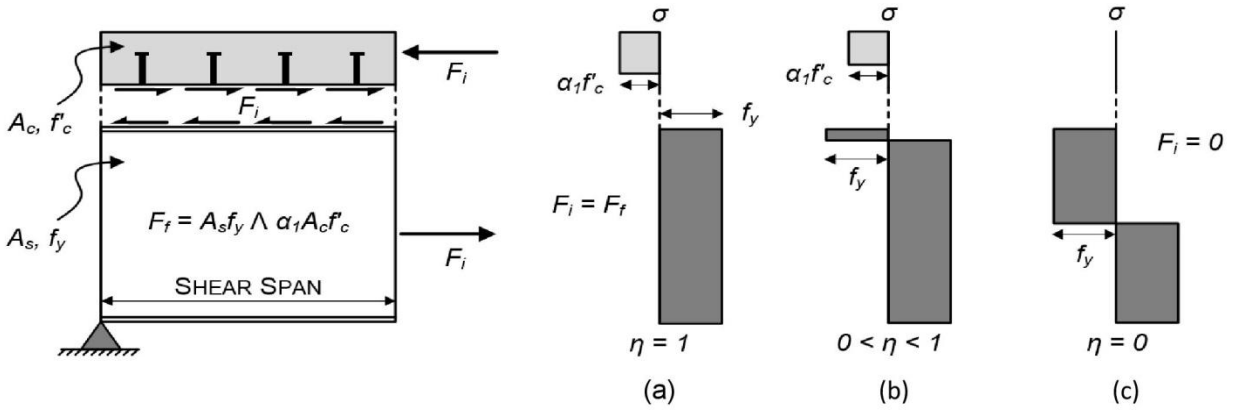

Figure 2–3: Degrees of shear connection (η)

When the strength of the shear connectors is less than the strength of the concrete deck, the equilibrium of forces is achieved when the resultant force in the concrete deck is equal in magnitude to the strength of the shear connectors as this is the maximum longitudinal shear force that can be transferred. Therefore, the strength of the shear connector controls and the composite section is said to have a partial shear connection ($0< \eta <1$). This condition is illustrated in Figure 2–3 (b) which depicts a portion of the steel girder acting in compression to equilibrate the insufficient compressive resultant transferred to the concrete deck. Finally, the composite member is said to have no shear connection (η = 0) when shear connectors are not present. As illustrated in Figure 2–3 (c), when the composite member has zero shear connection, the force in the concrete deck is equal to zero and the steel girder must have an overall resultant force of zero.

The degree of shear connection can be expressed mathematically in Equation 2-1 as the ratio of the ultimate capacity of the shear connection (F_i) to the minimum strength of the shear connectors required for full shear connection (F_F) (Oehlers et al., 1997).

$$\eta = \frac{F_i}{F_f} \tag{2-1}$$

The Canadian steel design code for buildings, CSA S16-09, Clause 17.9.4 restricts the degree of shear connection to be not less than 40% (CSA S16-09, 2012). Conversely, CSA S6, Clause 10.11.8.3 prohibits the use of partial shear connections (CSA S6, 2014). Researchers have questioned the rationality of these

limitations, hypothesizing that they may be too conservative, requiring an excessive number of shear connectors. Research has shown that reductions in shear connection as high as 45% only result in a reduction in strength of up to 85% of the full composite value (Yura et al., 2008).

The degree of interaction pertains to the continuity of the strain profile or the compatibility of strains at the interface of the concrete deck and steel girder. When a composite beam deforms in bending, the interfacial surfaces of the concrete deck and the steel girder cannot penetrate one another (in the vertical direction).Vertical loads applied on the composite beam will force the two members to deform with the same profile or deflected shape, and thus the members will have the same curvature. As a result, the strain profiles in the concrete and steel will have the same curvature or slope. Depending on the properties (stiffness and strength) of the shear connection between the two members, the concrete deck and steel girder may slip relative to one another at their interface, causing the resulting strain profiles to have an error in compatibility at the interface related to the magnitude of the slip (although the slopes of the strain profiles will be equal). Consequently, each material will have a unique neutral axis, separated by a distance, *h*, as shown in Figure 2–4.

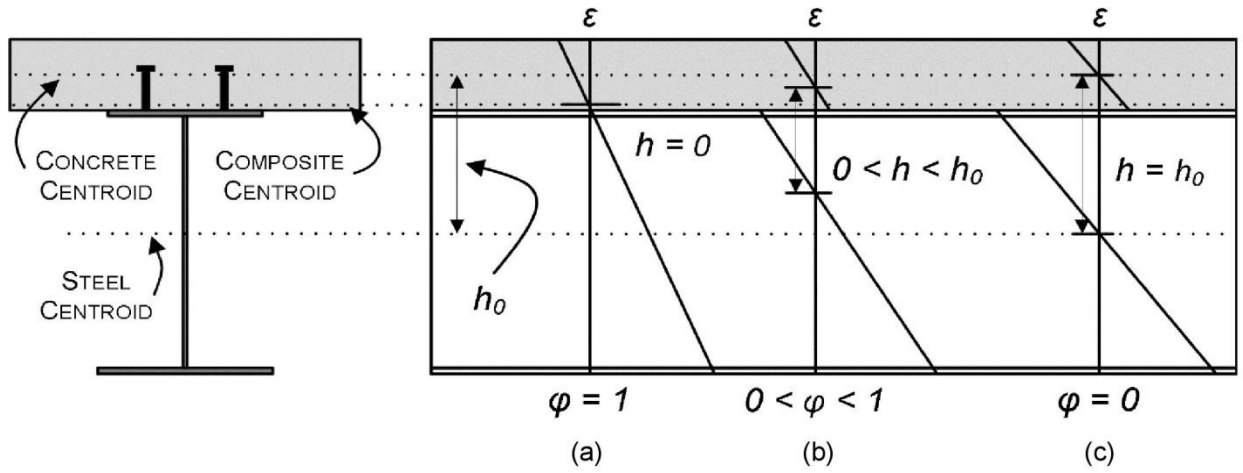

Figure 2–4: Degrees of Shear Interaction

The degree of shear interaction is controlled by the stiffness of the shear connectors. When the stiffness of the shear connectors between the concrete deck and the steel girder is infinitely rigid, as is the case with a chemically bonded composite section, the interfacial slip between the two components is prevented and the composite section assumes one centroid. This condition is shown in Figure 2–4 (a) and represents a full or complete shear interaction ($\varphi = 1$). As mentioned previously, all mechanical shear connectors require slip to develop the longitudinal shear forces. Therefore, all composite beams employing mechanical shear connectors will exhibit a partial shear interaction ($0 < \varphi < 1$). As shown in Figure 2–4

(b), when a composite beam has a partial shear interaction, the distance between the neutral axis of the concrete deck and steel girder will be non-zero and consequently, each member will have its own neutral axis. Lastly, if no shear connectors are present, the concrete deck and the steel girder will behave independently from one another and the neutral axis for each will coincide with their respective centroids. This is a condition of zero shear interaction ($\varphi = 0$) and is shown in Figure 2–4 (c). The distance between the neutral axes for a zero shear interaction condition is a maximum and is denoted as h_0.

The degree of shear interaction can be expressed mathematically in Equation 2-2 as one minus the ratio of the separation between of the neutral axes (h) to the maximum separation of the neutral axes for the case with zero shear interaction (h_0) (Oehlers et al., 1997).

$$\eta = 1 - \frac{h}{h_0} \tag{2-2}$$

2.1.3 Types of Shear Connectors

There are several forms of shear connectors used in composite section construction. Undoubtedly, the most commonly used shear connector for new construction is the welded, headed shear stud connector, which is welded to the upper flange of the steel girder using an arc stud welding gun following the Metal Arc Welding provisions described in Appendix H of CSA W59 (CSA W59-13, 2013). Clause 10.4.7 of CSA S6 specifies that only studs of Type B shall be used (CSA S6, 2014). The shear studs are equipped with heads to prevent deck uplift and pullout of the studs. There are two common assembly configurations when the use of headed shear studs is adopted. The shear studs may be arranged in pairs, evenly spaced along the length of the flange, or in discrete clusters at specified increments along the length of the flange. The former arrangement is implemented when the concrete deck is to be cast-in-place around the shear studs. The latter is conducive for when precast concrete decks are required. When the shear studs are arranged in discrete clusters, the concrete deck is typically cast with blockouts, intended to leave holes in the concrete deck, accommodating its assembly with the steel girder with the shear studs already welded to the flange in clusters. Subsequent to the placement of the precast deck, these stud pockets or blockouts are grouted to complete the shear connection between the steel girder and the concrete deck. Figure 2–5 illustrates the assembly of a composite beam with a cast-in-place concrete deck using headed shear stud connectors.

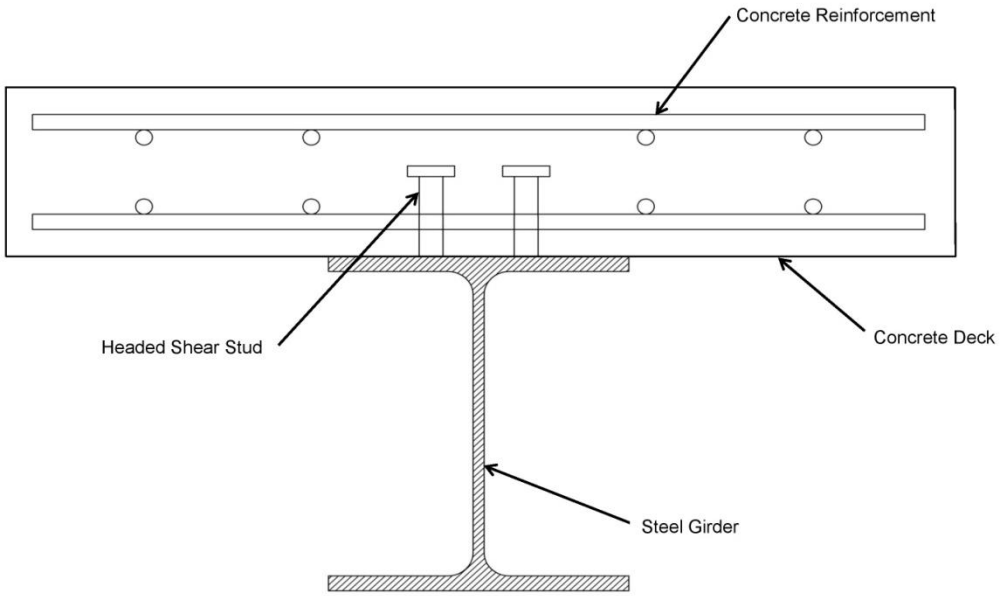

Figure 2–5: Cast-in-place concrete deck with welded, headed shear stud connectors

Welded, headed shear studs offer a reliable and economical shear connection between the steel girder and concrete deck. However, they can only be implemented on new construction bridges, they require destructive disassembly, they cannot be easily inspected during the service life of the bridge and finally, they are especially susceptible to fatigue failure. This inherent susceptibility to fatigue failure originates from the residual stresses introduced to the shear studs and flanges during the welding at the time of the shear stud installation, in addition to the geometric stress concentrations created by these welds.

An attractive alternative to welded, headed shear studs are slip-critical through-bolt shear connectors. Bolt provisions described in CSA S6, Clause 10.4.5, mandates that bolts used on bridge structures must comply with ASTM A325, A325M, A490, A490M, F1852 or F2280 (CSA S6, 2014). Furthermore, bolts used in structural applications must not be less than M16 or 5/8 inches in diameter. Lastly, the through-bolts must be tightened as per CSA S6, Clause 10.24.6.3, which specifies that pretensioned bolts shall be tightened to at least 70% of their minimum tensile strength (CSA S6, 2014). Figure 2–6 illustrates a typical construction configuration of a composite bridge where the shear connection is provided using through-bolts.

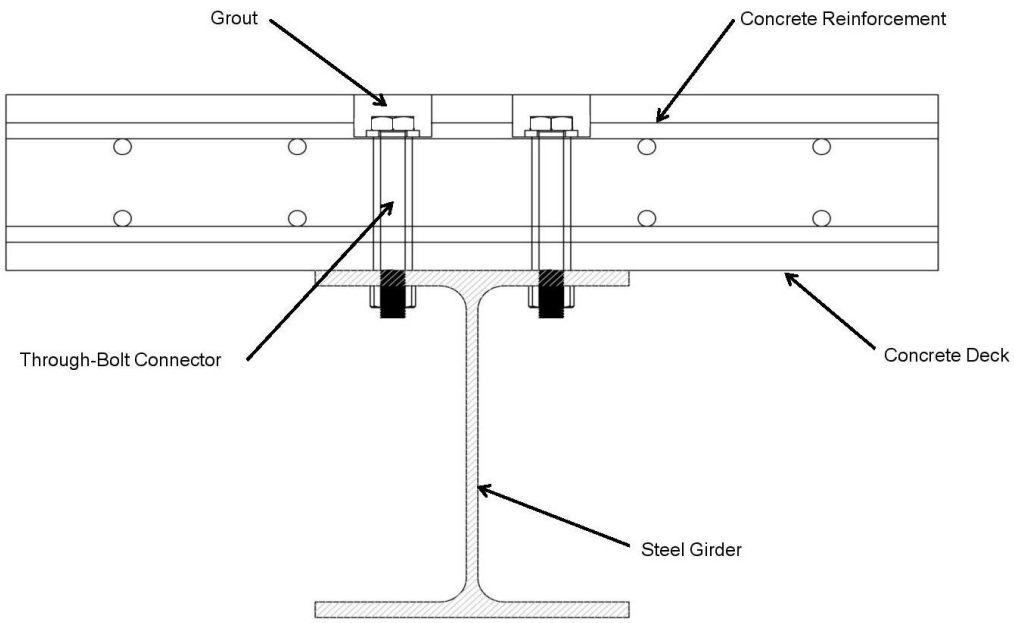

Figure 2–6: Precast concrete deck with slip-critical, through-bolt shear connectors

As shown in Figure 2–6, in a slip-critical shear connection, the diameter of the through-bolts is less than that of the sleeve in the concrete through which they pass. Therefore, when the through-bolts are initially loaded, the longitudinal shear forces are primarily resisted by the friction between the concrete deck and steel girder interface. Once the longitudinal shear force reaches a critical value, the concrete deck slips relative to the steel girder and the mechanism of shear resistance is now provided by the bearing of the through-bolts on concrete deck. This is more thoroughly discussed in Section 2.2.1. Through-bolt shear connectors offer several advantages over shear studs. Most importantly, through-bolt shear connections offer a weld free connection, making them far less susceptible to fatigue failure. Furthermore, the pretension in the through-bolts provides a normal force far larger than from the self-weight of the concrete deck alone, increasing the force of friction acting between the concrete deck and steel girder interface. As demonstrated by Oehlers & Seracino (2002) this increase in friction will reduce the magnitude of the longitudinal shear force required to be resisted by the through-bolts prior and subsequent to the onset of slip.

Oehlers & Seracino (2002) performed a finite element analysis in which they concluded that the frictional forces between the concrete deck and the steel girder are non-trivial and therefore reliably reduce, but do not eliminate, the longitudinal shear flow required to be resisted by the mechanical shear connectors through other mechanisms such as bearing, therefore extending the life of the shear connectors. This reduction in shear flow is explained mathematically in Equation 2-3.

$$q = V\left(\frac{A \cdot y}{I} - \frac{\mu}{l}\right) \tag{2-3}$$

where q is the total shear flow to be resisted by the mechanical shear connectors, V is the vertical shear force acting on the beam at the section of interest, $A \cdot y$ / I is the common shear flow equation, l is the length of the shear span and μ is the coefficient of friction between the concrete deck and the steel girder interface (Oehlers & Seracino, 2002).

Moreover, when through-bolt shear connectors are used, the inspection of the shear connectors can be performed much more easily than shear studs as the through-bolts are visible from the underside of the flange. If a through-bolt fails, it is likely that it will fall from the point of failure downwards, leaving a vacant hole on the underside of the composite structure which is visible to inspectors. Lastly, bridges constructed using through-bolt shear connectors are much easier to disassemble at the end of their useful life as the concrete deck may be removed in a non-destructive manner by simply loosening the through-bolts and hoisting the deck off the steel girder. Conversely, headed shear studs cannot be inspected as they are not visible after their installation and the disassembly of composite structures using shear studs requires sawing of the bridge deck, a both costly and dangerous operation.

Research performed by Kwon et al. (2007) proposed rehabilitating currently existing bridges that have been deemed structurally deficient by installing post-installed shear connectors, making their concrete decks and steel girders act compositely. Kwon et al. (2007) discovered that the installation of their proposed post-installed shear connectors may increase the capacity of the existing structure by up to 50% (Kwon et al., 2007). Figure 2–7 illustrates one of the more favorable post-installed shear connection designs proposed by Kwon et al. (2007).

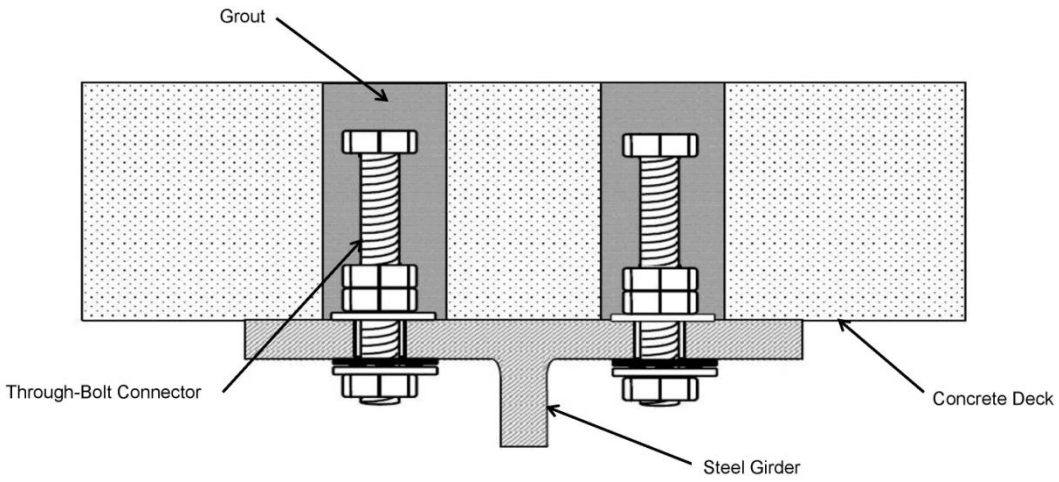

Figure 2–7: Double-nut through-bolt post-installed shear connectors (Kwon et al., 2007)

Figure 2–7 illustrates a bridge deck and girder whereby the composite action between the two was retroactively achieved by installing double-nut through-bolt shear connectors. The shear connectors were installed by coring through the concrete deck, drilling through the steel girder and placing the bolt assemblies through the manufactured voids. Composite action is then achieved by bolting the assemblies from the underside of the flange and placing a non-shrink grout in the cored voids in the concrete deck around the through-bolts.

Recently, research has been done on shear connection by adherence, in an effort to reduce construction time of composite bridges of steel girders and precast concrete decks (Bowser, 2010). When the concrete deck is cast-in-place directly on the steel girder, the chemical adhesion initially creates a fully composite behaviour. However, this adhesion cannot be relied upon as it typically breaks down after only a few loading cycles. Therefore, connections by adherence rely upon the friction characteristics of the connection to provide the composite behaviour between the concrete deck and the steel girder (Thomann & Lebet, 2008). The structural configuration proposed by Thomann & Lebet (2008) consists of a steel plate that has been welded along the length of the flange in the longitudinal direction and an epoxy resin and a coarse sand bonding layer which coats the flange. The concrete deck has a roughened slot along its longitudinal length which contours the steel plate welded to the flange. Any voids remaining between the concrete deck and steel girder are filled with a cement paste. This configuration is illustrated in Figure 2–8.

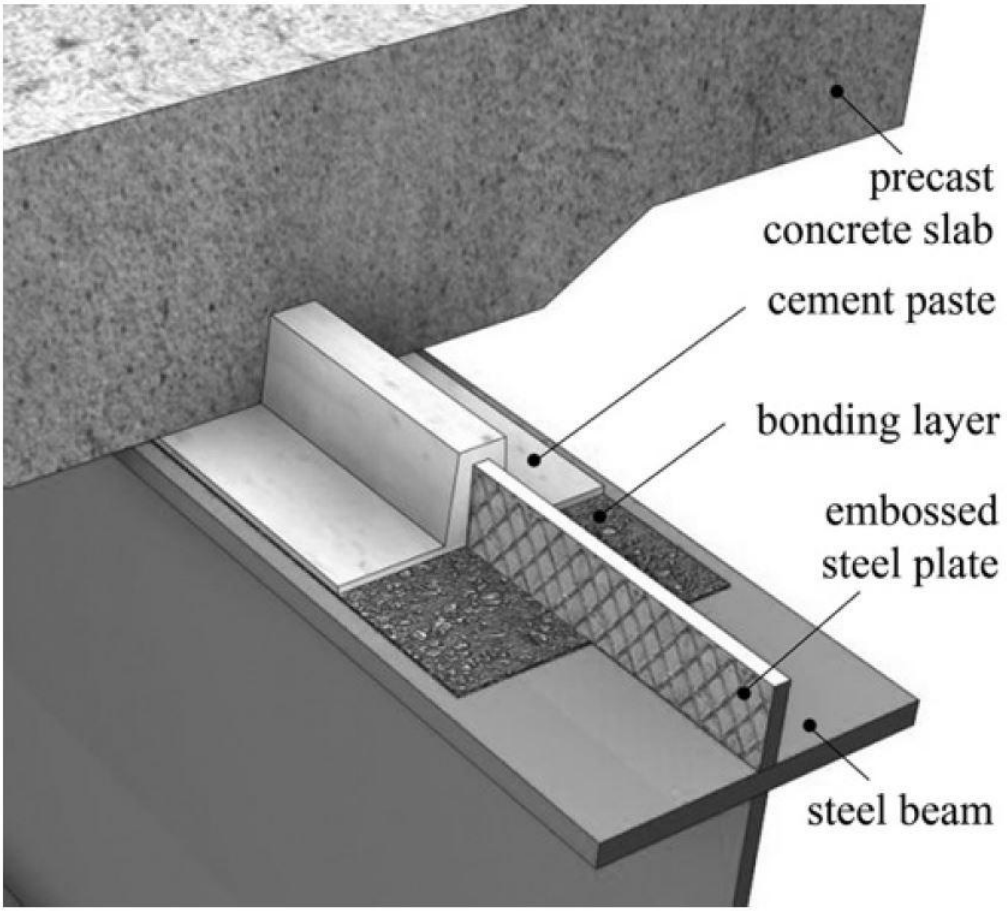

Figure 2–8: Connection by Adherence (Thomann & Lebet, 2008)

2.1.4 Push Tests Versus Beam Tests

The determination of the static or fatigue performance of a shear connector and the competency of the shear connector to induce composite action requires experimental testing. Push tests and beam tests are the two most common types of experiments used. Both of which may be used to generate the load-slip curves for shear connectors.

A push test experimental setup entails a steel girder positioned vertically between two concrete decks with the shear connectors of interest fastening each concrete deck to the flanges of the steel girder. The concrete decks are positioned on a solid foundation and a static or cyclic load is applied directly to the steel girder parallel to the concrete deck and steel girder interfaces, subjecting the shear connectors to direct shear as shown in Figure 2–9. Push tests typically have a concrete deck on either side of the steel girder to eliminate any eccentricities acting on the connection due to the applied load.

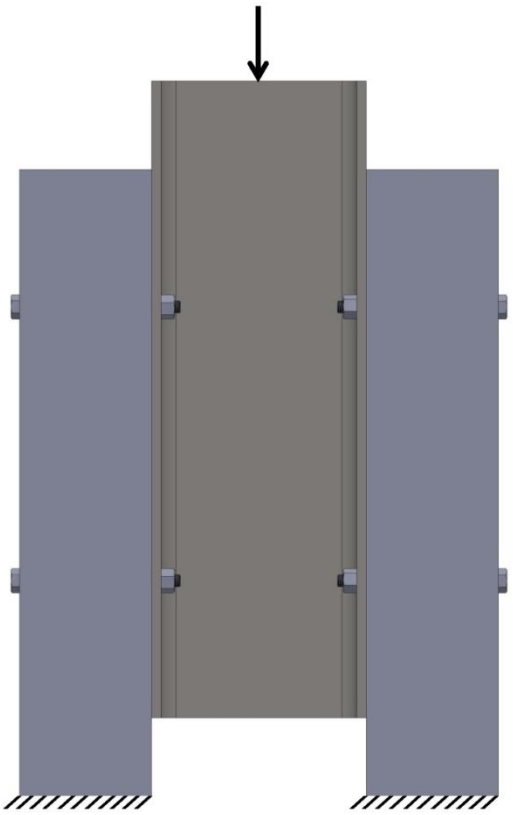

Figure 2–9: Typical push test specimen

The longitudinal shear force carried by each shear connector is calculated by dividing the total magnitude of the applied load by the number of shear connectors. This is possible because Slutter & Fisher (1966) discovered that the load distribution is relatively uniform between each of the connectors and the stress level is constant throughout the fatigue life. Push tests are relatively inexpensive to conduct in comparison to beam tests and therefore have been used extensively by several researchers such as Slutter & Fisher (1966), Kwon et al. (2010), and Chen (2013). Push tests have been widely accepted as adequate for determining the static and fatigue performance of shear connectors as Slutter & Fisher (1966) asserted that the results from push tests are similar to that of beam tests, indicating that where differences do occur, push tests yield more conservative results and may be treated as a lower bound. Therefore, due to their conservatism and lower fabrication costs than beam tests, push tests have been used by many researchers.

A beam test features a composite bridge structure comprised of a concrete deck fastened to a steel girder using the shear connectors of interest. The ends of the bridge are typically simply supported and the loading is applied to the concrete deck at the desired location perpendicular to the shear interface as shown in Figure 2–10.

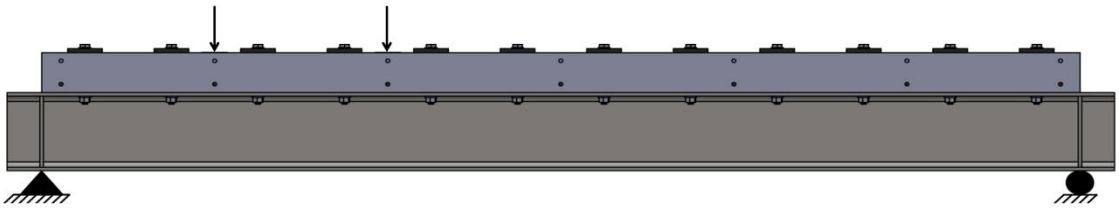

Figure 2–10: Typical beam test specimen

Dissimilar to the push test, the longitudinal shear force carried by each shear connector in the beam test cannot be determined by simply dividing the applied load by the number of shear connectors as the force distribution in a beam test is highly indeterminate and is not constant among all the shear connectors. The longitudinal shear force carried by each shear connector must be calculated by considering the first moment of area of the composite section. This is discussed thoroughly in Section 2.3.3. In general, the longitudinal shear force acting on each shear connector in a beam test are not equal and therefore the shear connectors are not expected to fail simultaneously. When one shear connector begins to crack, yield or slip, its stiffness is reduced and there is a redistribution of forces to the neighboring shear connectors which now attract more shear force than previously due to their relatively larger stiffness. This causes the damage (crack, yielding or slip) in the failing shear connector to grow more slowly as its neighboring shear connectors have alleviated some of the force it originally resisted (Sjaarda et al., 2018). This redistribution is not present in push test experiments.

Beam tests are relatively more expensive to fabricate and are more complicated to successfully instrument as the force distribution in the connectors is highly indeterminate and therefore, the successive failure of shear connectors is largely unpredictable. However, the behaviour of the shear connectors is potentially different when assessed using a push test versus a beam test. Several researchers including Johnson (2000), Yu-Hang et al. (2014), Porter (2016),.and Sjaarda et al. (2018) have advocated the use of beam tests, concluding that the inconsistencies in results between push tests and beam tests are significant, and suggest that push tests may not capture true connector behaviour, and may be too conservative. The primary difference between a push test and a beam test is the mechanism by which the longitudinal shear force is developed in the shear connectors (Sjaarda et al., 2018). In a push test, the longitudinal shear force developed in the shear connectors is dictated by simple equilibrium as they provide the only load path which the applied load may be transferred from the steel girder to the concrete decks. In this case, the force in the shear connectors is independent of the connector stiffness. Conversely, the shear connectors in a beam test resist the longitudinal shear forces acting between the concrete deck and steel girder by resisting slip caused by the strain profile discontinuity at the interface between the concrete deck

and steel girder. That is, the force in the connector is generated by an imposed deformation, and thus is strongly dependent on the stiffness (load-slip response) of the connector.

Moreover, the failure mechanism observed during a push test may not be representative of the failures experienced in an actual structure. Chen (2013) revealed in his push test experimentation of shear studs that plastic deformation of the shear studs was observed prior to the onset of fracture and in many cases, the concrete beneath the fractured shear stud was crushed. Conversely, Porter (2016) did not observe any plastic deformation to the shear studs prior to the onset of fracture and did not report any crushing of the concrete deck. Oehlers & Foley (1985) confirmed this phenomenon indicating that due to the nature of push tests, the concrete decks are more likely to experience splitting than when used in a composite beam. This emphasises the fact that the slip observed during a push test may be unrealistic in magnitude and not representative of the behaviour of shear connectors in composite bridges.

2.2 Static Resistance

The following section discusses in detail the significant research that has been completed prior to this research project regarding the static resistance of shear connectors as well as the pertinent design code requirements. Since through-bolt shear connectors are the focus of this research topic the following section will focus primarily on through-bolt shear connectors as well as welded, headed shear stud connectors as a reference for comparison.

2.2.1 Static Resistance of Shear Connectors

The static resistance of a shear connector is the resistance or strength of the connector subjected to loads which are constant, or applied at a rate sufficiently slow that they may be considered as constant with no inertial responses. The determination of a loading rate that is appropriately slow such that it may be considered static is dependent on the stiffness of the supporting structure. Knowledge of the static resistance of shear connectors is vital to the understanding of how the overall bridge will perform when subjected to large sustained loads such as snow loads or the accumulation of vehicles during periods of high intensity traffic.

The most common method of obtaining the static resistance of a shear connector is through the use of a push test. When a push test is used to quantify the static performance of a shear connector, the load-slip curve specific to the shear connector can be derived directly. Figure 2–11 illustrates a typical load-slip curve for headed shear studs (Left) and through-bolts (Right).

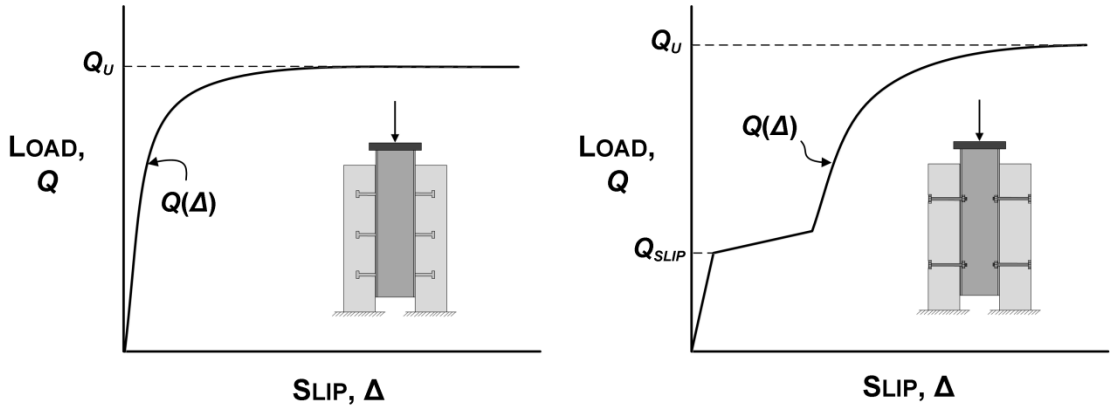

Figure 2–11: Push test load slip curves for headed shear studs (Left) and through-bolts (Right)

Load-slip curves offer critical information, characterizing the performance and behaviour of a shear connector. Firstly, the maximum capacity of the shear connector, labeled as Q_U in Figure 2–11, may be obtained directly as the load at which the shear connector fails. Moreover, the stiffness of the shear connector can be determined by calculating the slope of the load-slip curve. Lastly, the ductility of the shear connectors may be computed from the load slip curve by taking the ratio of the total slip at failure to the slip observed at the onset of yielding of the connector.

As illustrated in Figure 2–11, the load-slip response of the welded, headed shear studs connectors differs from the load-slip response of the through-bolt shear connectors. The load-slip responses are different primary due to the fact that the shear studs are embedded directly within the concrete decks whereas the through-bolts pass through prefabricated holes within the concrete decks and steel girder that are slightly larger in diameter than the through-bolts themselves. Therefore, when the shear studs are loaded statically in a push test experiment, they engage in bearing against the concrete immediately. As illustrated in Figure 2–11 (Left), the load resisted by the shear studs (Q) increases constantly as the relative slip between the concrete decks and the steel girder (Δ) increases until the shear studs begin to yield, after which the shear studs fracture at an ultimate load Q_u. Conversely, the load-slip behaviour of the through-bolt shear connectors, loaded in a push test experiment, displays three separate stages defined by Liu et al., (2014). During first stage, the applied load (Q) is less than the force of friction between the steel-concrete interfaces and therefore fails to induce slip. This explains the initial vertical segment of the load-slip curve presented in Figure 2–11 (Right). The second stage reveals the behaviour of the through-bolts at the onset of slip. During this stage, there is very little increase in load resisted by the through-bolts (Q) as the force of friction between the steel girder and concrete decks has been overcome. Therefore, the slip between the steel girder and concrete decks increases until the separation between the through-bolts and the inside surface of the holes within the concrete decks decreases to zero. This is illustrated in Figure 2–

11 (Right) as the nearly horizontal line following the onset of slip in the first stage. The final stage features the through-bolts bearing against the concrete decks immediately following the large increase in slip observed during the second stage. This is shown in Figure 2–11 (Right) as the nonlinear load-slip response up until the onset of failure (Q_u). This is explained in more detail in Section 5.1.1.

Ollgaard et al. (1971) performed 48 push test experiments with welded, headed shear stud connectors to assess the influence that the concrete properties has on the strength of the embedded shear stud connection. The concrete properties considered in the sensitivity analysis included the compressive strength, tensile strength, modulus of elasticity, and density. The failure criterion was established as the separation of the steel girder from one or both concrete decks. The failure of the specimens featured one of two separation modes. The shear studs either sheared off at the base where they connected to the flange, remaining embedded within the concrete, or the concrete failed in the vicinity of the shear studs. The latter separation mode involved the shear studs being pulled out of the concrete deck along with a portion of the concrete. Both separation modes were observed within the same specimen in several instances. Oehlers & Foley (1985) reported nearly identical failure modes for welded, headed shear studs. However, they indicated that failure of the concrete deck can be designed against if an adequate cover and sufficient reinforcement is provided.

Generally, Ollgaard et al. (1971) observed that the strength of the shear connectors decreased with substantial decreases in concrete compressive strength, concrete tensile strength, the modulus of elasticity of the concrete and the concrete density. However, a statistical regression analysis revealed that the inclusion of only the compressive resistance and modulus of elasticity of the concrete deck provided an accurate representation of the data with a high correlation. Ollgaard et al. (1971) concluded that the compressive resistance and the modulus of elasticity of the concrete deck are the controlling parameters which influence the strength of the shear connectors. Ollgaard et al. (1971) proposed Equation 2-4, an empirically derived relationship relating the concrete compressive strength (f'_c) and the modulus of elasticity of the concrete (E) in ksi to the strength of the shear stud connection (Q_u).

$$Q_u = 1.106 \cdot A_{sc} \left(f_c^{'} \right)^{0.3} \cdot \left(E_c \right)^{0.44} \tag{2-4}$$

where A_{sc} is the cross-sectional area of the shear stud connectors (in^2). Equation 2-4 can be simplified as shown in Equation 2-5 for design purposes as specified in CSA S16-09, Clause 17.7.2.2 (CSA S16-09, 2012).

$$Q_u = 0.5 \cdot \phi_{sc} \cdot A_{sc} \cdot \sqrt{f_c^{'} \cdot E_c} \leq \phi_{sc} \cdot A_{sc} \cdot F_u \tag{2-5}$$

where ϕ_{sc} is the material resistance factor of the shear connector, A_{sc} is in mm^2 and f'_c and E_c are in MPa. As illustrated in Equation 2-5, Clause 17.7.2.2 requires that the strength of the shear stud connection be less than the rupture strength of the shear studs in direct tension, which is determined by the product of the cross-sectional area and the ultimate strength (F_u) of the shear studs in mm^2 and MPa respectively (CSA S16-09, 2012). Moreover, Ollgaard et al. (1971) proposed Equation 2-6 where the load resisted by the shear studs (Q) is a function of the slip (Δ) in mm.

$$Q = Q_u \left(1 - e^{-0.71\Delta}\right)^{0.4} \tag{2-6}$$

Kwon (2008) performed static and fatigue tests on direct shear, push test specimens and static tests on full-scale beam tests to assess the performance of a variety of post-installed shear connectors. The shear connectors tested pertinent to this research project included through-bolts and double-nut through-bolts, described in Section 2.1.3. Kwon (2008) conducted two push tests on 7/8 inch diameter, ASTM A325 through-bolts and three push tests on 7/8 inch diameter ASTM A193 B7 threaded rods, double-nut through-bolts. The single shear push tests each featured one shear connector. Moreover, a clamping rod was included to prevent uplift of the steel section during testing. This testing configuration was adopted from the work of Kayir (2006) and is shown in Figure 2–12.

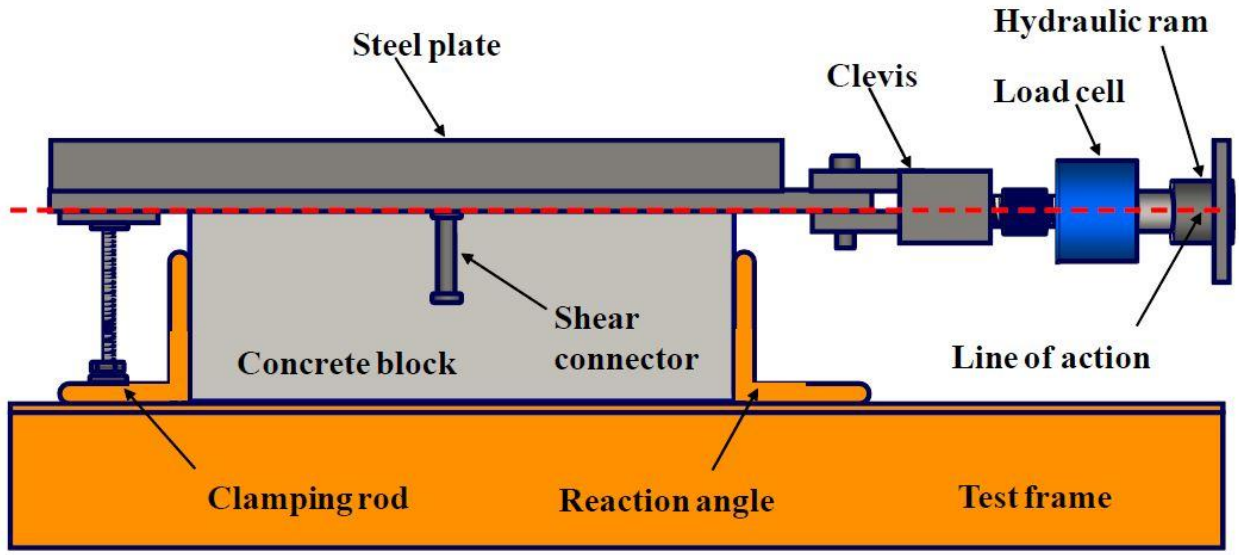

Figure 2–12: Direct shear test assembly (Kwon, 2008)

Kwon (2008) implemented the use of direct tension indicating washers to confirm the level of pretension in the through-bolts. The static push tests were conducted in displacement control until failure of the shear connectors was observed. Kwon (2008) reported that the double-nut through-bolts exhibited a higher

stiffness in the elastic range which he attributed to the increased bearing surface acting on the concrete due to the embedded double-nuts. It is speculated that this increase in bearing surface delayed the onset of concrete crushing. The ultimate failure of the double-nut through-bolts were shear failure at the steel-concrete interface. Moreover, Kwon (2008) described that the through-bolts exhibited a much larger slip than the double-nut through-bolt configuration, consistent with the large slip expected in stage two defined by Liu et al. (2014). Kwon (2008) also indicated that the through-bolts observed a relatively high initial stiffness at low load levels due to the shear resistance contribution of the friction between the steel and concrete. However, the failure mechanism associated with the through-bolt shear connectors was the crushing of the concrete as the through-bolts did not fail themselves.

Furthermore, Kwon (2008) and Kwon et al. (2010) performed full-scale beam tests to assess the stiffness, strength and ductility of composite beams using through-bolt shear connectors and double-nut through-bolt shear connectors. Each specimen was a simply supported beam, 38 feet in length and loaded at midspan. A non-composite beam with no shear connectors was tested to serve as a reference for comparison. Two beams with 32 shear connectors, providing a 30% degree of shear connection were tested. One featured 7/8 inch diameter ASTM A325 through-bolts and the other featured 7/8 inch ASTM A193 B7 threaded rods. The load deflection results for these experiments are illustrated in Figure 2–13.

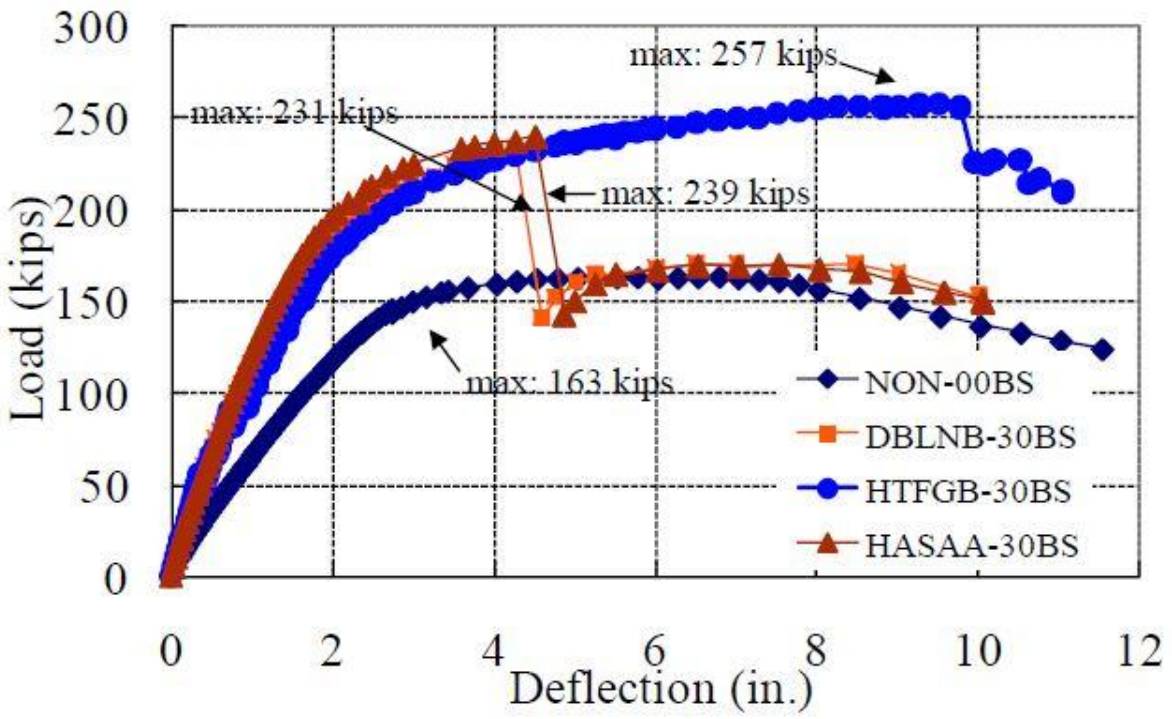

Figure 2–13: Load-deflection curves for full-scale composite beam tests. NON-00BS - Non-Composite Beam, DBLNB-30BS - Double-Nut Bolt Beam, HTFGB-30BS - High-Tension Friction Grip Bolt Beam, HASAA-30BS - Adhesive Anchor Beam (Kwon, 2008)

Figure 2–13 reveals that the non-composite beam behaved in a highly ductile manner, consistent with the behaviour expected of a fully supported steel beam. The ultimate strength of the non-composite beam was controlled by the plastic moment capacity of the steel girder. The specimen was loaded until local buckling of the flange and web occurred. While significant cracking of the concrete deck was observed, no crushing occurred. Moreover, as illustrated in Figure 2–13, the beam featuring the double-nut through-bolts exhibited a much greater initial stiffness and strength than the non-composite beam. The load capacity of this specimen dropped suddenly due to the failure of several shear connectors. Also shown in Figure 2–13, subsequent to the failure of multiple shear connectors, the double-nut through-bolt beam behaved very similarly to the non-composite beam with local buckling of the top flange and web. The test was stopped prior to the onset of crushing of the concrete deck. Finally, the beam with its shear connection provided by the through-bolts behaved in a manner that was even stiffer than the double-nut through-bolts and retained this stiffness for a longer period. This prolonged retention in stiffness was attributed to the friction acting between the steel girder and concrete deck which contributed to the resistance of the longitudinal shear forces, lessening the stresses on the through-bolts. However, once the

force of friction was overcome and subsequent to the onset of slip, the through-bolt beam behaved in a manner that was less stiff than the double-nut through-bolt beam. Kwon (2008) reported that the load carried by the through-bolt beam decreased with each occurrence of slip of a through-bolt shear connector. However, Kwon (2008) indicated that each load decrease was recovered through the dowel action of the through-bolts as they entered into bearing against the concrete. As illustrated in Figure 2–13, the through-bolts displayed a higher deformation capacity than the double-nut through-bolts due to the available slip potential offered by the oversized holes. This available slip potential, enabled a greater degree of force distribution between the shear connectors, resulting in an overall higher strength and ductility than the double-nut through-bolt shear connectors. Unlike the double-nut through-bolt shear connectors, only a single through-bolt failed at a deflection of 8.84 inches with no observable strength decrease. Shortly after, crushing of the concrete began and five more through-bolts failed between 9.75 and 10 inches of deflection. The failure of these through-bolts was accompanied by a relatively small decrease in strength as shown in Figure 2–13. Kwon (2008) reported that the interfacial slip between the steel girder and the concrete deck for the through-bolt beam was around 1/3 as much as the average slip observed with the push test specimens conducted on the through-bolt shear connectors.

Chen (2013) performed 13 double-shear push test experiments with the objective of attempting to increase the friction characteristics between the steel girder and concrete decks, thus reducing the longitudinal shear force required to be carried by the ASTM A325 through-bolt shear connectors. Along with varying the friction characteristics, the initial through-bolt pretension and diameter were also varied. Three of the push test experiments also featured trapezoidal shear lugs welded to the flanges of the steel girder to enhance shear transfer. The through-bolt diameters considered included 1/2", 5/8", and 3/4". A plain steel surface and a regular formed concrete surface were tested (S1), a steel surface coated with concrete sand and a regular formed concrete surface were tested (S2) and finally, a plain steel surface and a sandblasted concrete surface were tested (S3). Sikadur 330 adhesive was used to bond the concrete sand to the steel flanges (Chen et al., 2014). The test matrix adopted by Chen is illustrated in Table 2–1 below. Specimens including the use of welded shear lugs are denoted as SL.

Table 2–1: Chen (2013) testing matrix

	ASTM A325 Bolt Diameters		
Bolt Tension	1/2"	5/8"	3/4"
0 kN	SL	SL	-
53 kN	SL, S2, & S3	S2	S2
85 kN	-	S1, S2, & S3	-
125kN	-	-	S2 & S3

Each specimen experienced a shear failure of the through-bolt connectors, which failed within the threads where they intersected the concrete deck and steel girder interfaces. Chen (2013) reported that in many cases, the concrete was crushed by the bearing of the through-bolts against the inside diameter of the concrete holes. The load-slip curves observed from Chen's (2013) results featured the three separate stages defined by Liu et al. (2014) discussed above. Chen (2013) indicated that, as expected, the ultimate capacity of the through-bolts increased proportionally with the increase in through-bolt diameter. Moreover, the pretension level in the through-bolts was found to directly correspond to the load at which slip occurred. A larger pretension force produces a larger normal force and ultimately a larger force of friction acting between the steel girder and concrete decks. The ultimate capacity of the shear connections tested was the linear summation of the resistance due to friction acting between the steel girder and concrete decks and the dowel action of the bolts bearing against the concrete. However, the results indicated that whenever a friction enhanced surface was used, the coefficient of friction and by extension, the force of friction between the steel girder and concrete decks decreased from the base test which featured unmodified concrete and steel surfaces. Chen (2013) hypothesized that this phenomenon could be attributed to the surface treatments breaking down under the loading. When this occurred, the particulate residue of the surface treatments is believed to have remained trapped between the steel girder and concrete decks and acted as ball bearings, decreasing the friction between the steel girder and concrete decks.

2.2.2 Ultimate Limit State Design Requirements

The design of shear connectors used in composite bridges requires the consideration of both the ultimate limit state (ULS) and the fatigue limit state (FLS) as per CSA S6 (CSA S6, 2014). While the ULS rarely governs, the bridge must still satisfy the pertinent requirements. The ULS is the governing condition specifying the physical resistance and stability of a structure.

CSA S6, Clause 10.11.8.3 requires the transfer of the full longitudinal shear force between the concrete deck and steel girder, acting between the points of maximum and zero moment along the bridge span at the ULS (CSA S6, 2014). The longitudinal shear force acting between these two points is assumed to be resisted uniformly (equally) by the shear connectors present between the points, assuming no contribution from friction. Therefore, the total number of shear connectors required (N) between the location of maximum and zero moment is equal to the total longitudinal shear force (P) divided by the strength of each shear connector (q_{rs}) as shown in Equation 2-7. The strength of a single shear connector (q_{rs}) is determined based on Equation 2-5 above.

$$N = \frac{P}{q_{rs}} \tag{2-7}$$

The total longitudinal shear force that must be resisted is based on the crushing strength of the concrete and can be calculated using either Equation 2-8 or Equation 2-9. When the plastic neutral axis is located within the concrete deck, Equation 2-8 is used and Equation 2-9 is used when the plastic neutral axis is located within the steel section.

$$P = \phi_s \cdot A_s \cdot F_y \tag{2-8}$$

$$P = 0.85 \cdot \phi_c \cdot f_c^{'} \cdot b_e \cdot t_c + \phi_r \cdot A_r \cdot F_y \tag{2-9}$$

where ϕ_s, ϕ_r and ϕ_c are the material resistance factors for the steel girder, steel reinforcement and concrete deck respectively, A_s and A_r are the areas of the steel girder and steel reinforcement respectively (mm^2), F_y is the minimum specified yield strength of steel (MPa), f'_c is the specified compressive strength of concrete (MPa), b_e is the effective width of the concrete deck (mm) and t_c is the thickness of the concrete deck (mm).

The tensile capacity of the through-bolt shear connectors at the ULS (T_r) is determined by Equation 2-10.

$$T_r = A_b \cdot F_u \tag{2-10}$$

where A_b is the cross-sectional area of a single bolt and F_u is the specified minimum tensile strength (MPa).

2.3 Fatigue Resistance

The following section provides an overview of the fatigue of metals and discusses in detail the significant research that has been completed prior to this research project regarding the fatigue resistance of shear connectors. Lastly, the design code requirements for the fatigue resistance of shear connectors are discussed.

2.3.1 Fatigue of Metals

There are a variety of mechanisms by which metallic structural elements may fail. Creep, rupture, and fatigue are three of the more common failure modes. Fatigue failure was the primary interest of this research project as it is the most frequent mode of failure in metals, responsible for approximately 90% of all metallic failures (Callister & Rethwisch, 2010). Fatigue is the progressive weakening of a material due to the initiation and propagation of cracks when subjected to cyclic loading. The fatigue life of a

component is the linear summation of the crack initiation life (N_i) and the crack propagation life (N_p), after which final fracture occurs. For smooth elements, the fatigue life is typically assumed to be equal to the crack initiation life as it is much longer than the crack propagation life. Conversely, for welded elements, the crack initiation life is typically assumed to be zero as welds inherently consist of defects, internal stresses, and imperfections prior to the onset of cyclic loading. Metallurgical imperfections such as notches in the crystalline structure, abrupt discontinuities in the component geometry, and weldments all create stress concentrations. These stress concentrations are especially susceptible to the formation of cracks as the peak stresses observed by the component are a maximum at these locations. Fatigue cracks will only form under tensile loading, pulling the crystalline structure apart. Compressive loads are remedial in that they close the crack, preventing further crack formation. Once a fatigue crack has formed, the sharp tip of the crack creates a stress concentration, amplifying the plastic deformation caused by tensile stresses. The crack will continue to grow under the cyclic loading until the critical crack length has been reached and the remaining area is less than the minimum required to resist the applied load. At this instance, the component will then fail statically.

There are a variety of factors which influence the fatigue life of a structural component including the stress range, the mean stress, structural geometry, initial imperfections, and material properties such as ductility, stiffness, and yield strength (Cui, 2002). Typically, higher strength metals observe longer fatigue lives as they have a higher resistance to plastic deformations. Currently there exists two approaches for predicting the fatigue life of a component, cumulative fatigue damage theory and fatigue crack propagation theory. The cumulative fatigue damage theory is the most commonly used and therefore was the primary focus of this discussion. The cumulative fatigue damage theory predicts the failure of a component once the accumulated fatigue damage reaches a critical level, beyond which failure is expected. There are three methods used under this theory to calculate the cumulative damage: the stress-life method, the strain-life method, and an energy based approach, or fracture mechanics (Cui, 2002).

The stress-life method is the most frequently used approach by engineers for predicting the fatigue life of shear connectors in composite structures. The stress-life method correlates the fatigue life of a component, or the number of cycles to failure (N) to the applied true stress amplitude (σ_a) the component is subjected to. Fisher et al. (1969) revealed through physical tests and fracture mechanics that the relationship between the number of fatigue cycles and the stress range is linear when expressed logarithmically and can be rewritten mathematically as shown in Equation 2-11.

$$N = M \cdot \Delta\sigma_r^{-m} \tag{2-11}$$

where N is the number of fatigue cycles to failure, $\Delta\sigma_r$ is the stress range the component is subjected to and the terms M and m are constants that are established based on the regression analysis of physical testing.

Equation 2-11 provides the number of occurrences of the applied stress range that will result in the failure of a given component with a specific material and geometry. Equation 2-11 explicitly assumes that the stress range the component is subjected to is constant. This is rarely the case, especially in bridge structures where vehicles of dissimilar weights, traveling at varying speeds cross the structure consistently. Therefore, the Palmgren-Miner's Rule for non-uniform amplitude loading must be considered. The Palmgren-Miner's rule hypothesizes that the cumulative damage experienced by a component due to the application of repeating cycles of non-uniform magnitude may be expressed mathematically as shown in Equation 2-12 (Hwang & Han, 1985).

$$D = \sum_{i=1}^{k} \frac{n_i}{N_i} \tag{2-12}$$

where n_i is the number of cycles the component has been subjected to at each stress range, N_i is the total number of cycles the component can withstand before failure at a specific stress range and D is the damage incurred.

The Palmgren-Miner's Rule linearly combines the contribution to damage that each stress range within the loading history had on the total damage incurred by the component. It formulates a hypothesized equivalent constant stress amplitude that would yield a fatigue life similar to that of the non-uniform stress history. The cumulative damage, D, is typically set equal to 1 to determine the number of times the non-uniform stress amplitude history can be applied to the component before failure occurs.

2.3.2 Fatigue Resistance of Shear Connectors

The fatigue resistance of a shear connector is the resistance or strength of the connector subjected to cyclic loads. The two most common methods of obtaining the fatigue performance of a shear connector is through the use of push tests or full-scale beam tests where the loading is applied in a cyclic manner.

The amplitude of the cyclically applied loads may be repetitive or variable. Researchers Oehlers & Foley (1985) believe that based on the Palmgren-Miner's Rule, the occurrence of an overload does not affect the fatigue life unless it is significant enough to result in fracture, given the current remaining effective area. As the fatigue loading progresses, crack propagation will increase, decreasing the remaining effective area resisting the applied loads. Given the current remaining cross-sectional area, if a sudden overload is

applied with a magnitude sufficiently large to fail the shear connector statically, complete fracture will occur, therefore decreasing fatigue endurance of the shear connector. Moreover, Oehlers & Foley (1985) indicated that the range of the shear loading in composite beams causing tension on the shear connectors (R_{Tens}) is the critical or effective range which propagates a fatigue crack and not the entire range acting on the shear connectors (R_{Total_1}), which is the summation of the range in tension (R_{Tens}) and the range in compression (R_{Comp}). This is because the portion of the loading which subjects the shear connectors to a compressive loading closes any cracks, inhibiting further crack propagation. However, when the entire stress range loads the shear connectors in tension, the entire range (R_{Total_2}) is considered critical or effective in propagating fatigue cracks. This concept is illustrated in Figure 2–14.

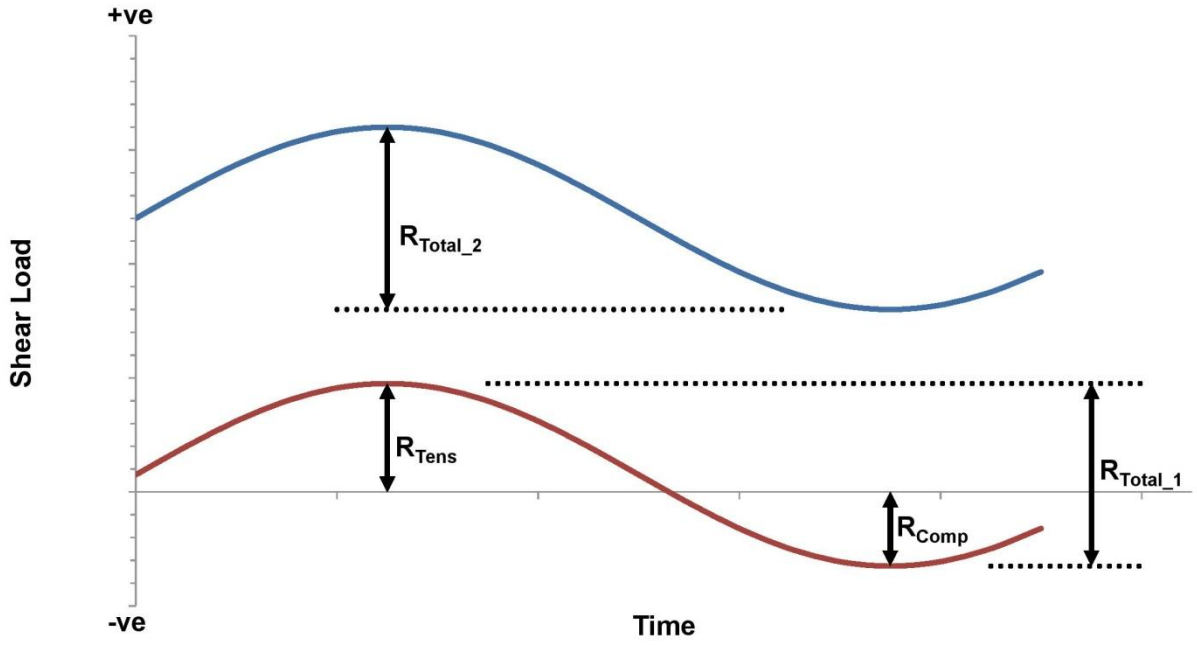

Figure 2–14: Fatigue loading range (Adapted from: Oehlers & Foley, 1985)

Slutter & Fisher (1966) and Seracino et al. (2003) confirmed this understanding by reporting that shear connectors subjected to stress reversals or bi-directional cyclic loading experienced longer fatigue lives than those subjected to unidirectional cyclic loading.

Similarly, Skorupa (1998) examined the effects of a variable amplitude loading on the propagation of fatigue cracks. Skorupa (1998) defined the load interaction effect which explains the occurrence of a different crack growth increment under variable amplitude loading when compared to constant amplitude loading with identical maximum and minimum stress levels. Skorupa (1998) concluded that the effects of variable amplitude loading on the crack growth rate is highly dependent on a number of factors including

material properties, geometry and external environmental conditions. It was found that variable amplitude loading can have the effect of hindering or accelerating the growth of fatigue cracks depending on the specifics of the specimen.

Porter (2016) addressed the effects of variable amplitude loading acting on composite bridge decks featuring welded, headed shear stud connectors to simulate the actual anticipated loading conditions a typical vehicular bridge may be subjected to. Twelve composite beam specimens were tested. Six precast specimens were fabricated exhibiting evenly spaced clusters of four shear studs, grouted into pockets cast in the concrete deck. The remaining six specimens were fabricated with the concrete deck cast-in-place around evenly spaced rows of two shear studs. The specimens were instrumented using a combination of linear variable differential transformers (LVDT) to record the interfacial slip at the steel-concrete interface and the overall beam deflection. Furthermore, strain gauges were used to determine the forces within the steel girder and local distortion strain gauges were installed with the intent of recording shear stud failures. The specimen geometry and instrumentation details used in Porter's (2016) experiments are illustrated in Figure 2–15.

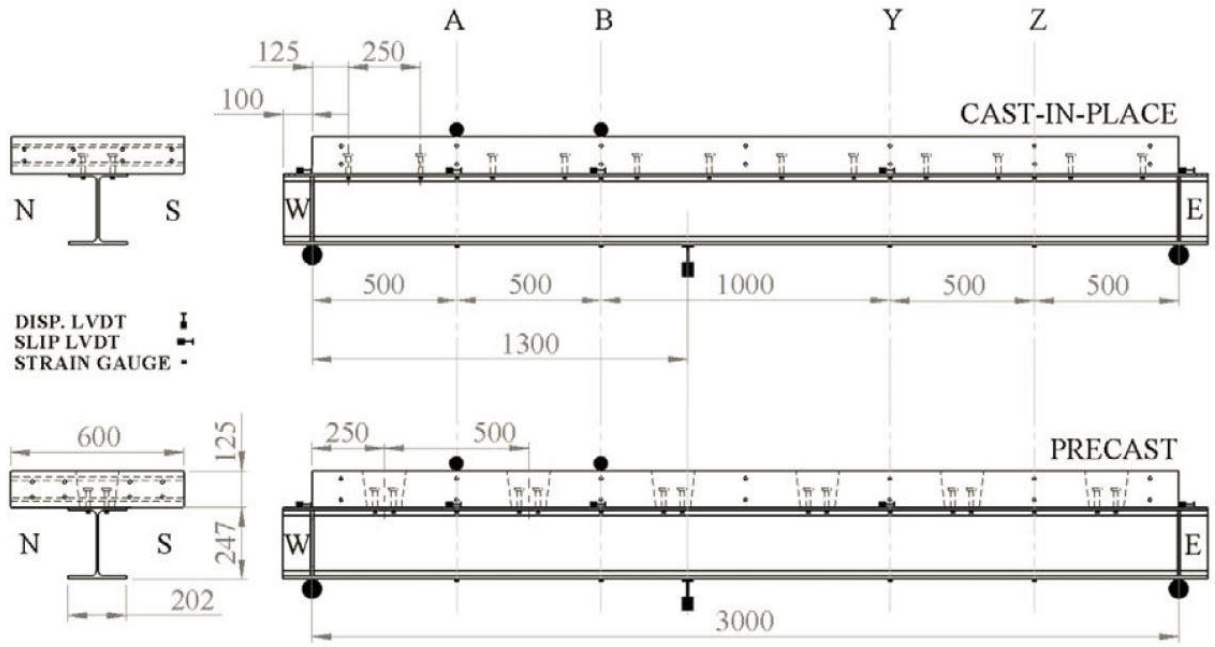

Figure 2–15: Specimen geometry and instrumentation layout. Cast-in-place (Upper) and precast (Lower) (Porter, 2016)

The specimens tested by Porter (2016) were simply supported and were subjected to two points loads, offset towards the left hand side of the beam, labelled as West in Figure 2–15. This loading configuration

was designed to create a varying shear profile along the length of the beam, inducing a relatively early failure in the more heavily loaded shear connectors towards the West end of the beam. Porter (2016) expected the shear studs at the West end of the beam to fail first, therefore simplifying the instrumentation and monitoring of the specimens. Prior to the commencement of fatigue testing, the cast-in-place and precast specimens were tested statically in load control to break the chemical adherence between the concrete deck and steel girder as well as to quantify the original strength of the specimens prior to the onset of fatigue damage. Further static tests were performed at the calculated 100% and 1000% fatigue lives of the shear studs. The variable amplitude loading history was acquired from data collected during a survey conducted by the Ministry of Transportation of Ontario (MTO) in 1995. The surveying involved randomly sampling the weights of over 10,000 trucks using the transportation infrastructure in Ontario. Porter (2016) randomized and scaled the data collected by the MTO to yield desired stress ranges on specific stud groupings. Porter (2016) defined three distinct phases of failure: the initiation of a fatigue crack, the onset of reduction in stiffness of the studs, and final fracture of the studs.

Based on the static test performed throughout the experimentation, Porter (2016) discovered that only the specimens subjected to the highest stress level of fatigue loading demonstrated significant increases in deflection throughout the course of their fatigue lives. The less heavily loaded specimens demonstrated little to no changes in deflection. Moreover, the fatigue testing revealed that, as expected, the welded headed shear studs failed at their welds. The local distortion strain gauges were successful in determining when the final failure of a stud occurred. The distortion gauge results displayed an increase to some maximum value, followed by a rapid decrease, indicating that the stiffness of the failed stud had decreased and consequently, the longitudinal shear force it once carried had been redistributed to the surrounding shear studs. Porter (2016) reported that typically the shear studs towards the ends of the beams failed first as these shear studs experienced the largest slip magnitude. Conversely, the shear studs directly beneath the location of the applied loading failed last as the longitudinal shear force was the lowest and the normal force was the greatest directly beneath the applied loads and therefore, the force of friction was also the greatest. This significant normal force and resulting friction between the concrete deck and steel girder, reduced the magnitude of the longitudinal shear force required to be resisted by the shear studs. Porter (2016) concluded that the shear studs in the precast specimens outperformed the shear studs in the cast-in-place specimens in terms of their fatigue performance. Porter (2016) found that the shear studs in the cast-in-place specimens experienced initial stresses prior to the onset of loading due to concrete shrinkage, reducing the overall fatigue life of the shear connectors.

Slutter & Fisher (1966) performed extensive fatigue testing on 56 single shear, push test specimens. They claimed that the current design procedures of composite beams were too conservative based on the static

testing performed by Slutter & Driscoll (1965) and fatigue testing performed by King et al. (1965) and Toprac (1965). Furthermore, the current design considerations for the fatigue of shear connectors imposed a factor of safety to the static strength of shear connectors, limiting the yielding of the shear connectors as the basis for the determination of fatigue strength. However, Slutter & Fisher (1966) reported that based on composite beam tests conducted at Leigh University and the University of Texas, no direct relationship was found to exist between the fatigue strength and the static strength of shear connectors. Therefore, furthering the understanding of the fatigue behaviour of shear connectors may result in more efficient designs, rendering significant cost savings. Of the 56 push test specimens, 35 featured four 3/4" shear studs, 9 featured four 7/8" shear studs, and the remaining 12 used 4" channel connectors. Each specimen was subjected to 250 cycles per minute (4.17 Hz) or 500 cycles per minute (8.33 Hz) depending on the behaviour and response of the specimen.

The experimentation was designed to assess the influence the stress range and minimum stress had on the fatigue performance of the shear connectors. All tests were conducted in a random order and three of each type of specimen were tested to discover the consistency of the results. The randomization of the testing was done to prevent uncontrolled factors such as concrete curing time and erratic behaviour of the testing equipment from biasing the results. Fatigue testing was conducted until fatigue fracture of all the connectors was observed. Slutter & Fisher (1966) reported that fatigue failures typically initiated at the reinforcement of the stud weld and penetrated into the flange of the girder. The flanges had concave depressions remaining at the locations of the fractured shear studs. Slutter & Fisher (1966) observed that the studs nearest to the loaded edge failed in fatigue first when tested at the higher stress range with the lower minimum stress. The remaining two studs typically failed statically by being sheared off. Conversely, Slutter & Fisher (1966) observed that all four shear studs failed due to fatigue simultaneously when tested at the lower stress range with the higher minimum stress. This behaviour is speculated to be a consequence of a more even stress distribution at the lower stress levels. The results revealed that the stress range was the more critical variable in comparison to the minimum stress in determining the fatigue performance of shear studs. Based on a regression analysis of their experimental results, Slutter & Fisher (1966) proposed the following semi-logarithmic equation, estimating the fatigue life (N) of a shear stud connector for a given stress range (S_r).

$$\log N = 8.072 - 0.1753 \cdot S_r \tag{2-13}$$

The shear stress range, S_r in Equation 2-13, is taken as the difference between the maximum and minimum shear stresses in ksi. Moreover, Slutter & Fisher (1966) observed that the stress level was maintained constant throughout the fatigue life in a push test, rendering a more conservative result over

beam tests which display a loss of interaction prior to failure, which allows for the forces to redistribute among the shear connectors. This redistribution of forces results in a shear stud stress state that is less than that predicted by elastic theory.

Yu-Hang et al. (2014) performed fatigue tests on seven simply supported composite beams, spanning 4 m with 16 mm diameter welded, headed shear studs, arranged in a single line along the length of the specimen. They concluded that the fatigue life of the shear studs was significantly influenced by the shear stress amplitude acting on the shear studs. Furthermore, they discovered that welded shear studs present in a composite beam, subjected to fatigue loading, predominately experience one of the three failure modes shown in Figure 2–16. Yu-Hang et al. (2014) reported that welded, headed shear studs typically fail either by shear failure at the base of the stud as shown in Figure 2–16 (a), cracking of the flange near the stud as shown in Figure 2–16 (b) or failure of the weld between the stud and the flange as shown in Figure 2–16 (c).

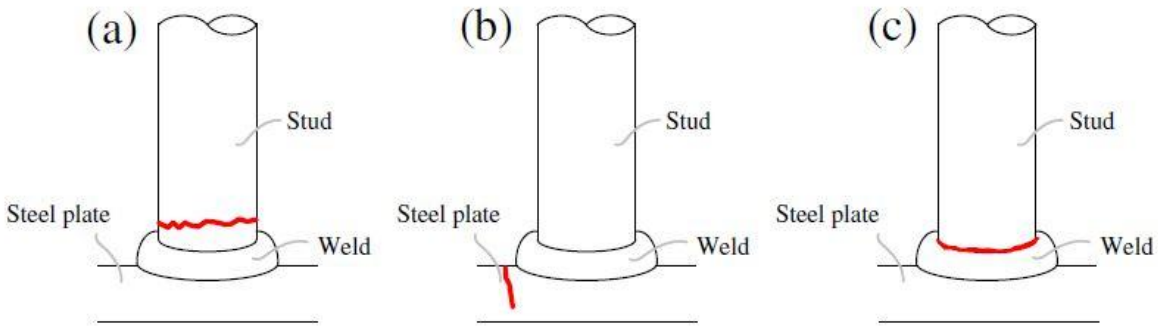

Figure 2–16: Typical fatigue failure modes for welded headed shear studs (Yu-Hang et al., 2014)

All three failure modes depicted in Figure 2–16 illustrate the propagation of fatigue cracks, originating at a stress concentration created by a material imperfection or weldment. Yu-Hang et al. (2014) reported that the welding quality plays a significant role on the fatigue strength of the connection.

Yu-Hang et al. (2014) observed that as the fatigue crack propagated, the remaining net area of the shear studs decreased. When the longitudinal shear force acting on the shear studs could no longer be resisted, the remaining net area sheared statically. Thus, the failure plane of the shear studs that failed due to fatigue displayed two discrete areas. One representing the fatigue crack propagation area and the other the static shear failure area. When the diameter of the shear stud was large relative to the thickness of the flange, the high heat caused by the welding generated residual stresses in the steel flange, resulting in the crack formation and ultimate failure of the flange. Therefore, Yu-Hang et al. (2014) recommend limiting the stud diameter to flange thickness ratio to prevent this failure mode.

Kayir (2006) conducted static and fatigue tests on multiple types of shear connectors including 3/4", ASTM A193 B7 threaded rods, double-nut through-bolt shear connectors, and 3/4", ASTM A325 through-bolt shear connectors. Direct tension indicating washers were used to determine the appropriate level of pretension in the connectors.

Three static tests were conducted for each type of shear connection, five fatigue tests were conducted on the double-nut through-bolt shear connectors and five fatigue tests were conducted on the through-bolt shear connectors. The specimens were loaded in direct shear in an identical testing configuration used by Kwon (2008), illustrated in Figure 2–12. The primary objective of the research conducted by Kayir (2006) was to assess the fatigue performance of a single shear connector subjected to high-cycle fatigue and low-cycle fatigue. Specimens subjected to high-cycle fatigue were loaded below the yield stress of the connectors and the specimens subjected to low-cycle fatigue were loaded above the yield stress of the connectors. The static tests and high-cycle fatigue tests were performed in load control. The low-cycle fatigue tests were performed in displacement control. All fatigue tests were performed with a constant minimum stress of about 6.2 MPa to prevent unintended load reversals. The high-cycle fatigue tests were stopped once five million cycles was reached and the low-cycle fatigue tests were stopped once four thousand cycles was reached. The fatigue testing matrix used by Kayir (2006) for the double-nut through-bolt shear connectors and the through-bolt shear connectors is illustrated in Table 2–2.

Table 2–2: Kayir (2006) fatigue testing matrix

High-Cycle Fatigue Testing	
Double-Nut 1	Through-Bolt 1
Double-Nut 2	Through-Bolt 2
Double-Nut 3	
Low-Cycle Fatigue Testing	
Double-Nut 4	Through-Bolt 1
Double-Nut 5	Through-Bolt 3
	Through-Bolt 4

The highest loaded double-nut through-bolt shear connector tested under high-cycle fatigue, failed by shearing of the connector in the concrete at the level where the second nut on the rod ended. This specimen also exhibited significant crushing of the concrete in front of the connector. The remaining two specimens did not fail due to fatigue and were tested statically to determine what effects the high-cycle fatigue damage may have had on their residual strengths. Kayir (2006) concluded that high-cycle fatigue tests do not reduce the ultimate capacity of shear connectors when compared to the initial static tests. Moreover, the highest loaded through-bolt shear connector, tested under high cycle fatigue, failed by

shearing of the connector above the steel-concrete interface within the steel plate. Some local concrete crushing in the vicinity surrounding the shear connector was observed and significant bearing and deformations of the steel plate were also reported.

None of the double-nut through-bolt shear connectors tested under low-cycle fatigue failed. However, a decrease in the load sustained by the connectors was observed throughout the low-cycle testing due to the crushing of the concrete. Both of the double-nut through-bolt test specimens were loaded statically subsequent to the low-cycle fatigue testing to determine what effects the low-cycle fatigue damage had on their residual strengths. Both failed statically in shear at the steel-concrete interface. Moreover, one of the three through-bolt specimens tested under low-cycle fatigue failed in shear above the steel-concrete interface. However, it should be noted that this specimen (Through-Bolt 1 in Table 2–2) was originally subjected to approximately 5.6 million cycles in the previous high-cycle fatigue testing. Both of the remaining two through-bolt test specimens were loaded statically subsequent to the low-cycle fatigue testing to determine the effect the low-cycle fatigue damage had on their residual strengths. While failures featured significant bearing on the steel plate, one ultimately failed due to shearing above the steel-concrete interface and the other failed due to the splitting of the concrete deck. Kayir (2006) concluded that low-cycle tests did in fact reduce the ultimate capacity of the shear connectors when compared to the original static tests however, not significantly. Kayir (2006) concluded that both the double-nut through-bolt shear connectors and the through-bolt shear connecters performed significantly better than the welded, headed shear studs loaded at similar levels which failed statically immediately upon the application of the first fatigue cycle in the low-cycle fatigue testing.

Further to the static push tests described in Section 2.2.1, Kwon (2008) and Kwon et al. (2010) conducted two cyclic push tests, assessing the fatigue performance of post-installed shear connectors. The specimens were fatigued in load control and were subjected to sinusoidal cyclic loads. One of the push tests featured 7/8", ASTM A325 through-bolts and the other featured 7/8", ASTM A193 B7 threaded rods, double-nut through-bolts. The through-bolt shear connectors were tested at a stress range of 240 MPa and the double-nut through-bolts were tested at a stress range of 310 MPa. Fatigue failure of the through-bolts and double-nut through-bolts was not observed after five million cycles. Kwon (2008) concluded that the fatigue resistances of post-installed shear connectors is considerably higher than the fatigue resistance of welded, headed shear studs. This can largely be attributed to the absence of weldments required for the post-installed shear connectors. Furthermore, Kwon et al. (2010) speculated that the high pretension force within the through-bolts and threaded rods may inhibit bending, further preventing failure in fatigue.

Kwon (2008) proposed the stress range of 240 MPa as the endurance limit for ASTM A325 bolts and ASTM A193 B7 threaded rods based on the absence of fatigue failures observed with the through-bolt shear connectors at this stress range. Even though the threaded rods did not fail in fatigue at 310 MPa, the limited testing data renders 240 MPa an acceptable conservative limit. Kwon et al. (2010) therefore proposed a relationship defining the endurance limit for the longitudinal shear force range acting on ASTM A325 bolts and ASTM A193 B7 threaded rods based on the endurance stress range of 240 MPa. This relationship is defined mathematically in Equation 2-14.

$$Z_r = 240 \cdot A_{sc} \tag{2-14}$$

where Z_r is the allowable longitudinal shear force stress range acting on the shear connector (N) and A_{sc} is the effective shear area of the shear connector (mm^2) which is taken as 80% of the gross cross-sectional area to account for the reduction in area due to the presence of threads (Kwon et al., 2010).

Kwon (2008) loaded the fatigued shear connectors statically to determine if their residual strengths were reduced by the fatigue loading. The maximum residual static strengths subsequent to the fatigue loading was 273 kN for the through-bolt shear connectors and 224 kN for the double-nut through-bolt shear connectors. Interestingly, these values were greater than the average static strengths from the static tests performed on the specimens that had not been fatigued, which were found to be 235 kN for the through-bolt shear connectors and 183 kN double-nut through-bolt shear connectors. This suggests that the fatigue loading had little effect on the residual static strength of the shear connectors. Conversely, Oehlers & Foley (1985) concluded based on their analysis of 129 push tests of welded, headed shear studs that the static strength reduces significantly after being subjected to fatigue loading, reporting residual strengths as low as 51% of the expected maximum static strength. Mainstone & Menzies (1967) reported similar reductions in strength. Therefore, the residual strength of cyclically loaded shear connectors varies depending on the magnitude and type of fatigue damage incurred.

2.3.3 Fatigue Limit State Design Codes

Further to the CSA S6 code requirements considering the ULS of shear connectors discussed in Section 2.2.2, the design of shear connectors used in composite bridges also requires the consideration of the FLS as per the current CSA S6 (CSA S6, 2014). The FLS is the governing condition requiring the bridge structure to be able to withstand the application of a specific number of cycles of a constant amplitude loading such that the cumulative fatigue effect is equivalent to that of the variable amplitude loading expected to act on the bridge throughout its lifetime (CSA S6, 2014). The fatigue loading limitations have been calibrated such that the anticipated cumulative fatigue effects of the actual loading

experienced by the bridge structure throughout its lifetime does not exceed the cumulative effect of two million cycles of the specified loading (CSA S6, 2014).

CSA S6, Clause 10.17.1 requires the consideration of the live load effects and the effects of local distortion when considering the performance of the bridge structure with regards to the FLS (CSA S6, 2014). For load-induced fatigue, structural details shall satisfy the limitation specified in Equation 2-15 for load-induced fatigue and Equation 2-16 for load-induced fatigue specifically in bridge decks as per Clause 10.17.2.2.

$$F_{sr} > 0.52 \cdot C_L \cdot f_{sr} \tag{2-15}$$

$$F_{sr} > 0.62 \cdot f_{sr} \tag{2-16}$$

where C_L is a reduction factor, f_{sr} is the calculated fatigue stress range due to the passage of the CL-625 truck as specified in Clause 3.8.3.2 (MPa) and F_{sr} is the fatigue stress range resistance which is calculated using Equation 2-17 (CSA S6, 2014).

$$F_{sr} = \left(\frac{\gamma}{N_c} \right)^{\frac{1}{m}} \geq \frac{F_{srt}}{2} \tag{2-17}$$

where F_{srt} is the constant amplitude threshold stress range (MPa), γ is the fatigue life constant pertaining to the detail category specified in Table 10.4 of CSA S6, m is a constant (taken as 3) established from a regression analysis of test data and N_c is calculated using Equation 2-18 (CSA S6, 2014).

$$N_c = 365 \cdot y \cdot N_d \cdot AADT_f \tag{2-18}$$

where y is the design life (typically set equal to 75 years), N_d is the number of design stress cycles experienced for each passage of the design truck as specified in Table 10.5 of CSA S6 and $AADT_f$ is the anticipated single-lane, average daily truck traffic (CSA S6, 2014).

It is important to note that Equation 2-17 is identical to Equation 2-11 proposed by Fisher et al. (1969) discussed earlier with $\Delta\sigma_r$ replaced with F_{srt} and the symbol γ used instead of M. The term F_{srt} represents the minimum stress range for an applied constant amplitude loading which will induce the growth of a fatigue crack. Theoretically, any nominal stress range less than this value will not result in the growth of a fatigue crack. CSA S6 indicates that the actual loading the bridge experiences is variable in amplitude and therefore can occasionally be twice as large in magnitude as that calculated (CSA S6, 2014). Hence, the

limiting stress range is taken as $F_{srt}/2$ as shown in Equation 2-17. The limiting constant amplitude stress ranges for the various fatigue life categories are displayed graphically in Figure 2–17.

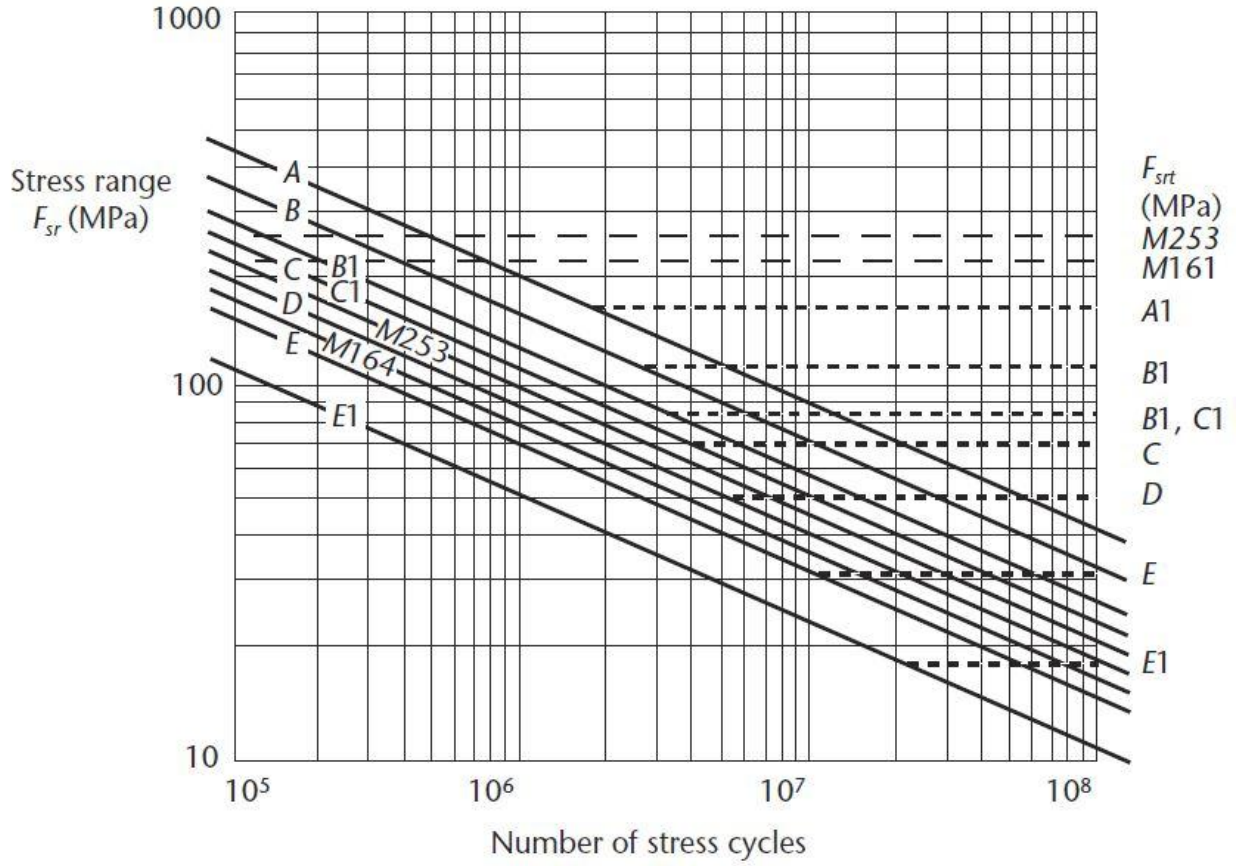

Figure 2–17: CSA S6.1 S-N curves for various fatigue detail categories (CSA S6.1, 2014)

CSA S6 permits the assignment of a particular component subjected to load-induced fatigue into one of eight predefined general categories specified in Table 10.7 (CSA S6, 2014). It is critical to mention that CSA S6 does not provide a detail category for slip-critical, through-bolt shear connections. Therefore, the only manner in which such a connection may be designed for is by treating them as welded, headed shear studs.

Furthermore, the CSA S6, Clause 10.17.2.7 requires that the fatigue stress range resistance calculated using Equation 2-17 be less than the design shear stress range (τ_{rs}) which is calculated using Equation 2-19 (CSA S6, 2014).

$$\tau_{rs} = 0.52 \cdot C_L \cdot \frac{V_{sc} \cdot Q \cdot S}{A_{sc} \cdot I_t \cdot n} \tag{2-19}$$

where V_{sc} is the design shear force along the length of the beam being considered (N), Q is the first moment of area of the transformed section at the interface between the concrete and the steel (mm^3), S is the shear stud group spacing (mm), A_{sc} is the cross-sectional area of a single shear stud (mm^2), I_t is the moment of inertia of the transformed composite section about the axis of bending (mm^4), and n is the number of shear studs in the group at the section being considered (CSA S6, 2014).

2.4 Modelling of Composite Beams

Often the use of computational models, both analytical and computer based, to augment or completely replace physical testing is an attractive solution to minimize costs and time required for data acquisition. Computational models are particularly valuable for the permutation of sensitivity analyses that would otherwise require exhaustive experimental testing. Two of the more popular forms of computational models are ones that can be expressed in discrete mathematical forms and those which employ the use of a finite element analysis (FEA) software. FEA is a numerical technique which finds approximate solutions to partial differential equations quantifying physical phenomena (Fish, 2007). Many researchers such as Kalfas et al. (1997), Kwon (2008), Bowser (2010), Chen et al. (2014), Liu et al. (2014), Porter (2016), and Pavlović & Veljković (2017) have adopted the use of FEA to simulate the response of composite structures.

Kalfas et al. (1997) proposed a finite element (FE) model created in COSMOS/M which simulated a push test experiment featuring welded, headed shear studs, connecting a steel girder to a concrete deck. Due to the symmetry of the push test experiment, only half of the push test specimen was modelled to improve computational efficiency. The shear stud connectors were approximated using beam elements due to the inherent flexibility offered by that element type. The results of the FE simulation were then compared to experimental results. Kalfas et al. (1997) reported a maximum deviation of about 14% between their simulated and experimental results.

Similarly, Liu et al. (2014) created a FE model using ABAQUS to simulate a push test experiment featuring through-bolts, connecting a steel girder to a geopolymer concrete deck. Liu et al. (2014) also took advantage of the symmetry of the experimental setup and only modelled three quarters of the push test specimens to improve computational efficiency. Unlike the beam elements used by Kalfas et al. (1997), Liu et al. (2014) used twenty node, quadratic brick elements to model the 3D through-bolt shear connectors. The adoption of this element type permitted the usage of ABAQUS's BOLT LOAD function which created a specified initial, pretension force in the through-bolt. The results of the FE simulation were then compared to experimental results to validate the FE model. Ultimately, it was found that the FE simulation results accurately predicted both the ultimate strength and the load-slip response of the

through-bolt connectors. Liu et al. (2014) were then able to perform a sensitivity analysis, assessing the influence on the overall load-slip behaviour from varying the bolt pretension, the clearance between the bolt and the deck and the strengths of the through-bolts and concrete deck.

2.5 Research Needs

The literature review presented in this Chapter provided a thorough background of the significant research that has been conducted prior to this research project, identifying discontinuities in the current knowledge which need to be addressed.

Firstly, the current CSA S6 (CSA S6, 2014) assumes that the fatigue performance of through-bolt shear connectors is identical to welded, headed shear stud connectors. It is anticipated that this assumption is overly conservative, rendering economically inefficient designs. Since the FLS typically governs the design of shear connectors over the ULS, research demonstrating the over conservatism associated with designing through-bolt shear connectors in a manner similar to welded, headed shear studs may result in a decreased number of through-bolts required and more efficient designs.

Moreover, the current design provisions for shear connectors were formulated from the regression analysis of push tests from multiple researchers with inconsistent testing procedures and failure criterion. Therefore, the understanding of the performance of through-bolt shear connectors acting in a composite beam subjected to flexure is required to validate or refute this practice.

Furthermore, little is understood about the mechanics of a through-bolt shear connector as they deform during a push test. Chen (2013) proposed an equation which predicts the ultimate capacity of through-bolt shear connectors. The work of Chen (2013) is described in detail in Chapter 5. A clearly defined formulation of the full load-slip behaviour of a through-bolt shear connector is required. The development of a theoretical derivation of a load-slip curve would reduce the requirement for performing push tests in the future.

Lastly, no research to date has implemented a successful instrumentation technique for monitoring the stresses experienced by the through-bolt shear connectors. The development and corroboration of such a technique is desired to objectively quantify the performance of the through-bolt shear connectors, revealing the true load-slip behaviour and provide indication when failure has occurred.

3 Experimental Program

This Chapter describes the complete development of the experimental component of this research project. Specimen design details, including selected material properties and dimensions are presented. Next, the fabrication of the various components of the specimens is explained along with the specimen instrumentation specifics. Finally, the specimen testing procedure, including the test frame configuration, loading conditions, and the data acquisition systems are discussed.

3.1 Specimen Description

Three specimens, named Specimen B1, B2, and B3 were fabricated for the fatigue and static structural testing. Three identical concrete deck elements, 600 mm wide, 125 mm deep and 3000 mm long were prefabricated for the experimental program along with three identical 3200 mm long, W250x49 steel girder sections made from 350W steel. As illustrated in Figure 3–1, holes for two rows of through-bolts were evenly spaced at 250 mm centre to centre along the lengths of the specimens, 102 mm apart.

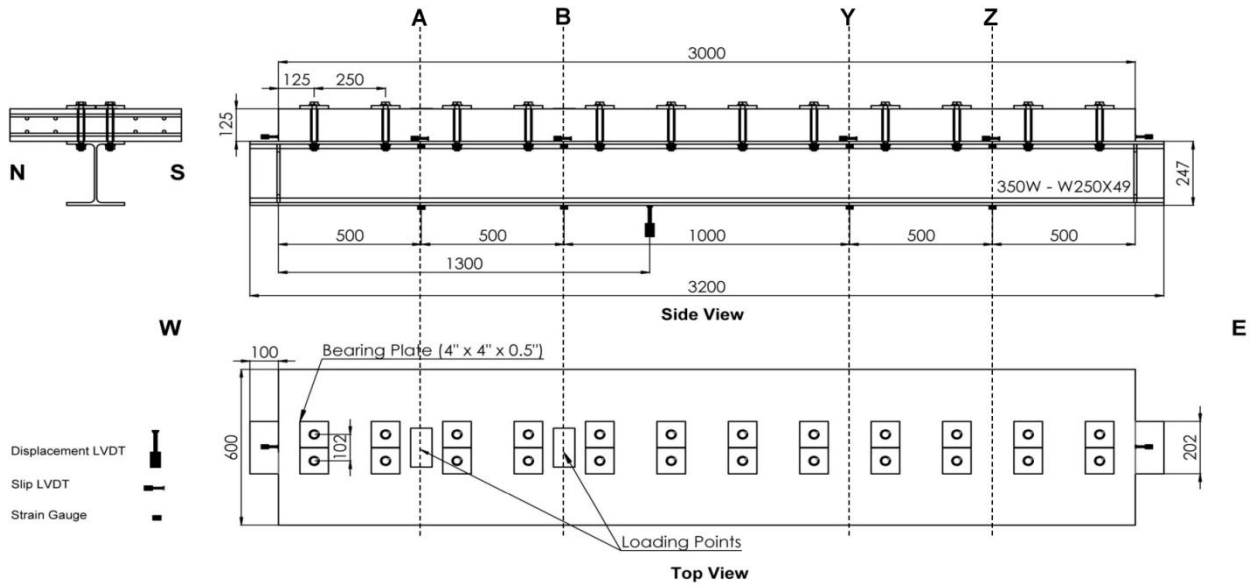

Figure 3–1: Specimen geometry (dimensions in mm)

The through-bolts chosen for this study were 5/8" (15.88 mm) diameter, ASTM A325 structural bolts. The through-bolts passed through sleeves cast into the concrete deck, formed using polyvinyl chloride (PVC) piping, with a 25 mm interior diameter and the holes drilled in the steel girders, with a diameter of 11/16" (17.46 mm). The oversized sleeve diameter was selected as a tolerance control measure, permitting some variance in the location of the holes in the concrete deck.

The adopted nomenclature used throughout this report for specifying locations along the specimens is based on the cardinal directions. Figures depicting the specimens in this report have the specimens oriented such that the West end is on the left and the East end is on the right. Therefore, the North side refers to the side face of the specimen, which protrudes into the page and consequently, the South side refers to the side face visible in the figures (unless otherwise noted).

The through-bolts are designated by their row number, beginning at Row 1 at the West end of the specimen and terminating at Row 12 at the East end of the specimen. Within each row there is a North (N) and a South (S) through-bolt. For example, through-bolts in Row 1 are referred to as N1 and S1 and therefore, through-bolts in Row 2 are referred to as N2 and S2, etc.

Lastly, the four section profiles of interest shown in Figure 3–1, named Profile A, B, Y, and Z, refer to locations 500 mm, 1000 mm, 2000 mm, and 2500 mm from the West support of the specimens.

3.2 Specimen Fabrication

This section explains in detail the procedures and methodologies used in fabricating and assembling the specimens. Information pertaining to the formwork assembly, concrete casting, steel girder preparation and bearing plate manufacture is provided, including justification for decisions where relevant.

3.2.1 Formwork Construction

The concrete specimens were cast in rectangular formwork, constructed from 19 mm formply shown in Figure 3–2, which has a moisture resistant film fused to the interior surfaces. Prior to casting, the interior surfaces of the formply were oiled to prevent the concrete from adhering to the formwork, allowing for an easier formwork removal after casting. The upper and lower reinforcement mats were then installed in the formwork using predrilled holes along the lengths of the formwork as anchor locations for the slightly oversized transverse bars.

Figure 3–2: Formwork assembly

Creating and accurately positioning the holes in the concrete decks proved to be a significant challenge. It was decided to fasten the PVC piping to the formwork at the precise, intended locations of the through-bolts prior to the casting of the concrete as opposed to drilling holes subsequent to the casting of the concrete to avoid the consequences of rework. The risk associated with casting the holes in the concrete deck was reasoned to be less than drilling holes subsequent to the curing of the concrete because drilling may cause concrete cracking and is difficult to correct if positioned improperly. Conversely, if PVC sleeves were positioned improperly (by a small amount), a file could be taken to the interior surface of the tube to remove material until the through-bolt is capable of being positioned. A rigid, plywood template, identifying the exact hole locations was created to reduce tolerance issues. This template was then used to mark the bolt hole locations in both the formply and the steel girders.

PVC piping with a 25 mm exterior diameter, was cut to the exact height of the concrete deck (125 mm) and clamped in position at the location of the holes using threaded rods. As illustrated in Figure 3–3, a fender washer and a hex nut assembly was installed at the top end of the threaded rod, which passes through the PVC sleeve and is anchored within the formply using T-nuts.

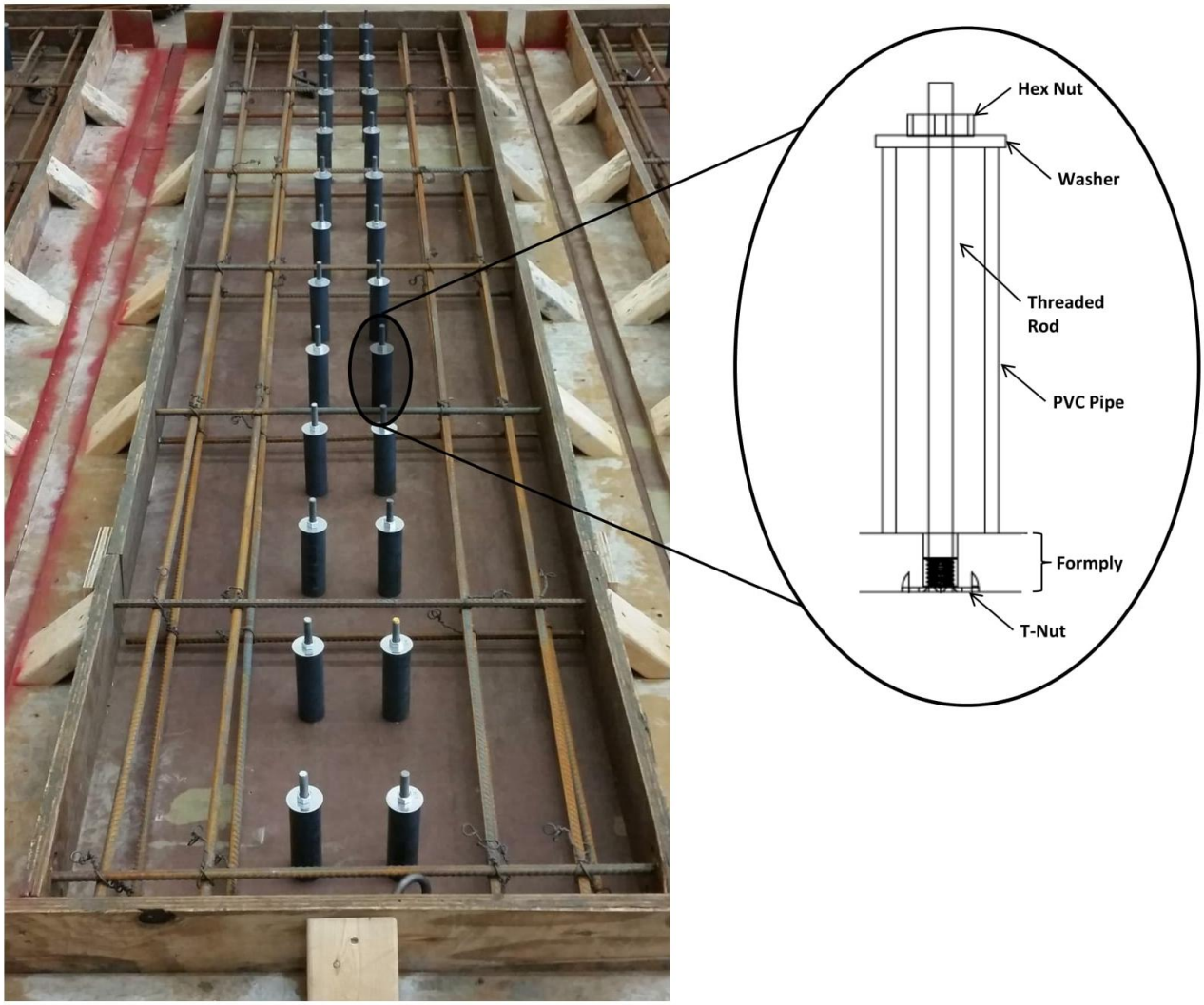

Figure 3–3: Concrete sleeve formwork

The T-nuts were installed in the formply from the bottom side at the precise location of the holes. Moreover, the T-nuts were recessed into the formply such that they were flush with the underside of the formwork to create an even, level surface for the concrete to cure.

3.2.2 Concrete Deck Fabrication

The concrete deck reinforcement was designed according to CSA S6 (CSA S6, 2014), which requires orthogonal reinforcement, providing a reinforcement ratio of at least 0.003 near the top and bottom surfaces of the concrete deck. Identical upper and lower reinforcement mats were assembled by fastening 400W weldable, low alloy 10M steel bars. As shown in Figure 3–4, the longitudinal reinforcement consisted of four 3000 mm segments and the transverse reinforcement consisted of seven 600 mm segments, with bar spacing as indicated in the figure.

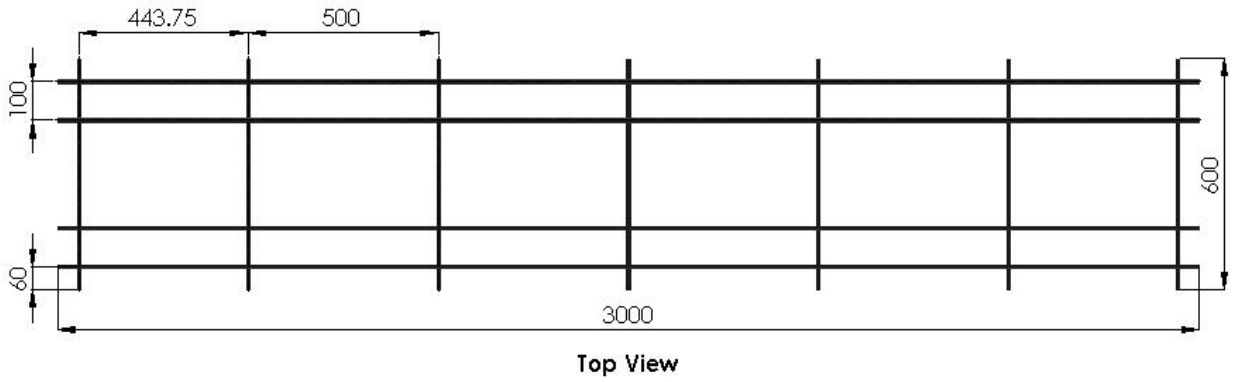

Figure 3–4: Reinforcement mat assembly (dimensions in mm)

A cover of at least 20 mm was provided for all steel reinforcement. The reinforcement spacing was selected to allow ample clearance for the through-bolts to avoid concrete cracking due to incomplete consolidation during the curing process. The reinforcement spacing was in compliance with the provisions of CSA S6, Clause 8.14.2 (CSA S6, 2014).

Calculations were performed to determine the necessity of spiral reinforcement in the concrete decks, around the holes where the pre-tensioned bolts were to be located. Equation 3-1, suggested by Stone & Breen (1984), was used to determine the cross-sectional area of spiral reinforcement (A_{SP}) in square inches required, given the intended pretension level in the through-bolts:

$$A_{SP} = \frac{f_1 - 0.6 \cdot f_{c1}^{'}}{4 \cdot f_y}(D)(s) \geq 0.05 \tag{3-1}$$

where f_y is the yield strength of the spiral reinforcement in psi, f_1 is the post-tensioning load divided by the concrete area confined by the spiral in psi, f'_{c1} is the specified compressive strength of the concrete in psi, D is the diameter of the spiral reinforcement (in) and s is the pitch of the spiral (in) (Stone & Breen, 1984). On this basis, it was determined that the minimum expected concrete strength at the time of testing would be sufficient to not require spiral reinforcement.

The concrete was poured directly into the form work using a conveyer belt, extending from the concrete truck and was provided from a ready-mix supplier, Hogg Concrete. The concrete was then vibrated to facilitate consolidation, preventing honeycombing. Moreover, embedded hoisting anchors were placed into the concrete at opposite corners immediately after pouring to assist with hoisting and repositioning the concrete decks. The concrete decks were screeded to provide a level height of 125 mm and finished using hand trowels. Finally, the concrete decks were moist cured by covering them with water-saturated

burlap blankets and high density polyethylene tarps for seven days. The burlap blankets were moistened daily during the initial seven days, after which, the formwork was stripped and the specimens were transported to long-term storage in the laboratory where they were stacked until testing.

The concrete was specified to have a 28 day compressive strength of 35 MPa and a slump of 100 mm. Sixteen concrete cylinders were cast to assess the concrete compressive strength after seven days, when the specimens were to be transported into long-term storage, after twenty eight days to assess to 28-day concrete compressive strength, and at the actual times the tests were to be performed. The average concrete compressive strength was determined to be 40.1 MPa at the time of testing.

3.2.3 Steel Girder Preparation

The oversized through-bolt hole diameter in the steel girders was specified to be 11/16" (17.46 mm) as per the provisions of CSA S16-09, Clause 22.3.5.1, which limits the nominal hole diameter to be no larger than 2 mm than the nominal bolt diameter (CSA S16-09, 2012). Furthermore, an 11/16" diameter hole allowed for some tolerance when assembling the specimens while minimizing the span that the bolt head has to bridge.

Bearing stiffeners were welded on both sides of the flanges, 100 mm from each end of the steel girders where the concrete deck ends and where the underlying supports would be centred. The bearing stiffeners were 10 mm thick and designed according to CSA S16-09, Clause 14.4 to prevent web yielding and web buckling (CSA S16-09, 2012) at the support locations. The completed specimen components are shown in Figure 3–5.

Figure 3–5: Concrete decks and steel girders

As shown in Figure 3–5, there were 24 holes in each concrete deck, which must align with the 24 holes in each steel girder to within sufficient tolerable limits such that the through-bolts may successfully pass through the holes in both the concrete decks and the steel girders.

3.2.4 Bearing Plate Fabrication

Simple bearing stress calculations revealed that the surface area provided by the structural washers was insufficient to prevent crushing of the concrete deck due to the intended pretension force in the through-bolts. Therefore, the use of bearing plates under the washers was deemed necessary.

The bearing plates were fabricated from structural steel by the research team. The dimensions of the surface of the bearing plate in contact with the concrete deck were calculated by first assuming a square layout, then dividing the total pretension force in the though-bolts by the compressive strength of the concrete. This insured that the bearing plates were sufficiently large enough to disperse the compressive bearing force throughout the concrete surface. The thickness calculation of the bearing plates proved to be a challenge as no standard provisions are readily available for a loaded bearing plate, bridging over an

oversized hole in concrete. An FE model was prepared to model the behaviour of the bearing plates acting in this manner. The thickness of the bearing plates was varied incrementally until two design criteria were met. Firstly, the maximum stresses observed in the bearing plates was to be less than the yield stress of the steel. Also, the local deformation of the bearing plates within the circumference of the oversized hole, was to be kept at a minimum such that the bearing plates did not induce normal stresses on the interior surfaces of the concrete holes. This was important to insure that the bearing plates did not exhibit significant dishing, which may have caused premature damage to the concrete deck prior to testing. The final dimensions adopted for the bearing plates were 4" x 4" x 0.5".

The bearing plates were cut from a 4" x 10' x 0.5" steel plate beam using a band saw. The centres of the bearing plates were precisely determined using an edge finder and an electronic position indicator. 11/16" diameter holes were then drilled at the centres of the bearing plates. This hole diameter leaves approximately 1.6 mm of clearance for the through-bolts to pass through. It is important to minimize the distance the head of the through-bolt must bridge to prevent a pull-out of the through-bolt. Further modifications discussed in Section 3.3 were made to the bearing plates after they were fabricated to facilitate the instrumentation of the through-bolts with strain gauges.

3.3 Instrumentation of Specimens

One of the primary objectives of this research project was to accurately determine the progression of through-bolt failure and the number of cycles resulting in failure so that a stress versus life (S-N) curve may be plotted. Moreover, capturing the global behavioural changes of the composite beam throughout the fatigue test is desirable as it offers valuable information necessary for comparison of the performance of the through-bolt shear connectors at the beginning and end of their fatigue life. Finally, the behaviour of the through-bolts and the overall behaviour of the specimens as they were loaded to their ultimate capacity was necessary for the development of load-slip curves for the through-bolt shear connectors.

A combination of strain gauges, displacement transducers (LVDTs) and string pot displacement transducers were used to quantitatively and qualitatively capture the performance and behaviour of the through-bolt shear connectors throughout the experimental testing. The instrumentation layout for the static and fatigue testing is illustrated in Figure 3–1.

Global behavioural changes of the specimens were assessed by monitoring the progression of the strain profiles in the steel girder and the interfacial slip between the concrete deck and the steel girder throughout the duration of each test. The strain profiles in the steel girders were determined using CEA-06-125UN-120, three wire, temperature compensated strain gauges, procured from Micro-Measurements, placed on the underside of the upper and lower flanges of the steel girders at Profiles A, B, Y, and Z.

Strain gauges on the underside of the upper and lower flanges of the steel girders at the midspan were added for Specimen B2 and B3. The surfaces of the flanges at the strain gauge locations were prepared prior to the installation of the strain gauges using a pneumatic belt sander for the initial polishing. The gauge locations were then wet sanded using increasingly fine grits of sand paper in an acidic solution. The strain gauges used in this research project were connected to three wires, which enabled automatic correction for fluctuations in atmospheric temperature throughout the duration of the testing. Using the strain values in the flanges of the steel girders, the strain profiles for the girders can be determined and the strain profiles in the concrete decks can be calculated implicitly. This is discussed in more detail in Section 4.1.3. Interfacial slip was monitored using five model 0241 DC LVDTs, with a displacement stroke of ±2.54 mm. The LVDTs were placed at the West and East ends of the specimens and at Profiles A, B, and Y.

The instrumentation layout for ultimate static strength testing was identical except only four LVDTs were installed at the West and East ends of the specimens and at Profiles A and Z. Also, for the ultimate static strength testing, model 0244 DC LVDTs with relatively larger strokes (±25.4 mm) were used as larger interfacial slips were anticipated. Lastly, using a transformed section deflection analysis, it was determined that the point of maximum vertical displacement of the specimens was located at 1300 mm from the West support for the offset loading arrangement used in the fatigue tests. A model 0244 DC LVDT, with a displacement stroke of ±25.4 mm was placed at this location to assess the deflection of the specimens throughout the experimentation. Conversely, for the ultimate strength testing, the specimens were loaded at the midspan. Therefore, the maximum deflection was expected to occur at the midspan of the specimen for this testing arrangement. In order to measure vertical deflections for these tests, SP2-12 string pot displacement transducers, with a stroke of 317 mm, were positioned beneath the specimens at the midspan. All of the DC LVTDs and string pot displacement transducers were procured from Micro-Measurements.

Accurately determining the progression of through-bolt failure and the number of cycles resulting in failure required continual observation of the forces in the through-bolts. This was rendered possible through the use of a novel through-bolt instrumentation technique developed by the research team, whereby strain gauges were applied to the shank of the through-bolts. The strain gauges used to instrument the through-bolts were the same as the ones used for the steel girder flanges. Application of the strain gauges required extensive sanding and polishing of the through-bolts such that the strain gauges could be placed on a smooth, clean surface, free of any imperfections. Modifications to the bearing plates were required before the through-bolts could be instrumented. Grooves were machined into the underside of the bearing plates to allow for the strain gauge wires to pass through from inside the PVC sleeve where

they attach to the strain gauges, to the exterior where they would be connected to the data acquisition system. Finally, two threaded holes were machined into the bearing plates on either side of the through-bolt hole to allow for a temporary brace to be installed. The intention of the brace is to secure the through-bolts to the bearing plates during the instrumentation process, preventing the bearing plates from sliding down the shank of the through-bolts and shearing off the strain gauges. The braces remained fastened to the bearing plates until the through-bolts were ready to be installed and pretensioned.

Figure 3–6 shows the progression of the preparation of the through-bolts beginning with the original through-bolt (Left) to the polished and cleaned through-bolt (Centre) to the fully assembled construction, including the temporary brace, with the strain gauge adhered to the shaft of the through-bolt (Right). Not shown in Figure 3–6 (Right) is the metallic receptor pad glued to the top of the bearing plate, intended to accept the copper wires from the strain gauges and connect them electrically to the insulated wires from the data acquisition (DAQ) unit.

Figure 3–6: Through-bolt strain gauge preparation

After the strain gauges were fastened to the through-bolts, solder was applied to the metallic tabs on the strain gauges and the metallic receptors. Copper wires of identical length were cut to connect the strain gauges to the metallic receptors. The enamel at the ends of the wires were removed, the ends were "tinned" and then the ends of the copper wires were soldered to the strain gauges and the metallic receptors. The copper wires were sized to be a little longer than necessary to allow for some movement and elongation of the through-bolts during the application of the pretension in the through-bolts and to accommodate possible movement during the testing. This excess length was folded neatly and tucked

inside the groove in the bearing plates. Tape was applied over the wires as an additional measure to prevent them from migrating during testing. This is shown in Figure 3–7.

Figure 3–7: Strain gauge wiring

Four views showing all sides of the fully instrumented through-bolts are presented in Figure 3–8.

Figure 3–8: Fully instrumented through-bolts

The first four rows and the last two rows of through-bolts were instrumented for Specimen B1, resulting in a total of twelve through-bolts instrumented. The decision as to which through-bolts to instrument for Specimen B1 was made based on the expected load levels each row would be subjected to and was intended to reduce the total number of through-bolts to be instrumented. The loading configuration and the consequent shear force profile are discussed in Section 3.5. Through-bolts Rows 1 and 2 were subjected to the highest shear force and were therefore of particular interest. The through-bolts in Rows 3 and 4 were instrumented to observe the through-bolt behaviour directly beneath the location of loading. Finally, the through-bolts in Rows 11 and 12 were instrumented as the slip level at the East end of the specimens was expected to be relatively high in comparison to the West end due to the greater flexural length on this end. Specimen B2 featured half the number of through-bolts installed as Specimen B1, with the through-bolts staggered along the longitudinal length. It was expected that more failures would occur with Specimen B2 than with Specimen B1 since there were fewer through-bolts used, resulting in fewer alternative load paths for force redistribution with successive through-bolt failures. Therefore, all twelve through-bolts installed in Specimen B2 were instrumented. Finally, Specimen B3 featured two rows of through-bolts at each of the specimen's ends (Rows 1 & 2 and 11 & 12), all of which were instrumented for the same reasons described for Specimen B2.

3.4 Assembly of Specimens

Subsequent to the completion of the fabrication and instrumentation of the specimen components, the specimens were assembled. The concrete decks were hoisted on top of the steel girders and the through-bolts were inserted into their respective holes. The specimens were then positioned within the testing frame and the instrumentation was connected to the DAQ. Once the instrumentation was connected and tested, the through-bolts were tightened as per CSA S6 Clause 10.24.6.3, which specifies that pretension load level in the through-bolts shall be tightened to at least 70% of their minimum tensile strength, which is calculated using Equation 2-10 (CSA S6, 2014). Therefore, the ASTM A325 through-bolts were tightened to a pretension of 85 kN. The through-bolts were tightened row-by-row, beginning at the midspan of the specimens, proceeding towards the West and East ends. This was done to force the potentially different contour profiles of the concrete decks and steel girders to match one another without creating any artificial kinks. The desired pretension load level of 85 kN was achieved using tension indicating washers, which were installed between the heads of the through-bolts and the bearing plates. The through-bolts that were instrumented with strain gauges were also monitored to confirm that the appropriate pretension magnitude was achieved.

A summary of the material and geometric properties of the completed specimens is provided in Table 3–1.

Table 3–1: Specimen Design Summary

Property	Component			
	Steel Girder W250x49	Concrete Deck	Concrete Reinforcement 10M	Through-Bolts ASTM A325
Strength (MPa)	350	40.1	400	635
Elastic Modulus (MPa)	200,000	30,857	200,000	200,000
Length (mm)	3,200	3,000	-	-
Depth (mm)	247	125	-	177.8
Width (mm)	202	600	11.3	15.88
Cross-Sectional Area (mm^2)	6,250	75,000	100	198

The transformed section properties of the assembled specimens, provided in Table 3–2, were calculated based on the geometric cross-section of the fully assembled specimens, assuming full shear connection by adopting a linear stress distribution over the depth of the section. The transformed section properties were taken at the concrete deck and steel girder interface. The composite cross-sections were transformed by converting the width of the concrete decks to an equivalent width of steel using the modular ratio (n) of the moduli of elasticity of the steel and concrete. Moreover, the transformed section moment of inertia was calculated including the longitudinal concrete reinforcement.

Table 3–2: Transformed cross-section properties

Property	Symbol	Value
Modular Ratio	n	7.03
Centroid of Transformed Section (From Top)	$\bar{y}$	128.1 mm
Transformed Section First Moment of Area	Q_{tr}	7.00×10^5 mm^3
Transformed Section Moment of Inertia	I_{tr}	2.24×10^8 mm^4
Effective Transformed Section Moment of Inertia (24 Bolts)	I_e	1.74×10^8 mm^4
Effective Transformed Section Moment of Inertia (12 Bolts)	I_e	1.57×10^8 mm^4
Effective Transformed Section Moment of Inertia (4 Bolts)	I_e	1.57×10^8 mm^4

As discussed in Section 2.1.2, a composite beam will behave fully compositely when the force resultant in the concrete deck is equal in magnitude to the force resultant in the steel girder at the ultimate limit state. When this condition holds true, the composite section is said to have a full shear connection or a degree of shear connection, calculated by Equation 2-1, equal to one ($\eta = 1$). A total of 44 through-bolt shear connectors would be required for the development of a fully composite section, assuming a point load applied at the midspan. The actual degree of shear connection provided for all the experiments conducted in this study was less than one (100%) and are summarized in Table 3–3.

Table 3–3: Composite beam specimens degree of shear connection

Specimen	Number of Bolts	Degree of Shear Connection (η)
B1	24	38.64%
B2	12	19.32%*
B2	12	28.98%**
B3	8	19.32%*

*Note: The degree of shear connection for Specimen B2 and B3 are identical when loaded with two point loads as they each featured the same number of through-bolts between the locations of zero and maximum bending moments.
**Note: Specimen B2 has a degree of shear connection of 28.98% when loaded with a single point load at the midspan, which is the same configuration as the one used for Specimen B3.

Since all shear connectors are flexible, the actual beam deflection was expected to be greater than predicted with an assumption of a perfectly rigid shear connection. As an approximation, the deflection for a beam with partial shear connection can be calculated considering the partial shear connectivity by reducing the transformed section moment of inertia to account for the increased flexibility as a result of the partial shear connection. CSA S16-09 Clause 17.3.1 permits the use of Equation 3-2 to calculate the effective moment of inertia, I_e, by correcting the transformed section moment of inertia, I_{tr}, and the moment of inertia of the steel section alone, I_s, to account for a partial shear connection, η (CSA S16-09, 2012). In the next chapters, deflection predictions made using this equation are compared to measured deflections at different stages of the fatigue and static strength tests. Equation 3-2 was used to compute the effective transformed section moments of inertia provided in Table 3–2.

$$I_e = I_s + 0.85 \cdot \eta^{0.25} \cdot (I_t - I_s) \tag{3-2}$$

3.5 Fatigue Testing Loading Procedure

The fatigue testing configuration consisted of the specimens supported at each end on pin-rollers and subjected to two point loads offset from the midspan. The loading configuration and the resulting shear force and bending moment profiles are illustrated in Figure 3–9. The loading offset was intended to create a varying shear profile along the length of the specimens, inducing a relatively early failure in the more heavily loaded shear connectors towards the West end of the specimens. This experimental design was intended to study the impact that a failed through-bolt shear connector had on the neighbouring through-bolts in terms of how the longitudinal shear redistributed and consequently how the overall composite behaviour was affected. Moreover, as shown in Figure 3–9, the loading offset induces approximately three times the shear force in through-bolt Rows 1 and 2 compared to through-bolt Rows 3 - 12, meaning that failure of these through-bolts was expected to occur first. This simplified the instrumentation and monitoring process as it was therefore not necessary to monitor and instrument all twelve through-bolt rows. The loading was applied to the specimens through two pin supports attached to a spreader beam.

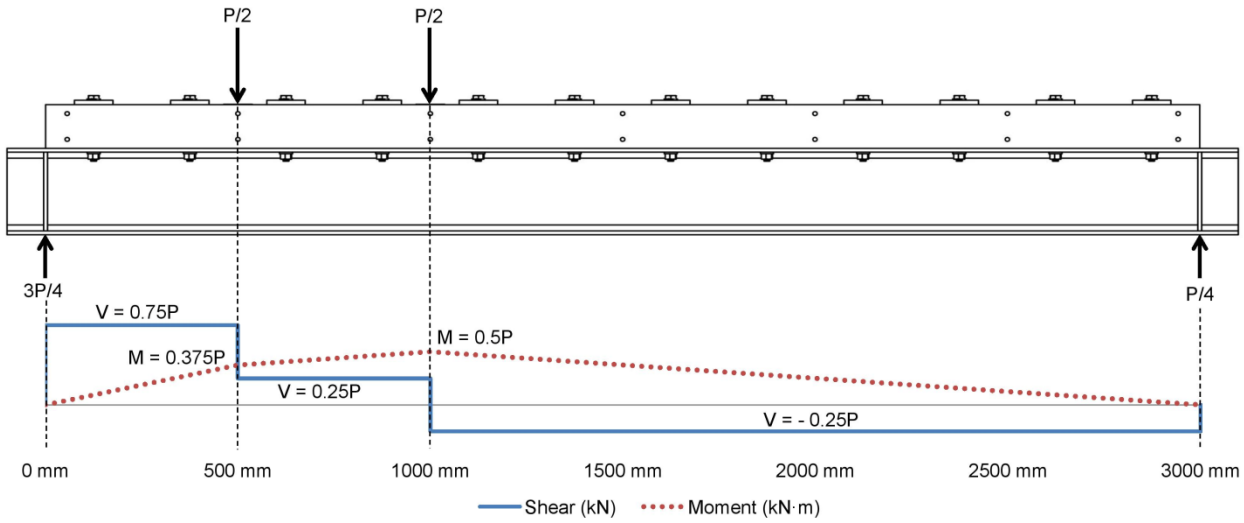

Figure 3–9: Static and fatigue testing configuration

3.5.1 Stiffness Testing

The specimen stiffness was evaluated by testing prior to any fatigue testing and at various stages throughout the experimentation. Initial stiffness tests were performed to confirm the load level at which the onset of slip between the concrete deck and the steel girder is apparent as well as to collect data on the behaviour of the specimen before any fatigue damage occurred. The load level for stiffness testing was then adopted as the minimum trial peak load used in the fatigue testing. Subsequent stiffness tests were performed to discover if any global behavioural changes in the specimens or local behavioural changes in the through-bolts had arisen due to the accumulation of fatigue damage.

The stiffness tests were performed in displacement control at a rate of 0.05 mm/s. Displacement control is typically preferable for capturing small variations in the load resisted by the specimens since the actuator continually imposes displacement at a constant rate regardless of the behaviour of the specimen. Conversely, if a crack were to form or if there was a sudden slip and the specimens were loaded in load control, the load cell on the actuator would provide an electronic load feedback to the controller indicating that the required loading increment has not yet been achieved and the controller would respond with instructions to rapidly increase the load until the required loading increment is reached. This may consequent in discrete variations being missed.

Two cycles were performed for each stiffness test so that the results of each cycle could be averaged. Furthermore, at the peak of each stiffness test, the actuator was paused for roughly ten seconds to allow for instrumentation stabilization. The resulting loading-unloading history can be seen in Figure 3–10.

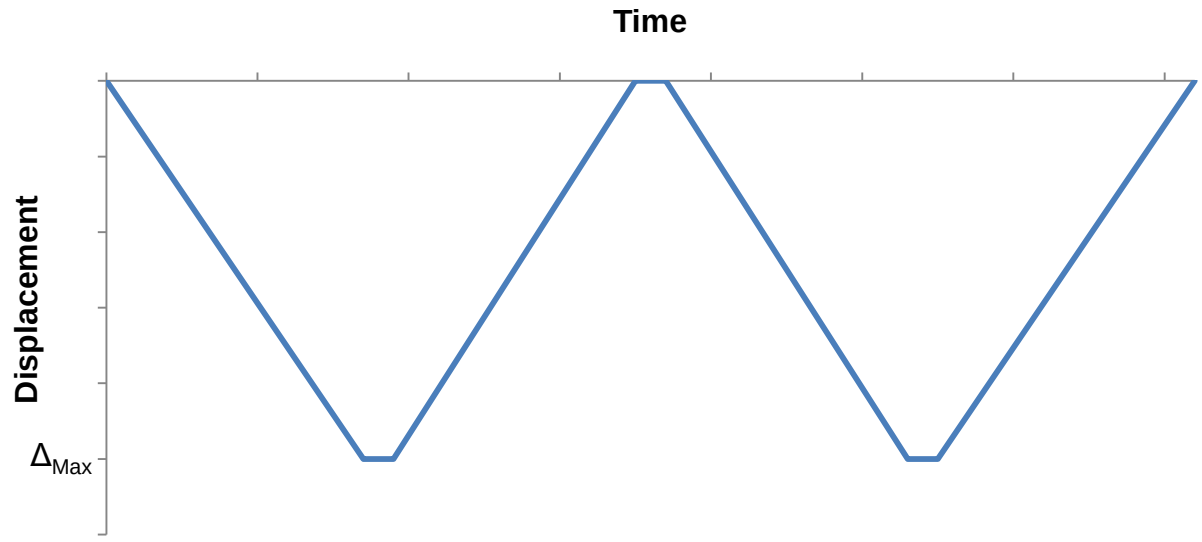

Figure 3–10: Loading-unloading history for stiffness test

The stiffness tests performed subsequent to the cyclic loading stages were performed until the displacement of the composite beam corresponding with the maximum load level in the previous cyclic testing was reached. This displacement is indicated in Figure 3–10 as Δ_{Max}.

The data collected during the stiffness tests included the interfacial slip between the concrete deck and the steel girder, the maximum vertical deflection of the specimen, and the strains in the steel girder flanges and the instrumented through-bolts.

3.5.2 Cyclic Loading

One of the primary focuses of this investigation was to assess the fatigue performance of the through-bolt shear connectors. This required subjecting the through-bolts to cyclic stresses by loading and unloading the specimen repeatedly. As the specimens were loaded, the through-bolts transferred the longitudinal shear forces between the concrete decks and steel girders, increasing the force carried by the through-bolts. When the specimens were subsequently unloaded, the strains in the through-bolts decreased. This oscillation of strains (and corresponding stresses) within the through-bolts was expected to initiate and propagate cracks within the through-bolts until the cracks reached a critical length and the remaining cross-sectional area was less than sufficiently required to resist the forces induced in the through-bolts. At this instance, fatigue failure of the through-bolts was expected to occur and was expected to be brittle.

The specimens were loaded cyclically in load control, using a sinusoidal function. The applied load range was varied from test to test. However, a 10 kN minimum loading was maintained on each specimen to

prevent impact loading caused by the load apparatus lifting off of the specimen. This is shown as the upper dashed red line in Figure 3–11.

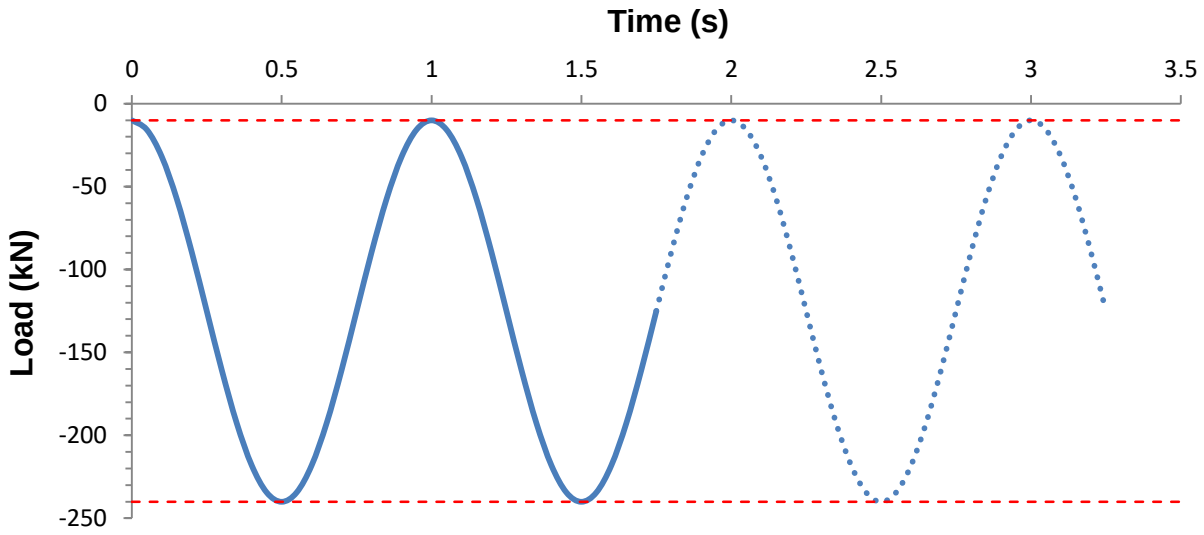

Figure 3–11: Cyclic loading history

The frequency at which the cyclic testing was performed ranged between 0.5 Hz and 2 Hz depending on the desired loading level. Higher load levels generally result in shorter tests since fatigue failure is expected to occur sooner. However, lower frequencies were used at the higher load levels to prevent damage to the actuator and the specimens.

3.6 Ultimate Static Strength Testing Loading Procedure

Another primary objective of this research project was to determine the load-slip curve for a through-bolt shear connector using a large-scale beam test, thus confirming the appropriateness of using a push test to establish load-slip behaviour. Therefore, two large-scale beam static tests were performed. The first using Specimen B2, which was essentially undamaged after the end of its fatigue test, and the remaining, using Specimen B3, which was not subjected to prior fatigue loading. Both specimens were loaded as shown in Figure 3–12 using a single line load at the midspan of the specimen to maximize the longitudinal relative slip expected between the concrete deck and steel beam. As before, both ends of the beams were supported by pin-rollers to minimize horizontal loading of the actuator during the test. The load was applied to the specimen through a solid 4" x 4" spreader beam that extended the width of the concrete deck.

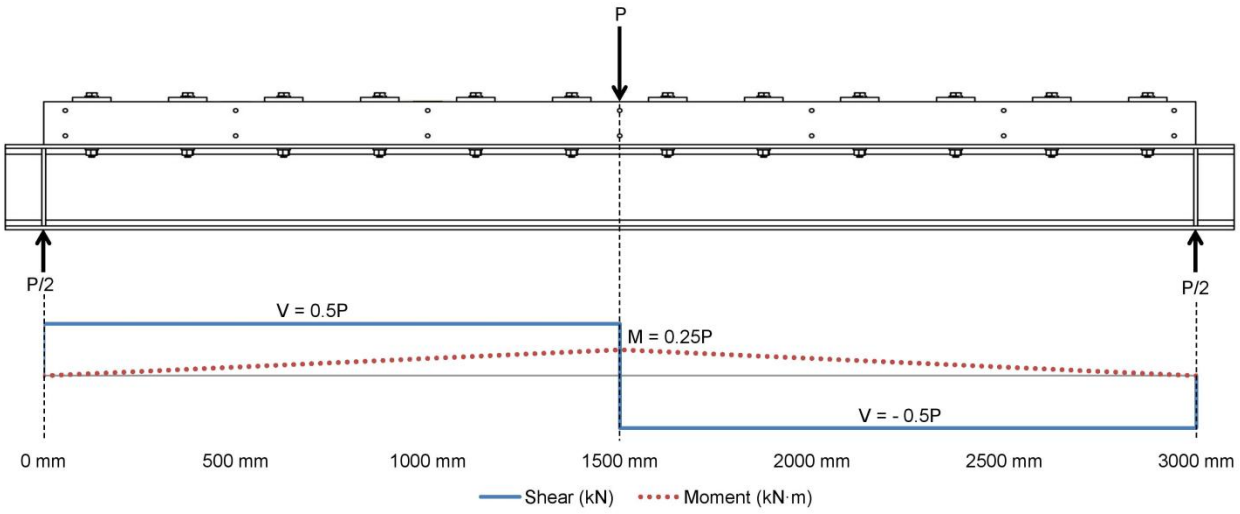

Figure 3–12: Ultimate static strength testing configuration

Specimen B2 featured twelve staggered through-bolts spaced uniformly along the length of the beam. The through-bolts were not altered in any way following the fatigue testing of this specimen. Specimen B3 featured four through-bolt shear connectors at either end of the specimen. This arrangement was chosen in an attempt to mimic the push tests conducted on through-bolt shear connectors performed by Chen (2013), which also had four shear connectors per side on each specimen. Additionally, the friction between the concrete deck and steel girder interface was reduced between the groupings of through-bolts at the ends of Specimen B3 by first polishing the steel girder and then using a high pressure, lithium based grease containing molybdenum disulfide, liberally placed between two 0.15 mm thick polyethylene sheets. This is illustrated in Figure 3–13. Therefore, Specimen B3 can be idealized as two push tests (one on either end) enabling a direct comparison between the results obtained from this test and the experimental findings of Chen (2013).

Figure 3–13: High pressure grease placed between polyethylene sheets

Figure 3–13 illustrates the application of the friction-reducing membrane, placed between the polyethylene sheets on the steel girder of Specimen B3. The thickness of the friction-reducing membrane did not create a significant gap between the steel girder and the concrete deck was placed directly on top of the assembly shown in Figure 3–13. Note that the friction between the concrete deck and steel girder 500 mm from either end where the four through-bolts was not reduced to ensure that the effects that friction plays on the overall shear resistance of the bolt group was captured.

3.6.1 Ultimate Static Strength Loading

Ultimate static strength tests were performed on Specimens B2 and B3 to determine the total ultimate static capacity of the composite beams with varying degrees of composite interaction.

The ultimate strength tests were conducted in displacement control at a rate of 0.01 mm/s. Similar to the stiffness tests described in Section 3.5.1, displacement control was selected for the ultimate strength tests to prevent sudden failure of the specimens at the instance when the peak load is reached (e.g. due to a through-bolt failure).

The specimens were loaded until the overall load slip curve began decreasing after the maximum observed loading was achieved. Because the specimens were loaded to failure, non-recoverable plastic damage was experienced by the specimens and therefore only one cycle was performed.

3.7 Laboratory Testing Frame and Data Acquisition

Structural steel testing frames, each equipped with a unidirectional hydraulic actuator, were used to load the specimens for each test type. Attached to the actuators were load cells and LVDTs, which measured the load applied to the specimens and the displacement of the actuators respectively.

The testing configuration for the stiffness and fatigue testing consisted of the specimen being placed in the centre of the testing frame, offset longitudinally such that the actuator was positioned above the West end of the specimen. The composite beams were supported at each end on rollers and subjected to two equal point loads, which were applied to the beam through two pin supports attached to a spreader beam. The loading pin supports were placed on top of 2 mm thick neoprene pads, which were intended to help distribute the load over the possibly uneven concrete surface. Pedestals at either end of the specimens transferred the load from the pin-roller supports to the concrete foundation of the laboratory (strong floor). Vertical threaded rods were bolted into the pedestals on either side of the roller supports to prevent transverse migration (drift) of the specimens during the fatigue testing. The complete testing configuration for the stiffness and fatigue testing is shown in Figure 3–14.

Figure 3–14: Laboratory testing frame and setup for stiffness and fatigue tests

The testing configuration for the ultimate strength testing consisted of the specimens placed in the centre of the testing frame such that the actuator was positioned directly above the midspan of the specimen. The specimens were subject to one line load, applied to the specimen at the midspan. The specimens were supported at each end on pin-rollers. Pedestals at either end of the specimen transfer the load from the pin-roller supports to the laboratory's structural strong floor. The complete testing configuration for the ultimate strength testing is shown in Figure 3–15.

Figure 3–15: Ultimate strength testing frame and setup

An MTS 407 control system provided the electronic instructions, powering the actuator for each test type. The control system received continual electronic feedback from the load cell and LVDT attached to the actuator and provided the appropriate instructions in response depending on whether an increase or decrease in the measured displacement and or force was required. The control system was equipped with built in interlocks, which terminate all actuator activities in the event that a predefined maximum displacement or loading was achieved. This was done to prevent unexpected damage to the actuator or specimen from occurring during the test. The system design software LabView provided instructions to the data acquisition (DAQ) unit for all structural testing performed in this project.

4 Experimental Results

The following chapter presents the findings and results of the experimental testing described in Chapter 3. Section 4.1 and Section 4.2 present the results of the stiffness and fatigue testing respectively. The results of the stiffness tests with through-bolts removed are presented in Section 4.3. Finally, the results of the ultimate static strength testing are presented in Section 4.4.

Each of the three specimens described in Chapter 3 were subjected to a different testing program to maximize the utility of the constructed specimens. When possible, some specimens were used in multiple tests. Table 4–1 summarizes the test matrix of the experimental program.

Table 4–1: Test matrix of the experimental program

Specimen	B1	B2	B3
Number of Through-Bolts	24	12	8
Experimental Testing	Stiffness and Fatigue (2,007,766 Cycles) ↓ Stiffness with Through-Bolt Removals	Stiffness and Fatigue (762,241 Cycles) ↓ Ultimate Strength	Ultimate Strength

The through-bolt instrumentation method described in Section 3.3 was validated and confirmed to be effective through the comparison with the tension indicating washers. At the completion of tightening as indicated by the tension indicating washers, the strain values within the through-bolts for all three specimens were on average 6.2% different from 2100 microstrain with one through-bolt as much as 17.8% different. A strain of 2100 microstrain is consistent with the predicted theoretical value that would be anticipated with 5/8" diameter through-bolts, subjected to a pretension level of 85 kN.

4.1 Stiffness Testing Results

The stiffness tests described in Section 3.5.1 were performed on Specimens B1 and B2 prior to fatigue testing and at various stages throughout the fatigue tests. The first stiffness test was performed to confirm the load level at which the onset of slip between the concrete deck and the steel girder became apparent and to collect data on the behaviour of the specimens before any fatigue damage was incurred. The first time Specimen B1 was loaded, the onset of slip was observed at 225 kN. Specimen B1 was further loaded until 240 kN to ensure that no further changes occurred. Therefore, 240 kN was adopted as the datum load level for comparison purposes between all stiffness tests discussed in this section.

The frequency at which the specimens were stiffness tested was relatively high near the beginning of the fatigue testing in comparison to the later portion of the fatigue testing program. This was done because the behaviour of the specimens was unknown prior to commencement of fatigue loading. Therefore, multiple stiffness tests were performed at the early stages of the specimens fatigue life to ensure that all behavioural changes were captured. Table 4–2 summarizes the stiffness tests performed on Specimen B1 and Specimen B2, indicating the number of cycles after which a stiffness test was performed and the calculated longitudinal shear stress level acting on the through-bolts resulting from the total load applied as shown in Figure 3–9.

Table 4–2: Summary of completed stiffness tests for Specimen B1 and Specimen B2

Number of Cycles Prior to Stiffness Testing	B1			B2		
	Applied Load (kN)	Shear Stress Level (MPa)		Applied Load (kN)	Shear Stress Level (MPa)	
		Bolt Rows 1-2	Bolt Rows 3-12		Bolt Rows 1-2	Bolt Rows 3-12
0	240	354.27	118.09	355	1048.05	349.35
10,000	240	354.27	118.09	355	1048.05	349.35
25,000	240	354.27	118.09	355	1048.05	349.35
100,000	240	354.27	118.09	355	1048.05	349.35
500,000	240	354.27	118.09	355	1048.05	349.35
1,000,000	240	354.27	118.09			
1,200,000	240	354.27	118.09			
1,200,000	355	524.02	174.67			
2,000,000	355	524.02	174.67			
2,007,766	500	738.06	246.02			

As shown in Table 4–2, Specimen B1 was stiffness tested at the end of its fatigue life at 2,007,766 cycles. Unfortunately, a failure of the actuator crippled the testing frame during the fatigue testing of Specimen B2. This prevented a final stiffness test of Specimen B2 at 762,241 cycles.

The applied load that the specimens were subjected to during the stiffness testing was equal to the peak load they experienced during the fatigue testing. It is important to note that the fatigue load level was increased for Specimen B1 after 1,000,000 cycles and again after 2,000,000 cycles. The longitudinal shear stress (τ) values reported in Table 4–2 were calculated using the common shear flow equation, Equation 4-1, which is identical to Equation 2-19, neglecting the calibration coefficient of 0.52 and the modification factor, C_L, which account for differences between the design truck used in the CSA S6 and the actual trucks, which are anticipated to cross the bridge structure (CSA S6, 2014). Neglecting these terms for the purpose of this research project is appropriate since the applied loads are precisely known and were not caused by a moving vehicle.

$$\tau_b = \frac{V_{sc} \cdot Q \cdot S}{A_{sc} \cdot I_t \cdot n} \tag{4-1}$$

Recall that V_{sc} is the design shear force along the length of the beam being considered, Q is the first moment of area of the transformed section at the interface between the concrete and the steel, S is the shear stud group spacing, A_{sc} is the cross-sectional area of a single shear stud, I_t is the moment of inertia of the transformed composite section about the axis of bending and n is the number of shear studs in the group at the section being considered (CSA S6, 2014).

Prior to the tightening of the through-bolts to the appropriate pretension load level, the contour profiles of the concrete decks and steel girders did not match along the entire span of the specimens. Differences in the original curvatures of the concrete decks and steel girders created small gaps at the steel-concrete interface such as the one shown in Figure 4–1.

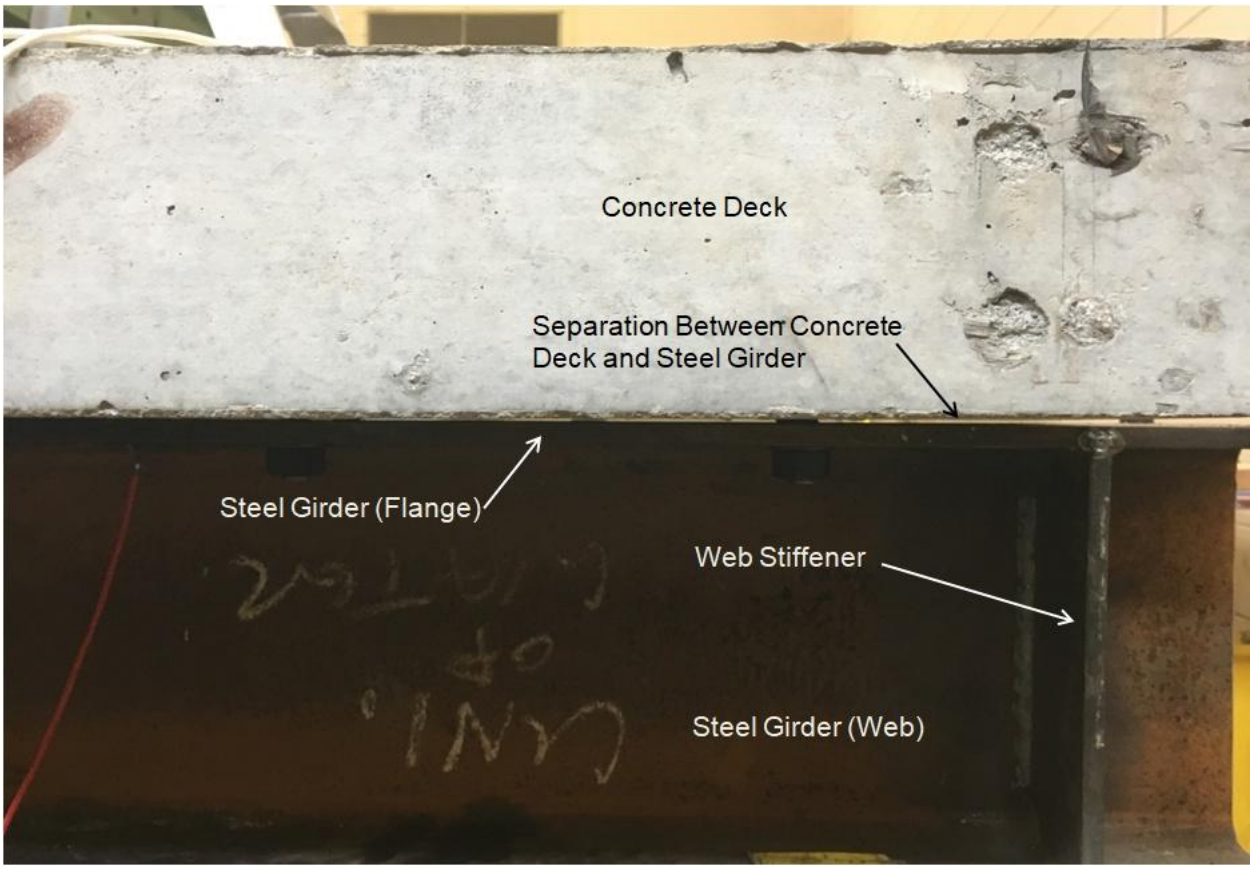

Figure 4–1: Differences in curvature between the concrete deck and steel girder resulting in a gap between the steel-concrete interface on the East end of Specimen B1

Differences in curvature between the concrete decks and steel girders, such as the one causing the gap shown in Figure 4–1, are a result of the combination of initial imperfections in the steel girders from the manufacturer and undulations in the floor, on which the concrete decks were cast. Once the pretension force was applied to the through-bolts, any separation between the concrete decks and steel girders were largely eliminated by forcing the concrete decks to contour the profiles of the steel girders. The stiffness of the concrete decks were considerably less than the stiffness of the steel girders and therefore, it was expected that the gap closure would largely be achieved by deformation of the concrete decks. Forcing the concrete decks to conform to the contours of the steel girders created cracks on the top surfaces of the concrete decks in regions where the concrete decks were cast with a positive curvature or the steel girders had a negative curvature. Examples of this are shown in Figure 4–2. Henceforth, these cracks are referred to as installation cracks to differentiate them from cracks formed during the loading of the specimens. Installation cracks also formed on the underside of the concrete decks where negative curvature of the concrete decks were present prior to the tightening of the through-bolts. However, this was not observed as frequently. The installation cracks in Figure 4–2 have been highlighted with black lines for clarity.

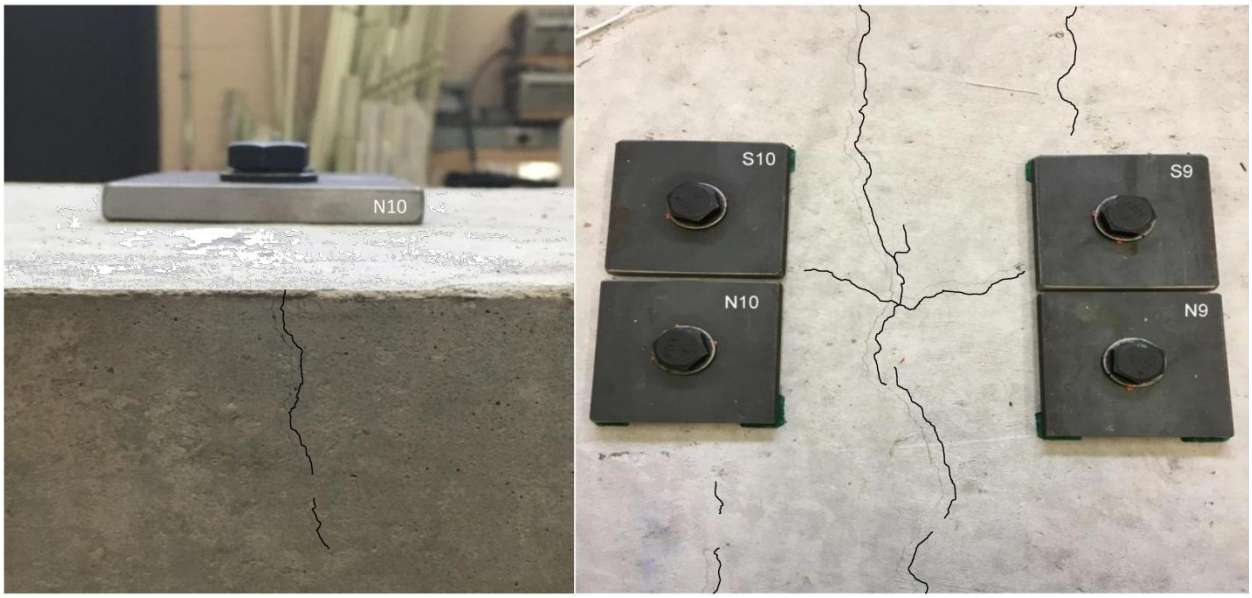

Figure 4–2: Installation cracks in concrete deck due to tightening of through-bolts

Installation cracks typically occurred on the top surface, extending the entire width of the concrete deck, and were approximately 0.1 mm wide. The installation cracks typically only penetrated roughly one third of the deck thickness and hence were treated as minor imperfections, which are not believed to have had any influence on the results. This is expected to hold true even when the installation cracks were present on the underside (tension sides) of the concrete deck. Moreover, installation cracks were consistently

situated either directly underneath a row of through-bolts as shown in Figure 4–2 (Left) or in between two consecutive rows of through-bolts as shown in Figure 4–2 (Right). As mentioned in Section 3.4, the through-bolts were tightened row-by-row, beginning at the midspan of the specimens, proceeding towards the West and East ends. This was done to force the potentially different contour profiles of the concrete decks and steel girders to match one another without creating any artificial kinks. However, the normal force provided by the pretension load in the through-bolts, clamped the concrete decks to the steel girders at the location of the through-bolts that had been previously tightened. This clamping action restricted the rotation of the concrete deck at the location of the row of through-bolts, forcing the deck to rotate and consequently crack directly beneath or just beyond the location of the row of through-bolts previously tightened.

4.1.1 Load-Deflection Results

The maximum deflections of Specimens B1 and B2 were recorded during the stiffness tests to determine if any global behavioural differences were apparent before and subsequent to any damage incurred from the fatigue testing. The vertical load versus deflection results for Specimens B1 and B2 can be seen in Figure 4–3 and Figure 4–4 respectively. The sign convention adopted for this research project is that the downwards direction is taken as positive; all loads and deflections reported as positive indicate they were acting in the downwards direction.

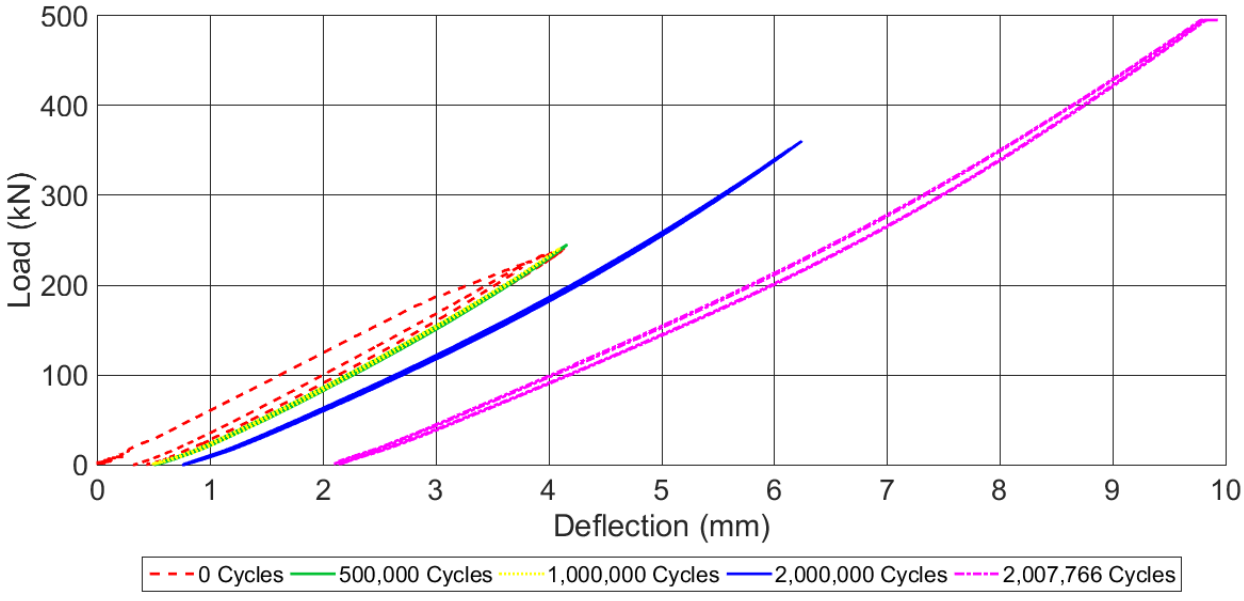

Figure 4–3: Load versus deflection plots for Specimen B1

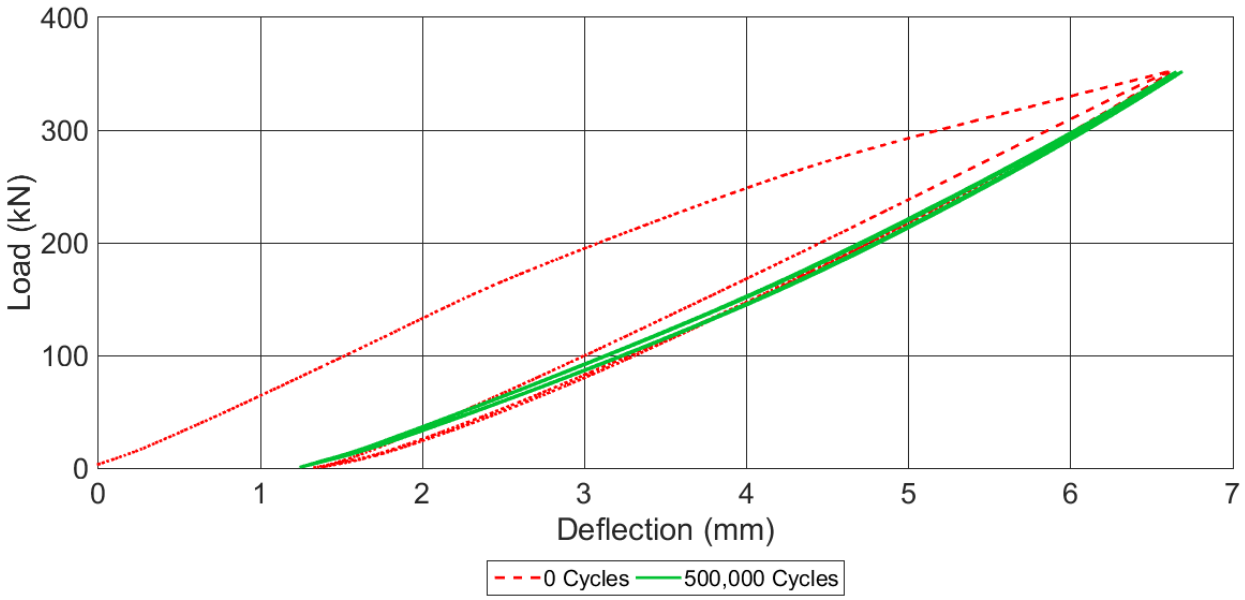

Figure 4–4: Load versus deflection plots for Specimen B2

Figure 4–3 and Figure 4–4 reveal that the stiffness of Specimen B1 decreased slightly and the stiffness of Specimen B2 did not decrease at all throughout the fatigue testing. The formation of fatigue cracks and the occurrence of concrete cyclic creep was anticipated to result in a less stiff, overall global response of the specimens. Similarly, the peak vertical deflections observed for Specimens B1 and B2 remained constant throughout fatigue testing except when Specimen B1 was subjected to higher load levels. This behaviour was unexpected, as it was theorized that the specimens would soften throughout their fatigue lives and thus experience larger deflections as the fatigue testing progressed. The results in Figure 4–3 and Figure 4–4 suggest that little or no fatigue damage was incurred by the specimens throughout the fatigue testing and that the degree of shear connection remained relatively unchanged.

One important observation concerned the change in the deflection at zero load of the specimens following the introduction of an increased maximum load level. This implies that the specimens experienced a reconfiguration of the through-bolt shear connectors, allowing for the concrete deck to establish a new favorable orientation with respect to the steel girder each time the specimen experienced a new load. This behaviour is more obvious with Specimen B1 as the load level it was subjected to was increased twice throughout its fatigue history, whereas the maximum load level that Specimen B2 was subjected to remained constant. However, both Specimen B1 and Specimen B2 exhibited this behaviour the first time they were loaded, the effects of which may have been accentuated due to additional settlement caused by the seating of the supports. The non-recoverable vertical displacement indicates that the concrete cracking observed throughout the fatigue testing, as well as possible cyclic creep of the concrete, may have

inhibited the elastic return of Specimen B1 to its original orientation. Furthermore, the interfacial slip between the concrete deck and steel girder may also be a contributing factor to the permanent displacement. This is discussed further in Section 4.1.2. Figure 4–3 and Figure 4–4 also reveal that the load-displacement behaviour of Specimens B1 and B2 are nonlinear on the descending branches as they approach zero load. This nonlinear behaviour substantiates the proposed hypothesis as the nonlinear behaviour may be a consequence of elastic strain energy accumulated within the concrete reinforcement, providing a force that partially restored the otherwise non-recoverable displacement incurred.

The peak vertical deflections for Specimens B1 and B2 at the 240 kN load level are presented in Table 4–3 for each stiffness test performed throughout during the fatigue testing, along with a comparison with the original displacements prior to the onset of fatigue loading. As discussed in Section 4.1, the load level of 240 kN was selected as the reference datum for comparison purposes.

Table 4–3: Summary of maximum deflections at the 240 kN load level

Number of Cycles Completed Prior to Stiffness Testing	B1			B2		
	Maximum Testing Load (kN)	Maximum Deflection at 240 kN (mm)	Change Relative to 0 Cycles	Maximum Testing Load (kN)	Maximum Deflection at 240 kN (mm)	Change Relative to 0 Cycles
0	240	3.993	0%	355	4.445	0%
10,000	240	3.928	-2%	355	5.486	23%
25,000	240	4.035	1%	355	5.222	17%
100,000	240	4.036	1%	355	5.300	19%
500,000	240	4.154	4%	355	5.279	19%
1,000,000	240	4.121	3%	355		
1,200,000	355	4.650	16%	355		
2,000,000	355	4.800	20%	355		
2,007,766	500	6.482	62%	355		

Table 4–3 reveals that the maximum deflection of Specimen B1 at the 240 kN level, increased dramatically after one million cycles, which corresponds to the instance where the fatigue load level was increased from 240 kN to 355 kN. Similarly, an even more substantial increase was observed in the maximum deflection of Specimen B1 at the 240 kN load level after two million cycles, which corresponds to the instance where the fatigue load level was increased once again, from 355 kN to 500 kN. It is believed that this increase in deflection at the 240 kN load level is primarily primarily due to the reconfiguration of the through-bolt positions with the increase in the peak fatigue load.

Conversely, as shown in Table 4–3, Specimen B2 observed a significant non-recoverable displacement immediately following the initiation of the fatigue loading, which then remained relatively constant following further cycling. The initial non-recoverable displacement exhibited by Specimen B2 is

theorized to have been relatively larger than the initial non-recoverable displacement observed by Specimen B1 because Specimen B2 had half the number of through-bolts providing the shear connection and the applied loading that Specimen B2 was subjected to was larger. Fewer through-bolts resulted in a reduction in the frictional component of shear resistance due to the reduced number of through-bolts with pretension forces acting on Specimen B2, clamping the concrete deck to the steel girder. As a result, slip would be expected to occur at a lower load level, and larger slip magnitudes would be expected. This is discussed further in Section 4.1.2. Upon unloading, the recovery of the slip would also be reduced due to the lower restoring force due to the dowel action of the through-bolts (due to reduced number of bolts in Specimen B2).

The vertical load-deflection results were overlaid on the same figure as the calculated theoretical deflections of the specimens for comparative purposes for Specimen B1 and Specimen B2 in Figure 4–5 and Figure 4–6 respectively. The vertical load-deflection results were modified in Figure 4–5 and Figure 4–6 by forcing the zero-load starting point of each hysteresis loop to begin at the origin (0 kN and 0 mm of slip). This was done to allow for a more direct comparison of the slopes between the various curves. The theoretical deflections for a fully composite beam and partially composite beam are provided along with the theoretical deflections of a single steel, W250x49 girder. The predicted deflections were calculated using linear elastic theory, adopting a transformed section moment of inertia for the fully composite calculation and the modified, effective transformed section moment of inertia, described by Equation 3-2 for the partially composite calculation. The moment of inertia of the steel W250x49 girder alone was used for the predicted deflection of the steel girder. Porter (2016) found that shear deformations accounted for approximately 9% of the total deflection predicted by the theoretical deflection calculations and were therefore not considered in the following permutations.

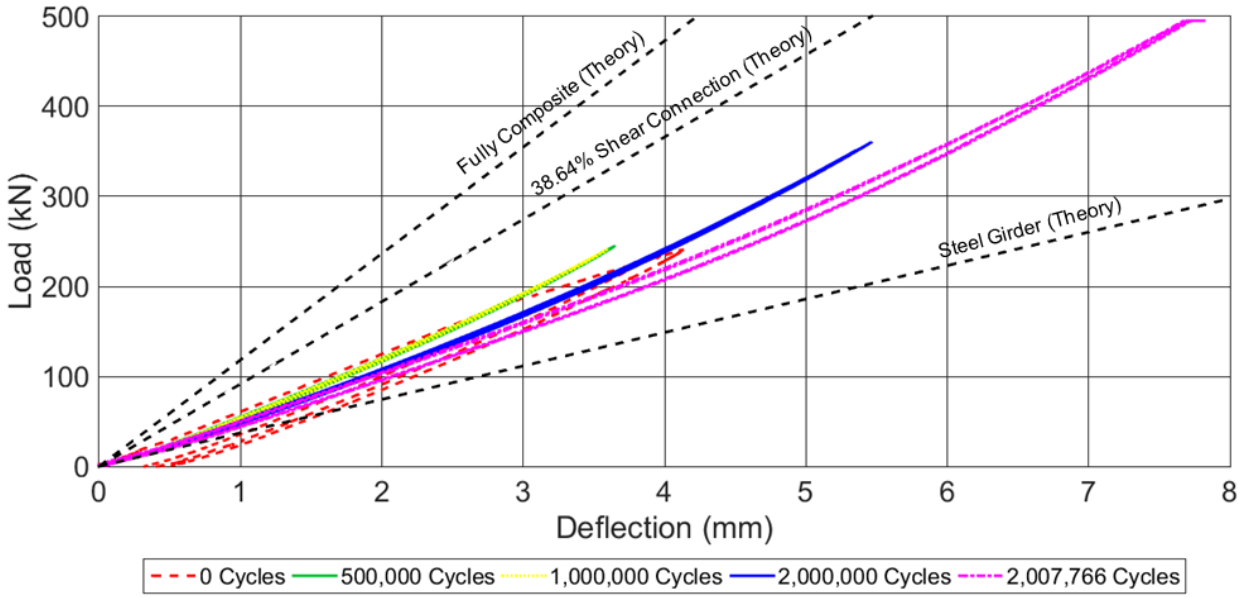

Figure 4–5: Comparative maximum deflection results for Specimen B1

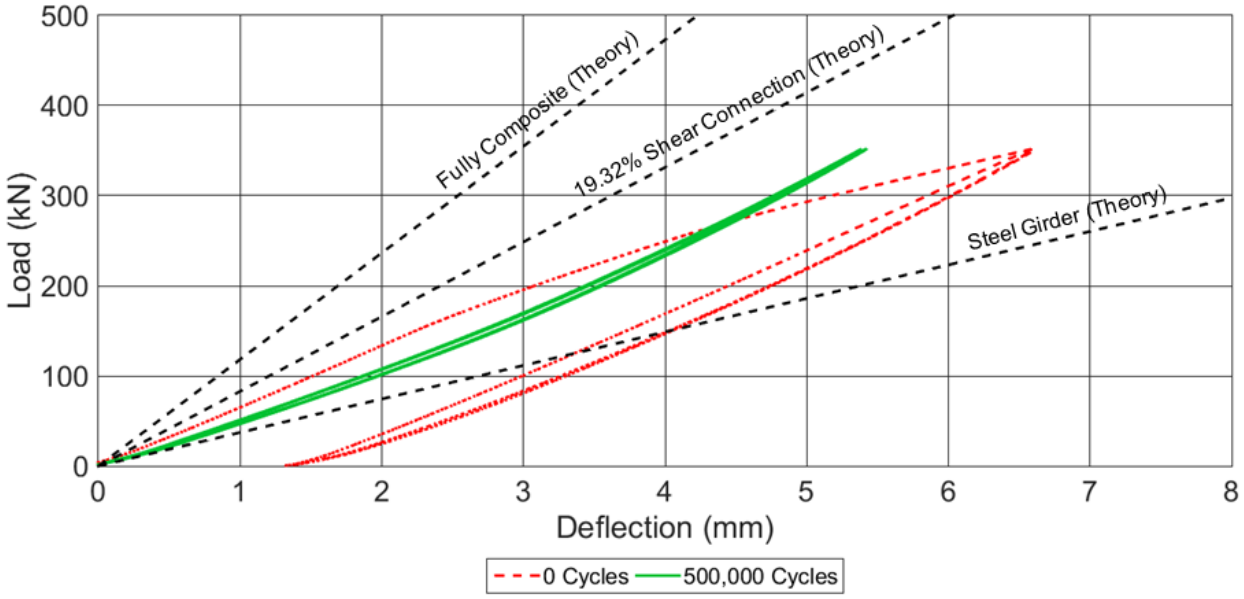

Figure 4–6: Comparative maximum deflection results for Specimen B2

Looking at these figures, it is apparent that the load-deflection behaviour of both Specimen B1 and Specimen B2 was between the predicted theoretical responses of the partially composite beam and the steel girder on its own. Moreover, it is evident that changes in the slope of the load-deflection curves throughout the fatigue testing for Specimen B1 were more significant than for Specimen B2.

Based on this comparison, the results suggest that using the modified, effective transformed section moment of inertia as described by Equation 3-2 for calculations involving partially composite sections, may be inappropriate as the equation appears to yield non-conservative results. This can likely be explained by the lack of explicit consideration in Equation 3-2 for the connector flexibility.

The calculated deflections assume linear elastic behaviour and therefore the theoretical deflections for a fully composite beam, a partially composite beam, and a single steel girder can be represented with straight lines with identical increases in deflection of 48% and 41% from 240 kN to 355 kN and 355 kN to 500 kN respectively. The Specimen B1 data, on the other hand, exhibited a change in slope (see Figure 4–5). The average peak deflections of Specimen B1 increased by 49% from 240 kN to 355 kN – a similar percentage increase to the one predicted by the theoretical calculations. However, the average peak deflection of Specimen B1 increased by 61% from 355 kN to 500 kN, which is considerably larger than the expected increase based on the calculated theoretical deflections. This larger than expected increase in deflection suggests that progressive concrete cracking or creep may have contributed to the overall deflection of Specimen B1.

4.1.2 Interfacial Slip

The interfacial slip between the concrete deck and steel girder was recorded during the stiffness tests using five LVDTs placed along the length of Specimen B1 and Specimen B2. The LVDTs were placed at 0 mm, 500 mm, 1000 mm, 2000 mm and 3000 mm from the West end of the specimens and were labelled as Slip 1 through Slip 5. The recorded slips were used to quantify any degradation in the shear connection as a consequence of the damage incurred from the fatigue testing. The sign convention adopted for this research project assumes that the relative slip of the concrete deck with respect to the steel girder is positive when this slip is towards the right and hence negative towards the left. When the specimens are loaded as shown in Figure 3–9, it is expected that the underside of the concrete decks will elongate relative to the upper flanges of the steel girders, resulting in imperfect composite behaviour. It is therefore expected that the recorded slips measured on the West side of the location of maximum moment will be negative and the slips measured on the East side of the location of maximum moment will be positive. Zero slip is anticipated at the location of maximum moment. Plots of Slip 1 (West end of specimens, X = 0 mm) for both Specimen B1 and Specimen B2 are provided in Figure 4–7 and Figure 4–8 respectively as representative samples of the trends and behaviour for each specimen.

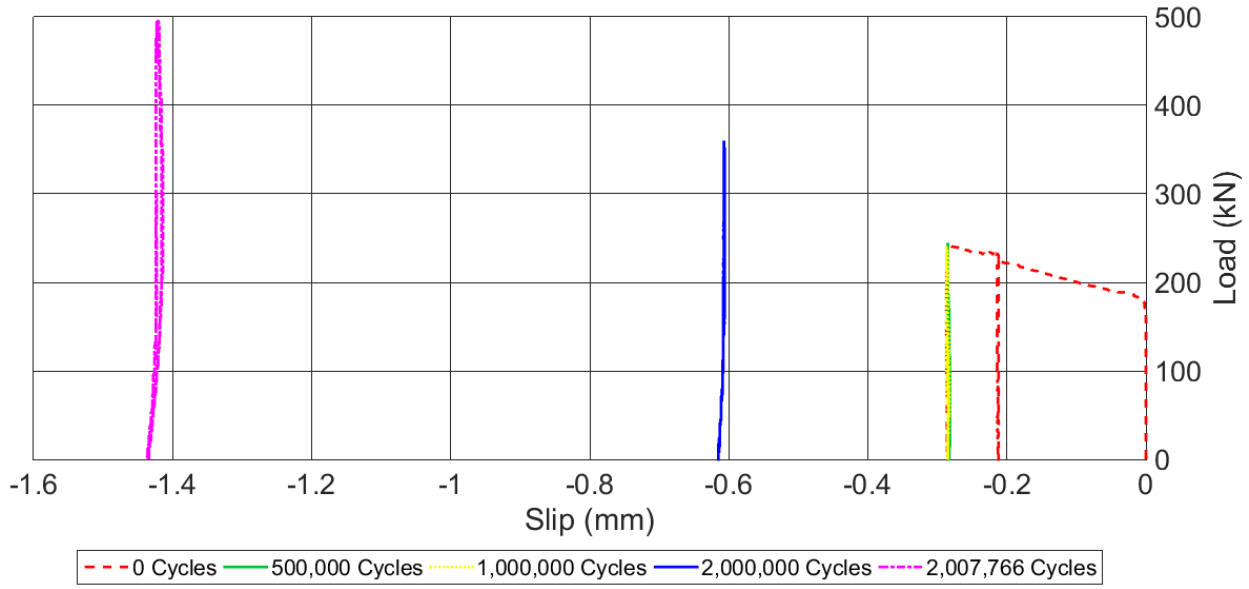

Figure 4–7: Slip 1 load-slip plot for Specimen B1

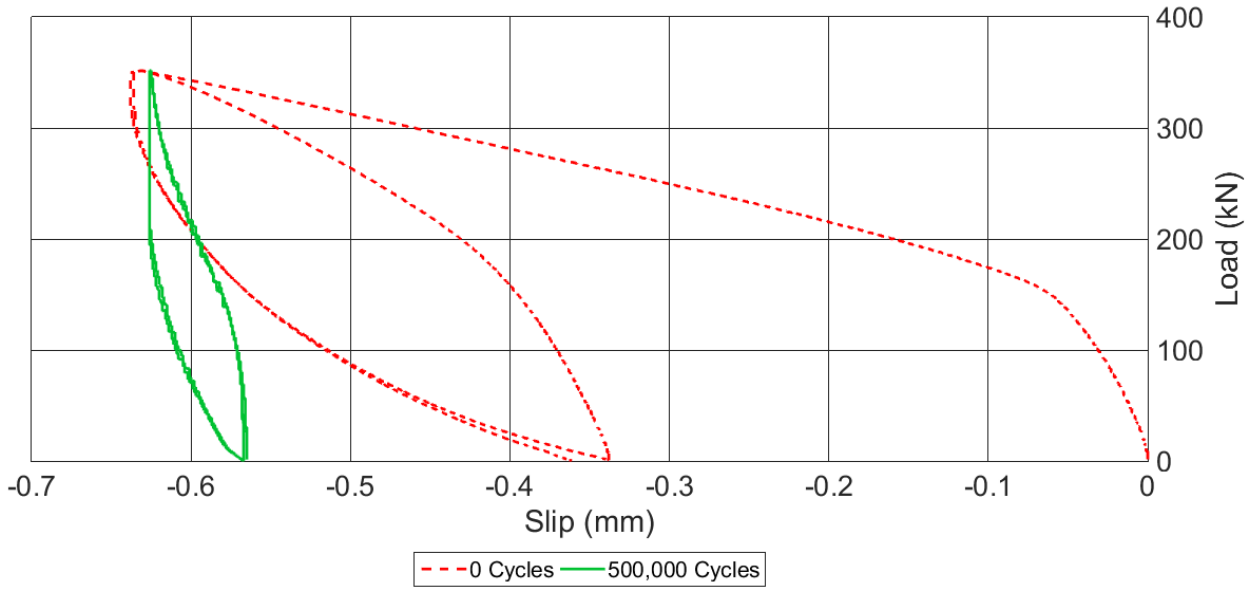

Figure 4–8: Slip 1 load-slip plot for Specimen B2

Similar to the vertical displacements, the unloaded position of the concrete deck relative to the steel girder changed following the introduction of an increased load level. This trend further supports the belief that the specimens experienced a reconfiguration of the through-bolt shear connectors (due to cracking of the concrete, slip between the concrete deck and steel girder interface, and change in the angle of inclination of the through-bolts) each time they experienced a higher load level for the first time. However, in contrast with the vertical deflection behaviour, the unloaded position of the concrete decks relative to the

steel girders changed throughout the fatigue lives of both Specimen B1 and Specimen B2. This implies that in addition to the reconfiguration of the through-bolt shear connectors each time a new load level was introduced, further reconfiguration occurred during the cyclic testing. This is evident in Figure 4–8 from the change in the magnitude of the slip measurements of the specimens at the same load level during the stiffness tests. This possibly occurred due to the load cycles applied during the fatigue testing, forcing the concrete deck and through-bolt shear connectors to reconfigure into a new equilibrium state.

The definition of change in slip used for the following analysis is the change in relative displacement of the concrete deck to the steel girder from the unloaded state to the maximum load level of interest. The resulting change in slip profile along the span at the 240 kN load level, has been plotted for Specimen B1 and Specimen B2 in Figure 4–9 and Figure 4–10 respectively.

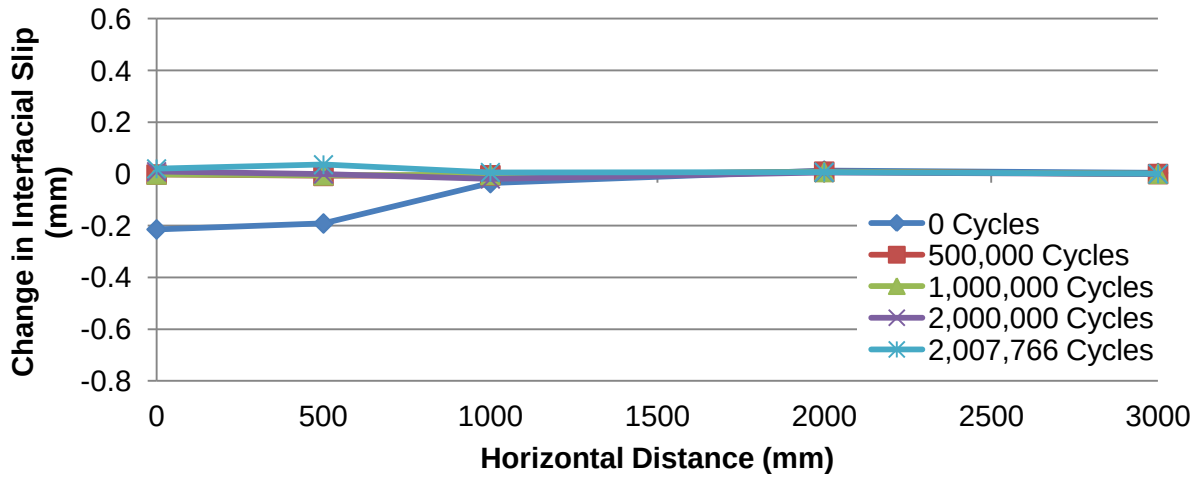

Figure 4–9: Change in interfacial slip profile for Specimen B1 at the 240 kN load level

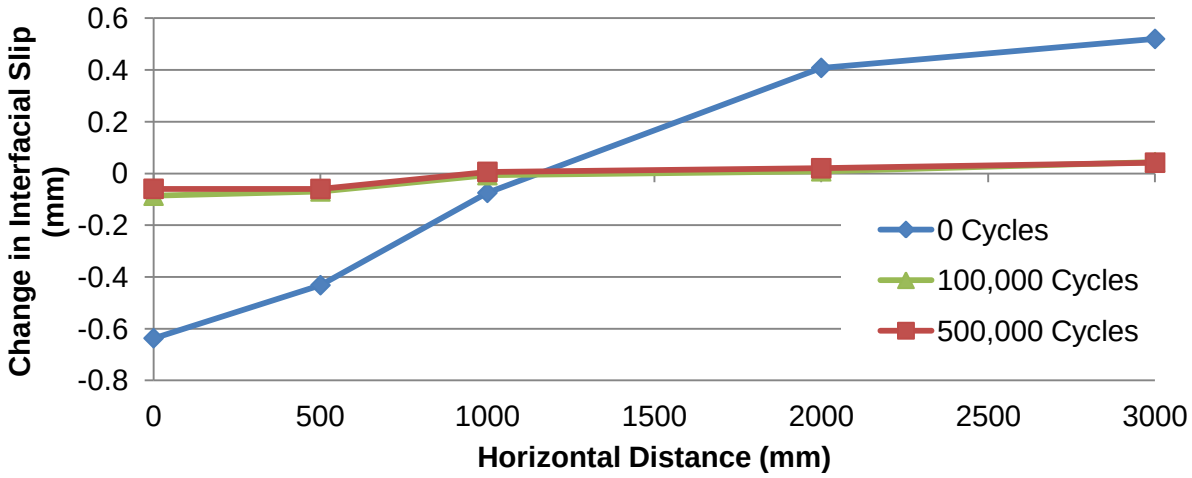

Figure 4–10: Change in interfacial slip profile for Specimen B2 at the 240 kN load level

As illustrated in Figure 4–9 and Figure 4–10, the largest change in slip observed by Specimen B1 occurred at the West end. This result was expected as the vertical shear force is highest at the West end, and thus the horizontal shear forces acting at the interface between the concrete deck and steel girder were expected to be the highest at the West end and may exceed the friction force required to initiate slip. On the other hand, a large change in slip was observed for Specimen B2 at both the West and East ends. The relatively large change in slip at the East end of Specimen B2 is rationalized by considering the limited normal force acting on the interface between the concrete deck and steel girder in this region. Since the applied load is closer to the West end of the specimen, the East end experienced less interfacial friction between the concrete deck and steel girder and thus less resistance to slip. This behaviour was not as prevalent in Specimen B1, which featured twice the number of through-bolts and consequently had twice the normal force acting on the slip interface.

Furthermore, the change in slip at Profile B (1000 mm from the West support) was close to zero for both Specimens B1 and B2. This was anticipated because, as shown in Figure 3–9, the maximum moment along the span occurs at this location, implying the longitudinal shear flow is zero. Therefore, since the shear flow is the driving mechanism inducing slip, zero slip is anticipated at Profile B.

It is also important to mention that the change in slip along the span length was larger for Specimen B2 relative to Specimen B1. Once again, this was expected since Specimen B2 featured half the number of through-bolts as Specimen B1 and therefore experienced half the friction due to the normal force provided by the pretension in the through-bolts, resulting in larger changes in slip.

Furthermore, Figure 4–9 and Figure 4–10 reveal that both Specimens B1 and B2 exhibited large initial changes in slip prior to fatigue loading, which were not recovered and almost zero change in slip subsequent to the fatigue loading except for instances where the applied loading was increased. This contradicts the expected behaviour, as it was hypothesized that the interfacial change in slip between the concrete deck and steel girder would progressively increase with accumulated fatigue damage. This behaviour also contradicts the results reported by Porter (2016) who noted a large increase in slip following significant fatigue damaged incurred by the welded, headed shear studs.

4.1.3 Strain Profiles and Concrete Deck Force

The strain profiles of the steel girders were measured along the length of the specimens and recorded during the stiffness tests using strain gauges placed on the upper and lower flanges at Profiles A, B, Y, and Z. The strain gauges were installed on the upper and lower flanges of the steel girders to define the strain profiles present in the steel girders along the span. The motivation for creating strain profiles was to quantify any loss in shear connection due to the accumulation of fatigue damage. and to accurately determine the forces carried by the through-bolts. The forces carried by the through-bolts found using this method may be used as an alternative, confirming the calculated theoretical longitudinal shear stresses reported in Table 4–2. Porter (2016) attempted to install strain gauges on the upper and lower surfaces of the concrete decks, defining the strain profiles along the entire depth of the specimens, revealing the exact forces transferred by the shear connectors to the concrete decks. Unfortunately, Porter (2016) found the results from these strain gauges to be unusable due to the cracking of the concrete throughout the progression of the fatigue tests. Therefore, the force transferred by the through-bolt shear connectors to the concrete decks were inferred from the equilibrium of the overall structure.

The strain profiles for Specimen B1 and Specimen B2 at the 240 kN load level are provided in Figure 4–11 and Figure 4–12 respectively. As per the common convention, negative strains indicate compression and positive strains indicate tension. The strain profiles are plotted on the specimen cross-section geometry as a location reference. Moreover, the theoretically calculated strain profile at the 240 kN load level, assuming a fully composite section, is plotted for comparison purposes. As illustrated in both Figure 4–11 and Figure 4–12, the neutral axes for the specimens is 244 mm from the bottom when a full shear connection is present. This is illustrated graphically as where the black dashed line representing the theoretical strain profile for a fully composite section, crosses the zero strain ordinate within the upper flange of the steel girder. It was expected that as the fatigue testing progressed, the shear connection would become less stiff thus resulting in a downward shift of the neutral axis.

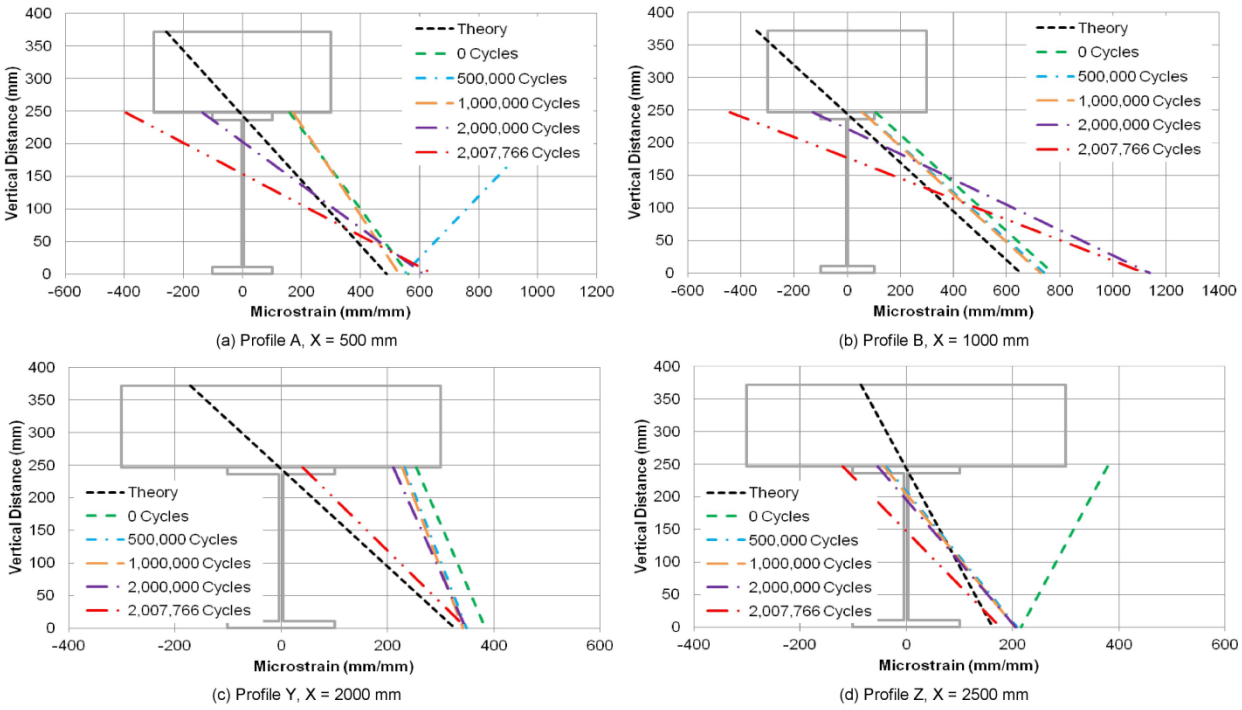

Figure 4–11: Strain profiles at (a) A, (b) B, (c) Y, and (d) Z for Specimen B1 at the 240 kN load level

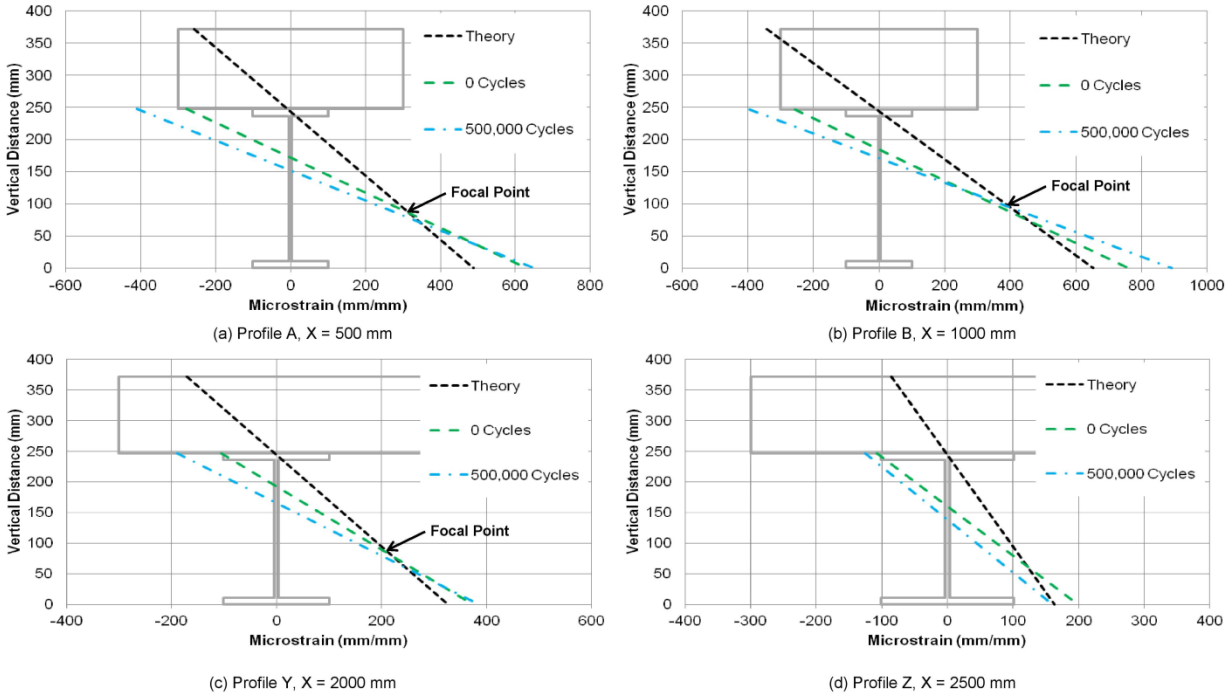

Figure 4–12: Strain profiles at (a) A, (b) B, (c) Y, and (d) Z for Specimen B2 at the 240 kN load level

It is important to note that both Specimens B1 and B2 did not have a sufficient number of through-bolts to render a theoretical fully composite section. This is illustrated in both Figure 4–11 and Figure 4–12 by the green dashed lines, representing the strain profiles prior to any fatigue loading, which already feature slopes less than that of the fully composite beam. Therefore, as discussed in Section 2.1.2, it is concluded that the specimens feature a significantly flexible or partial shear connection.

As expected, the slopes of the strain profiles for both specimens decreased, or equivalently, the curvature increased, and the neutral axis shifted downwards throughout the fatigue testing. This, continual decrease in slope (increase in curvature) indicates a corresponding incremental increase in the strain discontinuity between the strain profiles in the steel girders and the concrete decks, signifying a decrease in shear connection. This has the effect of decreasing the overall stiffness of the specimens and increasing the occurrence of slip at the interface. Moreover, the decrease in slope (increase in curvature) results in a migration of the neutral axes in the steel girders. As the neutral axis in the steel girders migrates downwards, the force carried by the through-bolts decreases until the neutral axis corresponds with the geometric centroid of the steel girders, 123.5 mm from the bottom. When this occurs, the steel girders and the concrete decks are each in static equilibrium independent from one another and therefore, the force carried by the through-bolt shear connectors is zero (that is, behaviour is non-composite). This is discussed in more detail later in this section.

Interestingly, the slope of the strain profiles appeared to decrease uniformly across the entire span for both Specimens B1 and B2. It was originally expected that Profile A would experience the greatest loss in shear connection as this region of the specimen experienced the largest amount of slip. Moreover, it was expected that Profile B would experience the least loss in shear connection as this was the location of the maximum moment. This behaviour suggests that the decrease in the degree of shear connection was moderately low and changed very little from prior to the introduction of fatigue loading. Figure 4–11 indicates that Specimen B1 exhibited negative curvature at Profile A at 500,000 cycles and Profile Z at 0 cycles. These strain readings are believed to be erroneous as negative curvature is not possible at ends of the specimen. However, the strain gauges were believed to be providing accurate readings during other portions of the testing.

Oehlers & Seracino (2002) explained that the total internal moment resultant at a cross-section is the linear summation of the moment couples in the concrete deck, M_C, the steel girder, M_S, and the moment couple resulting from the shear interaction provided by the through-bolts, M_{Comp}. The moment couples in the concrete deck and steel girder result from the unbalanced compressive and tensile forces in each structural element. Figure 4–13 illustrates the interaction of these internal forces where C_C and C_S are the

compressive forces in the concrete deck and steel girder respectively and T_C and T_S are the tensile forces in the concrete deck and steel girder respectively. Moreover when the composite beam is subjected to positive bending moments, C_R is the resultant (net) compressive force acting on the concrete deck portion of the cross-section and T_R is the resultant (net) tensile force acting on the steel cross-section.

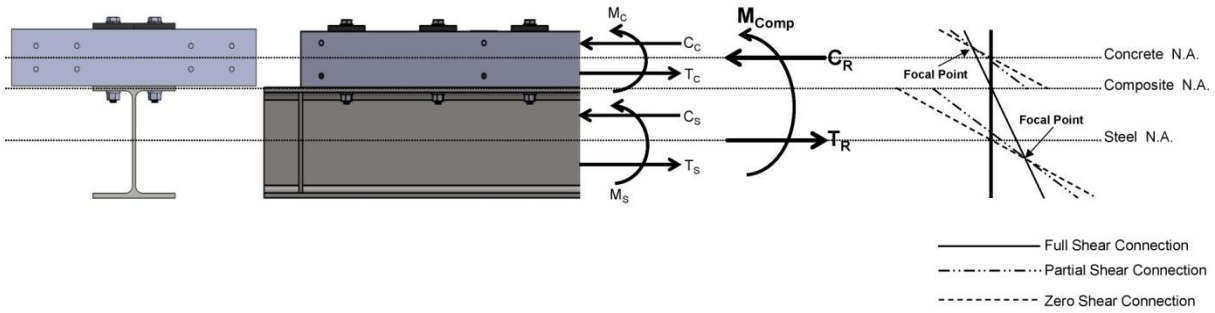

Figure 4–13: Equilibrium of internal force couples acting on the cross-section

Equilibrium of the cross-section requires that the overall compressive resultant acting on the cross section, C_R, must be equal to the overall tensile resultant acting on the cross-section, T_R. This is rendered possible through the transfer of the longitudinal shear by the through-bolts and the friction acting between the concrete deck and steel girder interface. While the interfacial friction is always present between the concrete deck and the steel girder, it is relatively small and cannot be relied upon. Therefore, the interfacial friction is typically neglected and the shear connectors are assumed to independently carry the entire longitudinal shear force at the interface.

If the resultant forces in the concrete deck were equal in magnitude and the resultant forces in the steel girder were also equal in magnitude, then $C_R = T_R = 0$ as the concrete deck and steel girder would each be independently in equilibrium. Therefore, $M_{Comp} = 0$, implying zero shear connection between the concrete deck and the steel girder.

A fully composite beam requires $C_R = T_R$ where C_R is limited by the crushing of the concrete due to C_C. While partially composite beams still require $C_R = T_R$, the total longitudinal shear force transferred across the concrete deck and steel girder interface, C_R or equivalently T_R, is limited by the strength of the shear connectors. It is only when the strength of the shear connectors equals (or exceeds) the compressive resistance of the concrete that a fully composite section is achieved. Therefore, the progressive fatigue damage and the consequential decrease in stiffness of the through-bolt shear connectors, deteriorates the remaining shear connection, reducing the magnitude of C_R. This has the effect of decreasing M_{Comp} and by extension, the overall moment capacity of the composite section.

The net compressive forces in the concrete decks were calculated using the strain profiles in the steel girders at Profiles A, B, Y and Z. Using Hooke's law, the stress profiles and the corresponding forces, C_S and T_S, were found from the strain profiles. The difference between C_S and T_S provided the overall tensile resultants acting on the cross-sections, T_R, which by equilibrium are equal and opposite to the resultant compressive forces acting in the concrete decks, C_R. Table 4–4 and Table 4–5 summarize the resultant compressive forces in the concrete decks during the fatigue testing of Specimens B1 and B2 respectively at the 240 kN load level. Also shown in Table 4–4 and Table 4–5 is the percentage difference of the force in the concrete decks from the predicted value according to theoretical forces for a fully composite section.

Table 4–4: Concrete deck compression resultant results for Specimen B1 at 240 kN load level

Profile	A		B		Y		Z	
X (mm)	500		1000		2000		2500	
	Deck Force, C_R (kN)	Diff. w.r.t. Theory	Deck Force, C_R (kN)	Diff. w.r.t. Theory	Deck Force, C_R (kN)	Diff. w.r.t. Theory	Deck Force, C_R (kN)	Diff. w.r.t. Theory
Theory	295.0		393.3		196.7		98.3	
0	441.5	49.7%	538.4	36.9%	390.1	98.4%	363.1	269.3%
500,000	987.9	234.9%	490.5	24.7%	354.6	80.3%	104.5	6.3%
1,000,000	430.4	45.9%	481.8	22.5%	348.7	77.3%	99.1	0.8%
2,000,000	292.4	-0.9%	616.3	56.7%	341.1	73.5%	92.4	-6.0%
2,007,766	154.4	-47.7%	415.6	5.7%	237.5	20.8%	34.7	-64.7%

Table 4–5: Concrete deck compression resultant results for Specimen B2 at 240 kN load level

Profile	A		B		Midspan		Y		Z	
X (mm)	500		1000		1500		2000		2500	
	Deck Force, C_R (kN)	Diff. w.r.t. Theory	Deck Force, C_R (kN)	Diff. w.r.t. Theory	Deck Force, C_R (kN)	Diff. w.r.t. Theory	Deck Force, C_R (kN)	Diff. w.r.t. Theory	Deck Force, C_R (kN)	Diff. w.r.t. Theory
Theory	295.0		393.3		295.0		196.7		98.3	
0	214.9	-27.1%	306.5	-22.1%	284.2	-3.7%	163.6	-16.8%	55.8	-43.2%
500,000	146.6	-50.3%	302.8	-23.0%	231.6	-21.5%	120.1	-38.9%	20.7	-78.9%

The resultant compressive forces in the concrete decks presented in Table 4–4 and Table 4–5 are also presented graphically in Figure 4–14 and Figure 4–15. Similar to the strain profiles, the concrete deck

forces for Specimen B1 shown in Figure 4–14 at Profile A at 500,000 cycles and Profile Z at 0 cycles are believed to be erroneous and do not provide indication of behaviour.

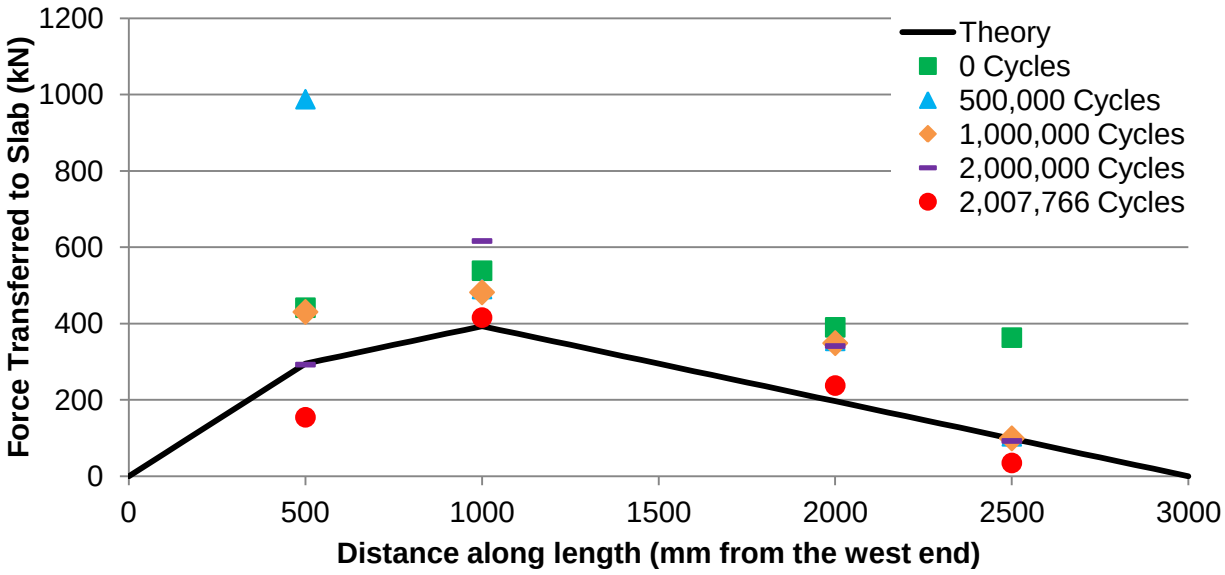

Figure 4–14: Variation of concrete deck compression resultant along length for Specimen B1 at the 240 kN load level

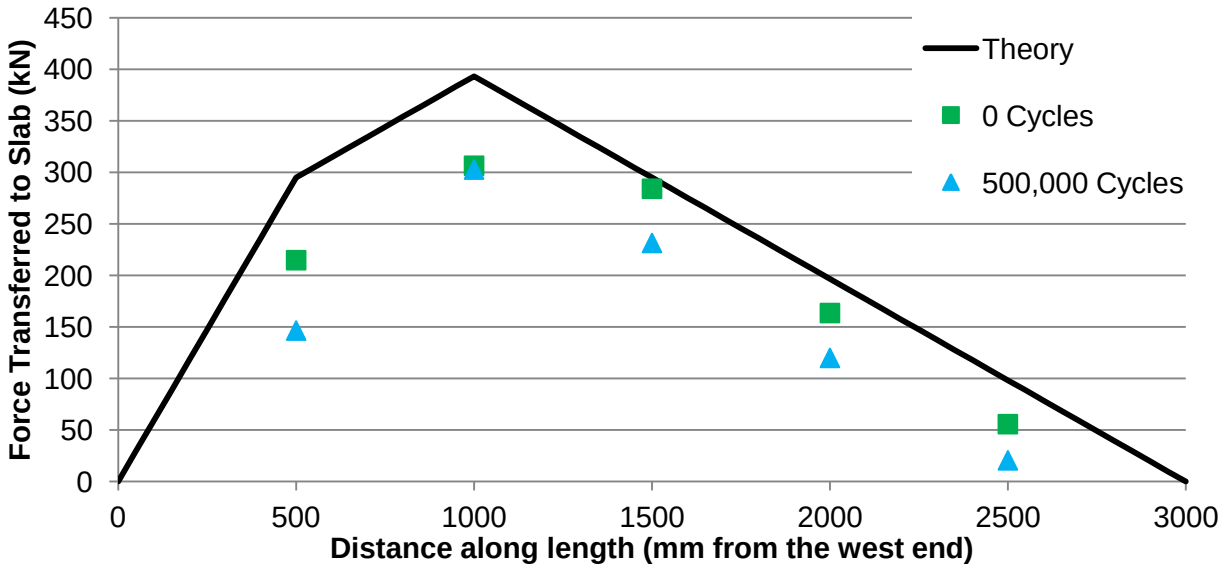

Figure 4–15: Variation of concrete deck compression resultant along length for Specimen B2 at the 240 kN load level

Figure 4–14 and Figure 4–15 suggest that the degree of shear connection in terms of the force transfer to the concrete deck, appears to have reduced during the duration of the fatigue loading. As discussed

earlier, it was originally expected that Profile A would experience the greatest loss in shear connection as this region of the specimens experienced the largest amount of slip. Moreover, it was further expected that Profile B would experience the least loss in shear connection as this is the location of the maximum moment and hence experienced the least amount of slip. Figure 4–14 and Figure 4–15 confirm both of these hypothesises as Profile A saw the largest change and Profile B saw virtually no change in the net compressive forces in the concrete decks for both specimens. While Profile A experienced the largest change in the net compressive force in the concrete decks, the actual change experienced was still relatively minor and not significantly larger than the change experienced by Profile Y and Profile Z. Moreover, Figure 4–14 and Figure 4–15 reveal that the longitudinal shear transfer was less for Specimen B2 than for Specimen B1, consistent with what was expected because Specimen B2 featured less through-bolts.

4.2 Fatigue Testing Results

The fatigue testing described in Section 3.5.2 was performed on Specimen B1 and Specimen B2. The fatigue testing was intended to quantify the fatigue performance of the through-bolt shear connectors, revealing the number of cycles required for the occurrence of failure and providing a direct comparison to the fatigue performance of welded, headed shear studs. Additionally, the redistribution of forces amongst the remaining through-bolts subsequent to the progressive failure of the most highly loaded through-bolts was of particular interest to observe the residual performance of the composite structure. The fatigue testing unfortunately did not result in the fatigue failure of any through-bolt shear connectors, as the fatigue performance of the through-bolt shear connectors far exceeded expectations. Fatigue testing on Specimen B1 was stopped after 2,007,766 cycles when a fatigue crack was observed in the web of the steel girder at the West end of the specimen. As shown in Figure 4–16, the fatigue crack emanated from the weldment fastening the web stiffener to the girder web. The fatigue testing was stopped as a safety precaution. The fatigue crack shown in Figure 4–16 has been highlighted with a black line for clarity.

Figure 4–16: Fatigue crack in the web of the steel girder at the West end of Specimen B1

The fatigue testing on Specimen B2 was stopped after 762,241 cycles due to the failure of an actuator mounting bolt in the test frame. Table 4–6 summarizes the applied shear stress ranges and number of cycles for each specimen and group of through-bolt rows, calculated using Equation 4-1.

Table 4–6: Fatigue test summary

Specimen	Number of Cycles	Bolt Rows 1-2 Shear Stress Range (MPa)	Bolt Rows 3-12 Shear Stress Range (MPa)
B1	1,000,000	438.70	146.23
	1,000,000	658.05	219.35
	7,766	934.62	311.54
	Equivalent Shear Stress Range (MPa)	571.99	190.66
B2	762,241	1453.37	484.46
	Equivalent Shear Stress Range (MPa)	1453.37	484.46

The equivalent longitudinal shear stress ranges presented in Table 4–6 were calculated using the Palmgren-Miner's rule, given by Equation 2-12 assuming a slope of 3 for the S-N curve to calculate the number of cycles to failure. The equivalent longitudinal shear stress ranges represents the linear summation of the contribution to damage that the loading history at each longitudinal shear stress range had on the overall damage incurred. The magnitude of the equivalent longitudinal shear stress range represents a hypothesized constant stress amplitude that would result in a fatigue life similar to that of the actual, non-uniform stress history. It is important to note that the equivalent longitudinal shear stress ranges reported in Table 4–6, calculated using Equation 4-1, neglect the contribution of friction. The actual longitudinal shear stress ranges acting on the through-bolts were less than those reported due to the contribution the interfacial friction between the concrete deck and steel girder had on resisting the longitudinal shear forces. The interfacial friction resisted a portion of the longitudinal shear forces acting between the interface of the concrete deck and steel girder, thus lessening the longitudinal shear force required to be resisted by the through-bolts. The equivalent longitudinal shear stresses were computed for the purposes of plotting the S-N curve for the through-bolts.

The autopsy of Specimen B1 and Specimen B2 revealed that no cracks developed within the through-bolt shear connectors present in each specimen. Moreover, when removed, the through-bolts did not display any signs of permanent deformation or other forms of damage. The initial location of the bearing plates, prior to the commencement of the fatigue testing, were recorded on the concrete decks using an acetone marker, outlining the positions of the bearing plates. Upon observation of the specimens after the completion of fatigue testing, it was apparent that the bearing plates on the top surface of the concrete decks did not shift during the fatigue loading. Furthermore, straight lines were drawn with chalk along the hex nuts and the exposed threads at the bottom of the through-bolts prior to testing to reveal if the hex nuts loosened during the fatigue tests. Once again, upon observation of the specimens subsequent to the completion of the fatigue testing, it was clear that the hex nuts remained as they were after tightening of the through-bolts.

Both Specimens B1 and B2 experienced the propagation and enlargement of the installation cracks in the concrete decks as discussed in Section 4.1. The installation cracks grew from their original 0.1 mm to roughly 0.3 mm in most cases. Some installation cracks near the point loads expanded to as large as 0.75 mm. Specimen B1 experienced crack propagation and further crack formation in addition to the installation cracks subsequent to one million applied cycles. Generally, the cracks on the compression side of the concrete deck would close at the peak of each load cycle and then reopen when the load was at a minimum.

The DAQ unit was equipped with a peak-detecting algorithm, recording the peaks and valleys of the strains and displacements during the fatigue testing. A MATLAB script was prepared to process the large data sets. The MATLAB script plots the peaks and valleys recorded by the DAQ software and also computes and plots the ranges of the data. Computing the range of the strains and displacements from the peaks and valleys provided required the subtraction of the valleys from the peaks at evenly spaced increments. The MATLAB script traversed through the data, finding two non-similar, adjacent data points, x_1 and x_2 which correspond to the unloaded and fully loaded state of the actuator respectively. If the two adjacent points were not dissimilar by more than a specified percentage, typically between 10% and 25%, or the two adjacent points did not coincide with the loaded and unloaded actuator states, the two points were discarded and the next set of adjacent points was considered. Once two suitable points were identified, the range was taken as the difference between x_2 and x_1. Therefore, a positive range implied that x_2 was larger than x_1, indicating that the magnitude of the strain or displacement increased as the specimen was loaded. Lastly, the MATLAB script reduced the congestion of each plot by searching for two adjacent points, x_2 and x_1, that are separated from the previously identified suitable adjacent points, $x_{2\text{-}1}$ and $x_{1\text{-}1}$, by 600 or 1000 data points, depending on the total number of data points provided and ignoring points in between.

4.2.1 Variation of Beam Deflection

The maximum deflections of Specimens B1 and B2 measured 1300 mm from the West supports were recorded during fatigue testing to determine if softening of the specimens was occurring. It was theorized that as the fatigue testing progressed, the overall maximum deflections of the specimens would increase as a result of the decrease in stiffness due to crack propagation within the through-bolts, cyclic creep of the concrete decks, crack growth in the concrete decks, and slip at the concrete deck and steel girder interface. Figure 4–17 and Figure 4–18 display the maximum deflection ranges for Specimens B1 and B2 respectively.

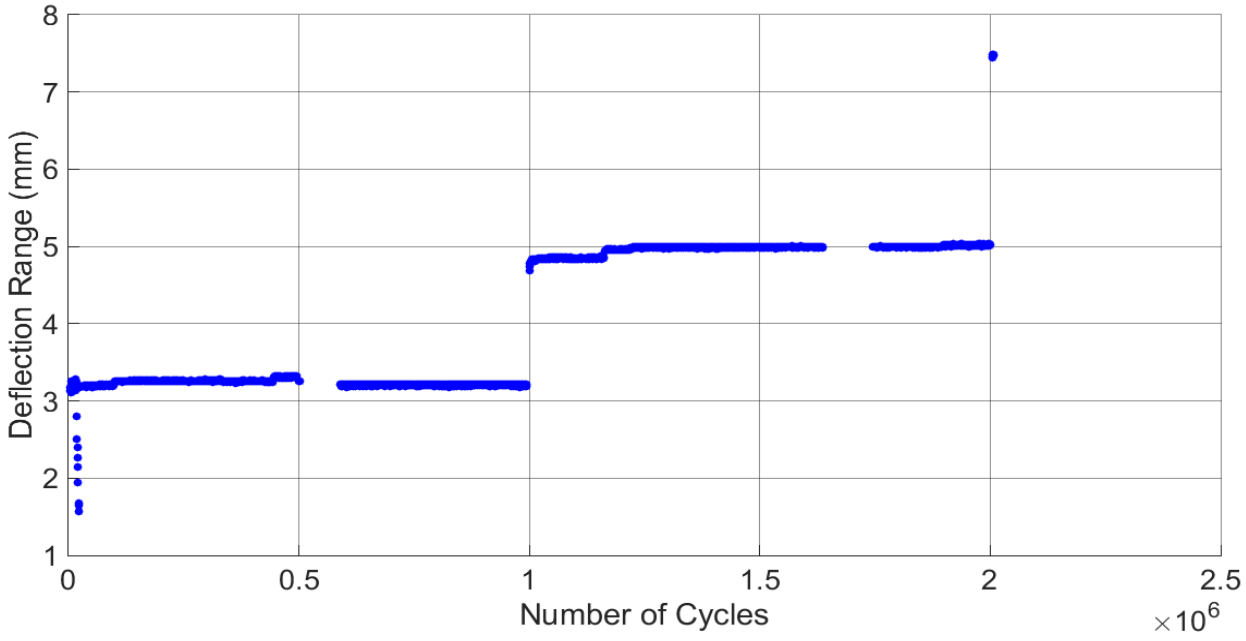

Figure 4–17: Maximum deflection range versus number of cycles for Specimen B1

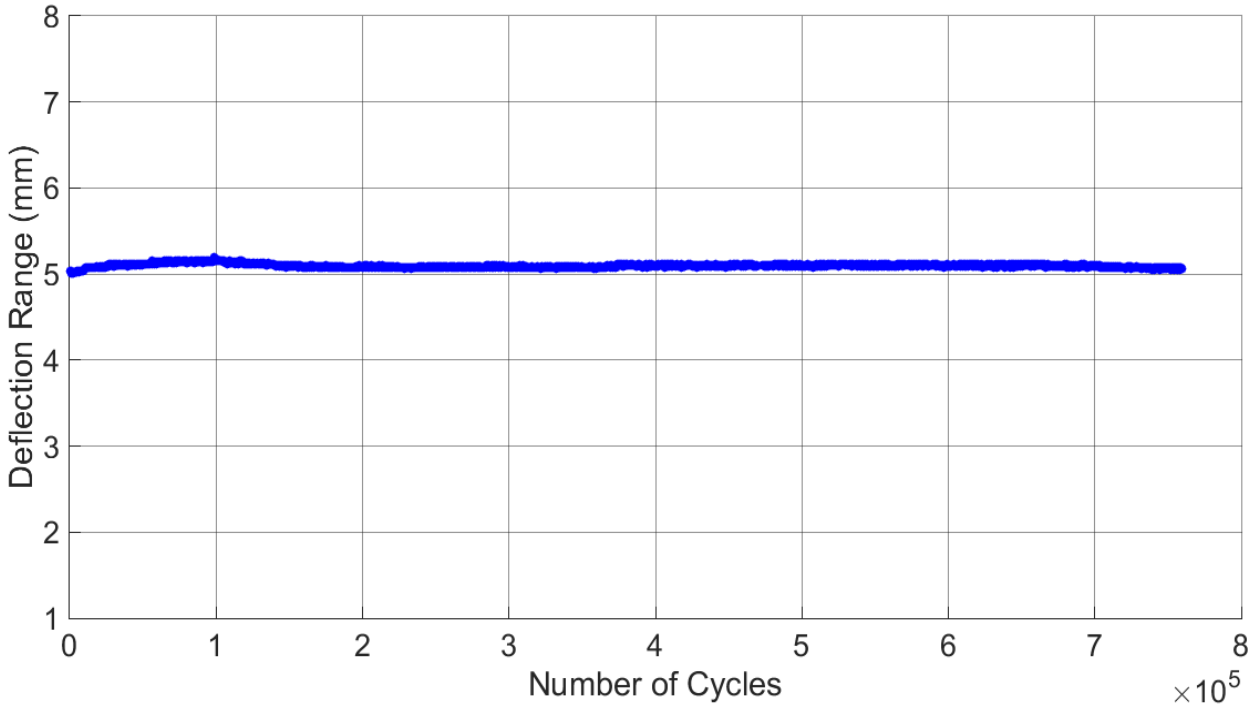

Figure 4–18: Maximum deflection range versus number of cycles for Specimen B2

The deflection results reveal that the overall maximum deflection of both Specimens B1 and B2 did not change significantly due to the fatigue loading. The abrupt increases in deflection present in Figure 4–17

for Specimen B1 were due to the introduction of larger load levels at one million cycles and again at two million cycles. The deflection results further support the conclusion that the through-bolts did not experience significant fatigue damage throughout the fatigue testing. Specimen B1 observed an average range of deflection of approximately 3.2 mm when subjected to a load range of 230 kN, 5.0 mm when subjected to a load range of 345 kN and 7.5 mm when subjected to a load range of 490 kN. Specimen B2 was continuously subjected to a load range of 345 kN throughout the duration of its fatigue life and observed an average range of deflection of approximately 5.1 mm. Contrary to what was expected, the average deflection range observed by Specimen B2 was very similar to the average range of deflection observed by Specimen B1 at the common load range of 345 kN. Since Specimen B2 featured half as many through-bolts, it was expected that it would experience greater deflections. Because the deflection ranges for both Specimens B1 and B2 are very similar, it is suspected that the concrete decks and steel girders for each specimen experienced negligible changes in interfacial slip during fatigue loading cycles.

4.2.2 Variation of Interfacial Slip

The interfacial slip between the concrete decks and steel girders were recorded throughout the fatigue testing using five LVDTs placed along the length of the specimens. The LVDTs were placed at 0 mm, 500 mm, 1000 mm, 2000 mm and 3000 mm from the West ends of the specimens and labelled as Slip 1 through Slip 5. As described in Section 4.1.2, the adopted sign convention assumes that relative slip of the concrete decks with respect to the steel girders is positive when the interfacial movement is towards the right (East in Figure 3–1). The recorded slips were used to further quantify any degradation in shear connection as a consequence of any fatigue damage incurred. It was expected that the slip magnitude would increase throughout the duration of the fatigue testing due to the softening of the through-bolt shear connectors. Moreover, it was also expected that the interfacial coefficient of friction between the concrete decks and steel girders would gradually decrease due to the continual polishing of the concrete decks sliding back and forth, therefore further increasing the relative slip.

Specimen B1 demonstrated virtually no increase in the range of interfacial slip (that is, the change in slip during a given load cycle) along the length of the specimen over the course of its fatigue loading, indicating that very little or no fatigue damage was incurred throughout the fatigue testing. Similar to the maximum deflection results, the interfacial slip results between the steel girder and concrete deck for Specimen B1, observed large, abrupt increases in slip when the applied load range was increased at one million cycles and again at two million cycles. However, as illustrated in Figure 4–19, the range of the interfacial slip remained constant for Slip 1 through Slip 5.

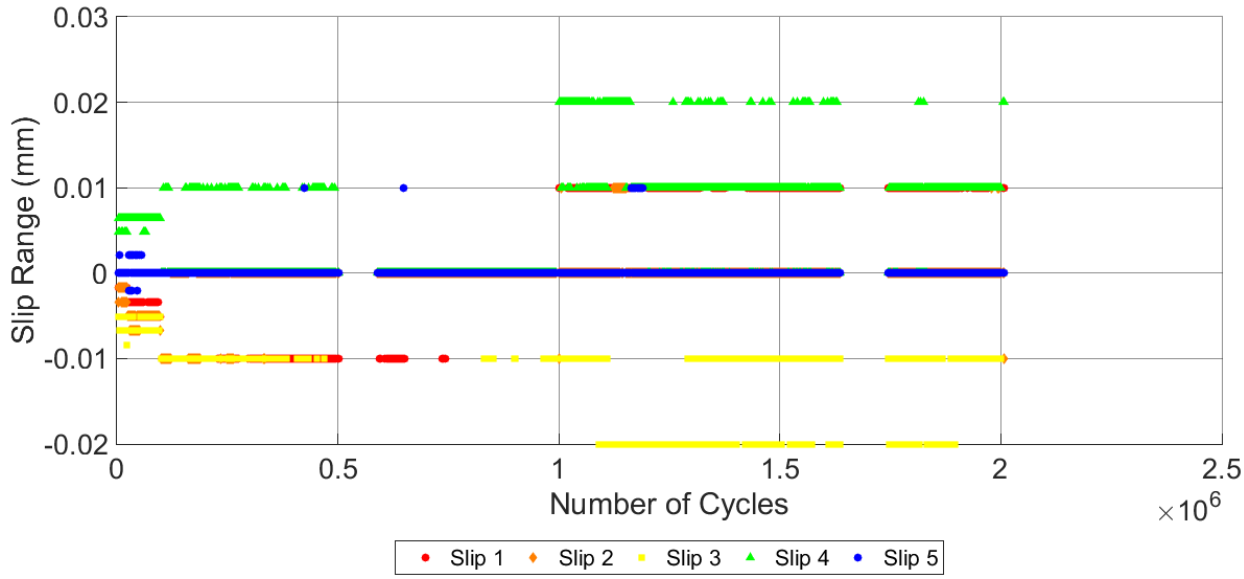

Figure 4–19: Interfacial slip range versus cycles for Specimen B1

Specimen B2 also demonstrated effectively no increase in the range of interfacial slip (change in slip during a given load cycle) along the length of the specimen over the course of its fatigue life. As illustrated in Figure 4–20, the interfacial slip range for Slip 1 through Slip 5 remained constant, indicating once again that very little or no fatigue damage was incurred throughout the course of the fatigue testing of Specimen B2.

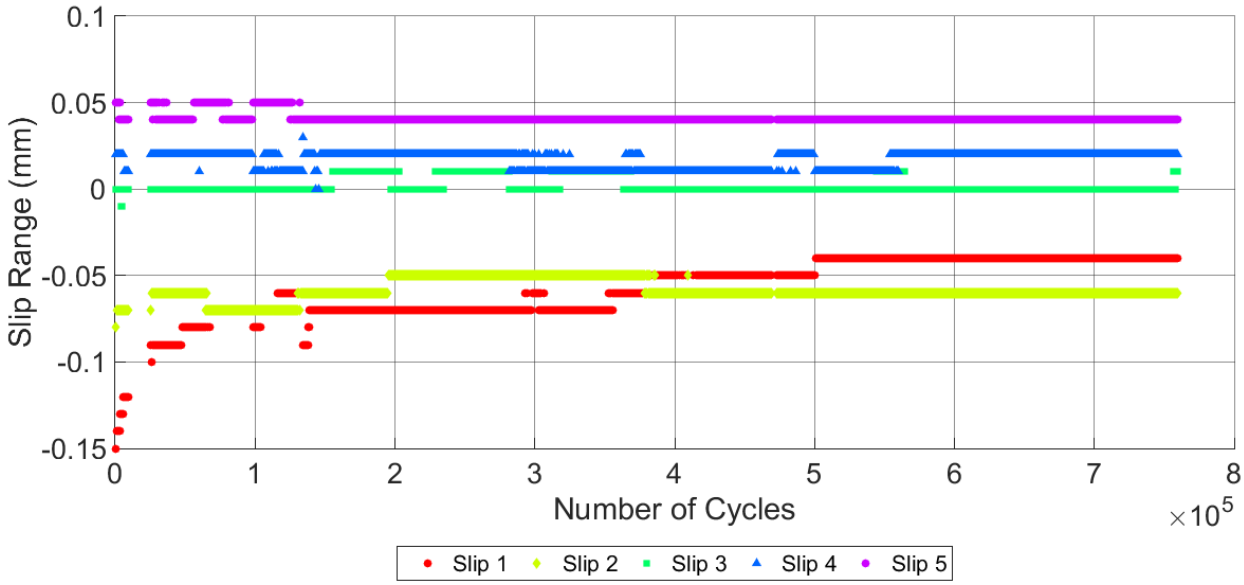

Figure 4–20: Interfacial slip range versus cycles for Specimen B2

4.2.3 Variation of Through-Bolt Strain

As explained in Section 3.3, the first four rows and the last two rows of through-bolts were instrumented for Specimen B1 and all twelve staggered through-bolts along the length of Specimen B2 were instrumented with strain gauges. The through-bolts were instrumented to directly quantify any fatigue damage incurred by the through-bolts as a consequence of the fatigue testing. Moreover, the through-bolts were instrumented to observe and identify the instance of a through-bolt failure and the effects that the failure of one through-bolt had on an adjacent through-bolt.

Immediately subsequent to the installation of the through-bolts, the through-bolt strains for both Specimen B1 and Specimen B2 were all approximately 2100 microstrain, consistent with the calculated theoretical strain that would be anticipated with 5/8" diameter through-bolts, subjected to a pretension level of 85 kN. As described in Section 3.4, the through-bolts were tightened row-by-row, beginning at the midspan of the specimens, proceeding towards the West and East ends. This resulted in a decrease in strain level of some of the interior most through-bolts as slight separations between the concrete decks and steel girders at the ends, such as the one shown in Figure 4–1, may have been straightened when the exterior most rows of through-bolts were installed, thus relieving the interior through-bolts.

Figure 4–21 provides a sample illustration of the variation of the through-bolt strain data using Through-Bolt N3 on Specimen B1 as an example. Note that Figure 4–21 shows the actual strain measurements recorded by the DAQ and not the strain range. Figure 4–21 reveals that the through-bolt strains observed large, abrupt decreases when the load range applied to Specimen B1 was increased at one million cycles and again at two million cycles as opposed to the increases in deflection and relative slip observed at these instances. Moreover, Figure 4–21 reveals that the strains in the through-bolts decreased throughout the progression of the fatigue testing in a parabolic fashion.

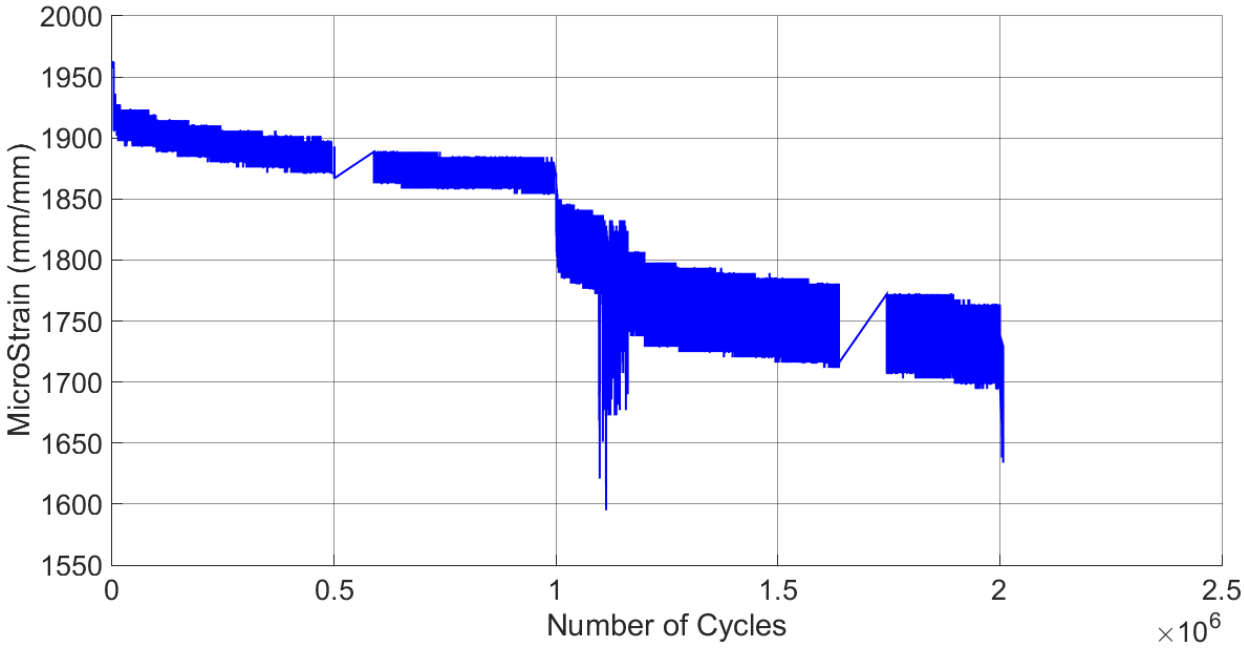

Figure 4–21: Through-Bolt N3 strain data versus number of fatigue cycles for Specimen B1

The large, abrupt decreases in the through-bolt strain when the load range applied to Specimen B1 was increased at one million cycles and again at two million cycles is a result of tensile forces carried by the through-bolts being alleviated by the larger applied loading. This effect is particularly pronounced in Figure 4–21, because Through-Bolt N3 is underneath the applied load. Similar trends and behaviour were observed for the other through-bolts. However, the magnitudes were much less for the through-bolts farther from the applied loading.

Similar to Specimen B1, a typical trend in the strain data was found for all of the through-bolts in Specimen B2. Therefore, Figure 4–22 provides a sample illustration of the through-bolt strain data using Through-Bolt S1 as an example. Figure 4–22 reveals that similar to Specimen B1, the through-bolt strains decreased throughout the progression of the fatigue testing in a parabolic fashion.

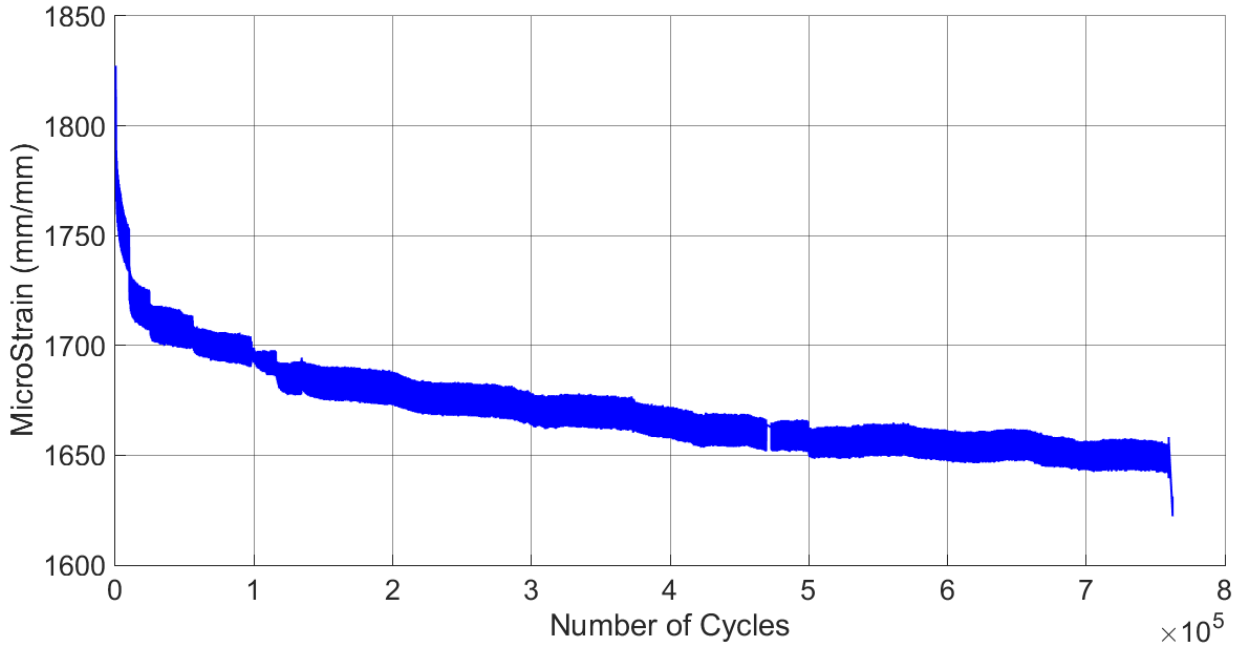

Figure 4–22: Through-Bolt S1 strain data versus number of fatigue cycles for Specimen B2

Since it was concluded from the findings of the autopsy that the hex nuts did not come loose during the fatigue testing, the loss of pretension in the through-bolts and the corresponding decrease in through-bolt strains for Specimen B1 and Specimen B2, might indicate a perpetual decrease in stiffness of the specimens due to the fatigue loading or shrinkage and or cyclic creep in the concrete decks. It was observed that if the specimens were left to rest over the course of multiple days in between cyclic testing, the strains present in the through-bolts would be slightly less when testing resumed than when previously recorded. King et al. (1965) reported similar observations with the local distortion gauges used on the flanges underneath welded, headed shear studs. These occurrences suggest that the concrete decks may be experiencing shrinkage, creep, or both. It is hypothesized that the concrete decks experienced localized creep around the bolts due to the pretension in the through-bolts. This creep effectively reduced the thickness of the concrete decks in the affected areas, thus relaxing the strain within the through-bolts over time. This theory offers an explanation as to why the strains experienced by the through-bolts in both Specimen B1 and Specimen B2 decreased continuously throughout the fatigue testing but did not exhibit any signs of fatigue damage. This theory also supports the conclusions drawn from examining the maximum deflection and interfacial slip results, which is consistent with the little or no visible fatigue damage experienced by both Specimen B1 and Specimen B2.

4.2.4 Fatigue-Life Analysis of Experimental Data

A statistical stress-life (S-N) analysis was not possible given that only two specimens were tested under fatigue loading and no failures of the through-bolt shear connectors were observed. However, the results of the "runout" tests were plotted on an S-N curve and compared with the Category A and Category D fatigue details from the CSA S6 (CSA S6, 2014) code and data points collected from a review of the literature conducted by Sjaarda et al. (2017). Figure 4–23 compares the equivalent longitudinal shear stress range and the corresponding total number of cycles that the most heavily loaded through-bolts (Rows 1-2) and the least heavily loaded through-bolts (Rows 5-12) were subjected to during the fatigue testing of Specimen B1 and Specimen B2.

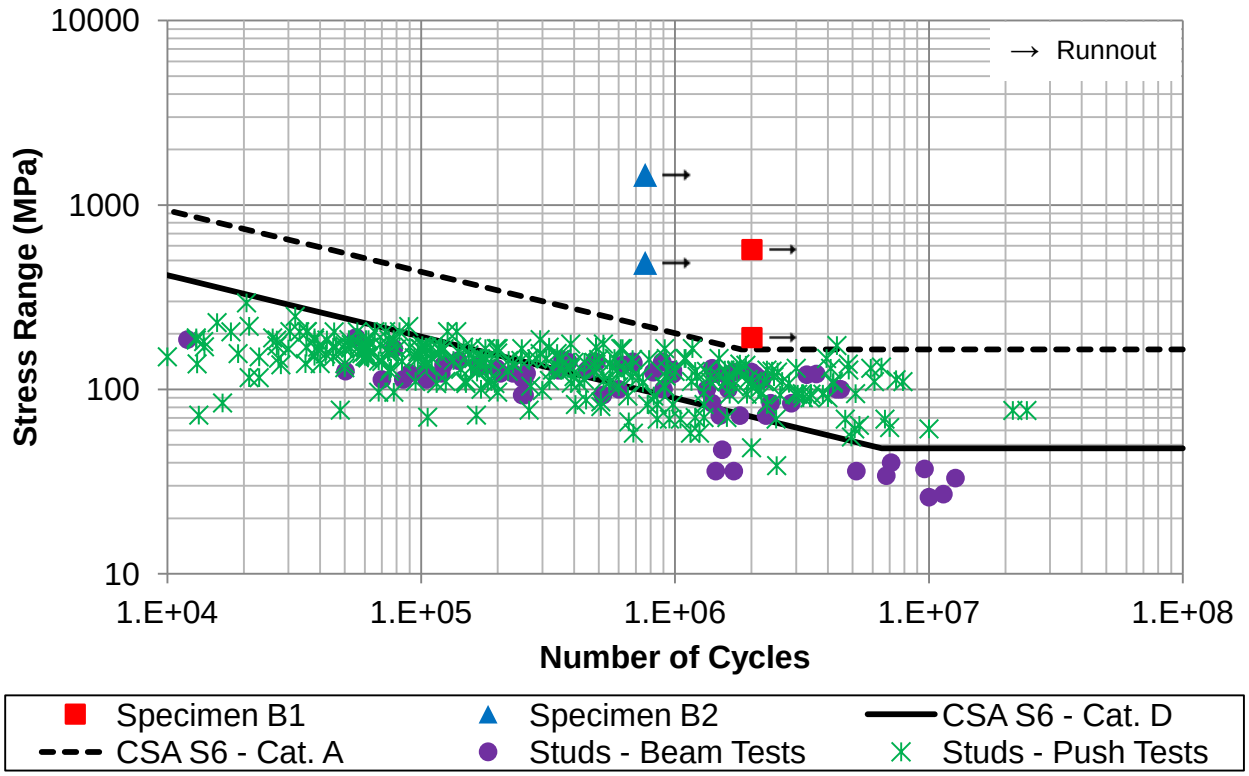

Figure 4–23: Equivalent longitudinal shear stress range S-N plot for Specimen B1 and Specimen B2

The data points representing the fatigue results for Specimen B1 and Specimen B2 have rightward facing arrows adjacent to them, indicating that the number of cycles that would induce a fatigue failure of the through-bolts is larger than the number reported (i.e. the test was a "runout"). The data points illustrated in Figure 4–23 from the review of the literature primarily represent welded stud failures. However, specimen flange failures, weld failures, and "runouts" are also included.

Figure 4–23 illustrates that, as expected, the through-bolt shear connectors outperformed the welded, headed shear studs, despite the lack of actual failures observed. The most heavily loaded through-bolts in Specimen B1 and Specimen B2 were subjected to approximately 521 and 3244 times the number of cycles predicted to result in failure using the CSA S6 Category D design line respectively. Moreover, both the most heavily loaded and least heavily loaded through-bolts outperformed the tested shear studs reported in the literature regardless of the shear stud testing approach employed (push test or beam test).

4.3 Stiffness Tests with Through-Bolt Removals

Since no through-bolt failures were observed in the fatigue tests of Specimens B1 and B2, a series of additional stiffness tests were performed on Specimen B1 with individual through-bolts sequentially removed to see what effect a through-bolt failure would have on the overall stiffness of the specimen. These tests are described in the following sub-sections.

4.3.1 Stiffness Tests with Through-Bolt Removals – Testing Procedure

For each stiffness test the specimen was loaded and unloaded quasi-statically with one additional through-bolt removed from the previous test. The tests were performed in the same manner as described in Section 3.5.1. The order of the simulated failures was similar to the welded, headed shear stud failure sequence generally observed by Porter (2016) and is described in Table 4–7.

Table 4–7: Stiffness tests with through-bolt removals testing matrix

Test Sequence	Through-Bolts Removed	Load Level (kN)
1	-	500
2	N1	355
3	S1	355
4	N2	355
5	S2	355
6	N12	355
7	S12	355
8	N11	355
9	S11	355
10	N10	355
11	S10	355
12	N9	355
13	S9	355
14	All	355

As shown in Table 4–7, the first stiffness test performed was to capture any behavioural changes of Specimen B1 after being subjected to 2,007,766 cycles during the preceding fatigue test. (Note: the results

of this test were also used in Section 4.1.) Porter (2016) observed that typically, the shear studs failed in locations with the largest interfacial slips, beginning in regions of highest longitudinal shear. Moreover, all shear studs reportedly failed within their respective row before the longitudinal shear force redistribution was significant enough to induce a failure in subsequent rows (Porter, 2016). Therefore, as described in Table 4–7, the through-bolt removal sequence began with Rows 1 and 2. Porter (2016) also found that following the failure of the studs in Rows 1 and 2, the shear studs at the far East end of the specimens began to fail next as they experienced the largest slips. As well, the interface between the concrete decks and steel girders in this region experienced a relatively lower normal force in comparison to the West end of the specimens where the normal force due the applied loading limited slip between the concrete decks and steel girders. Following the failure of Rows 1 and 2, Porter (2016) reported that subsequent failures began at Row 12 and progressively migrated towards the West end of the specimens, terminating at Row 9. After the failure of the shear studs in Row 9, further testing was typically ceased (Porter, 2016).

4.3.2 Stiffness Tests with Through-Bolt Removals – Load-Deflection Results

The maximum deflection of Specimen B1 was recorded during the through-bolt removal investigation to determine what effect the removal of each subsequent through-bolt row, or equivalently, the theoretical failure of each subsequent through-bolt row, had on the global behaviour of the specimen. The maximum deflection results are displayed in Figure 4–24. Note that the legend values for all figures in this section, indicate the number of through-bolts that were removed.

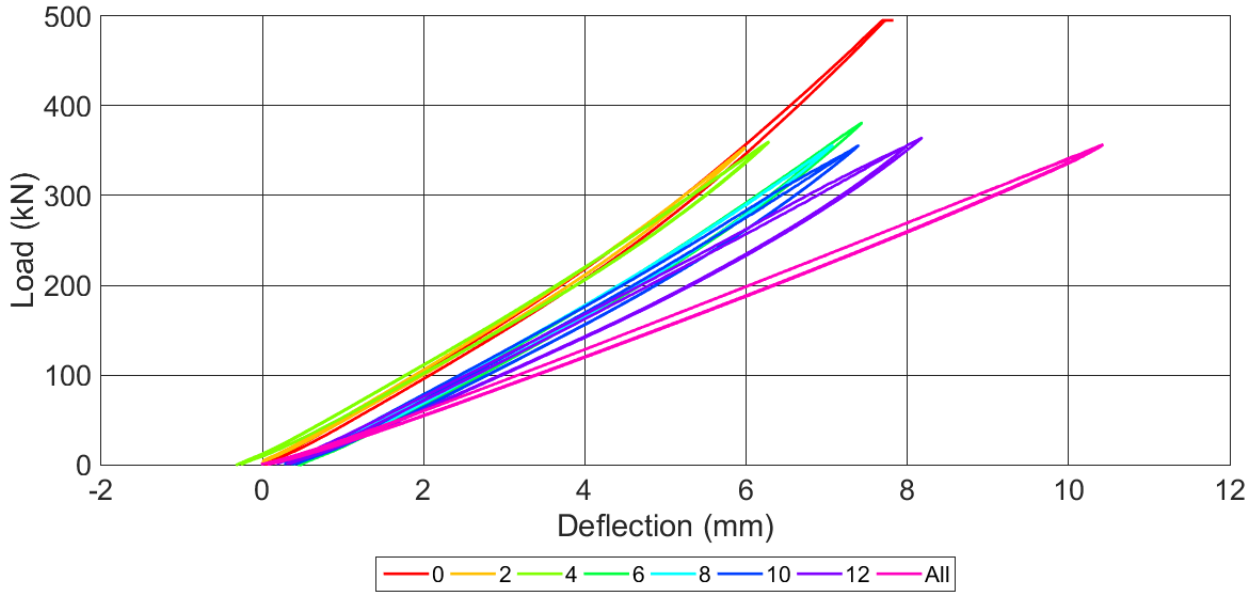

Figure 4–24: Stiffness tests with bolt removals – maximum deflection results

As is evident in Figure 4–24, the stiffness of the load-deflection curves for Specimen B1 decreased noticeably with each through-bolt row of removed. This behaviour was expected as the removal of each through-bolt reduces the degree of shear connection, resulting in a less stiff specimen response. As illustrated in Figure 4–24, a significant decrease in the maximum deflection occurred after the removal of six through-bolts. This corresponds to the removal of through-bolt Row 12. Since the loading was applied at the West end of the specimen, through-bolt removals at the East end of the specimen had a more profound effect on the stiffness of Specimen B1 since there was no applied normal force augmenting the shear connection due to the interfacial friction between the concrete deck and steel girder in this region.

Once again, a change in the unloaded position of the specimen was observed following the removal of each through-bolt row. This implies that the removal of each through-bolt row allowed for the repositioning of the specimen, establishing a new position of the concrete deck relative to the steel girder.

The maximum peak deflection exhibited by Specimen B1 at the 355 kN load level is presented in Table 4–8 for the stiffness tests performed after the removal of each through-bolt row along with a comparison to their original displacements prior to the removal of any through-bolt.

Table 4–8: Summary of maximum deflection at 355 kN load level with through-bolts removed

Number of Bolts Removed	Deflection (mm)	Change Relative Original Specimen
0	5.975	0%
2	5.981	0%
4	6.204	4%
6	7.011	17%
8	7.066	18%
10	7.379	23%
12	7.991	34%
24	10.376	74%

Table 4–8 reveals that the maximum deflection of the overall specimen at the 355 kN level, increases considerably after the removal of the first three rows of through-bolts and then fairly constantly afterwards. The maximum deflection values are plotted in Figure 4–25.

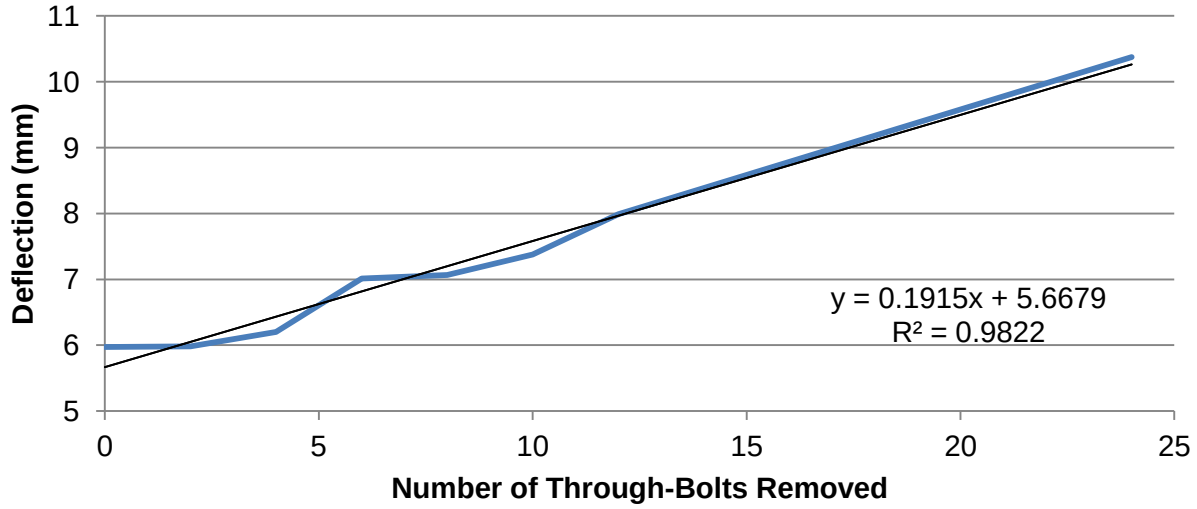

Figure 4–25: Maximum deflection versus number of through-bolts removed

As illustrated in Figure 4–25, the incremental increase in maximum deflection subsequent to each through-bolt row removed was fairly constant. A linear regression analysis, modelling the relationship between the maximum deflection and the number of through-bolts removed is displayed in Figure 4–25. The results of this regression analysis indicate that for each through-bolt removed, the maximum deflection increased by approximately 19% with an R^2 value of 98%.

The maximum deflection results for the through-bolt removal investigation were overlaid on the same figure as the calculated theoretical deflections for comparative purposes. The theoretical deflections for a fully composite beam and a single steel W250x49 girder are provided. The load-deflection plots shown in Figure 4–26 feature the zero-load starting point of each hysteresis loop beginning at the origin (0 kN and 0 mm of slip). This was done to allow for a more direct comparison of the slopes.

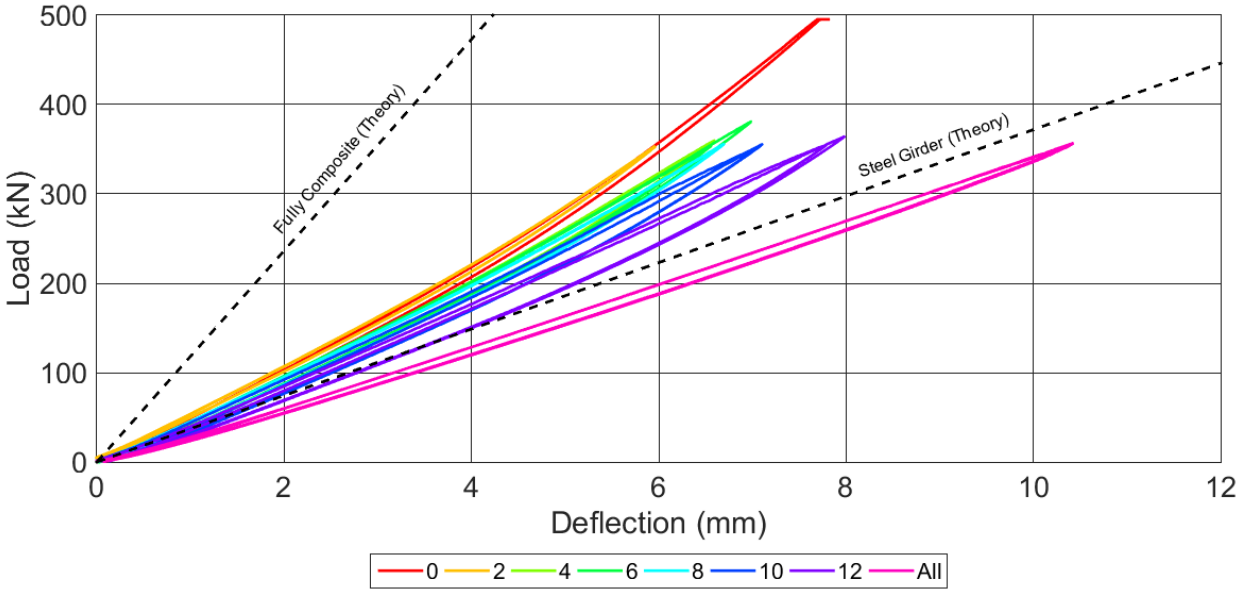

Figure 4–26: Stiffness tests with through-bolt removals – comparison with theoretical stiffness models

Figure 4–26 indicates that as each row of through-bolts was removed, the load-deflection curve of Specimen B1 approached the predicted theoretical response of a steel girder. Moreover, the behaviour of the non-composite beam very closely approximates the theoretical response of the steel girder, indicating that steel girder controls the behaviour of the specimen when no composite interaction is present. It is important to recall that the theoretical deflection calculations neglected the effects of shear deformations as Porter (2016) found that shear deformations accounted for only approximately 9% of the total deflection. Therefore, it is understandable that the deflection curve for Specimen B1 is slightly below the theoretical deflection curve for the steel girder on its own.

4.3.3 Stiffness Tests with Through-Bolt Removals – Interfacial Slip

The interfacial slips between the concrete deck and steel girder were recorded during the through-bolt removal investigation. The recorded slips were used to quantify any degradation in shear connection as a consequence of the removal of each subsequent through-bolt. Same as before, the relative slip of the

concrete deck with respect to the steel girder is positive when the movement is towards the right and hence negative towards the left. Plots of Slip 1 (West end, X = 0 mm) and Slip 5 (East end, X = 3000 mm) are provided in Figure 4–27 and Figure 4–28 respectively as representative examples.

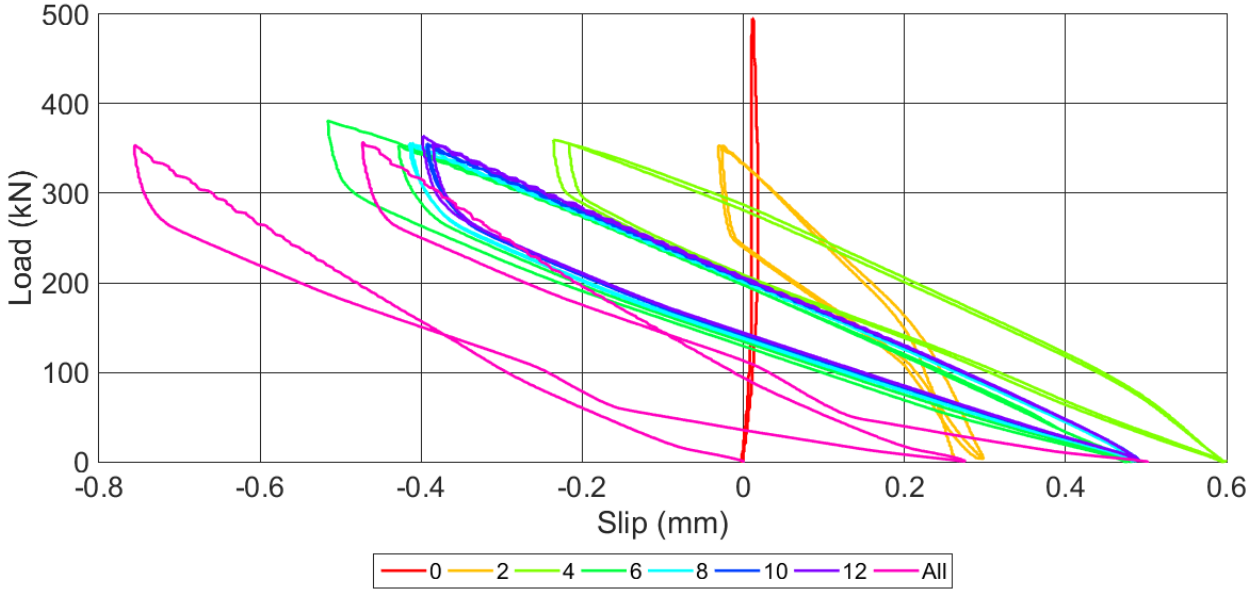

Figure 4–27: Stiffness tests with through-bolt removals – Slip 1 load-slip plot

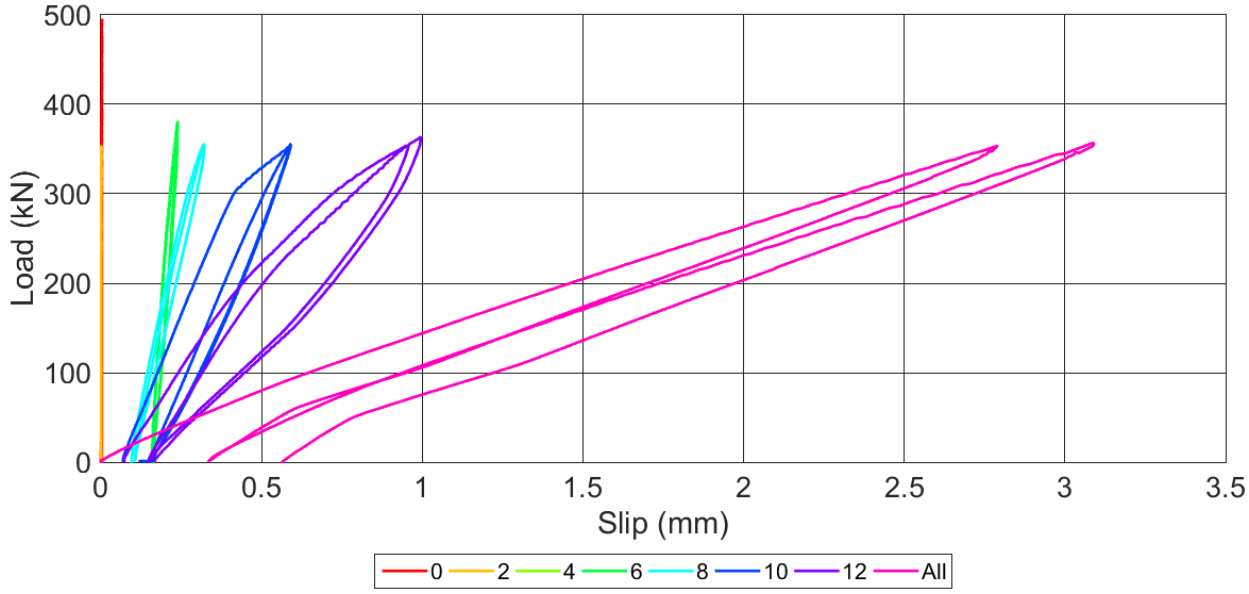

Figure 4–28: Stiffness tests with through-bolt removals – Slip 5 load-slip plot

Similar to the vertical displacements, the unloaded position of the concrete deck relative to the steel girder changed following the removal of each through-bolt row. This is expected, since the progressive removal

of through-bolts reduces the shear transfer between the concrete deck and steel due to friction and other mechanisms (e.g., dowel action, direct shear), and thus decreases the composite action. As a result, interfacial slip increases as through-bolts are removed. Figure 4–27 reveals a change in the sense of the interfacial slip after the removal of two through-bolts. When through-bolts were removed, the concrete deck became less constrained and could move in ways that it previously could not. Also, once the through-bolts were removed, the elastic restoring forces within the steel girder and concrete deck were not resisted by the presence of through-bolts. Moreover, Figure 4–27 and Figure 4–28 reveal that the slopes of the load-slip curves decrease significantly after the through-bolts in the immediate vicinity of the LVDT of interest were removed. For instance, as shown in Figure 4–27, the load-slip curve displayed virtually no slip until after the first row of through-bolts was removed. The first row of through-bolts corresponds to Through-Bolts N1 and S1, which were the closest through-bolts to the LVDT recording Slip 1. Once these through-bolts were removed, the slope of the load-slip curve for Slip 1 decreased significantly. The same behaviour was observed for Slip 5. As shown in Figure 4–28, the load-slip curve displayed virtually no slip until after the third row of through-bolts had been removed, including Through-Bolts N12 and S12, which were closest to the LVDT recording Slip 5. A slip profile along the span with each row of through-bolts removed is plotted in Figure 4–29.

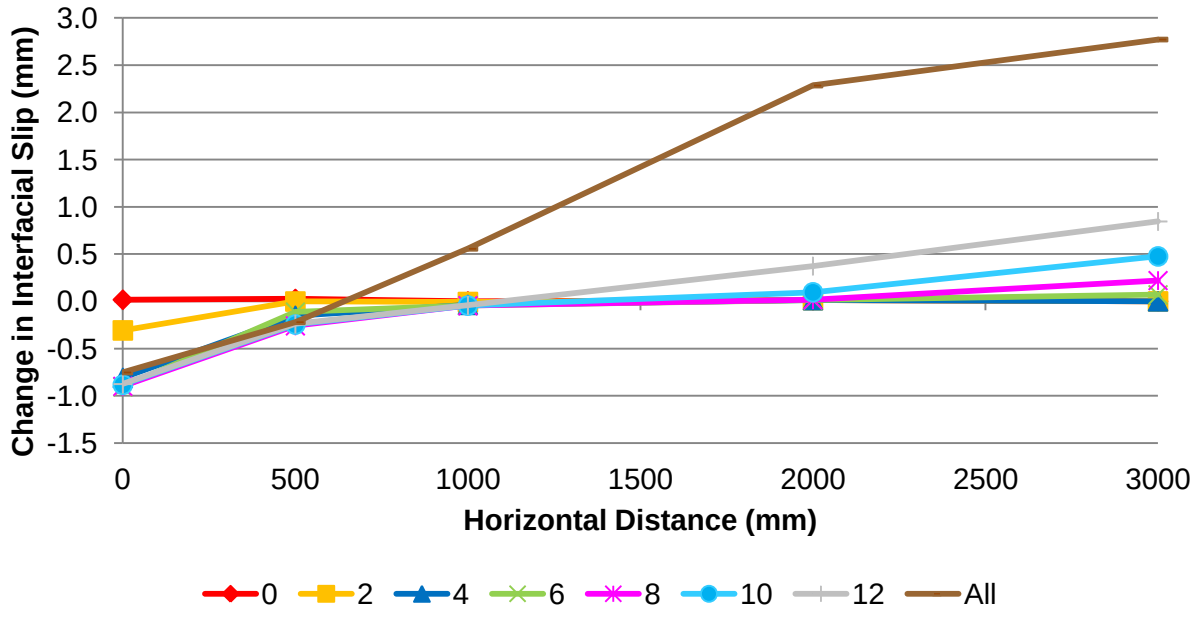

Figure 4–29: Stiffness tests with through-bolt removals – interfacial slip profile at 355 kN load level

Figure 4–29 reveals that the largest slips exhibited by Specimen B1 occurred at both the West and East ends of the specimen. This result was expected as the longitudinal shear forces acting at the interface

between the concrete deck and steel girder are the highest at the West end of the beam and the through-bolts were removed from the specimen ends first.

Furthermore, Figure 4–29 reveals that Specimen B1 exhibited relatively small initial slips prior to the removal of any through-bolts. Increasingly larger slips were observed as more and more through-bolts were removed with the highest slips occurring when all through-bolts were removed. This behaviour was expected as it is intuitive that the interfacial slip between the concrete deck and steel girder would progressively increase with the decrease in mechanical shear connectors resisting the slip. Additionally, as the number of through-bolts decreased, the normal force acting between the concrete deck and steel girder decreased, which resulted in less friction resisting the slip.

4.3.4 Stiffness Tests with Through-Bolt Removals – Strain Profiles and Concrete Deck Force

The strain profile of the steel girder was measured along the length of Specimen B1 and recorded during the stiffness tests with through-bolt removals at Profiles A, B, Y, and Z. Strain profiles were created to quantify any loss in shear connection due to the removal of each subsequent through-bolt.

The strain profiles for Specimen B1 at the 355 kN load level are illustrated in Figure 4–30. Once again, the strain profiles are plotted overtop the specimen cross-section geometry. The theoretical strain profile, assuming a fully composite section, is plotted for comparison purposes.

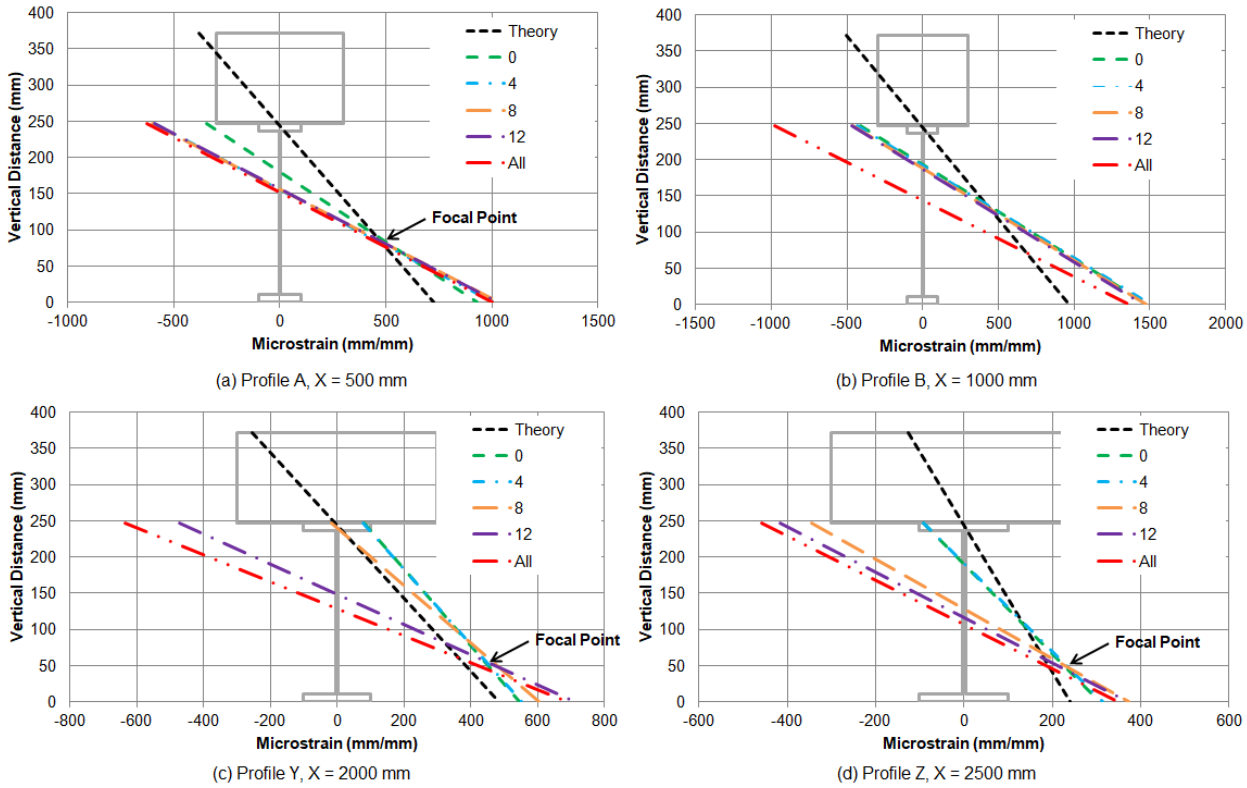

Figure 4–30: Stiffness tests with through-bolt removals – strain profiles at the 355 kN load level

As expected, the slopes of the strain profiles for Specimen B1 decreased throughout the progression of the removal of the through-bolts. This continual decrease in slope indicates a corresponding incremental increase in the strain discontinuity between the strain profiles in the steel girder and the concrete deck, representing a decrease in shear connection and increase in slip. This decrease in slope, or equivalently, increase in curvature, is accompanied by a repositioning of the neutral axis in the steel girder as a result in the decrease in the degree of shear connection. As the neutral axis in the steel girder migrated downwards, the force carried by the through-bolts became less and less until the neutral axis of the steel girder corresponded with the geometric centroid of the steel girder 123.5 mm from the bottom. Similar to the maximum deflection results, Figure 4–30 reveals a significant decrease in the slope (increase in curvature) of the strain profiles after the removal of six rows of through-bolts.

The net compressive forces in the concrete deck were calculated using the strain profiles in the steel girder at Profiles A, B, Y, and Z using the same procedure as described previously. Table 4–9 summarizes the resultant compressive forces present in the concrete deck at the 355 kN load level as the through-bolts were progressively removed. Also shown in Table 4–9 is the percentage change of the force in the

concrete deck from the predicted value according to theoretical force for a fully composite section. The resultant compressive forces in the concrete decks in Table 4–9 are shown graphically in Figure 4–31.

Table 4–9: Concrete deck compression resultant Results at the 355 kN load level with through-bolts removed

Profile	A		B		Y		Z	
X (mm)	500		1000		2000		2500	
	Deck Force, C_R (kN)	Change rel. to Theory	Deck Force, C_R (kN)	Change rel. to Theory	Deck Force, C_R (kN)	Change rel. to Theory	Deck Force, C_R (kN)	Change rel. to Theory
Theory (Full Comp.)	436.3	-	581.8	-	290.9	-	145.4	-
0	357.3	-18.1%	653.4	12.3%	383.2	31.7%	131.6	-9.5%
2	347.4	-20.4%	654.5	12.5%	384.4	32.2%	148.3	2.0%
4	255	-41.6%	654.9	12.6%	384.4	32.2%	136.9	-5.9%
6	260.9	-40.2%	613	5.4%	360.3	23.9%	115.2	-20.8%
8	265	-39.3%	618	6.2%	358.2	23.1%	16.6	-88.6%
10	264.9	-39.3%	611.6	5.1%	288.2	-0.9%	-28.9	-119.9%
12	267.7	-38.6%	603.2	3.7%	147.1	-49.4%	-27.5	-118.9%
All	230.7	-47.1%	231.6	-60.2%	31.5	-89.2%	-68.3	-147.0%

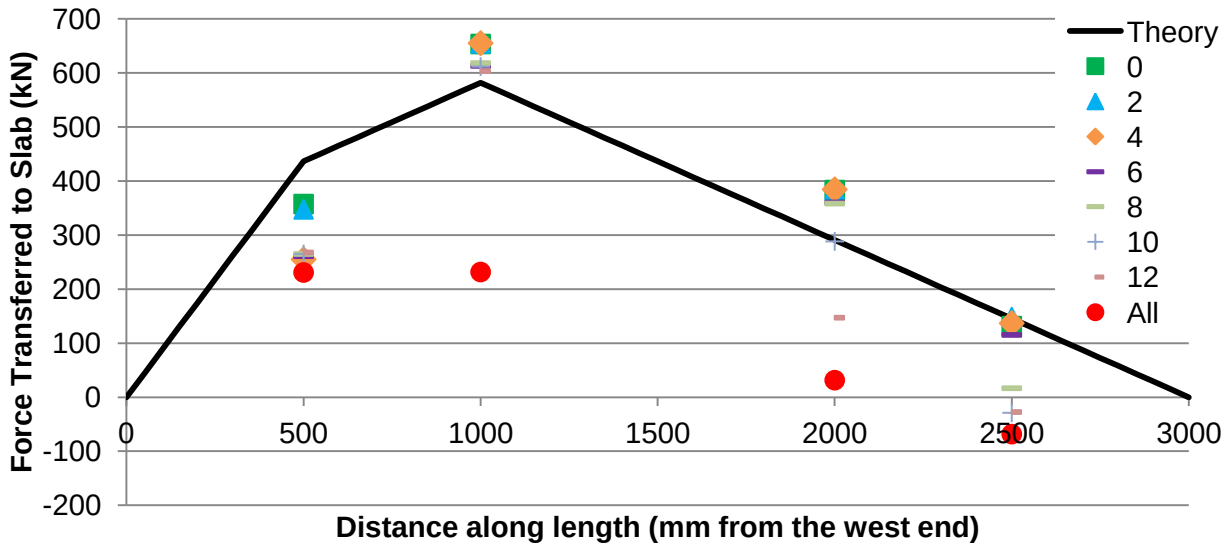

Figure 4–31: Stiffness tests with through-bolt removals – concrete deck compression resultant force at 355 kN load level

An important observation from Figure 4–31 is the two non-zero axial forces within the concrete deck at Profiles A and B for the configuration where all of the through-bolts have been removed. As illustrated in Figure 3–9, Profiles A and B correspond to the location of the applied loading. This implied that the interfacial friction acting between the concrete deck and steel girder, provided a non-trivial mechanism of longitudinal shear transfer where a sufficiently large normal force existed.

These findings provided sufficient information to compute the actual coefficient of friction acting between the concrete deck and steel girder for Specimen B1. The coefficient of friction was computed by taking the ratio of the force of friction to the applied normal force. The force of friction in this case was the average force acting on the concrete deck between Profiles A and B (231.15 kN) and the applied normal force was equal to the applied loading acting on the concrete deck at the same location (355 kN) alone since all of the through-bolts were removed. These values yield a coefficient of friction of 0.65. Interestingly, CSA S6, Clause 8.16.7.6.4.1 specifies a coefficient of friction of 0.6 in a concrete and steel shear interface (CSA S6, 2014), which is close to 0.65.

4.4 Ultimate Strength Test Results

One of the primary objectives of this research project was to determine the load-slip curve for through-bolt shear connectors using a large-scale beam test, thus confirming the appropriateness of using a push test to approximate the connector behaviour and assess its performance. Therefore, two static beam tests to failure were performed. The first was performed on the already fatigue tested Specimen B2 and the second was performed on the untested Specimen B3. Both specimens were loaded as described in Section 3.6 using a single line load (across the width of the slab) at the midspan to maximize the longitudinal shear force acting on the connectors along the entire length of the beam. Since it was concluded that the fatigue damage incurred by Specimen B2 was minimal, it is believed that this damage did not significantly influence the results described in this section.

The twelve staggered through-bolts in Specimen B2 were left unaltered after fatigue testing as it was suspected that little or no fatigue damage was incurred. Specimen B3 featured four through-bolt shear connectors at either end of the specimen. This through-bolt arrangement was chosen to mimic the push tests conducted on the same through-bolt shear connectors by Chen (2013), which also had four shear connectors on each concrete deck–steel girder shear plane. This made a direct comparison possible between the results obtained from the described beam test and the experimental findings of Chen (2013).

4.4.1 Ultimate Strength Tests – Specimen Failure Results

The ultimate static strength tests were conducted until either the failure of the through-bolts or until excessive deformations were observed, rendering further testing unsafe.

Specimen B2 was loaded until the overall deflections resulted in the specimen beginning to slide off the roller supports at the far ends. At this instance, the bottom flange had already yielded and the top flange already experienced compression buckling. Moreover, the top surface of the concrete deck had experienced significant crushing and the bottom of the concrete deck experienced significant cracking due to the application of the point load. The cracks on the underside of the concrete deck provide an indication that the specimen was likely behaving in a non-composite manner towards the end of the test. The overall final failure condition of Specimen B2 is shown in Figure 4–32.

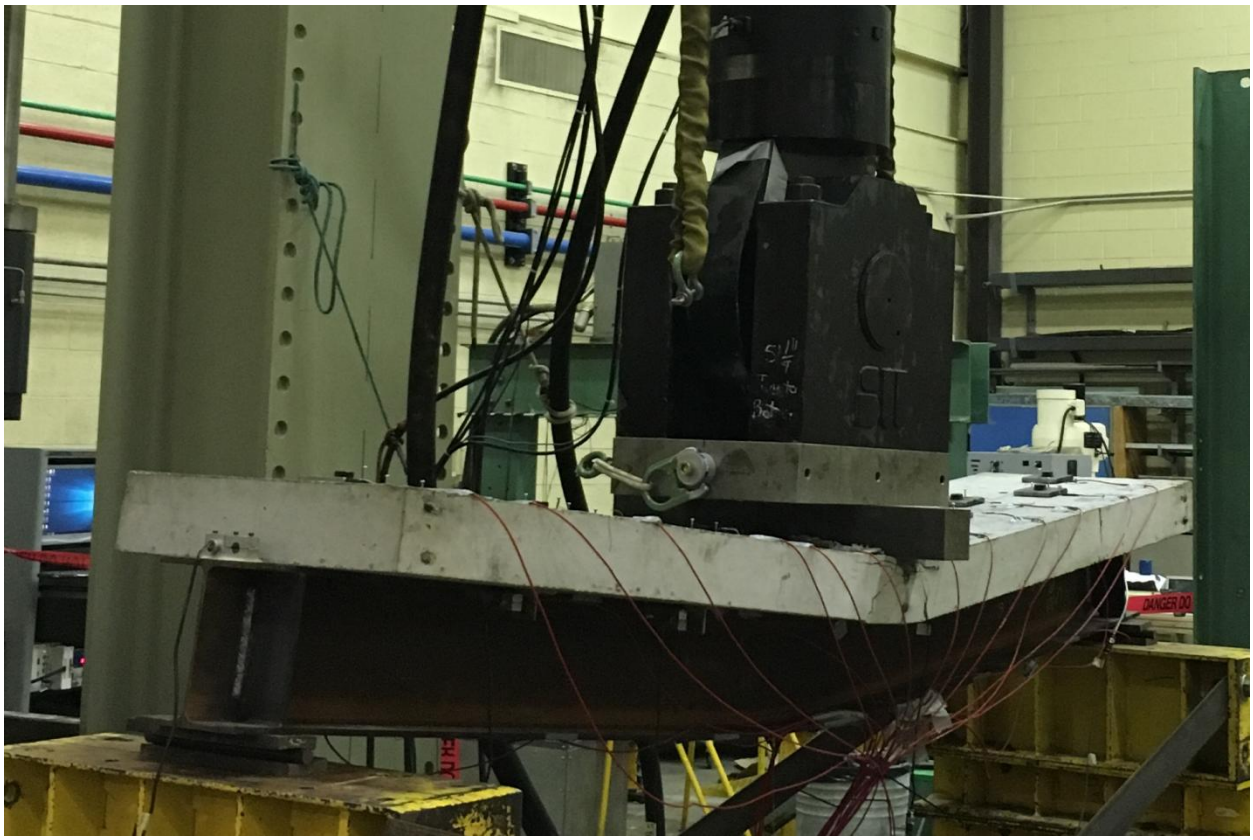

Figure 4–32: Specimen B2 at the end of ultimate strength testing

An autopsy of Specimen B2 revealed that the through-bolts experienced significant plastic deformation. However, none had completely fractured into two pieces. As shown in Figure 4–33, the through-bolt rows at the ends of the specimen (Rows 1 and 12) experienced the most significant plastic deformation. Also shown in Figure 4–33, the remaining rows experienced a decreasing amount of plastic deformation from the specimen ends towards the middle where through-bolt Rows 5 and 6 observed no plastic visible deformation. This behaviour was expected because the load was applied at the midspan of the specimen meaning that the normal force was the highest and the maximum bending moment was at the midspan.

Therefore, no slip was expected at the midspan of the specimen. Conversely, the far ends of the specimens were furthest away from the applied load and therefore experience the least normal force and based on mechanics, were anticipated to display the largest plastic deformation due to interface slip.

Figure 4–33: Specimen B2 through-bolts S1 - N12 (Left to Right)

Specimen B3 was loaded until all four of the through-bolts at the East end of the specimen had failed in shear. The overall deflections observed by Specimen B3 were slightly less than that observed by Specimen B2 at the time the testing was stopped. However, the occurrence of the last through-bolt failure was followed by a slight increase and then decrease in load, at which time it was concluded that the specimen has already surpassed its peak maximum obtainable load and the test was terminated. Similar to Specimen B2, the bottom flange of Specimen B3 yielded and the top flange also experienced compression buckling. After the conclusion of the testing of Specimen B2, it was decided that whitewashing the steel girder and concrete deck of Specimen B3 would be beneficial to observe the formation of yield lines during the testing. A calcium carbonate mixture was prepared and painted onto the side of Specimen B3, which when cured was very brittle. As shown in Figure 4–34, the brittleness of the whitewashing resulted in cracking in locations of high stress intensity causing yielding.

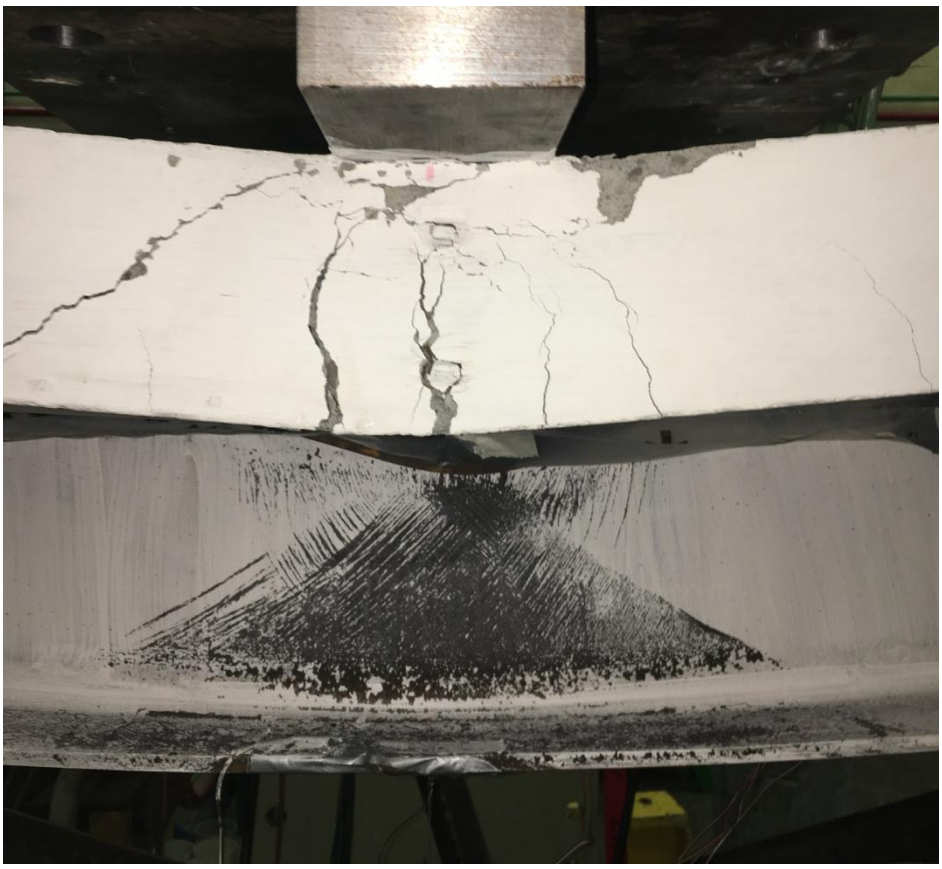

Figure 4–34: Whitewash cracking at the midspan of Specimen B3 at failure

Moreover, similar to Specimen B2, the top surface of the concrete deck of Specimen B3 experienced crushing due to the application of the point load and the bottom of the concrete deck experienced significant cracking, similarly indicating the presence of tensile forces within the bottom of the concrete deck. The overall final failure condition of Specimen B3 is shown in Figure 4–35.

Figure 4–35: Ultimate strength testing frame and setup of Specimen B3

An autopsy of Specimen B3 revealed that the all of the through-bolts on the East end of the specimen had sheared off completely. As shown in Figure 4–35, the shearing of Through-Bolts N11 and S11 was accompanied by a significant release of energy, which caused them to be ejected from the specimen along with their bearing plates. The through-bolt rows at the West end of the Specimen B3 experienced significant deformations. However, they did not fail and remained intact. It is suspected that Specimen B3 may have exhibited an unsymmetrical failure mechanism with through-bolts only on the East end of the specimen failing because the through-bolts on this end had a slightly lower initial pretension prior to the

commencement of the ultimate strength test. The initial through-bolt pretension magnitudes for the West and East ends of Specimen B3 are presented in Table 4–10.

Table 4–10: Specimen B3 Initial Through-Bolt Pretension Magnitudes

Location	West End				East End			
Through-Bolt	N1	S1	N2	S2	N11	S11	N12	S12
Initial Strain (Microstrain)	2186.8	2069.9	2268.8	2208.5	2078.0	2071.5	2016.7	2387.8
Initial Pretension Level (kN)	86.62	81.99	89.87	87.48	82.31	82.05	79.89	94.58
Initial Average Pretension (kN)	86.49				84.71			

The through-bolts on the East end of Specimen B3 failed in shear within the threads at the location of interface between the concrete deck and steel girder. A typical failed through-bolt is shown in Figure 4–36 and Figure 4–37.

Figure 4–36: Typical through-bolt failure

Figure 4–37: Typical failure shear surfaces of hex nut (Left) and through-bolt (Right)

4.4.2 Ultimate Strength Testing Load-Deflection Results

The midspan deflections of Specimens B2 and B3 were recorded during the ultimate strength tests to determine the global load-deflection curve as the specimens were loaded to failure statically. The comparative stiffness and ultimate capacity of the two specimens was of particular interest and the effects that the failure of one or multiple through-bolts on the overall load-deflection curve was also of significance. The maximum deflection results are plotted in Figure 4–38.

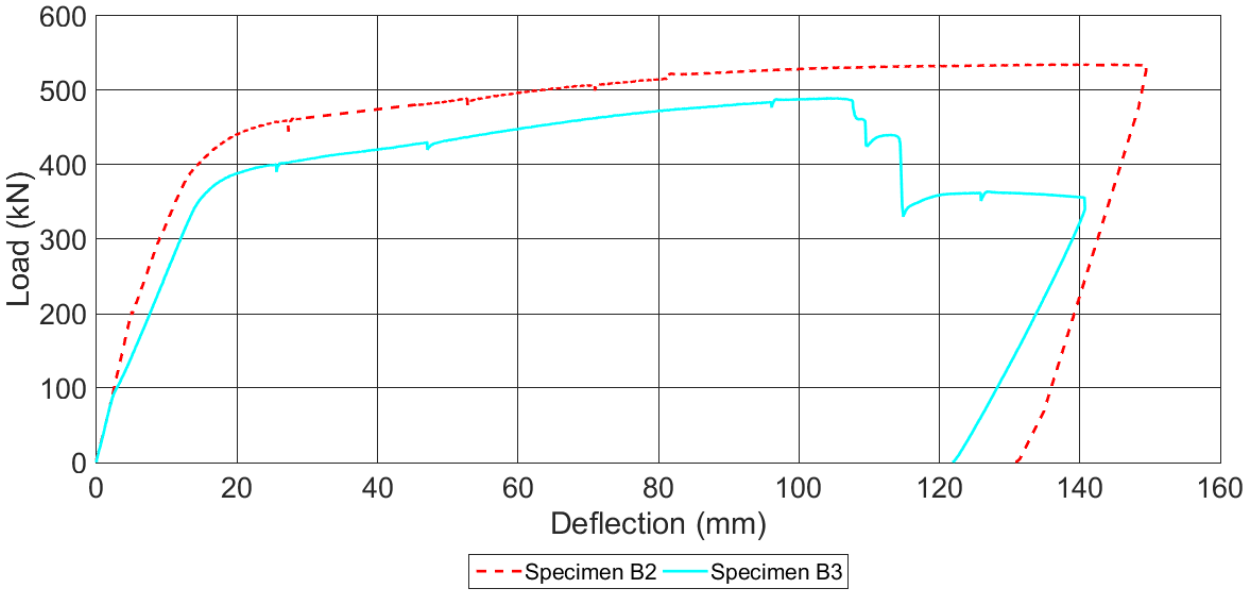

Figure 4–38: Midspan load vs. deflection results for Specimens B2 and B3

As expected, the stiffness observed for Specimen B2 was identical to the stiffness observed for Specimen B3 up until the onset of slip of the specimens, which first occurred at the East ends of the specimens at 97.4 kN for Specimen B3 and then at 200.2 kN for Specimen B2. This is observable in Figure 4–38 as the slope of the load-deflection curve for Specimen B2 (39.2) was approximately equal to the slope of the load-deflection curve for Specimen B3 (38.1) up until the onset of slip, which occurred first for Specimen B3 at 97.4 kN on the East end. This behaviour was expected because Specimen B3 included fewer through-bolts, resulting in an overall lower normal force preventing slip between the deck and steel girder. Moreover, Specimen B3 had all of the through-bolts grouped at the ends of the specimen, with a lubricated interface between the concrete deck and the steel girder between the through-bolt groupings. Conversely, Specimen B2 featured a continuous spacing of through-bolts along the span length with no lubrication provided, rendering the full use of the frictional characteristics between the concrete deck and steel girder along the entire span length, increasing the force of friction required to be overcome for the occurrence of slip.

Furthermore, as anticipated, the stiffness of the load-deflection curve for Specimen B2 was greater than the stiffness of the load-deflection curve for Specimen B3 after the onset of slip as illustrated in Figure 4–38 by the difference in slope of the load-deflection curves. Lastly, Figure 4–38 reveals that the failure of a through-bolt is preceded by an increase in the load carried by Specimen B3 until the sudden fracture of a through-bolt occurs, resulting in an immediate decrease in the specimen load. This pattern continues for each subsequent through-bolt failure. Following the failure of a through-bolt, the load becomes redistributed to the remaining through-bolts until they too become overloaded and fail.

4.4.3 Ultimate Strength Testing Interfacial Slip

The interfacial slip between the concrete decks and steel girders was recorded during the ultimate strength tests using LVDTs placed along the length of Specimen B2 and Specimen B3. The same five LVDTs that were present during the fatigue testing of Specimen B2 were used located at 0 mm, 500 mm, 1000 mm, 2000 mm, and 3000 mm from the West end of the specimen. As before, the recorded slip measurements from these LVDTS were labelled as Slip 1 through Slip 5. It was determined that Slip 3 was unnecessary, given the symmetrical loading configuration during the ultimate strength tests. Therefore, Specimen B3 featured four LVDTs, which were placed at 0 mm, 500 mm, 2500 mm and 3000 mm from the West end of the specimens and were labelled as Slip 1, Slip 2, Slip 4, and Slip 5 respectively. The recorded slips were used to quantify the magnitude and direction of interfacial slip between the concrete decks and steel girders during the testing.

Plots of Slip 1 (West end of specimens, X = 0 mm) and Slip 5 (East end of specimens, X = 3000 mm) for both Specimen B2 and Specimen B3 are provided in Figure 4–39 and Figure 4–40 respectively as representative samples of the trends and behaviour for each specimen. It is important to note that larger overall maximum deflections were anticipated for the ultimate static strength testing in comparison to the previously discussed fatigue testing. Therefore a string pot replaced the LVDT measuring the maximum deflection. However, the same LVDTs, measuring the relative slip on Specimen B2 for the fatigue testing were used for the ultimate static strength testing of Specimen B2. During the test, however, it was discovered that these LVDTs did not have a sufficient stroke capacity to accommodate the significant levels of slip observed during the ultimate strength testing. Slip 1 was reset during the test to capture the full slip magnitude. Unfortunately, the remaining LVDTs were not reset and therefore do not represent the complete load-slip curve at their respective locations. This error was corrected for the ultimate testing of Specimen B3 by installing LVDTs with a longer stroke range.

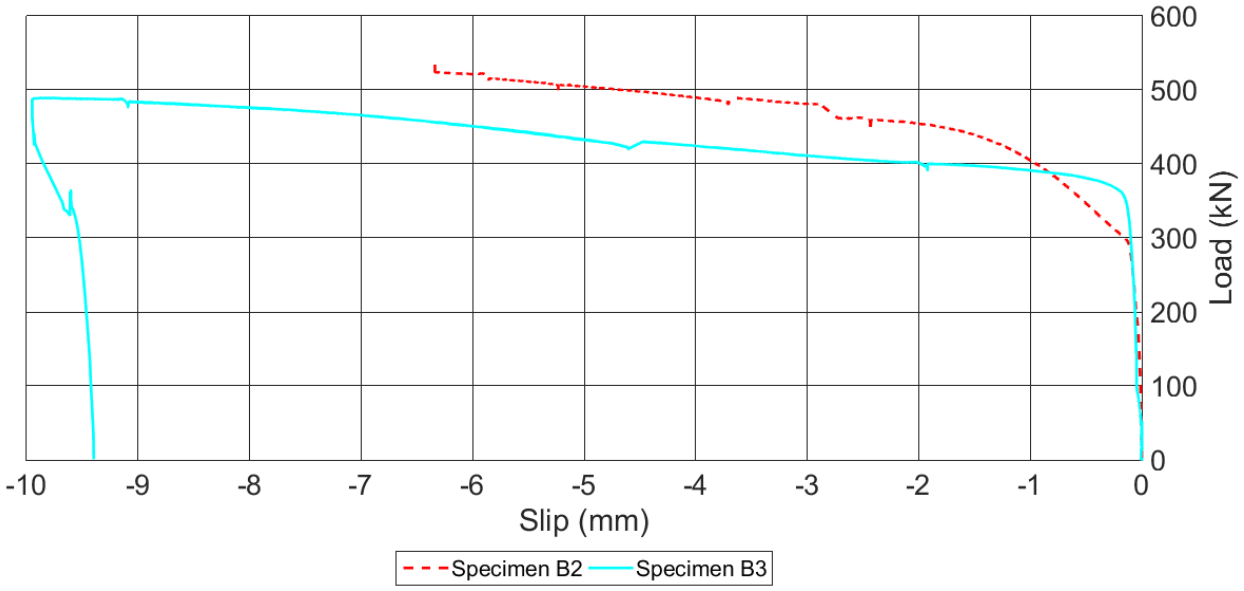

Figure 4–39: Slip 1 load-slip plots for Specimens B2 and B3

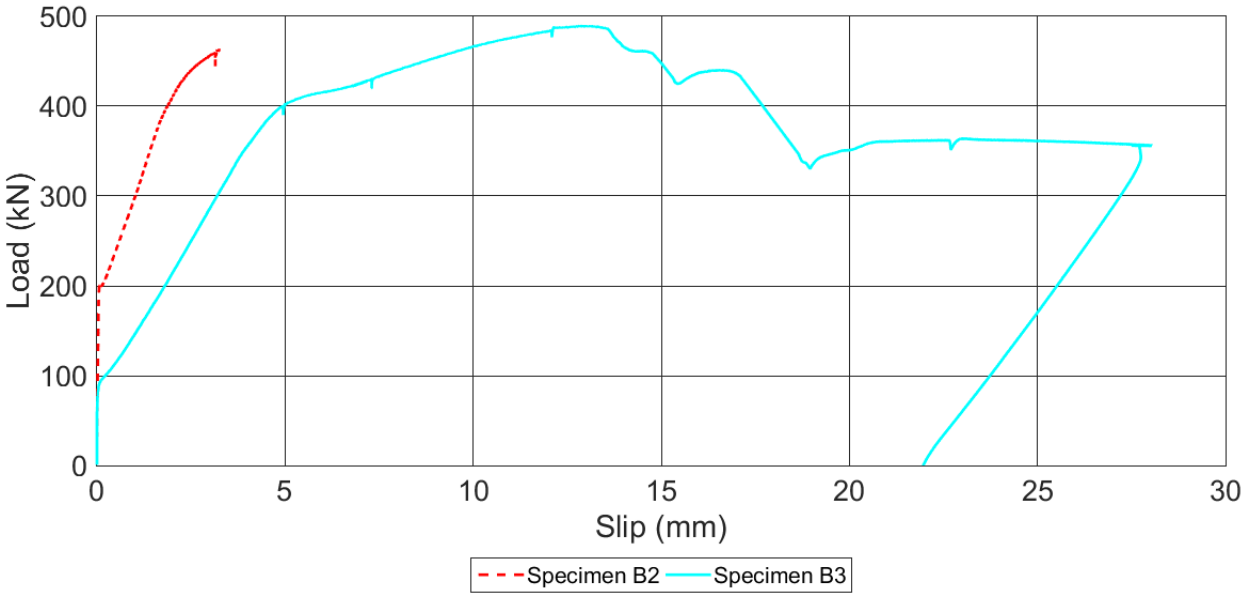

Figure 4–40: Slip 5 load-slip plots for Specimens B2 and B3

The Specimen B2 test did not result in any through-bolt failures, the load-slip curves in Figure 4–39 are smooth and continuous with no abrupt changes in curvature. Conversely, the load-slip curve for Specimen B3 in Figure 4–40 shows two small drops in load at approximately 14.8 mm and 15.0 mm of slip and one large drop in load at approximately 17.2 mm of slip. All of the through-bolt failures occurred on the East end of the specimen. Consequently, the Slip 1 load-slip curve in Figure 4–39 does not show similar drops in load as none of the through-bolts at the West end of the specimen failed.

Subsequent to the 356.7 kN and 406.4 kN load levels, the slope of the load-slip curves for Specimen B3, decreased in Figure 4–39 and Figure 4–40, implying a change in the mechanism resisting the interfacial slip between the concrete deck and steel girder. It is hypothesized that at this load level, the concrete deck slipped a sufficient amount, approximately -0.16 mm on the West end and 5.23 mm on the East end of Specimen B3, such that the through-bolts engaged in bearing on the inside surface of the bolt holes in the concrete deck. These two slip magnitudes are different because the through-bolts were positioned within the specimens by hand and could not have been placed in the exact centre lines of the holes in the concrete deck and steel girder. Another interesting observation is that the slope of the loading portion of the load-slip curves after the onset of slip up until the load level where the through-bolts were believed to engage in bearing, appears to match the slope of the unloading legs of the load-slip curves for Specimen B3. This is a particularly interesting observation for Slip 1 because none of the through-bolts fractured at the West end of Specimen B3 during the test. This suggests that the through-bolts remained deformed plastically during unloading, and the interfacial friction between the concrete deck and steel

girder was the primary mechanism responsible for resisting the interfacial slip during the unloading sequence.

4.4.4 Ultimate Strength Testing Strain Profiles and Concrete Deck Force

The strain profiles of the steel girders were measured along the lengths of the specimens and recorded during the ultimate strength tests at Profiles A, B, Y, and Z as the specimens were loaded to failure. Strain profiles were created for Specimen B3 as this was the only specimen test that resulted in failures of the through-bolts. The strain profiles were created to quantify changes in the depth of the neutral axis as the through-bolts progressively failed and the specimen approached the ultimate limit state.

The strain profiles for Specimen B3 were generated at various load levels. The load-slip curve for the East end of the specimen was used as the reference for determining the points of interest to be investigated as the East end of Specimen B3 experienced through-bolt failures during the ultimate strength testing. The strain profiles for Specimen B3 were generated for the load level prior to the onset of slip, the load level following the onset of slip, the load level corresponding to when the through-bolts began engaging in dowel action, at the peak load level, and at the load level corresponding to the fracture of the first through-bolt. The results of this investigation are illustrated in Figure 4–41.

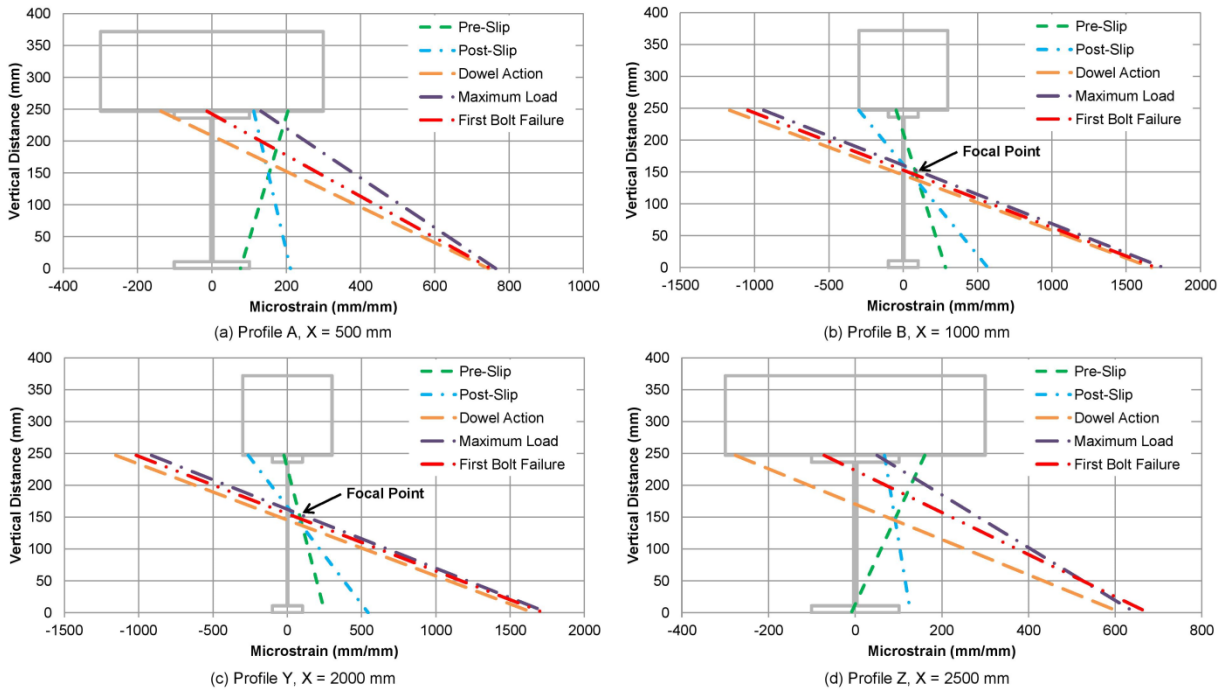

Figure 4–41: Strain profiles at (a) A, (b) B, (c) Y, and (d) Z for Specimen B3 at various load levels

Figure 4–41 (b) and (c) present strain profile results for the sections closest to the midspan, and reveal that prior to the onset of slip, the neutral axis of Specimen B3 coincided with the theoretically determined location, 244 mm from the bottom when a full shear connection is present. Immediately following the onset of slip, the neutral axis shifted downwards to approximately 162 mm from the bottom. After this, the neutral axis position varied only slightly with further increases in load. Note that at the later stages of the test, compression buckling of the compression flange was occurring, likely rendering the assumption of linear strain distributions to be of questionable validity. Figure 4–41 (a) and (d) – the sections closest to the supports – show strain profiles that are less easy to interpret, due to the likely presence of "arch action" at the supports. Given the unique configuration of Specimen B3 with through-bolts only near the ends of the specimen and friction intentionally limited, the behaviour of Specimen B3 was expected to be different from a fully composite or partially composite beam with regards to the strain profiles and the changes in the strain profiles.

The net compressive forces in the concrete deck were calculated using the strain profiles in the steel girder at Profiles A, B, Y, and Z using the same procedure as described previously. Figure 4–42 displays the resultant compressive forces present in the concrete deck at the various load levels.

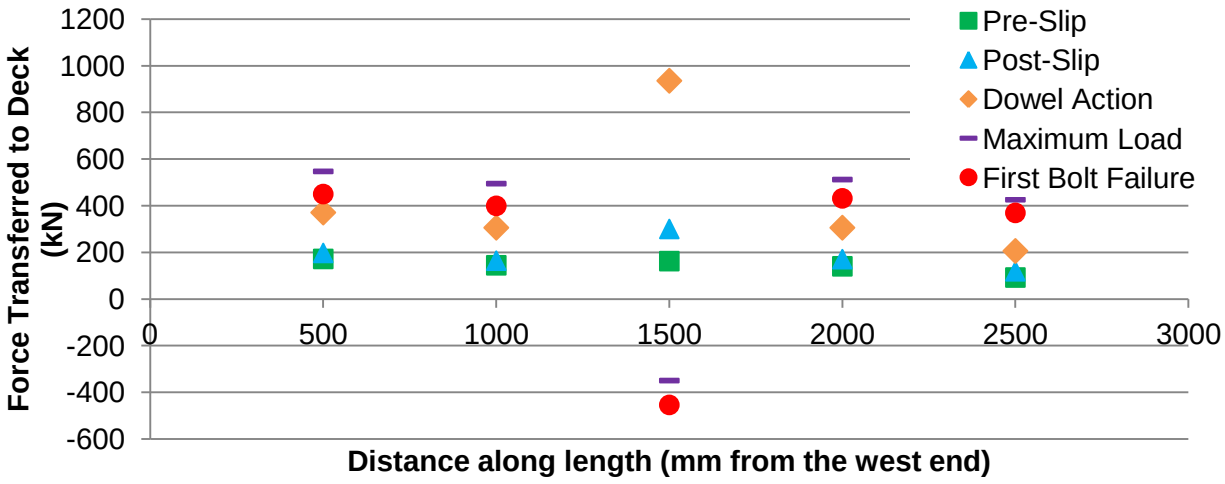

Figure 4–42: Variation of concrete deck compression resultant along length for Specimen B3 at various load levels

The results presented in Figure 4–42 were used to compute the actual coefficient of friction acting between the concrete deck and steel girder for Specimen B3. Unlike in Section 4.3.4 where the coefficient of friction for Specimen B1 was calculated for the condition where all the through-bolts were removed, the applied normal force for Specimen B3 was set equal to the tensile forces in the four through-bolts

acting on the concrete deck at the East end of Specimen B3. The East end was considered as slip occurred on this end first. The strain values in through-bolt Rows 11 and 12 at the instance of slip were used to determine the total compressive force acting on the concrete deck (333.0kN). The contribution that the applied loading at the midspan had on the normal force acting on the concrete deck at the far East end of the specimen was neglected. Moreover, the force of friction in this case was the axial force acting on the concrete deck at Profile Z (109.0 kN) at the instance of slip. These values yield a coefficient of friction of 0.33. This coefficient of friction was far lower than the value previously calculated for Specimen B1 (0.65). While this coefficient of friction was considerably different from the coefficient of friction specified by CSA S6, Clause 8.16.7.6.4.1 (0.6) (CSA S6, 2014), it was reasonably close to the coefficient of friction reported by Chen (2013) from his push test experiments (0.22).

4.4.5 Through-Bolt Load-Slip Behaviour

The load-slip curves for the through-bolts in Specimen B3 were derived using the procedure described by Oehlers & Seracino (2002) in Section 4.1.3. Using the strain gauges placed on the flanges of the steel girder at Profile A and Profile Z, the resultant force carried by the steel girder was calculated. The force resultant within the concrete deck was then set to equilibrate the girder force.

Using a MATLAB script, this analysis was performed for each data point collected throughout the ultimate strength test to obtain the variation in concrete deck force at the West and East ends of Specimen B3. The calculated concrete deck forces at the West and East ends of the specimen were then plotted against the slip level obtained at the specimen ends.

As discussed in Section 3.3, there were two LVDTs on either end of Specimen B3, one at the specimen ends and one just on the inside of the through-bolt groupings at Profile A and Profile Z. The slip values recorded by the two LVDTs on either side of the through-bolt groupings on both ends of the specimen were virtually identical, indicating that the slip between the concrete deck and steel girder was constant from the beam ends to the location of the strain gauges placed on the upper and lower flanges of the steel girder at Profile A and Profile Z. Therefore, the LVDTs at the ends of the specimen were chosen for the derivation of the load-slip curves for Specimen B3.

The load-slip curves for Specimen B3 are presented in Figure 4–43 and Figure 4–44 for through-bolt Rows 1, 2 and 11, 12 respectively. It is important to note that these load-slip curves do not provide the load-slip curve for any one bolt in particular but rather the average load-slip curve for all four through-bolts on either end of Specimen B3. Therefore, as illustrated in Figure 4–44, the load-slip curve for the through-bolt group reveals the drops in force as each through-bolt failed.

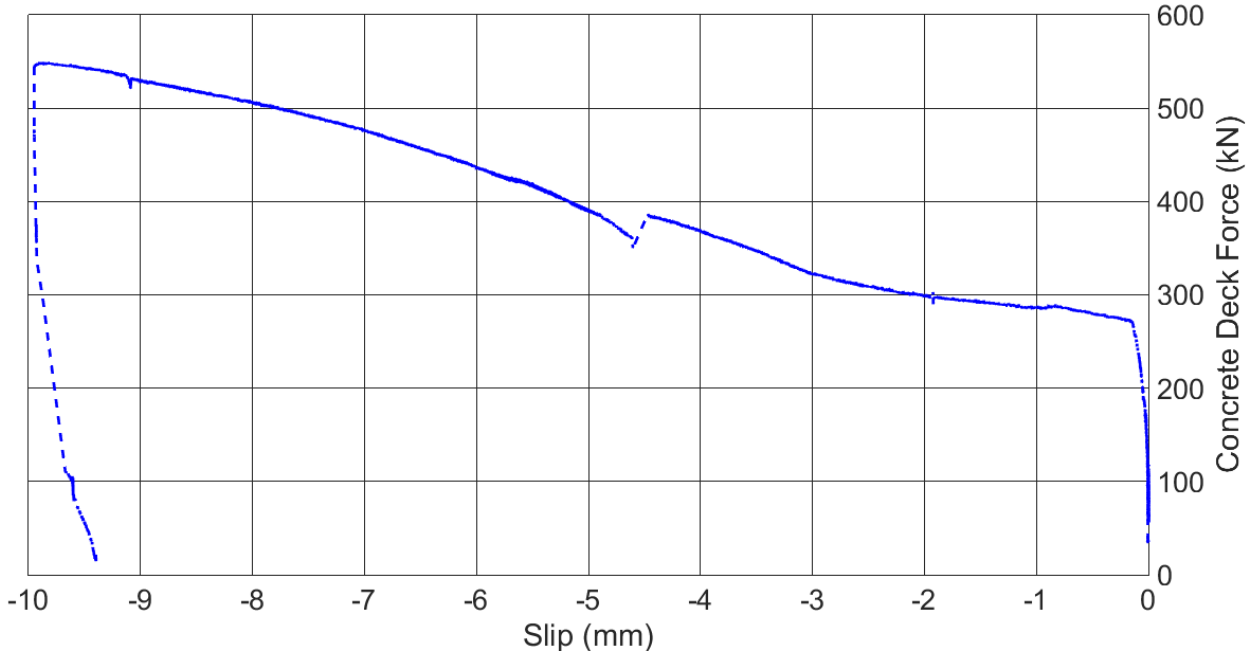

Figure 4–43: Load-slip curve for Specimen B3, through-bolt Rows 1 and 2

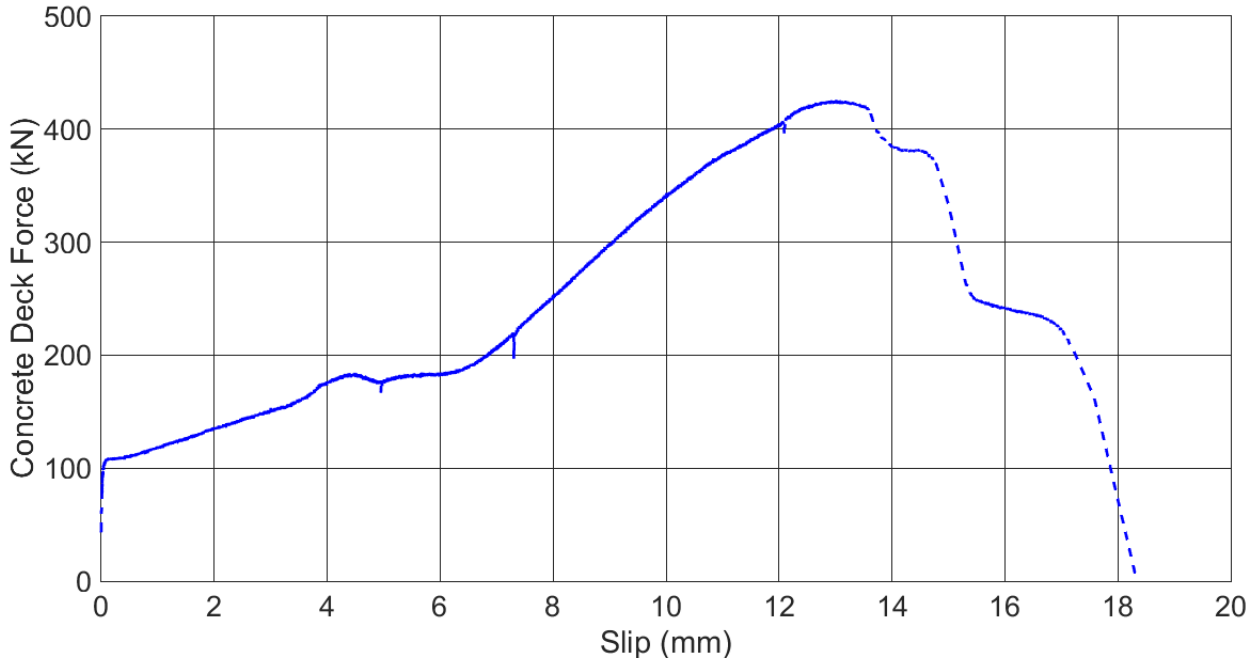

Figure 4–44: Load-slip curve for Specimen B3, through-bolt Rows 11 and 12

Figure 4–44 reveals that that following the initiation of slip at approximately 120 kN, the concrete deck began slipping consistently with only small increases in applied load until the displacement relative to the steel girder was such that the through-bolts engaged in bearing on the inside surface of the concrete deck.

The mechanism of load transfer to the concrete deck from the steel girder slowly changed from purely interfacial friction between the concrete deck and steel girder to a combination of friction and dowel action of the through-bolts. The through-bolt dowel action contribution to the overall load transfer increased in until it reached a global maximum of 425.9 kN. Shortly after reaching this maximum, Through-Bolt S12 reached its critical shear stress and failed abruptly. The load previously carried by S12 was redistributed to the remaining three through-bolts on the East end of the specimen and consequently caused Through-Bolt N12 to fail shortly after. Finally, Through-Bolts N11 and S11 failed simultaneously, eliminating all remaining mechanical shear connection between the concrete deck and steel girder at the East end of Specimen B3. This caused the force in the concrete deck at the East end to decrease to zero. The decrease in force was not abrupt because while there were no further through-bolts on the East end of the specimen transferring longitudinal shear forces, friction was still present between the concrete deck and steel girder. Table 4–11 summarizes the failure sequence of the through-bolts on the East end of Specimen B3.

Table 4–11: Specimen B3 Through-Bolt Failure Sequence

Failure Sequence	Through-Bolt	Total Applied Load (kN)	Deck Force (kN)	Interfacial Slip (mm)
1	S12	458.2	369.3	14.8
2	N12	447.8	332.7	15.0
3	N11	428.7	207.6	17.2
3	S11	428.7	207.6	17.2

4.4.6 Comparison Between Beam Test and Push Test Through-Bolt Load-Slip Behaviour

The load slip curve from the push test experiments conducted by Chen (2013) on the same through-bolts considered in this research project, are overlaid on the load-slip curve for Specimen B3 as a method of comparison between the behaviour of a through-bolt shear connector as determined using a push test versus a large-scale beam test. Recall that one objective of this project was to determine the suitability of using a push test to determine the load-slip behaviour of through-bolt shear connectors.

The load-slip curve from the push test experiments conducted by Chen (2013) is overlaid on the load-slip curves for Specimen B3 in Figure 4–45 and Figure 4–46 for through-bolt Rows 1 and 2 and 11 and 12 respectively. The data reported by Chen (2013) have been reduced by a factor of eight because it represents the total force carried by the eight through-bolt connectors in his push test specimens. Also, Specimen B3 featured four through-bolts on either end of the beam and therefore, the results in Figure 4–45 and Figure 4–46 have been reduced by a factor of four to render comparisons possible. Moreover, the load-slip curve for the East end of the specimen in Figure 4–46 was truncated at the first instance of a

through-bolt failure at 14.8 mm as the curve is intended to represent the behaviour of a single through-bolt.

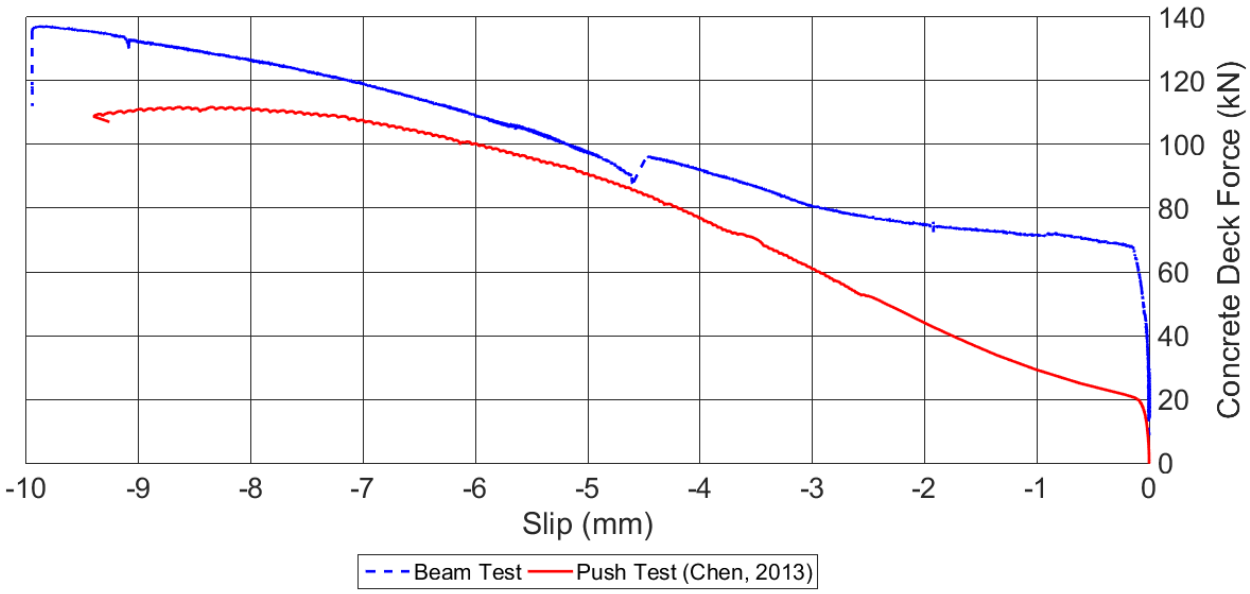

Figure 4–45: Load-slip curve for Specimen B3, through-bolt Rows 1 and 2 compared to results from Chen (2013)

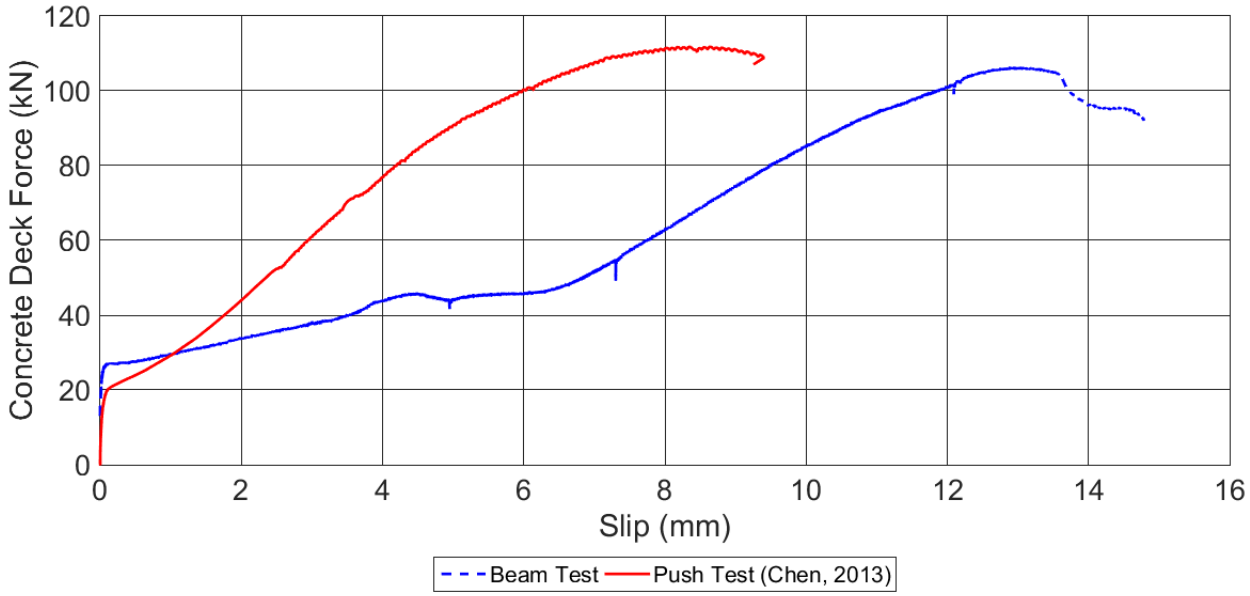

Figure 4–46: Load-slip curve for Specimen B3, through-bolt Rows 11 and 12 compared to results from Chen (2013)

While the load-slip curves presented in Figure 4–45 and Figure 4–46 respectively, each appear similar to the load-slip curve reported by Chen (2013), it is important to recall that the through-bolts on the West end of Specimen B3 had not yet failed at the end of this test. Conversely, the load-slip curve reported by Chen (2013) terminates at the ultimate capacity of the push test specimen, after the failure of the through-bolts. Therefore, the load-slip curve for the East end of the specimen, presented in Figure 4–46, is of particular interest for comparison to the load-slip curve reported by Chen (2013).

Figure 4–46 reveals that both the large-scale beam test and the push test feature a similar level of slip and a similar peak load prior to the onset of failure of the through-bolts. However, the slopes of the two load-slip curves are quite different, with the through-bolt shear connectors behaving in a less stiff manner when tested in a beam test relative to when they are tested in a push test. Moreover, the level of slip required to produce a failure of the through-bolt shear connectors is predicted to be much higher when tested using a beam test. The first instance of a through-bolt failure was observed at 14.8 mm of slip during the beam test, which is approximately 57% larger than the first occurrence of a through-bolt failure at 9.4 mm of slip when tested using a push test. This could be due to the randomized initial positioning of the through-bolts within the holes in the concrete deck and steel girder. For instance, if the through-bolts were positioned in an orientation such that they were closer to the inside edges of the holes in the concrete deck, then they would have engaged in bearing sooner and therefore stiffen the overall shear connection. This concept is described more thoroughly in Chapter 5. Lastly, the failure mechanism of the through-bolts when tested in a large-scale beam test is similar to when they are tested in a push test as observed by Chen (2013) (see Figure 4–47).

Figure 4–47: Comparison of through-bolt failures from beam test (Left) and push test (Right)

5 Analysis of Through-Bolt Connection Static Load-Slip Behaviour

The following chapter presents a mechanistic load-slip model and a non-linear FE model, each developed to predict the behaviour of a through-bolt push test specimen, and their comparison to test results completed by Chen (2013). The mechanistic model calculations may be performed by hand. However, a mathematical computer software (such as Excel or Matlab) should be used for enhanced computational efficiency. The FE model was developed using the commercial software ABAQUS.

The specifics of both models are described, including boundary conditions, material properties and all pertinent assumptions. The results of the mechanistic model and the push test FE model were validated through comparison to experimental results provided by Chen (2013).

5.1 Through-Bolt Mechanistic Model

Previously, Chen (2013) presented an equation (presented in Section 5.1.1) that predicts the ultimate capacity of a through-bolt connection. In this section, this model is extended for full load-slip behaviour prediction.

5.1.1 Mechanistic Model Formulation

The mechanistic model predicts the load slip curve by partitioning the total response of the through-bolts into the three separate stages defined by Liu et al. (2014) discussed in Section 2.2.1, assuming specific boundary conditions for each. These three stages are depicted in Figure 5–1.

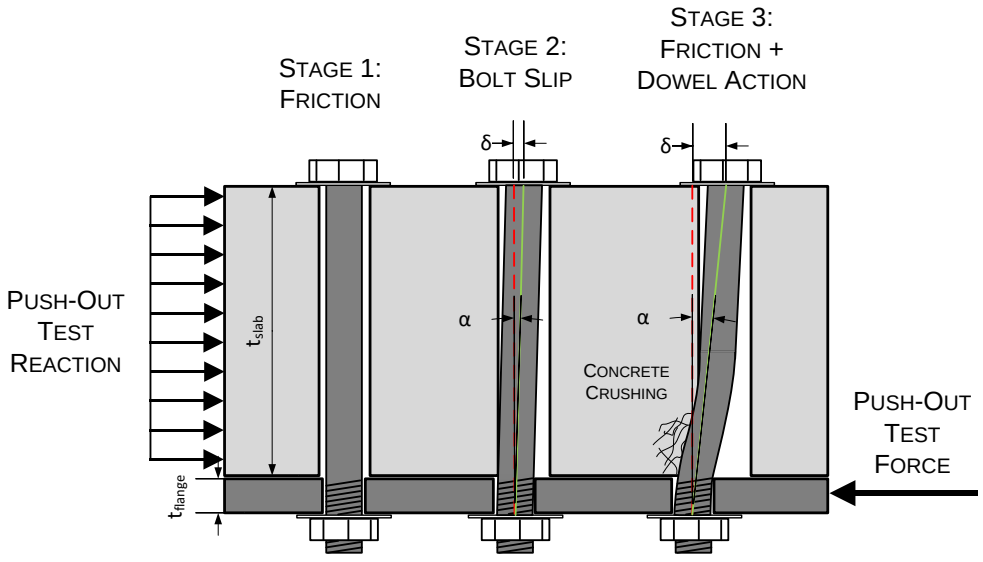

Figure 5–1: Three stages of mechanistic model analysis

An underlying assumption adopted in the mechanistic model is that subsequent to deformation, the through-bolt's ends remained fixed in the position they were initially installed in the bolt holes. This assumption simplifies the approximation of the deformed geometry of the bolt. The autopsy of the failed push test specimens performed by Chen (2013) revealed that the pre-tensioning of the through-bolts prevented slip of the bolt ends relative to the surfaces they pressed against.

Stage 1 of the response of the through-bolts during a push test, as shown in Figure 5–1, explains the initial vertical segment of the load-slip curve presented in Figure 5–2. During this stage, the applied shear force in the connection is less than the force of friction at the steel-concrete interface and therefore fails to induce slip. The through-bolt's ends are approximated as pinned at both ends during this stage. While theoretically some interfacial slip may be present during this stage, the contribution, if any, to the total interfacial slip observed at ultimate is negligible and therefore is assumed to be zero. Therefore, Stage 1 is illustrated with the load-slip curve as perfectly vertical in Figure 5–2, indicating zero interfacial slip.

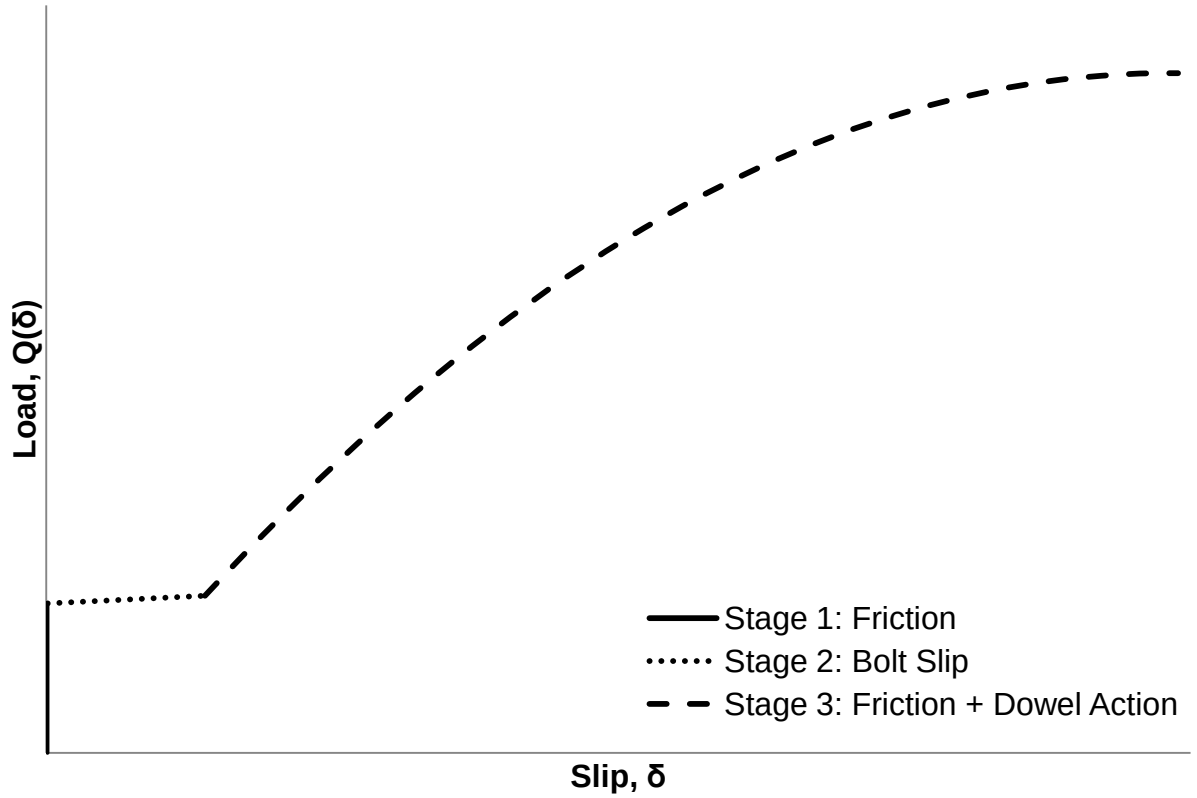

Figure 5–2: Idealized through-bolt load-slip curve

The slip load is calculated from the product of the slip coefficient (K_S), provided by Chen (2013), and the initial pretension level in the through-bolts. The initial pretension value is calculated using CSA S6 Clause 10.24.6.3, which specifies that the pretension load in the through-bolts shall be at least 70% of their minimum tensile strength (CSA S6, 2014). The initial strain in the through-bolts is then calculated using Hooke's Law. All subsequent strain calculations performed are added to this initial strain value.

Stage 2 of the response of the through-bolts during a push test represents the behaviour of the through-bolts at the onset of slip. Figure 5–2 reveals that immediately following the force of friction being overcome, Stage 2 features a large initial increase in interfacial slip between the steel and concrete interfaces, accompanied by virtually no increase in load. The magnitude of this large interfacial slip is equal in magnitude to the separation between the through-bolts and the interior surface of the bottom of the holes in the concrete decks. Stage 2 of the response of the through-bolts during a push test represents the uninterrupted slip of the through-bolts as they are brought into contact with the concrete decks from their original orientation during their installation. As a simplifying measure, the mechanistic model assumes that the through-bolts engage in bearing against the concrete decks immediately after the onset of slip. This was done to avoid the necessity of assuming an initial through-bolt orientation with respect to the bottom of the holes in the concrete decks.

The through-bolts are assumed to be installed (perfectly) perpendicular to the connection. Subsequent to the initiation of slip, the orientation of the through-bolts becomes slightly inclined due to the relative slip between the concrete and steel. The vertical distance between the ends of the through-bolts is assumed to remain constant, and thus the bolt inclination due to slip results in an axial deformation (elongation) of the bolts. The mechanistic model calculates the strain increase ($\Delta\varepsilon$) in the through-bolts as a function of slip (δ) using the deformed (slip) orientation of the bolt (see Stage 2 in Figure 5–1). It is important to mention that the mechanistic model does not predict the maximum slip magnitude. Linearly varying slip values, beginning at zero and terminating at the maximum value reported by Chen (2013) were used to generate the load-slip curve. Bending of the through-bolts are neglected (bolt ends are assumed to be pinned) when calculating the strain increase due to slip. The total strain in the through-bolts are taken as the strain increase ($\Delta\varepsilon$) due to slip plus the initial strain in the through-bolts due to the pretension force (ε_{bi}). The calculation of the total axial strain in the through-bolts (ε_b) is expressed mathematically in Equation 5-1.

$$\varepsilon_b(\delta) = \varepsilon_{bi} + \Delta\varepsilon$$
$$\varepsilon_b(\delta) = \varepsilon_{bi} + \frac{\sqrt{\delta^2 + t_{deck}^2} - t_{deck}}{t_{deck}} \tag{5-1}$$

where t_{deck} is the thickness of the concrete deck. This calculation neglects the thickness of the flange as it is relatively minor in comparison to the thickness of the concrete deck and it is assumed that the rotation of the through-bolts initiate on the inner surface of the flange against the concrete deck. While the autopsy revealed that some rotation of the through-bolts did occur within the flanges, this rotation was promptly terminated once the through-bolts engaged in bearing against the interior surfaces of the holes in the flanges due to the stringent tolerances.

The force in the through-bolts (T_b) is proportional to strain in the through-bolts (ε_b), and is determined by assuming a bilinear stress-strain curve defined by the yield stress, σ_{by}, the ultimate stress, σ_{bu}, the ultimate strain, ε_{bu}., the modulus of elasticity and the strain-hardening modulus. The force in the through-bolts is expressed mathematically in Equation 5-2.

$$\begin{aligned} T_b(\varepsilon_b) &= E \cdot \varepsilon_b \cdot A_b && \text{when } 0 \le \varepsilon_b \le \frac{\sigma_{by}}{E} \\ T_b(\varepsilon_b) &= \left[\sigma_{by} + E_2 \cdot (\varepsilon_b - \frac{\sigma_{by}}{E}) \right] A_b && \text{when } \frac{\sigma_{by}}{E} > \varepsilon_b \end{aligned} \tag{5-2}$$

where A_b is the cross-sectional area of a single through-bolt, E is the modulus of elasticity of the through-bolts and E_2 is the strain-hardening modulus that defines the post-yielding slope of the bilinear stress-strain curve.

The shear resistance of the through-bolts due to the interfacial friction of the connection is computed as a function of slip (δ), knowing the total force transmitted across the interface by each through-bolt (T_b) and the angle at which the deformed through-bolts are inclined (α) (see Figure 5–1) through the following relationships:

$$\alpha(\delta) = \tan^{-1}\left(\frac{t_{deck}}{\delta}\right) \tag{5-3}$$

$$Q_{friction}(\delta) = n \cdot T_b \cdot \left[K_s \cdot \sin(\alpha) + \cos(\alpha) \right] \tag{5-4}$$

where n is the number of through-bolts, t_{deck} is the thickness of the concrete decks and K_s is the coefficient of friction, or slip coefficient, between the steel and concrete interfaces. The coefficient of friction must be determined experimentally.

Also illustrated in Figure 5–1 is the deformation of the through-bolt as a consequence of the bolt bearing against concrete in Stage 3 of the response of the through-bolts during a push test. The autopsy of the

failed push test specimens revealed that the through-bolts deformed in flexure as they began to bear against the concrete near the steel flanges. The deformed shape of the through-bolts at the ultimate load level exhibited a double curvature, analogous to a fixed end condition. This flexural deformation is a consequence of the dowel action of the through-bolts, which contributes to the overall shear resistance of the connection. The contribution that the dowel action (Q_{dowel}) provides to the overall shear resistance is calculated as a function of slip (δ) using the mechanistically derived fixed-end force relationship, given by Equation 5-5:

$$Q_{dowel}(\delta) = \frac{12 \cdot E \cdot I \cdot \delta}{L^3} \tag{5-5}$$

where I is the moment of inertia of the through-bolts and L is the flexural length through which the through-bolts are deformed. Note that experiments by Chen (2013) showed that the deformations of the through-bolts due to dowel action, occurred over a flexural (deformed) length of the through-bolts, which was less than the total length of the through-bolts.

The flexural length, L, must be known in order to quantify the contribution the dowel action has on the overall load-slip curve. This length can be postulated by considering the bearing strength of the concrete as illustrated in Figure 5–3 where the length, L, in Equation 5-5 can be replaced with $L_{bearing}$.

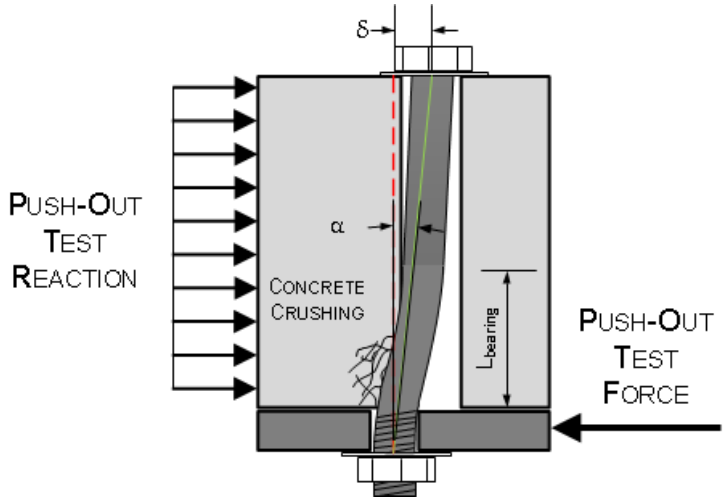

Figure 5–3: Stage 3 of the through-bolt load-slip behaviour showing concrete bearing length

As a simplifying measure, it was assumed that the bearing surface of concrete crushed by the through-bolts have an average width equal to the diameter of the through-bolts, projected onto the concrete. $L_{bearing}$ is defined by Equation 5-6, which was formulated by equilibrating the horizontal components of the

maximum allowable dowel action component of the overall shear resistance ($Q_{dowel(max)}$), defined below, and the compressive capacity of concrete.

$$L = L_{bearing} = \frac{Q_{dowel(max)} \cdot \sin(\alpha)}{f_c' \cdot d_b} \tag{5-6}$$

where f'_c is the compressive strength of the concrete decks and d_b is the diameter of the through-bolts.

It is intuitive that as the push test specimen slips, the length which the through-bolts bear against the concrete increases proportionally. The dependence of slip on bearing length is apparent in Equation 5-6.

Therefore, the contribution that the dowel action (Q_{dowel}) provides to the overall shear resistance given by Equation 5-5, can be rewritten with the flexural length, L, replaced with $L_{bearing}$ as shown in Equation 5-7. However, because the dowel action of the through-bolt is restricted to occur over the flexural length, the full slip magnitude (δ) cannot be used as this is the relative slip of the two far ends of the through-bolts. Therefore, the magnitude of slip of the through-bolt's end within the flange relative to the location along the shank of the through-bolt at the end of the flexural length was computed for each slip increment and is defined as δ'.

$$Q_{dowel}(\delta) = \frac{12 \cdot E \cdot I \cdot \delta'}{L_{bearing}^{\ 3}} \tag{5-7}$$

The ultimate failure condition is defined as the limiting capacity of the through-bolt's shear resistance considering the interaction between combined shear and tension. This relationship is based on the work of Chen (2013). Equation 5-8 shows the interaction formula and Equation 5-9 is a reorganization to solve for the maximum through-bolt shear capacity.

$$\left(\frac{Q_{dowel}}{0.6 \cdot n \cdot A_b \cdot \sigma_{bu}}\right)^2 + \left(\frac{n \cdot T_b}{n \cdot A_b \cdot \sigma_{bu}}\right)^2 \leq 1 \tag{5-8}$$

$$Q_{dowel(max)} = 0.6 \cdot n \cdot A_b \cdot \sigma_{bu} \sqrt{1 - \left(\frac{n \cdot T_b}{n \cdot A_b \cdot \sigma_{bu}}\right)^2} \tag{5-9}$$

The overall shear resistance of the through-bolts is the linear summation of the friction and dowel action shear resistance components, combining Stages 1, 2 and 3 from Figure 5–1. Equation 5-10 presents the final relationship used to approximate the full load-slip behaviour of a push test featuring through-bolts.

$$Q(\delta) = Q_{friction} + Q_{dowel} \tag{5-10}$$

where $Q_{friction}$ is given by Equation 5-4 and Q_{dowel} is given by Equation 5-7 and is limited by $Q_{dowel(max)}$ provided by Equation 5-9.

5.1.2 Mechanistic Model Results

A sample full load-slip response curve as predicted by the mechanistic model is illustrated in Figure 5–4. Initially, the applied load is resisted by the friction at the steel-concrete interface until the force of friction is overcome at the slip load. This is evident by the non-zero load intercept of the load-slip curve, indicating that the applied loading was resisted without the onset of slip until the slip load is reached, predicted to be 150 kN. This is consistent with the first of the three incremental stages described by Liu et al. (2014). However, beyond the slip load, the predicted response does not show a "plateau" region where there is little or no increase in shear resistance (applied load) as the slip increases. As mentioned earlier, this is because the initial position of the through-bolts within the holes of the concrete decks and steel girder was assumed to be such that dowel action of the through-bolts began immediately following the onset of slip. Finally, the predicted load-slip response behaves in a non-linear manner due to the combined effects of the dowel action of the through-bolts bearing against the concrete and the forces of friction acting between the concrete decks and steel girder. This behaviour describes the response of a push test experiment in its third and final stage as explained by Liu et al. (2014).

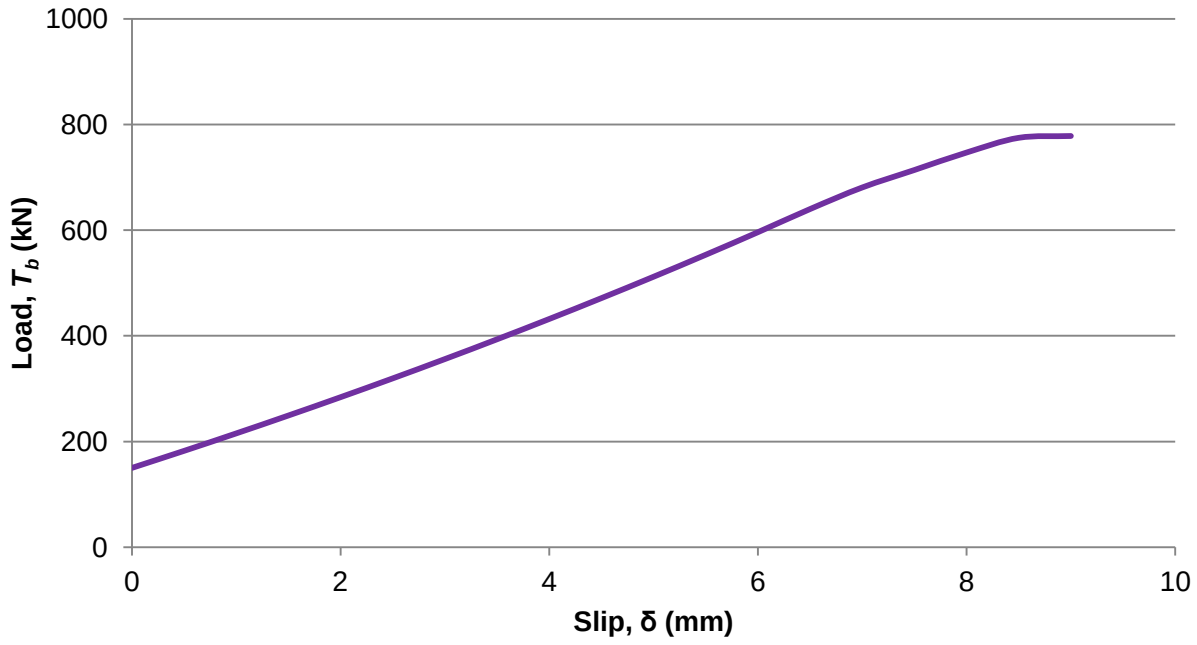

Figure 5–4: Non-linear load-slip mechanistic model results for 5/8" diameter through-bolts

5.1.3 Comparison of Mechanistic Model Predictions With Experimental Results

The simulated load-slip curves predicted by the mechanistic model were compared to the experimental results from Chen (2013) as a means of validation. The comparison between the predicted and experimental results for 1/2", 5/8", and 3/4" diameter through-bolts are illustrated in Figure 5–5, Figure 5–6, and Figure 5–7 respectively. Also shown for comparison purposes, is the predicted ultimate capacity of the through-bolts defined by Chen (2013) for each of the respective through-bolt diameters.

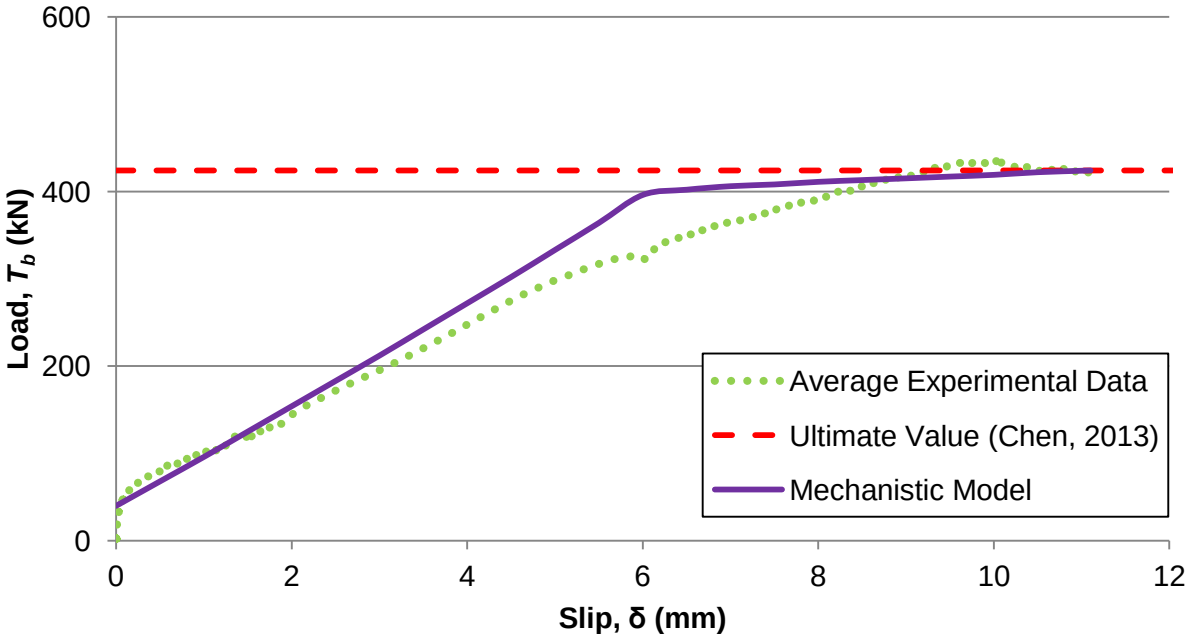

Figure 5–5: Comparison between experimental data and mechanistic model load-slip prediction for 1/2" diameter through-bolts

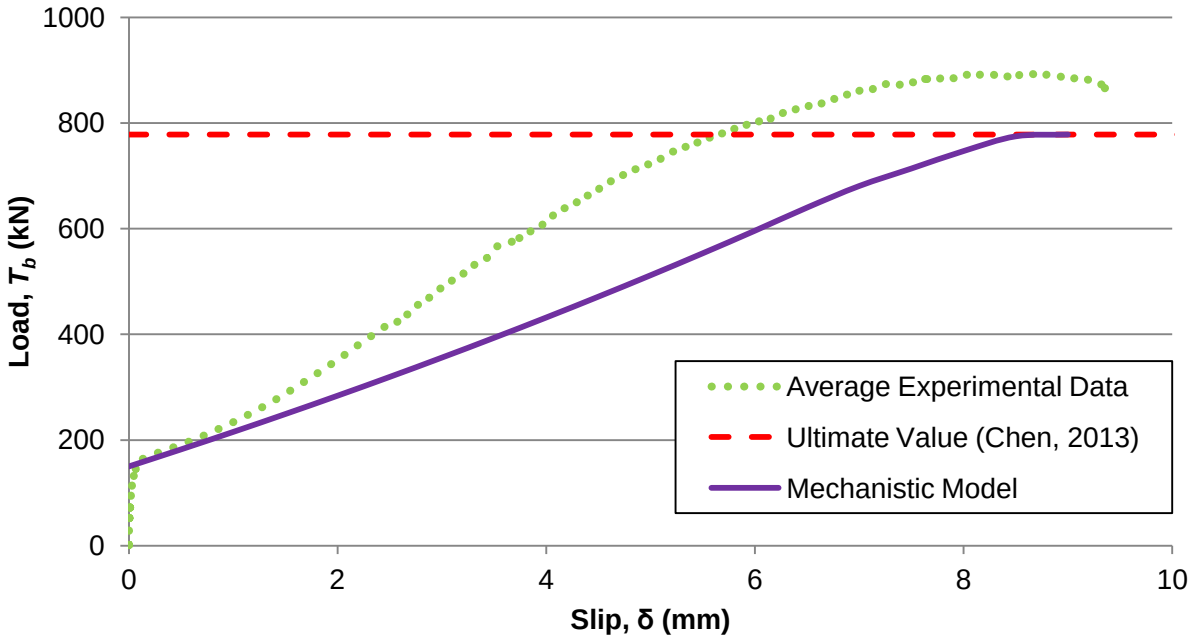

Figure 5–6: Comparison between experimental data and mechanistic model load-slip prediction for 5/8" diameter through-bolts

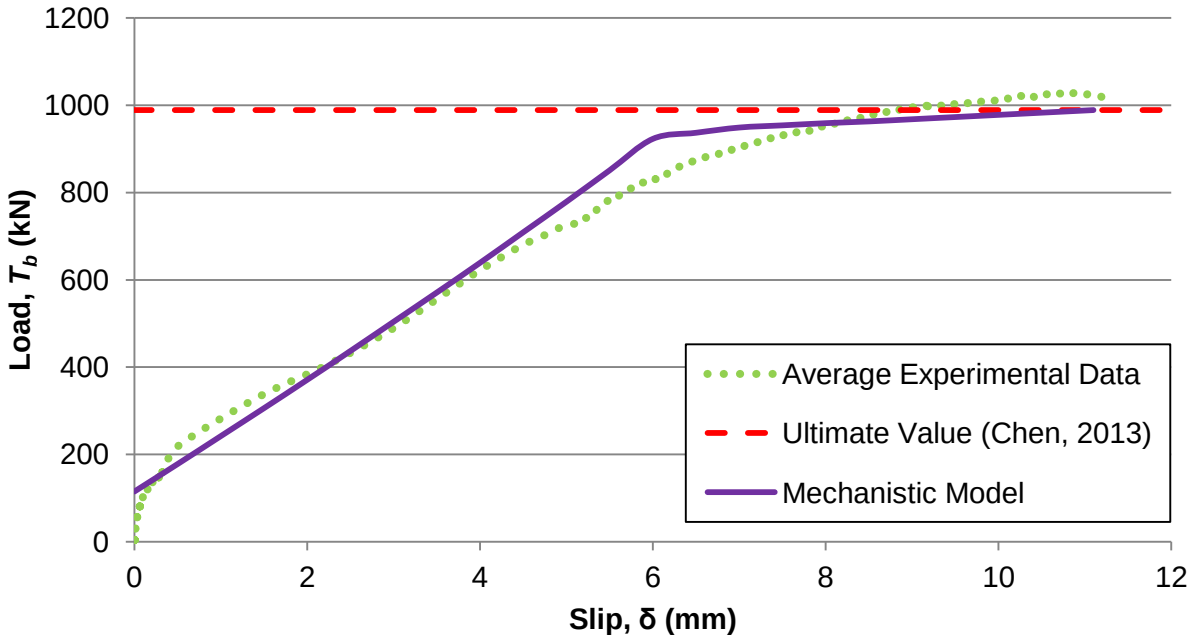

Figure 5–7: Comparison between experimental data and mechanistic model load-slip prediction for 3/4" diameter through-bolts

As shown in Figure 5–5, Figure 5–6 and Figure 5–7, the predicted load-slip curves from the mechanistic model emulates the behaviour of the experimental push tests reasonably well. It can be seen that the predicted initiation of slip in each case is virtually identical to the slip level observed during the experiments. This was expected as the slip coefficient (K_s) reported by Chen (2013) was used in the mechanist model. Moreover, the profile of the predicted load-slip curve correctly approximates the profile from the experimental data, confirming the adequacy of the mechanistic model in terms of its prediction of the through-bolts' stiffness and the relative engagement of the doweling and friction contributions to the overall shear resistance.

One discrepancy between the predicted load-slip curves and the experimentally observed load slip curves, common to the results for all through-bolt diameters, is the abrupt change in curvature once the theoretical maximum through-bolt shear capacity, described in Equation 5-9, has been exceeded. As explained in Section 5.1.1, the load resisted by the through-bolt shear connectors is the linear summation of the friction and the dowel action. While the dowel action is limited by the interaction described by Equation 5-9, the friction between the concrete deck and steel girder is a function of the force transmitted across the interface by the through-bolts (T_b) and the angle at which the deformed through-bolts are inclined (α). Both of which vary throughout the entirety of the load-slip prediction. However, the since the dowel action is substantially larger relative to the force of friction, the abrupt change in curvature of the overall load-slip curve is apparent when Q_{dowel} is held constant at a value equal to $Q_{dowel(max)}$, given by Equation 5-9.

The mechanistic model was used to perform a sensitivity analyses on the various parameters affecting the ultimate shear capacity of the through-bolt shear connection, allowing the influence of each parameter to be assessed. First, the influence that varying the slip coefficient and the bolt diameter has on the ultimate shear capacity of the through-bolt shear connection was assessed, holding the initial pretension load level constant at 85 kN. The results of this analysis are displayed graphically in Figure 5–8.

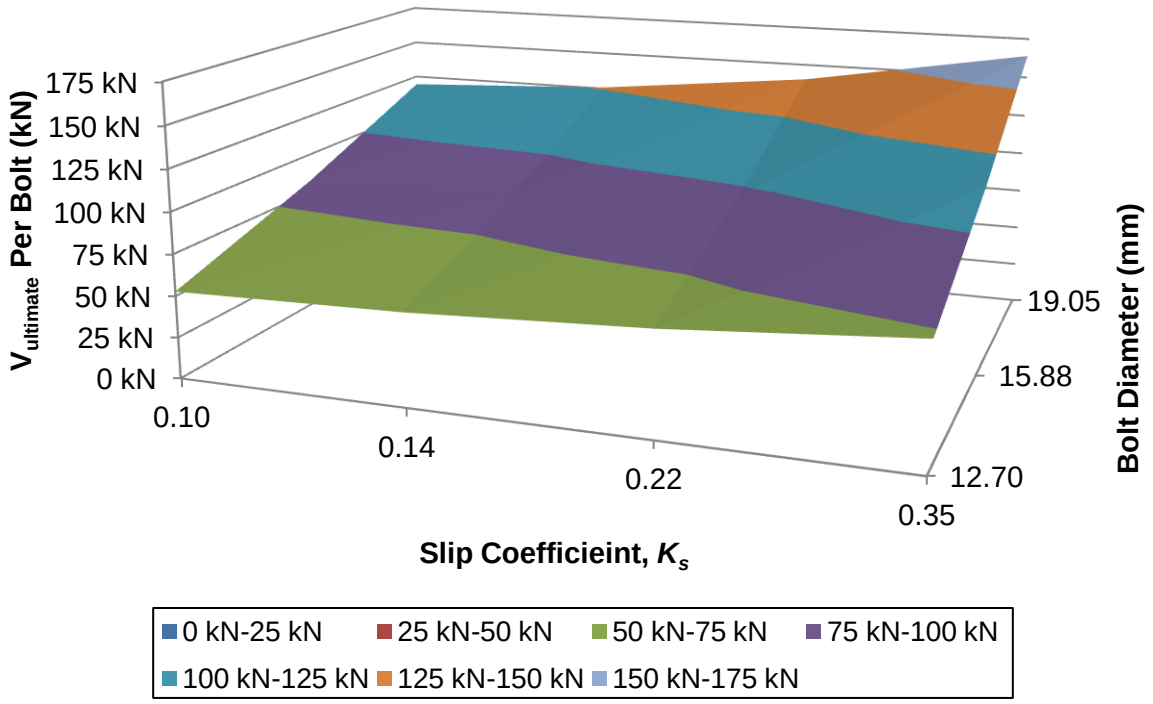

Figure 5–8: Influence of slip coefficient and bolt diameter on ultimate shear capacity of the through-bolt shear connection

As expected, Figure 5–8 illustrates that both increasing values of the slip coefficient and the bolt diameter independently have the same effect of increasing the ultimate shear capacity of the through-bolts shear connection. This conclusion is intuitive because a larger through-bolt diameter offers more material to resist the applied loading and a larger slip coefficient implies that friction assumes a more influential role in resisting the applied loading, lessening the reliance on the through-bolts themselves.

Moreover, the influence that varying the slip coefficient and the pretension load level has on the ultimate shear capacity of the through-bolt shear connection was assessed. This analysis was performed by associating the pretension level with the corresponding through-bolt diameter as per CSA S6 Clause 10.24.6.3 (CSA S6, 2014). The results of this analysis are displayed graphically in Figure 5–9.

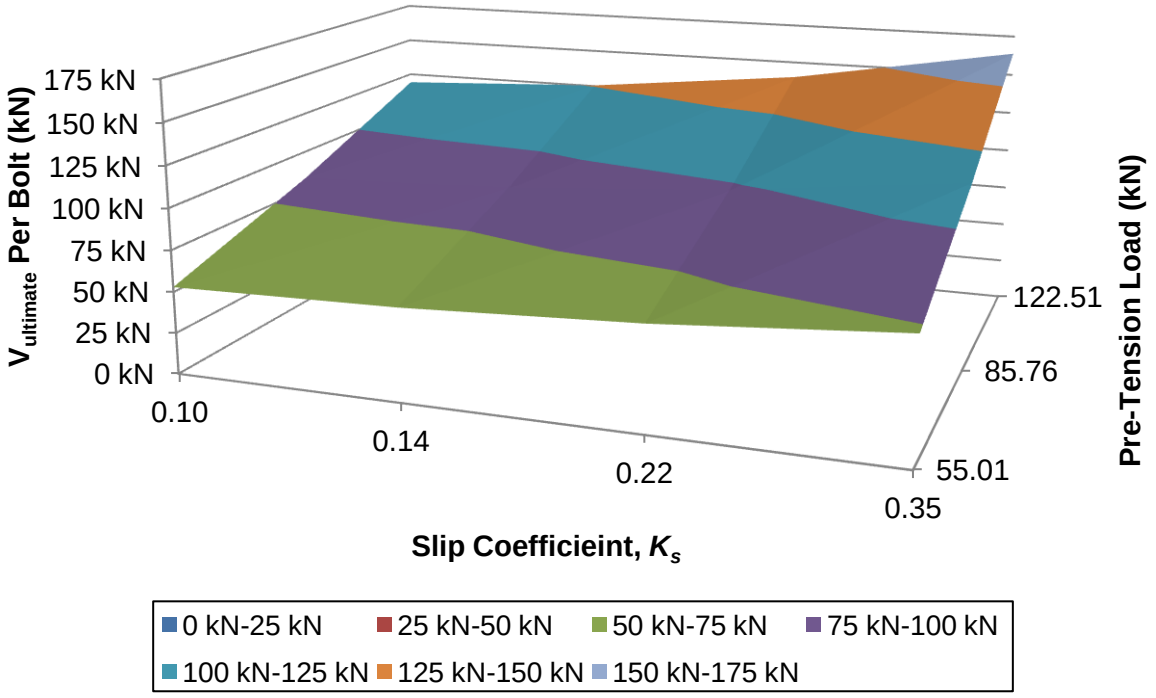

Figure 5–9: Influence of slip coefficient and pretension load on ultimate shear capacity of the through-bolt shear connection

Interestingly, the results of this analysis are almost identical to the ones shown in Figure 5–8 where the slip coefficient and through-bolt diameter were varied and the pretension load level was held constant. This indicates that the pretension load level on acting on the through-bolts assumes a less important role than the slip coefficient and the diameter of the through-bolts. Therefore, the two primary factors influencing the ultimate shear capacity of the through-bolt shear connection, the slip coefficient and the through-bolt diameter have been plotted on a two-dimensional coordinate system in Figure 5–10, permitting a more detailed quantification of the relationship between the slip coefficient and through-bolt diameter and the ultimate shear capacity.

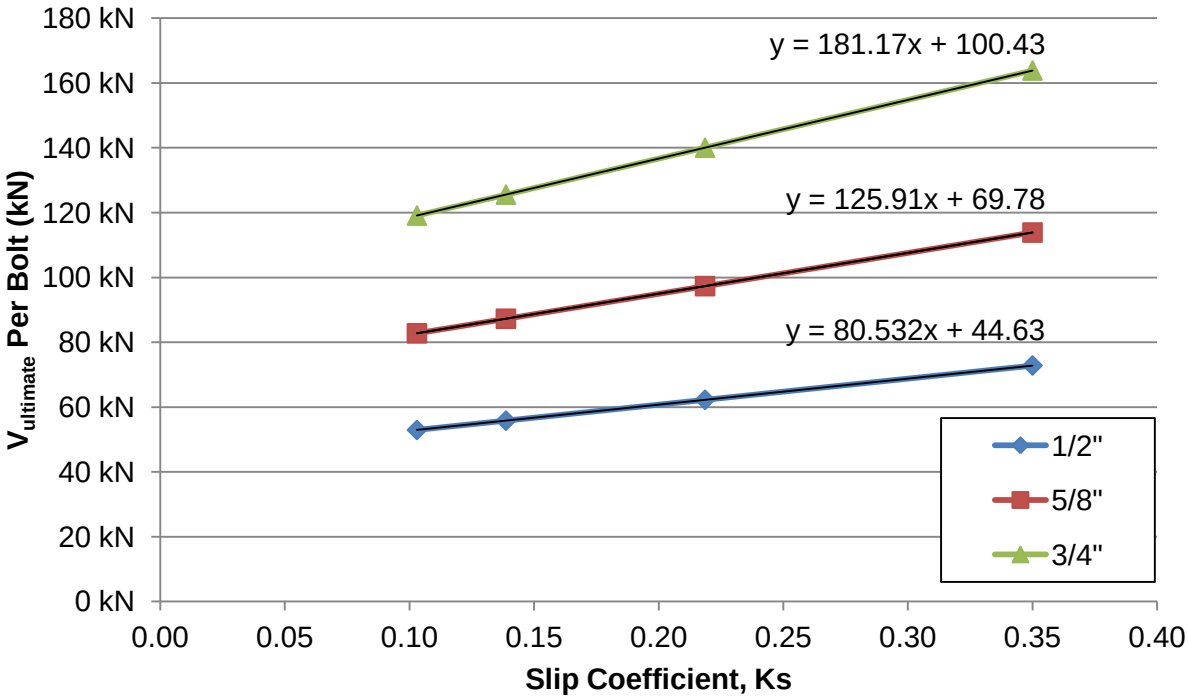

Figure 5–10: Relationship between slip coefficient and pretension load on ultimate shear capacity of the through-bolt shear connection

As illustrated in Figure 5–10, the effect that varying the slip coefficient has on the ultimate shear capacity of the shear connection is linear. It is important to note that the intercepts of each of the linear regression equations are not equal to zero. This implies that with a slip coefficient equal to zero, the shear connections will have varying ultimate shear capacities depending on the through-bolt diameters, with larger through-bolt diameters offering larger ultimate shear resistances.

5.2 Finite Element Push Test Model Description

The following presents a three dimensional FE model that simulates a through-bolt push test experiment, predicting the load-slip behaviour of the composite specimen and its comparison to test results. The push test FE model was prepared using ABAQUS version 6.13 (Dassault Systèmes, 2013) and considers both material and geometric nonlinearity. Due to the symmetry of the push test composite specimens used by Chen (2013), only half of the assembly was modelled to improve computational efficiency. Four distinct steps were established to replicate the circumstances of the push test experiments performed by Chen (2013). Boundary conditions and interaction constraints were defined in the initial step of the analysis. The through-bolts were pretensioned in the subsequent two steps and the vertical displacement was imposed in the final step.

5.2.1 Material Property Definitions

Nonlinear material properties were assigned to the steel girder, concrete reinforcement, concrete deck and through-bolt shear connectors. The material properties were defined in ABAQUS using tabulated true stress and true strain values for the steel components and engineering stress and engineering strain values for the concrete deck. The stress-strain relationship of the steel girder and steel reinforcement were approximated as linear-elastic, perfectly plastic with a modulus of elasticity of 200 GPa, a Poisson's Ratio of 0.2 and a yield stress of 350 MPa and 400 MPa for the girder and steel reinforcement respectively (CSA S16-09, 2012).

The stress-strain relationship of the concrete in compression assumes the linear-elastic, strain-hardening relationship proposed by Hognestad (1951), shown in Figure 5–11 (Left) and mathematically described by Equation 5-11.

$$\begin{aligned} f_c &= f_c'' \cdot \left[2 \cdot \frac{\varepsilon_c}{\varepsilon_c'} - \left(\frac{\varepsilon_c}{\varepsilon_c'} \right)^2 \right] && \text{when } \varepsilon_c \le \varepsilon_c' \\ f_c &= f_c'' - \left(\frac{0.15 \cdot f_c''}{0.0038 - \varepsilon_c'} \right) \left(\varepsilon_c - \varepsilon_c' \right) && \text{when } \varepsilon_c' \le \varepsilon_c \le 0.0038 \end{aligned} \tag{5-11}$$

where ε_c is the strain level in the concrete, f'_c is the 28 day compressive concrete strength, obtained from a cylinder test, f''_c is 90% of f'_c and ε'_c is defined as:

$$\varepsilon_c' = \frac{1.8 \cdot f_c''}{E_c} \tag{5-12}$$

The compressive strength of the concrete was determined by standardized concrete cylinder compression tests, the results of which were reported by Chen (2013). A Poisson's Ratio of 0.3 was adopted and the modulus of elasticity was calculated using the following equation proposed by Hognestad (1951):

$$E_c = 12411 + 460 \cdot f_c' \tag{5-13}$$

Clause 8.8.3 of CSA S6 (CSA S6, 2014) states that the tensile strength of concrete shall be neglected for flexural resistance calculations. However, due to the inherent nature of the push test, tensile stresses are present and assuming an isotropic behaviour of concrete is non-conservative. Therefore, the tensile capacity of the concrete was assumed to be non-zero. The stress-strain relationship of the concrete deck in tension was modelled using an average or "smeared" relationship, also shown in Figure 5–11 (Right) and mathematically described by Equation 5-14.

$$f_t = E_c \cdot \varepsilon_t \qquad \text{when } \varepsilon_t \le \varepsilon_r$$
$$f_t = \frac{\alpha_1 \cdot \alpha_2 \cdot f_r}{1 + \sqrt{500 \cdot \varepsilon_t}} \qquad \text{when } \varepsilon_t > \varepsilon_r \tag{5-14}$$

where ε_t is the tension strain level in the concrete, E_c is the modulus of elasticity from Equation 5-13, α_1 is a factor accounting for the concrete bond characteristics to the concrete reinforcement (1.0 for deformed reinforcing bars), α_2 is a factor to account for sustained or repeated loading (1.0 for short term loading) and f_r is the modulus of rupture, defined by Equation 5-15.

$$f_r = 0.6 \cdot \sqrt{f'_c} \tag{5-15}$$

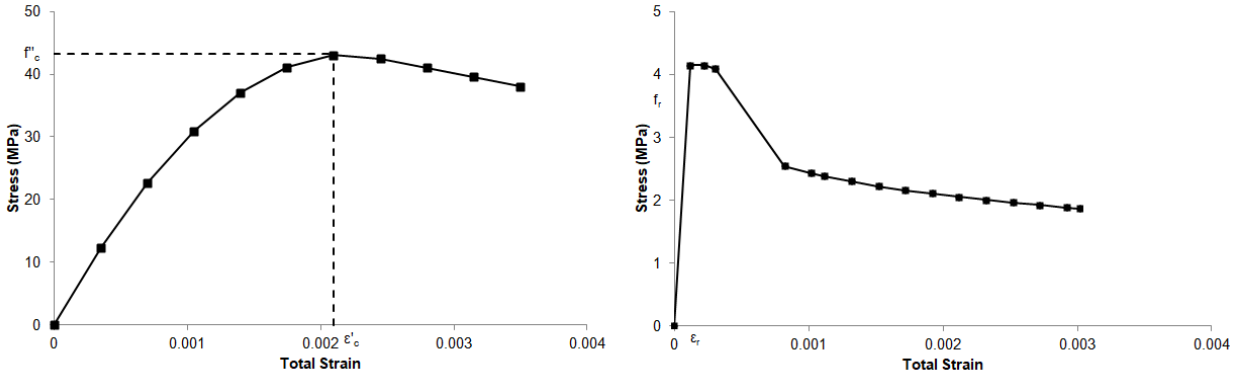

Figure 5–11: Concrete stress-strain relationship. Compression (Left), Tension (Right).

As illustrated in Figure 5–11 (Right), a small plateau was provided at the peak of the concrete tension stress-strain relationship to help improve convergence.

The stress-strain relationship of the steel through-bolts, shown in Figure 5–12, was assumed to follow a bilinear stress-strain relationship with an initial modulus of elasticity of 200 GPa, a yield stress (f_y) of 635 MPa and a strain-hardened modulus of elasticity of 1294 MPa. A tensile rupture strain (ε_u) of 0.23, as proposed by CSA S16-09 (2012), was adopted and a Poisson's Ratio of 0.2 was assumed.

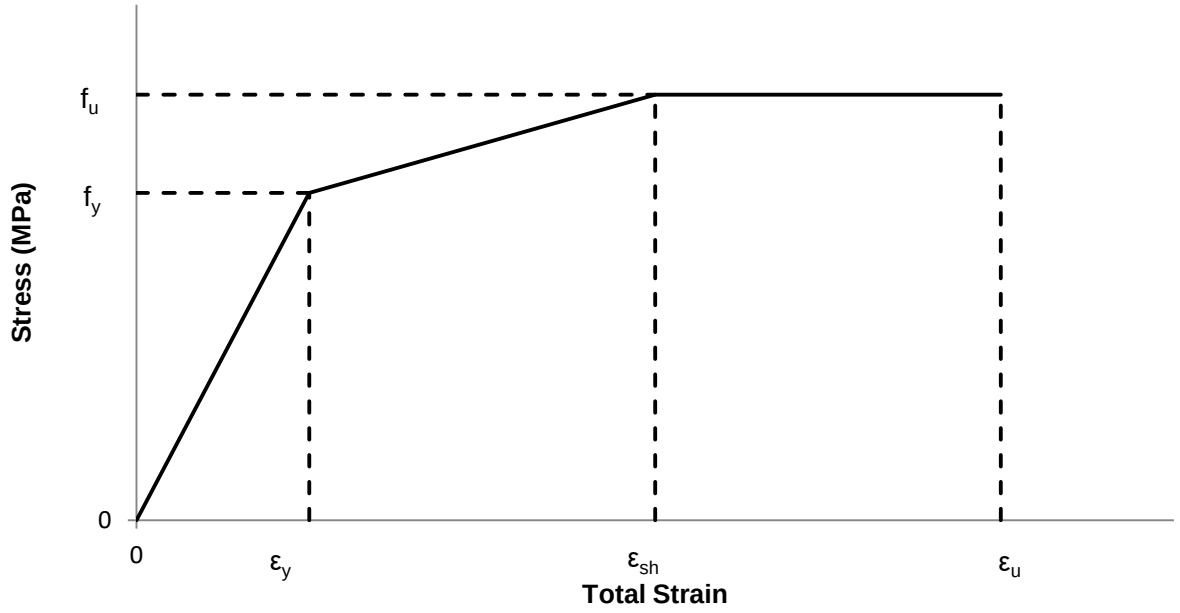

Figure 5–12: Through-bolt stress-strain relationship

5.2.2 Finite Element Mesh

Twenty node, quadratic, hexahedral, C3D20R elements were the selected element type for the through-bolts and steel girder in the push test FE simulation. C3D20R quadratic elements were used to mesh these components because their geometric flexibility allowed for a uniform mesh of the complicated physical geometry of the through-bolts and steel girder, each consisting of multiple curved features. The quadratic shape functions of the C3D20R elements better model curved features than their linear counterparts as they do not introduce artificial stress concentrations by approximating curves with linear line segments.

The concrete deck was modelled using eight node, linear, hexahedral, CD38R elements. CD38R elements were chosen for the concrete deck to reduce the mesh complexity, improving simulation efficiency. This simplification is appropriate as the stresses in the concrete deck were not of particular interest with regards to the scope of this study.

Lastly, the concrete reinforcement was modelled using two node, linear, T3D2 truss elements. The reinforcement was approximated as perfect 3D cylinders with no ribbing. This was an assumption intended to simplify the modelling and meshing of the concrete reinforcement geometry in ABAQUS.

Reduced integration was selected for all components to improve intermesh accuracy. A relatively fine mesh was used to discretize the through-bolts as the stresses and plastic strains in the through-bolts were of specific interest for this study. A comparatively coarser mesh was used to discretize the steel girder and

an even coarser mesh was used to discretize the concrete deck, as the stresses and plastic strains in these components were relatively less important for the purpose of this study. Moreover, there were fewer characteristic geometric features forming the deck and therefore, fewer elements were required to properly approximate its geometry. The mesh used in the push test FE model is depicted in Figure 5–13.

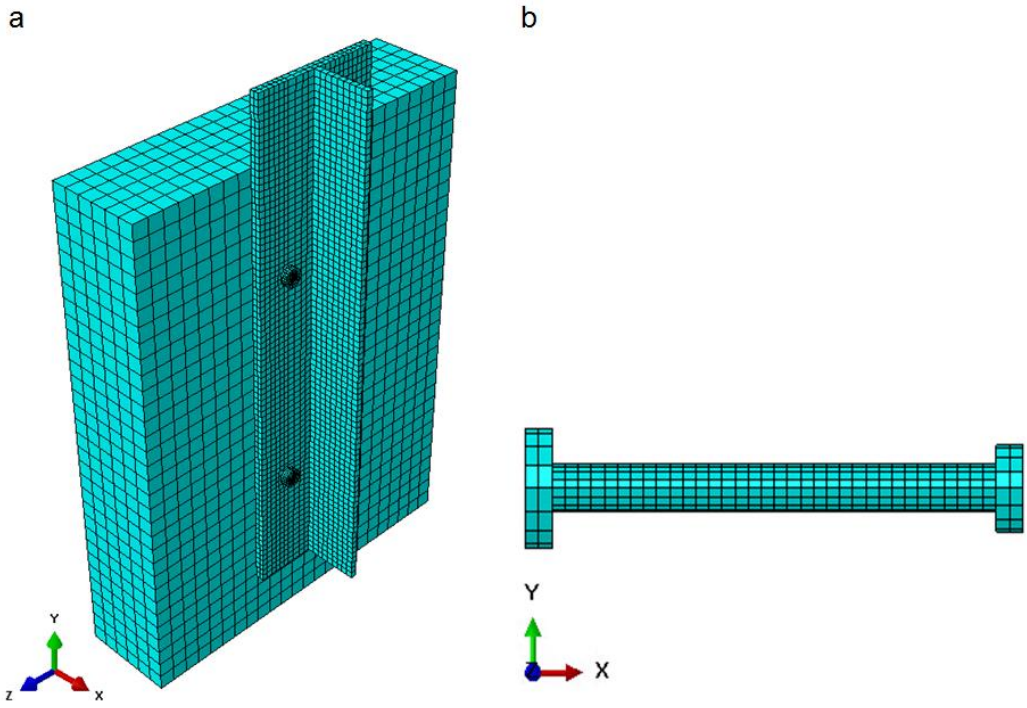

Figure 5–13: Push test FE model mesh overview a) Overall model b) Through-bolt shear connector

5.2.3 Boundary Conditions and Constraints

The boundary conditions and constraints selected in the push test FE model were chosen to approximate the conditions present in the experiments performed by Chen (2013). However, it should be mentioned that the exact positioning of the through-bolts within the holes in the concrete decks and the steel girders during the experiments conducted by Chen (2013) are not known. Therefore, initially it was assumed that gravity must have pulled the steel girder downwards before the tightening of the through-bolts was implemented. Hence, the through-bolts were positioned 1 mm from the bottom of the interior surfaces of the concrete holes. A 1 mm gap was arbitrarily chosen as opposed to 0 mm because having the bolts initially resting on the concrete resulted in convergence issues as the through-bolts pretension loading was applied. Furthermore, since the tolerance between the through-bolts and the holes in the steel flange were comparatively much smaller than with the holes in the concrete deck, it was assumed that the through-bolts were placed in the exact centres of the holes in the steel girder. The consequences of these assumptions are discussed later.

While in reality, a perfect pinned or fixed connection does not exist, the boundary conditions depicted in Figure 5–14 were selected as they most closely reflect the actual conditions of the experiments.

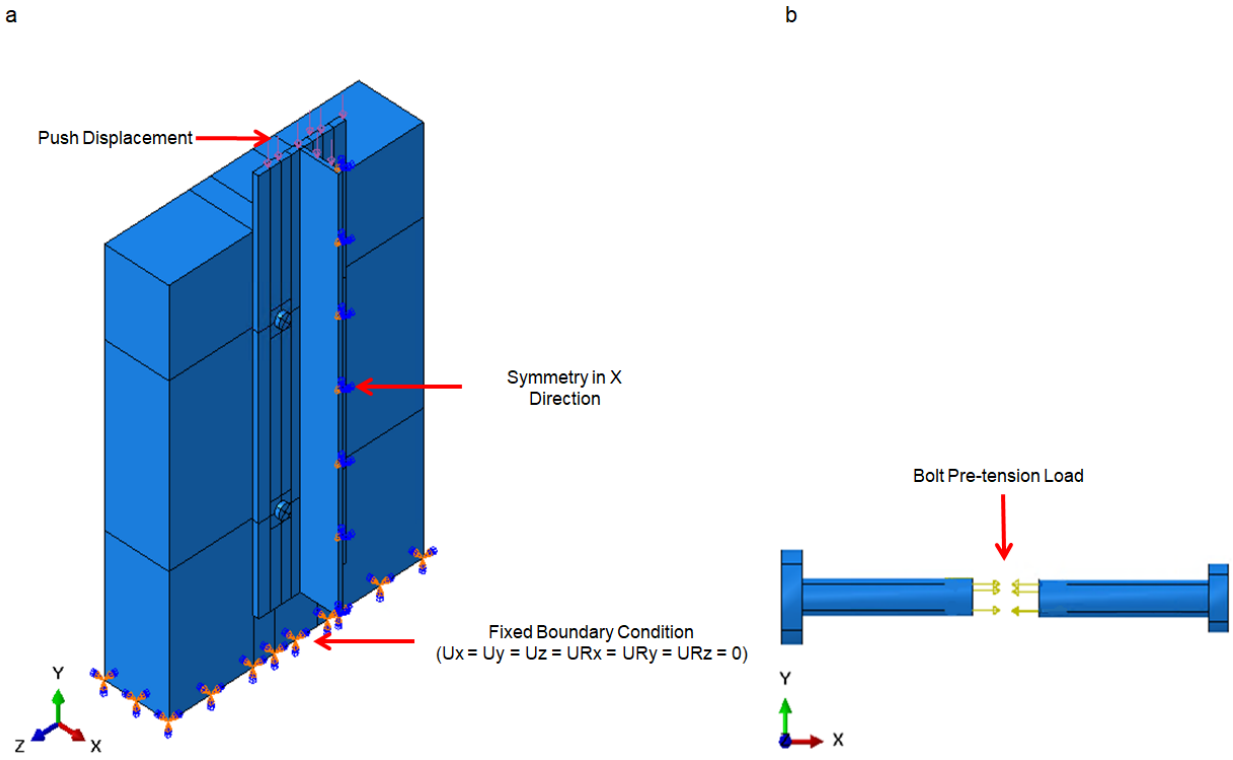

Figure 5–14: Push test FE model boundary conditions and loading assignments. a) Overall model b) Through-bolt

As described earlier, only half of the specimen's assembly was modelled. Therefore, a symmetry condition was applied along the web of the steel girder in the global X-direction, labeled in Figure 5–14, to account for the presence of the remaining half of the assembly not modelled. The symmetry condition assigned a zero value to the displacement component perpendicular to the cut surface of the web, prohibiting the formation of artificial interruptions in geometry during the deformation of the solid (Fish, 2007).

The base of the concrete deck was assumed to behave as a fixed support. This is a reasonable assumption because the steel platform on which the push test specimen was tested did not yield or deform during the experimentation.

The interfacial behaviour between the various components was modelled using several interaction constraints and contact properties. The orthogonal behaviour of the steel girder and concrete deck interface was characterized as "hard contact," prohibiting the merger of the two materials during the

simulation. The tangential behaviour was defined using an isotropic penalty friction formulation with a specified coefficient of friction of 0.22 (Chen, 2013). Moreover, a "finite sliding" interaction was assumed to allow for the separations between the concrete deck and the flanges of the steel girder which were expected to experience out of plane distortions known as flange curling. The interfacial behaviour between the shank of the through-bolts and the interior surfaces of the holes in the concrete and steel was also modelled using a hard contact interaction constraint. The same coefficient of friction as between the concrete deck and steel girder (0.22) was assumed between the through-bolts and the concrete deck. However, the tangential behaviour was assumed to be frictionless between the through-bolts and the steel girder as the coefficient of friction between two smooth metallic surfaces is comparatively low. Moreover, the distance that the through-bolt came into contact with the flange was limited to the width of the flange (11 mm) and is relatively minor in comparison to the width of the concrete deck (152 mm). Therefore, this assumption was not expected to have any significant effects on the outcome of the simulations.

Furthermore, for simplicity, the concrete reinforcement was assumed to be perfectly bonded within the concrete deck by assigning an "embedded region" contact between the concrete and the reinforcement. This is a simplifying assumption that circumvents the requirement for modelling the imperfect adhesion of the concrete to the reinforcement.

As illustrated in Figure 5–13, the washers at the ends of the through-bolts were modelled monolithically with the shanks of the through-bolts to reduce the modelling complexity. Moreover, the washers at the ends of the through-bolts were tied to their respective bearing surfaces against the concrete deck and flange of the steel girder. As discussed in Section 5.1.1, the ends of the through-bolt were found to have remained in their original alignment in the bolt holes subsequent to deformation as concluded based upon the autopsy of the failed push test specimens. Therefore, the tie constraint applied to the ends of the through-bolts was deemed appropriate.

The pretension force applied to the through-bolts was applied in the second step using ABAQUS's BOLT LOAD function which created a specified initial concentrated tension force in the through-bolt as shown in Figure 5–14. The applied BOLT LOADs were modified in the subsequent step using ABAQUS's FIX AT CURRENT LENGTH method, which allowed the force in the through-bolts to vary as the simulation progressed. If this method was not implemented, the ABAQUS solver would have continually adjusted the length of the through-bolts to maintain the originally specified pretension force. This is achieved by contracting or elongating the shanks of the through-bolts at the midspan cross-section plane shown in Figure 5–14. This contraction or elongation would have introduced a geometric incompatibility within the

through-bolts as the two halves of the through-bolts' shank would overlap or separate at the interface of these surfaces (ABAQUS, 2013). This behaviour is not correct as the force carried by the through-bolts is expected to increase throughout the duration of the push test.

Lastly, in the final step, the push test FE model was loaded in displacement control to replicate the experiments performed by Chen (2013). An applied displacement of 20 mm was uniformly imposed onto the top flange of the steel girder in the negative global Y-direction as shown in Figure 5–14. This applied displacement was considerably larger than the maximum displacements observed by Chen (2013). This was done intentionally as to not introduce bias into the simulation with regards to the maximum predicted load as well as to observe the behaviour of the model as it attempts to resist larger internal forces. The RIKS method was used in this step as it offered a more stable convergence for geometrically nonlinear failures (Liu et al., 2014).

5.2.4 Finite Element Analysis Results

Defining a suitable failure criterion proved to be a challenge as Chen (2013) allowed the actuator to continue loading the push test specimens subsequent to the onset of concrete crushing and significant distortion of the through-bolts. The objective of the experimentation performed by Chen (2013) was to load the through-bolts up to their ultimate capacity without the consideration of the condition of the concrete deck or flange of the steel girder. Therefore, to capture the onset of failure of the through-bolts in the push test FE simulation, it was decided to interpret the stabilization of the maximum Von Mises stress in the through-bolts that equalled the theoretical rupture stress in the through-bolts (1030 MPa) as the onset of failure. ABAQUS output results following this occurrence were deemed as unreliable and therefore, all results presented herein were extracted from ABAQUS at this instance.

A sample non-linear load-slip response as predicted by the push test FE model is illustrated in Figure 5–15. As expected, the three incremental stages described by Liu et al. (2014) are apparent. Initially, the applied load was primarily resisted by the interfacial friction between the concrete deck and steel girder interface until the force of friction was overcome at the slip load. This is evident by the high initial slope of the load-slip curve, indicating that the applied loading was resisted without the onset of slip until the slip load, predicted to be approximately 152 kN. This is consistent with Stage 1 of the response of a push test experiment. Beyond the slip load, a rapid increase in slip with virtually no increase in load is observed. The frictional forces previously resisting the applied loads have been overcome and the through-bolts slip freely for approximately for 1 mm until they contact the concrete deck in direct bearing. This is consistent with Stage 2 of the response of a push test experiment. Following this rapid increase in slip, the slope of the load-slip response increased due to the bearing action of the through-bolts

on the concrete deck. The mechanism resisting the applied load has changed from purely friction to primarily dowel action, augmented by friction. This behaviour describes the response of a push test experiment in its third and final stage.

The failure criteria discussed above was observed to have occurred at approximately 550 kN. Figure 5–15 displays the simulation results prior to the onset of this defined failure criteria as a solid blue line. Subsequent to the onset of the defined failure criteria, the simulation results are displayed as a blue hashed line. The post-failure results are displayed to illustrate that the model behaved in a stable manner following the supposed failure of the through-bolts.

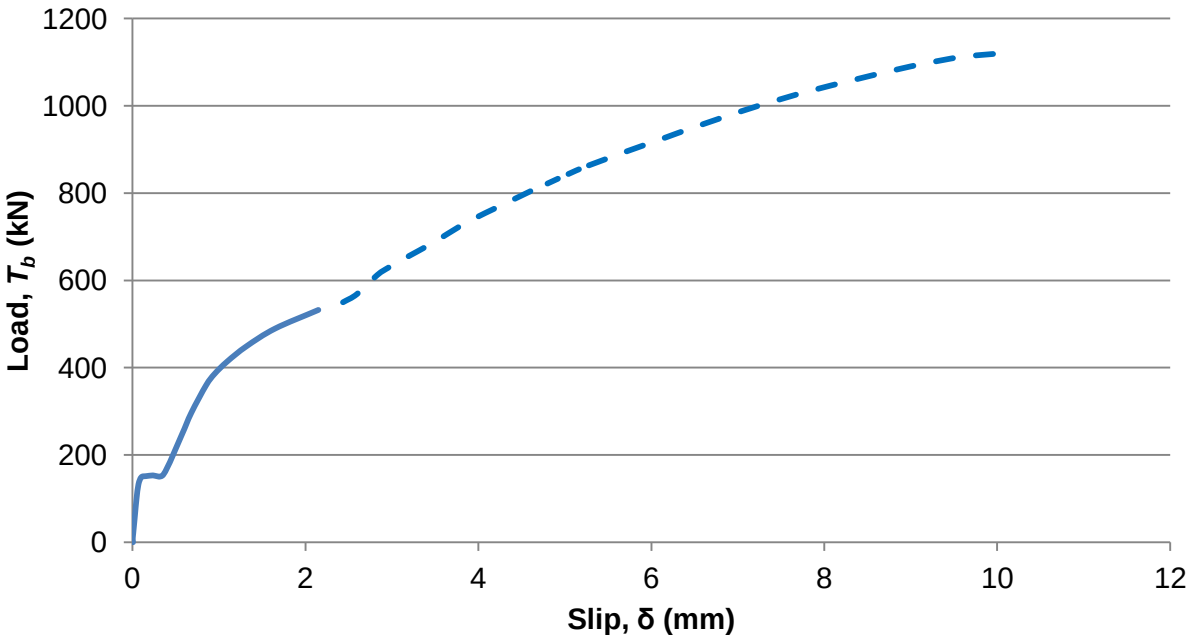

Figure 5–15: Load-slip finite element simulation results for 5/8" diameter through-bolt

5.2.5 Comparison of Finite Element Model Predictions with Experimental Results

The simulated load-slip curves were generated by the push test FE model for three different through-bolt diameters and were compared to the experimental results reported by Chen (2013) as a means of validation. The comparison between the simulated and experimental results are illustrated in Figure 5–16, Figure 5–17 and Figure 5–18 which feature 1/2" diameter through-bolts, 5/8" diameter through-bolts, and 3/4" diameter through-bolts respectively. Each plot has the predicted ultimate capacity of the through-bolts defined by Chen (2013) for comparison purposes. Also, as before, the following figures display the simulation results prior to the onset of the defined failure criteria as a solid blue line and subsequent to the onset of failure as a blue hashed line.

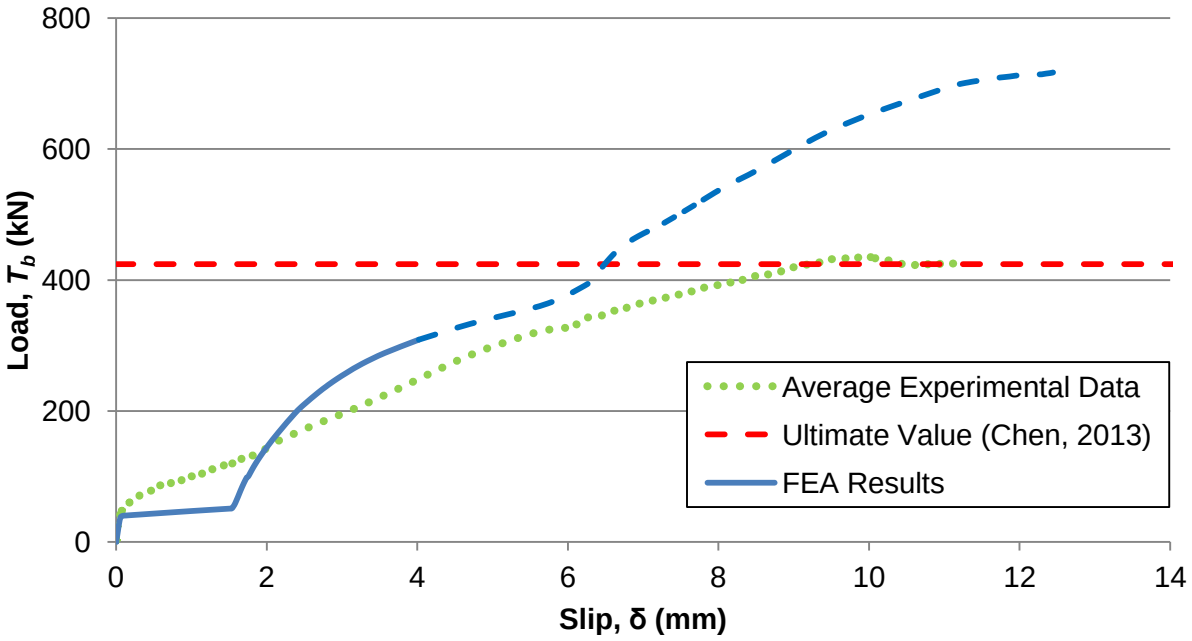

Figure 5–16: Comparison between experimental data and push test FE load-slip prediction for 1/2" diameter through-bolts

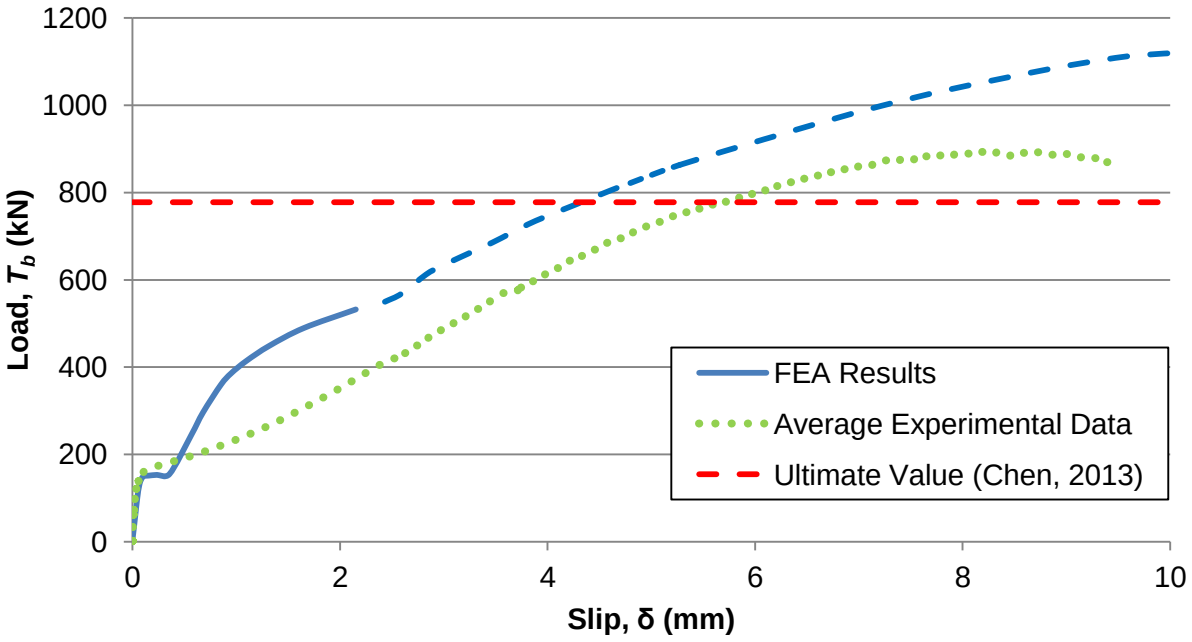

Figure 5–17: Comparison between experimental data and push test FE load-slip prediction for 5/8" diameter through-bolts

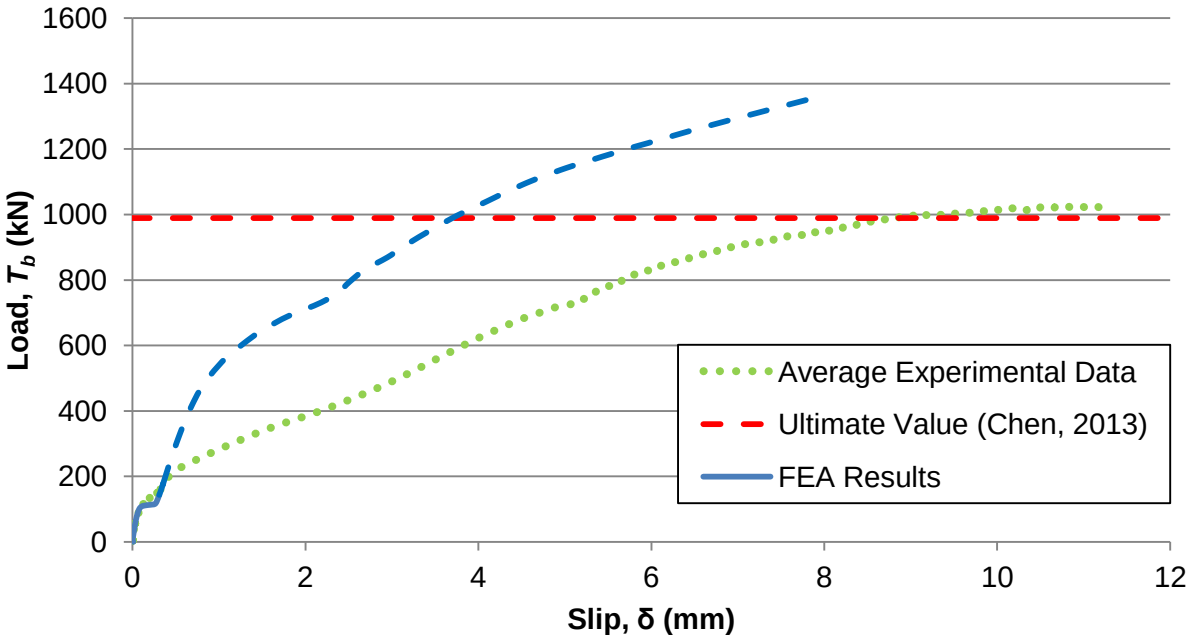

Figure 5–18: Comparison between experimental data and push test FE load-slip prediction for 3/4" diameter through-bolt

As shown in Figure 5–16, Figure 5–17 and Figure 5–18, the predicted load-slip responses from the push test FE models emulate the behaviour of the experimental push test reasonably well. It can be seen that the predicted initiation of slip is virtually identical to the slip levels observed during the experiments. This implies a reasonable level of effectiveness of the ABAQUS BOLT LOAD function and accuracy of the assumed coefficient of friction from Chen (2013).

However, the push test FE simulations predict a rapid increase in slip with virtually no increase in load immediately following the onset of slip. While this is consistent with the second stage defined by Liu et al. (2014), the experimental results differ in that they indicate a continual, smooth load increase following slip. Moreover, the push test FE simulation results appear much stiffer than the experimental results subsequent to the initial slip. Both of these occurrences suggest that the push test FE models have an inherent strength not present during the experiments.

One possible source of this fictitious strength may be a consequence of the assumption described earlier pertaining to the perfect geometrical symmetry of the initial arrangement of the through-bolts. It is well accepted that the through-bolts could not have feasibly been installed in a perfectly symmetrical orientation with regards to their distances above the interior surfaces of the holes in the concrete decks and steel girders. Therefore, as a pedagogical exercise, the positioning of the through-bolts within the

holes were arbitrarily modified in the vertical direction, from their originally assumed 1 mm displacement from the bottom, interior surface of the concrete holes to investigate the implications of this original assumption. While largely arbitrary, the assumed modifications were selected to produce an overall smoothening of the load-slip response. Table 5–1 summarizes the initial through-bolt position modifications that were made. The values indicated in the table are the new initial separations between the through-bolts and the interior, bottom surfaces of the concrete holes.

Table 5–1: **Initial through-bolt separations from bottom of interior surface of holes in concrete deck**

	Through-Bolt Diameter		
Through-Bolt Location	1/2" (12.70 mm)	3/8" (15.88 mm)	3/4" (19.05 mm)
Top left	0.50 mm	1.00 mm	1.50 mm
Top right	1.00 mm	2.00 mm	1.50 mm
Bottom left	1.75 mm	3.00 mm	4.00 mm
Bottom right	1.50 mm	1.50 mm	3.00 mm

It was expected that different trial arrangements of the initial locations of the through-bolts may further improve the accuracy of the results since each simulated load-slip curve above differs with respect to the magnitude of slip observed and the slope of the curve following the initial instance of slip. This is intuitive as it is very improbable that Chen (2013) installed the through-bolts at the exact same locations from test to test. As a result, it is understandable that any assumed initial through-bolt location which generates accurate results for one test will not necessarily be similarly successful for another. Therefore, as shown in Table 5–1, the assumed initial positioning of the through-bolts within the holes were not identical for each test. The push test FE simulations were run with the modified initial through-bolt locations and the results are shown in Figure 5–19, Figure 5–20, and Figure 5–21.

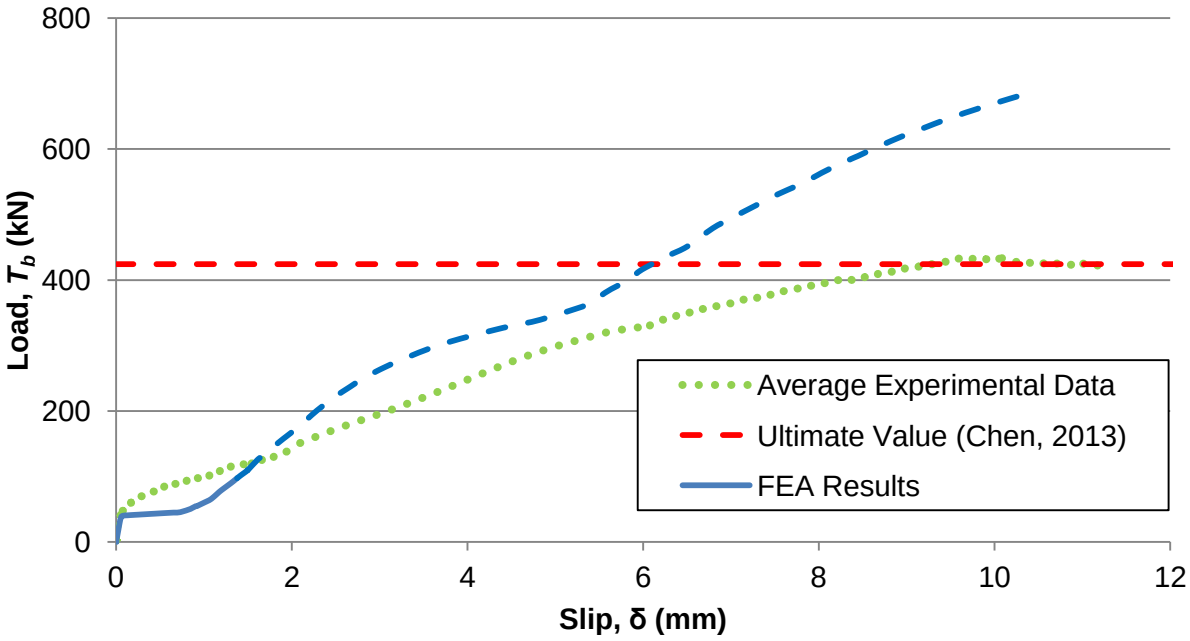

Figure 5–19: Comparison between experimental data and push test FE load slip prediction with modified initial through-bolt locations for 1/2" diameter through-bolt

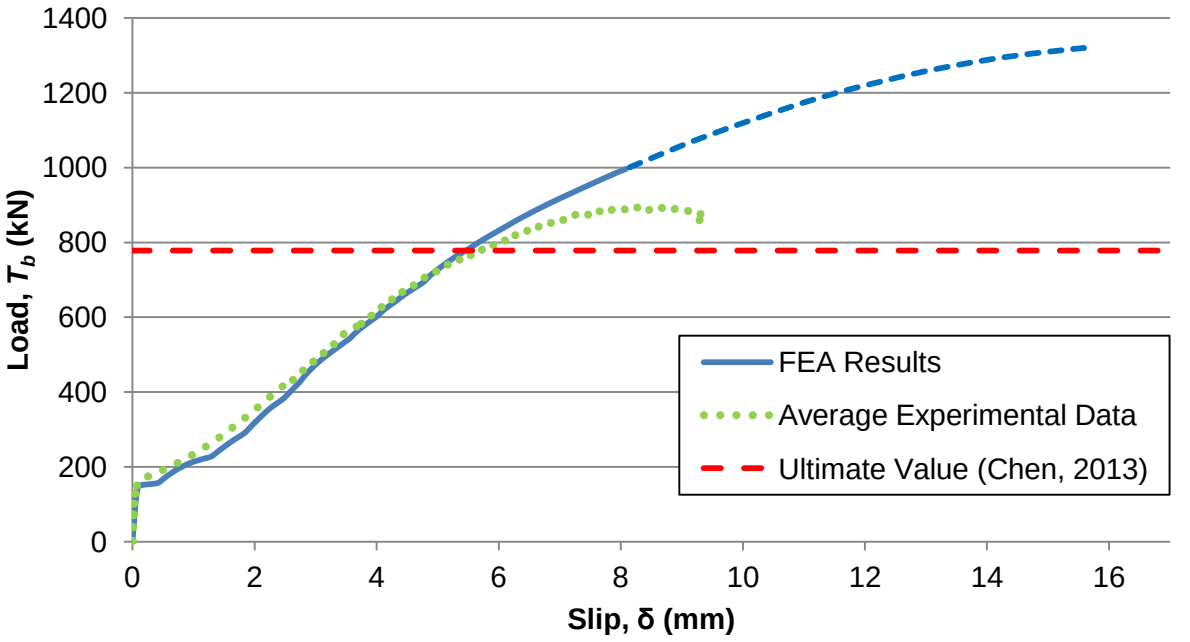

Figure 5–20: Comparison between experimental data and push test FE load slip prediction with modified initial through-bolt locations for 5/8" diameter through-bolt

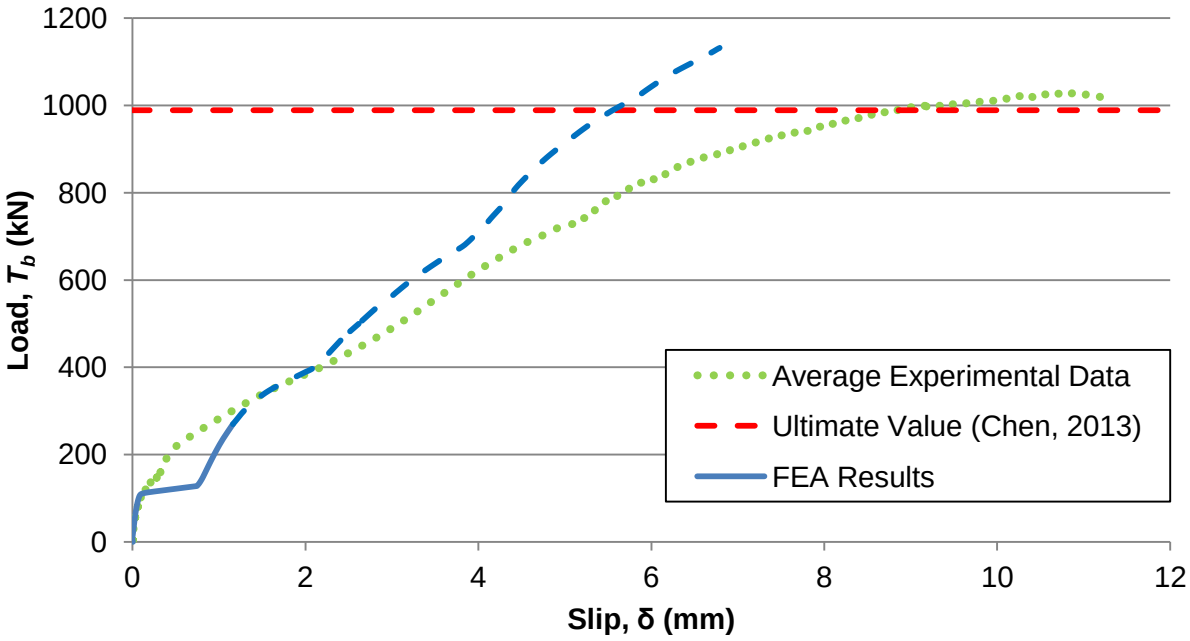

Figure 5–21: Comparison between experimental data and push test FE load slip prediction with modified initial through-bolt locations for 3/4" diameter through-bolt

As expected, the predicted load-slip responses from the push test FE models with the modified initial through-bolt locations, more closely approximate the behaviour of the experimental push tests. As shown in Figure 5–19, Figure 5–20, and Figure 5–21, the predicted initiation of slip have not changed, remaining virtually identical to the slip levels observed during the experiments. Nevertheless, the push test FE simulations now predict a smooth, continual increase in load following the initiation of slip, with a slope almost identical to that observed during the experiments.

With the initial positions of the through-bolts modified from their original symmetric arrangement with all through-bolts 1 mm above the bottom of the holes in the concrete deck, there was no longer a rapid increase in slip immediately following the onset of the force of friction being overcome. Previously, all of the through-bolts deformed the same initial 1 mm with virtually no increase in load before bearing against the concrete, thus engaging simultaneously, resulting in a rapid increase in stiffness. Now that the initial positions of the through-bolts have been modified such that they begun deforming at different initial distance from the concrete, each through-bolt slips by a different amount and engaged at different load levels. The dowel action contribution from each through-bolt became apparent at four different load levels, appearing as four separate and distinct increases in stiffness, which combined to smoothen out the

overall load-slip curves. This is opposite to the original simultaneous engagement of the dowel action from each through-bolt shown in Figure 5–16, Figure 5–17 and Figure 5–18.

Another simulation was run, replicating a sensitivity experiment conducted by Chen (2013) to further validate the push test FE model. Chen (2013) conducted an additional experiment whereby the pretension level in the through-bolts were varied from the requirements specified by CSA S6 Clause 10.24.6.3 as a sensitivity analysis. The push test FE simulation was identical to the one depicted in Figure 5–20, featuring the 5/8" diameter through-bolt, including the same assumed initial through-bolt locations described in Table 5–1 for the 5/8" diameter through-bolts. The only differences were that the through-bolts were now pre-tensioned to a maximum load of 55 kN instead of the original 85 kN and Chen (2013) reported a reduction in the coefficient of friction from the original 0.22 to 0.11. The results of this simulation are displayed in Figure 5–22.

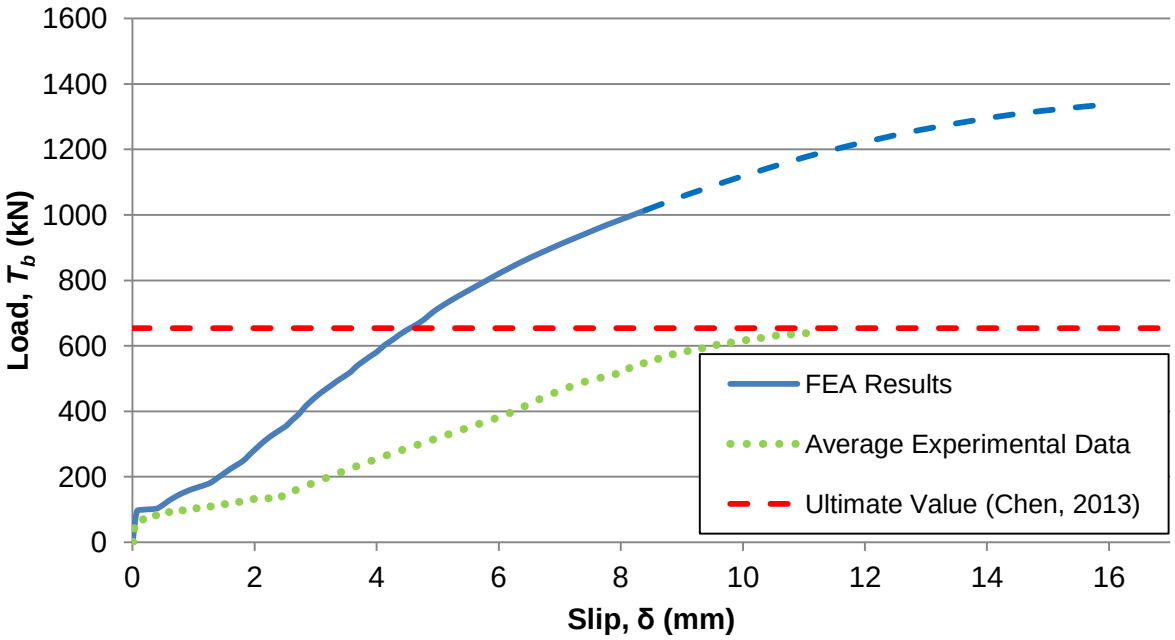

Figure 5–22: Comparison between experimental data and push test FE load-slip prediction for 5/8" diameter through-bolt with 55 kN of pretension

While the push test FE model predicted a slip load value of approximately 100 kN, reasonably comparable to the reported experimental value of approximately 65 kN, the load-slip curve of this simulation did not replicate the experimental results as closely as the previous model. Once again, it was expected that further trial arrangements of the initial positioning of the through-bolts may further improve the accuracy of the results. Therefore, the initial through-bolt locations within the holes in the concrete

deck were further modified such that the simulation began with the initial through-bolt locations described in Table 5–2. The push test FE simulation was run with the modified initial through-bolt locations and the results are displayed in Figure 5–23.

Table 5–2: Initial through-bolt separations from bottom of interior surface of holes in concrete deck with modified pretension level

Through-Bolt Location	3/8" (15.88 mm)
Top left	3.00 mm
Top right	5.00 mm
Bottom left	7.00 mm
Bottom right	4.00 mm

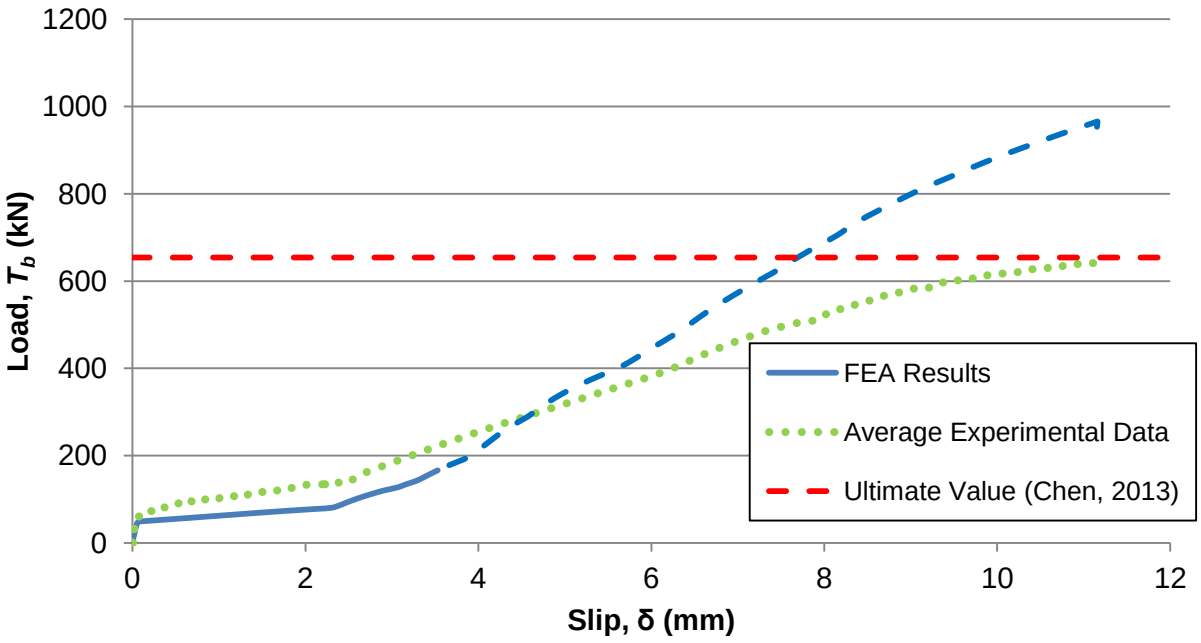

Figure 5–23: Comparison between experimental data and push test FE load-slip prediction with modified initial through-bolt locations for 5/8" diameter through-bolt with 55 kN pretension

As illustrated in Figure 5–23, the predicted response from the push test FE model, featuring the further modified initial through-bolt locations, better approximates the behaviour of the experimental push test. Interestingly, as shown in Figure 5–23, the predicted initiation of slip decreased from the previous 100 kN to 50 kN which more closely resembles the slip level observed during the experiments (65 kN). The push test FE simulation now predicts a continual load increase following slip, with a rate of increase almost identical to that observed during the experiments up until roughly 4 mm of slip.

The results of the above simulations further support the hypothesis that the through-bolt shear connectors were installed in slightly different orientations for each specimen in the experiments conducted by Chen (2013). Moreover, it is apparent that any asymmetrical through-bolt installation positions can have profound effects on the overall static performance of the shear connection as illustrated by significant changes in the load-slip responses from one simulation to the other. It is apparent that when all of the through-bolts were positioned symmetrically within the specimens, all of the through-bolts deformed uniformly and by the same amount before bearing against the concrete. Thus, the through-bolts engaged simultaneously, resulting in a rapid increase in the stiffness of the connection. Once any variability with regards to the initial through-bolt orientation was introduced during their installation, each through-bolt engaged in dowel action, bearing against the concrete at different load levels. Therefore, the randomized initiation of the dowel action contribution from each through-bolt had the effect of smoothening out the load-slip curve, decreasing the overall stiffness of the shear connection.

The Von Mises stress contour plot of the 5/8" diameter through-bolt with 85 kN of pretension, bearing against the steel flange at the time of the proposed failure criteria is presented in Figure 5–24.

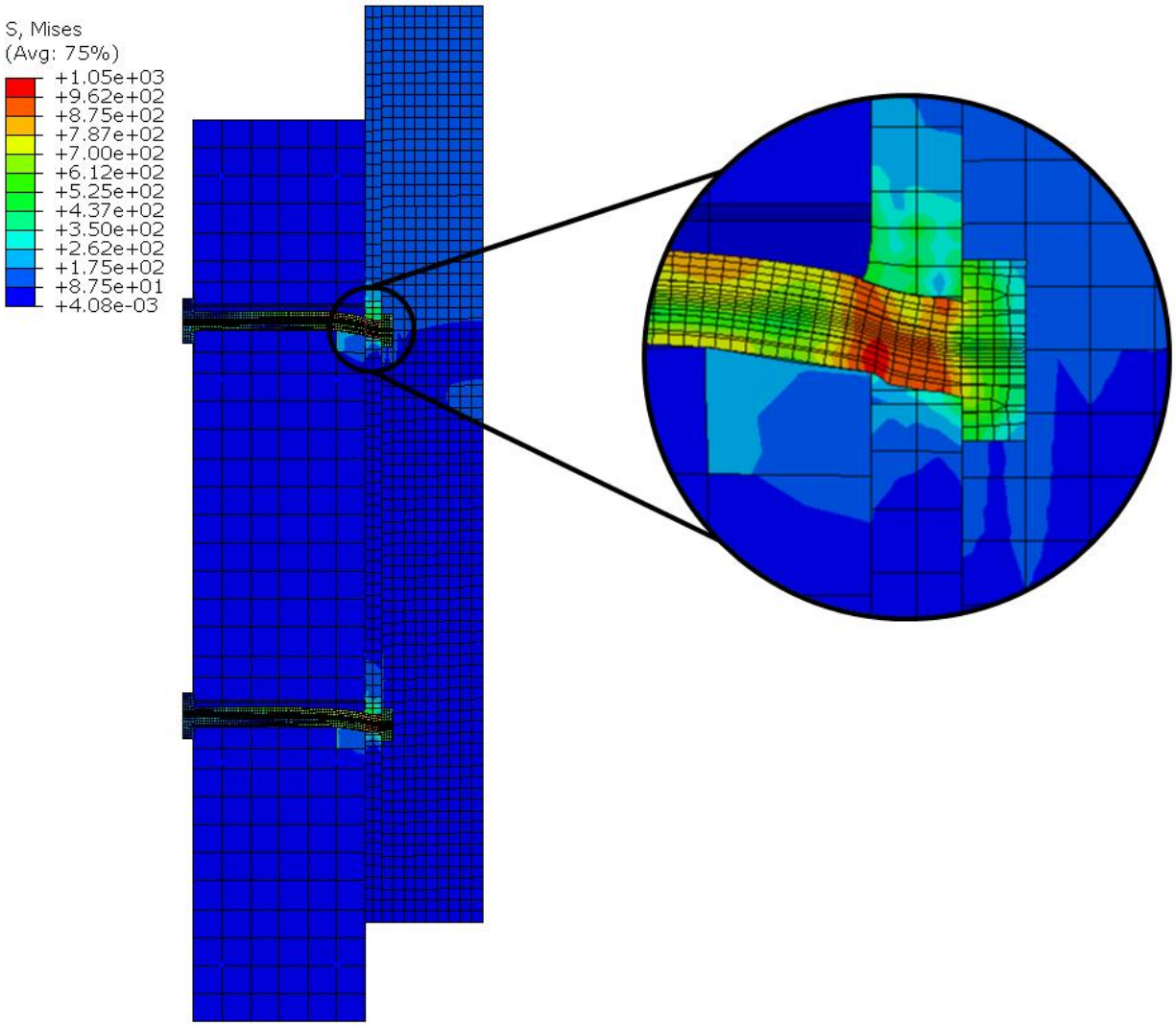

Figure 5–24: Von Mises stress contour plot demonstrating the shearing of 5/8" diameter through-bolts with 85 kN of pretension

As expected, Figure 5–24 reveals that the maximum stresses observed in the through-bolts, at the time of the proposed failure criteria, occurred at the shear plane between the concrete deck and flange of the steel girder. This is consistent with the experimental observations which indicated that the failure mechanism of the through-bolts was a shear failure at this same location (Chen, 2013).

The predicted deformed shape of the 5/8" diameter through-bolts with 85 kN of pretension in the push test FE model is compared to a through-bolt used in the experiments conducted by Chen (2013) in Figure 5–25. It should be noted that simulation output in Figure 5–25 was extracted at the instance that the failure of the most heavily loaded through-bolts was anticipated to occur. One of the non-failed through-bolts

from Chen's (2013) experimentation was used as a comparison to the FE model of a through-bolt on the verge of failure.

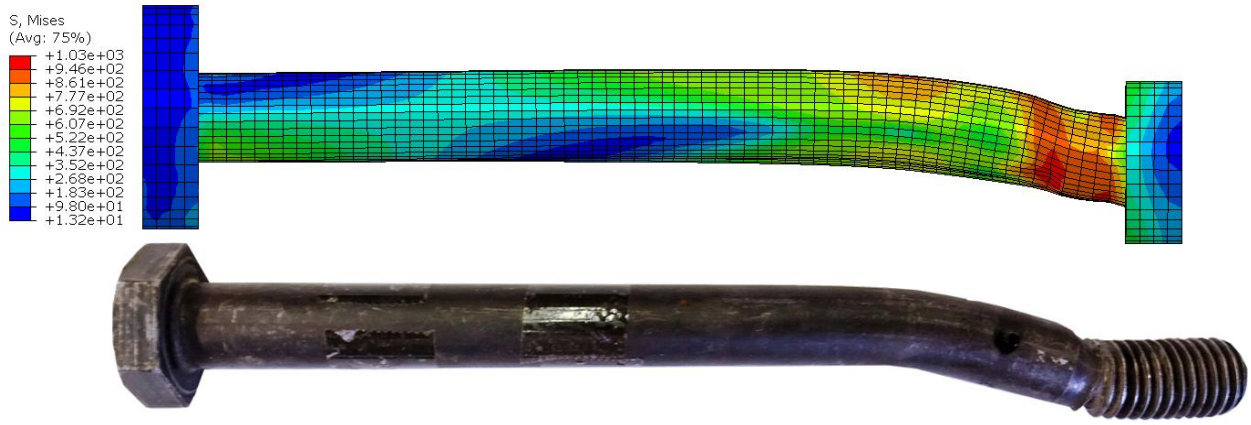

Figure 5–25: Comparison between deformed experimental specimen and push test FE prediction of a 5/8" diameter through-bolts with 85 kN of pretension

The deformed shape predicted by the push test FE model matches the profile of the deformed through-bolt used in the experiments performed by Chen (2013) very closely, capturing the same magnitude of transverse deflections and the same longitudinal length engaged in flexure. The results of this simulation further substantiate the appropriateness of assuming a flexural length, $L_{bearing}$, in Equation 5-7 that is less than the total length of the through-bolt. Figure 5–25 also reinforces the expectation that the location of the maximum stress in the through-bolts occured at the shear plane between the concrete and the steel flange.

6 Conclusions and Recommendations

This research project investigated the behaviour of ASTM A325 through-bolts when used as shear connectors in steel-precast composite girders, considering both the static and fatigue performance. This chapter presents the main conclusions resulting from this research project. Following this, recommendations are provided for future researchers to address remaining knowledge gaps and for engineers considering the use of through-bolt shear connectors on future projects.

6.1 Conclusions

The research presented in this thesis furthered the current state-of-understanding of the behaviour of slip-critical, through-bolt shear connectors in steel-precast composite bridge girders, addressing gaps in the current knowledge identified in Section 2.5. The significant findings of this research project are summarized in this section and are presented in the order they are introduced in Chapters 4 and 5.

6.1.1 Stiffness Testing

Prior to the stiffness testing, it was discovered that differences between the original profiles of the concrete decks and steel girders created gaps at the steel-concrete interfaces. Once the pretension force was applied to the through-bolts, any separation between the concrete decks and steel girders were eliminated, thus forcing the concrete decks to contour the steel girders. This action created installation cracks approximately 0.1 mm wide within the concrete decks.

The stiffness testing revealed that Specimen B1 and B2 did not observe any substantial changes in maximum deflection, stiffness or interfacial slip throughout their fatigue lives. However, changes in the specimen deflection under zero load following the introduction of an increased load level were observed for Specimen B1. This implies that the specimen experienced a slight shifting of the concrete deck position with respect to the steel girder each time a higher load level was introduced.

Based upon the findings of load-deflection results, it was concluded that the modified, effective transformed section moment of inertia, calculated using Equation 3-2, may be unsuitable for calculations involving partially composite sections. A comparison between the experimental results and the behaviour predicted by the equation suggests that the equation consistently yields non-conservative results, predicting an artificially stiffer response than observed during the experimentation.

Lastly, the net compressive forces in the concrete decks were calculated using the strain profiles in the steel girders. The results of this exercise further confirmed that the degree of shear connection was largely unchanged from the original state prior to the introduction of fatigue loading.

6.1.2 Fatigue Testing

The fatigue testing did not result in the failure of any through-bolt shear connectors. The fatigue performance of the through-bolt shear connectors far exceeded expectations. Fatigue testing on Specimen B1 was stopped after 2,007,766 cycles, when a fatigue crack was observed in the web of the steel girder, emanating from the weldment fastening the web stiffener to the web of the steel girder on the West end of the specimen. The fatigue testing on Specimen B2 was stopped after 762,241 cycles due to the failure of the actuator loading the specimen. The most heavily loaded through-bolts in Specimen B1 and Specimen B2 were subjected to approximately 521 and 3244 times the number of cycles predicted to result in failure by assuming the CSA S6 Category D fatigue detail respectively.

Both Specimens B1 and B2 experienced propagation and enlargement of the installation cracks discussed in Section 4.1. The installation cracks grew from their original 0.1 mm to roughly 0.3 mm most cases, some growing to as large as 0.75 mm near the point loads. Specimen B1 experienced further cracking in addition to the original installation cracks subsequent to one million applied cycles.

The maximum deflection and the interfacial slips observed during the fatigue testing did not change significantly, further supporting the conclusion that the through-bolts did not experience significant fatigue damage.

The described through-bolt instrumentation method was validated and confirmed to be effective through the comparison with the tension indicating washers. At the completion of tightening as indicated by the tension indicating washers, the strain values within the through-bolts were all on average 6.2% different from 2100 microstrain with one through-bolt as much as 17.8% different, consistent with the strain that would be anticipated with 5/8" diameter through-bolts, subjected to a pretension level of 85 kN.

Finally, the through-bolt strains observed abrupt decreases in strain when the load range applied to Specimen B1 was increased at 1,000,000 cycles and again at 2,000,000 cycles. Also, in contrast with the maximum deflection and interfacial slip results, the strains in the through-bolts decreased throughout the progression of the fatigue testing in a parabolic fashion. The parabolic decrease in through-bolt strains is believed to be a consequence of shrinkage and or creep experienced by the concrete decks due to the compressive forces acting on the concrete decks from the pretension in the through-bolts.

6.1.3 Stiffness Testing with Through-Bolt Removals

A failure scenario was replicated by progressively removing the through-bolt shear connectors following the fatigue testing of Specimen B1. Static stiffness tests were performed after the removal of each through-bolt. The results revealed that the stiffness of the overall load-deflection curve for Specimen B1

decreased and the peak, maximum deflection observed by Specimen B1 increased with the consecutive removal of through-bolts. The overall load-deflection of Specimen B1 approached the predicted response of a steel girder on its own, revealing that the steel girder stiffness controlled the behaviour of the specimen when no interaction was present. Also, the stiffness change was observed to be constant, with deflection increasing by approximately 19%, with the removal of each through-bolt.

Furthermore, the slope of the strain profile for Specimen B1 decreased throughout the progression of the removal of the through-bolts. This, continual decrease in slope indicates a corresponding incremental increase in the strain discontinuity between the strain profiles in the steel girder and the concrete deck, indicating a decrease in the degree of shear connection provided. The neutral axis in the steel girder migrated downwards and the force carried by the through-bolts decreased until the neutral axis of the steel girder corresponded with the geometric centroid of the steel girder. At this instance, the steel girder and the concrete deck were each in a static equilibrium independent from one another and therefore, the force carried by the through-bolt shear connectors was essentially zero.

The coefficient of friction for Specimen B1 was computed to be 0.65. This value was very similar to the coefficient of friction specified in CSA S6, Clause 8.16.7.6.4.1 (0.6) (CSA S6, 2014).

6.1.4 Ultimate Strength Testing

The autopsy of Specimen B2 revealed that the through-bolts experienced significant flexural deformation however, none had failed at the end of the ultimate strength test of this specimen. The through-bolt rows at the ends of the specimen (Rows 1 & 12) experienced the most plastic deformation. The remaining rows experienced a decreasing amount of plastic deformation from the specimen ends to the middle where through-bolt Rows 5 & 6 experienced very little deformation. Conversely, the shear failure of all four through-bolts occurred at the East end of Specimen B3. The bottom flanges for both Specimens B2 and B3 experienced yielding and the top flanges experienced compression buckling.

The stiffness of Specimen B2 observed in the ultimate strength test was nearly identical to the stiffness observed for Specimen B3 up until the onset of slip, which first occurred at the East ends of the specimens at a load of 200.2 kN for Specimen B2 and 97.4 kN for Specimen B3. This behaviour revealed that prior to the onset of slip, the mechanism primarily responsible for providing the shear connection was the interfacial friction between the concrete deck and steel girder interface. Following the onset of slip, the stiffness of the load-slip curve for Specimen B2 was greater than the stiffness of the load-slip curve for Specimen B3 since Specimen B2 featured more through-bolts.

The coefficient of friction for Specimen B3 was computed to be 0.33. This coefficient of friction was far lower than the value previously calculated for Specimen B1 (0.65). However, it was reasonably close to the coefficient of friction reported by Chen (2013) from his push test experiments (0.22).

Since Specimen B2 did not experience any through-bolt failures, the load-slip curves for Specimen B2 were smooth and continuous. Conversely, the failure of each through-bolt in Specimen B3 resulted in a sudden decrease in the load resisted by Specimen B3.

Load-slip curves for the through-bolts in Specimen B3 were prepared using the average load-slip curve for all four through-bolts at each end. The load-slip curve for the East end reveals that following the initiation of slip at an applied specimen load of approximately 120 kN, the concrete deck begun slipping with little increase in load until it had slipped a sufficient amount relative to the steel girder such that the through-bolts engaged in bearing on the inside surface of the concrete deck. The mechanism of load transfer to the concrete deck from the steel girder slowly changed from purely interfacial friction between the concrete deck and steel girder to a combination of friction and dowel action of the through-bolts. The through-bolt contribution to the overall transfer of load to the concrete deck increased after slip in a parabolic fashion until the concrete deck force reached a global maximum of 425.9 kN. Shortly after reaching this maximum, Through-Bolt S12 reached its critical maximum shear stress and failed abruptly. The load previously carried by this through-bolt was then redistributed to the remaining three through-bolts on the East end of the specimen and consequently caused Through-Bolt N12 to fail shortly afterwards. Finally, Through-Bolts N11 & S11 failed simultaneously, eliminating all remaining mechanical shear connection between the concrete deck and steel girder. This resulted in the force in the concrete deck to decrease to zero.

Lastly, the generated load-slip curves were compared to the load-slip curves from the push test experiments conducted by Chen (2013) as a means of comparing the behaviour of a through-bolt shear connector as determined using a push test versus a large-scale beam test. The beam test and the push test resulted in similar peak maximum shear loads prior to the onset of failure of the through-bolts. However, the slopes of the two load-slip curves were quite different, with the through-bolt shear connectors behaving in a much less stiff manner when tested in a beam test relative to when they were tested in a push test. Moreover, the slip required to produce a through-bolt failure is seen to be much higher in a beam test than in a push test. The first instance of a through-bolt failure was observed at 14.8 mm of slip between the concrete deck and steel girder in the beam test, which is approximately 57% larger than the first occurrence of a through-bolt failure at 9.4 mm of slip in a push test.

6.1.5 Mechanistic Model

The load-slip behaviour of a through-bolt push test specimen was predicted using a mechanistic model. Comparison of the load-slip curves generated by the mechanistic model with the experimental results obtained by Chen (2013) revealed that the mechanistic model is capable of accurately predicting the load-slip behaviour of through-bolt shear connectors.

6.1.6 Finite Element Analysis

The load-slip behaviour of through-bolts in a push test were predicted using computational FE models. The comparison of the load-slip curves generated by the FE models to the experimental results obtained by Chen (2013) revealed that the FE models are also able to predict the load-slip behaviour of through-bolt shear connectors.

Moreover, the FE simulations revealed that any asymmetry in the installation of the through-bolts has a noticeable effect on the overall static behaviour of the shear connection. It was observed that when positioned symmetrically within the specimens, all of the through-bolts deformed uniformly and by the same amount before bearing against the concrete. Thus, the through-bolts engage simultaneously, resulting in a rapid increase in the stiffness of the shear connection. Once any variability with regards to the initial through-bolt position is introduced, each through-bolt will start to bear against the concrete at a different load level. Therefore, the randomized initiation of the dowel action contribution from each through-bolt has the effect of smoothing out the load-slip curve, decreasing the overall stiffness of the shear connection.

Lastly, the push test FE models were also successful in accurately predicting the deformed shape of the through-bolts subjected to a push test, capturing the same magnitude of transverse deflection and the same longitudinal length engaged in flexure. This further substantiates the appropriateness of assuming a flexural length, $L_{bearing}$, in Equation 5-7 that is less than the total length of the through-bolt.

6.2 Recommendations for Future Research

Several recommendations are suggested in this section for further developing the current state-of-understanding of the behaviour of slip-critical, through-bolt shear connectors.

It is suggested to use Monte Carlo simulation in conjunction with the push test FE model and randomly vary the initial positions of the through-bolts in the concrete holes to establish the statistical influence that these variations have on the connection behaviour. Furthermore, a parametric study is suggested, using FE analysis to assess the effects of friction, bolt diameter, and geometric arrangement on the behaviour of this connection type.

It is recommended that researchers modelling push test experiments on through-bolts continue to use load-slip curves derived from either push test experiments or the FE model presented in Section 5.2. The FE model has an advantage over the mechanistic model in that the FE model can be used to estimate the ultimate slip magnitude at failure. Conversely, it is recommended that researchers modelling large-scale or full-scale bridges with through-bolt shear connectors use the load-slip curve for a single through-bolt presented in Figure 4–46, derived through the large-scale beam testing.

Two attempts were made to estimate the coefficient of friction between steel and concrete based on the experimental data obtained in this study, which yielded different results. Further investigation to better characterize this parameter would be beneficial for future modelling efforts.

Lastly, it is recommended that researchers conduct further large-scale beam testing featuring through-bolts as the mechanism of shear connection. It is suggested that smaller diameter through-bolts be considered or that tests be performed with higher loads on larger beams, in order to potentially cause a fatigue failure of the through-bolts.

6.3 Recommendations for Future Practice

Several recommendations are suggested in this section for industry experts who wish to consider using through-bolt shear connectors in composite bridge construction.

It is recommended that CSA S6 (CSA S6, 2014) review the assumption that the fatigue performance of through-bolt shear connectors is identical to welded, headed shear stud connectors. Further large-scale beam testing, featuring through-bolt shear connectors is recommended. However, it is believed that this assumption is overly conservative, rendering economically inefficient designs.

With regards to the installation cracks due to the tightening of the through-bolts, it is recommended that a grout be installed, occupying any potential voids separating the concrete deck and steel girder. This should minimize any discrepancies in the contour profiles of the concrete deck and steel girder, thus limiting or preventing the occurrence of installation cracks.

Lastly, it is recommended that the use of a laser scanner be adopted to locate the prefabricated holes within the concrete decks and steel girders to determine the globally optimal root mean square value (geometric incompatibility error) between all possible combinations between the concrete decks and steel girders. This will reduce or prevent the necessity for rework due to tolerance issues.

References

ABAQUS, (2013). Version 6.13, Dassault Systèmes, USA.

Bowser, M. G. (2010). Development of a Shear Connection for a Portable Composite Bridge (Master's thesis, University of Waterloo).

Callister, W. D., & Rethwisch, D. G. (2010). *Materials science and engineering An Introduction.* NY: John Wiley & Sons, Inc.

Canadian Standards Association. (2012). CAN/CSA-S16-09 Design of Steel Structures. *Canadian Standards Association: Mississauga, ON, Canada.*

Canadian Standards Association. (2013). CAN/CSA-W59-13 Welded Steel Construction (Metal Arc Welding). *Canadian Standards Association: Mississauga, ON, Canada.*

Canadian Standards Association. (2014). CAN/CSA-S6-14 Canadian Highway Bridge Design Code. *Canadian Standards Association: Mississauga, ON, Canada.*

Canadian Standards Association. (2014). CAN/CSA-S6.1-14 Canadian Highway Bridge Design Code Commentary. *Canadian Standards Association: Mississauga, ON, Canada.*

Chen, Y. T. (2013). *Innovative shear connections for the accelerated construction of composite bridges* (Master's thesis, University of Waterloo).

Chen, Y. T., Zhao, Y., West, J. S., & Walbridge, S. (2014). Behaviour of steel–precast composite girders with through-bolt shear connectors under static loading. *Journal of Constructional Steel Research*, *103*, 168-178.

Cui, W. (2002). A state-of-the-art review on fatigue life prediction methods for metal structures. *Journal of marine science and technology*, *7*(1), 43-56.

Dalehenley, M. (2009). “Shear Connections For The Development of a Full-Depth Precast Concrete Deck System”. M.S. Thesis. Texas A&M University.

Fish, J., & Belytschko, T. (2007). A first course in finite elements. Chichester, England; Hoboken, NJ: John Wiley.

Fisher, J. W., Frank, K. H., Hirt, M. A., & McNamee, B. M. (1969). Effect of weldments on the fatigue strength of steel beams, Final Report, September 1969 (70-25).

Hognestad, E. (1951). *Study of combined bending and axial load in reinforced concrete members*. University of Illinois at Urbana Champaign, College of Engineering. Engineering Experiment Station..

Hwang, W., & Han, K. S. (1985). Cumulative damage models and multi-stress fatigue life prediction. *Journal of Composite Materials*, *20*(2), 125-153.

Johnson, R. P. (2000). Resistance of stud shear connectors to fatigue. *Journal of Constructional Steel Research*, 56(2), 101–116. http://doi.org/10.1016/S0143-974X(99)00082-6

Kalfas, C., Pavlidis, P., & Galoussis, E. (1997). Inelastic behaviour of shear connection by a method based on FEM. *Journal of Constructional Steel Research*, *44*(1-2), 107-114.

Kayir, H. (2006). *Methods to develop composite action in non-composite bridge floor systems: Fatigue behavior of post-installed shear connectors* (Doctoral dissertation, MS Thesis, Department of Civil, Architectural and Environmental Engineering, University of Texas at Austin).

King, D. C., Slutter, R. G., & Driscoll Jr, G. C. (1965). Fatigue strength of 1/2 inch diameter stud shear connectors, Highway Research Record No. 103, Publication No. 294.

Kwon, G. U. (2008). *Strengthening existing steel bridge girders by the use of post-installed shear connectors*. The University of Texas at Austin.

Kwon, G., Engelhardt, M. D., & Klingner, R. E. (2010). Behavior of post-installed shear connectors under static and fatigue loading. *Journal of Constructional Steel Research*, *66*(4), 532-541.

Kwon, G., Hungerford, B., Kayir, H., Schaap, B., Ju, Y. K., Klingner, R., & Engelhardt, M. D. (2007). *Strengthening existing non-composite steel bridge girders using post-installed shear connectors* (No. FHWA/TX-07/0-4124-1).

Liu, X., Bradford, M. A., & Lee, M. S. (2014). Behavior of high-strength friction-grip bolted shear connectors in sustainable composite beams. *Journal of Structural Engineering*, *141*(6), 04014149.

Mainstone, R. J., & Menzies, J. B. (1967). Shear connectors in steel-concrete composite beams for bridges. 1: Static and fatigue tests on push out specimens. Concrete, 1967, No.9, 291-302.

Oehlers, D. J., & Foley, L. (1985). The fatigue strength of stud shear connections in composite beams. *Proceedings of the Institution of Civil Engineers*, *79*(2), 349-364.

Oehlers, D. J., Nguyen, N. T., Ahmed, M., & Bradford, M. A. (1997). Partial interaction in composite steel and concrete beams with full shear connection. *Journal of Constructional Steel Research*, *41*(2-3), 235-248.

Oehlers, D. J., & Seracino, R. (2002). A tiered approach to the fatigue assessment of composite steel and concrete bridge beams. *Proceedings of the Institution of Civil Engineers-Structures and Buildings*, *152*(3), 249-257.

Ollgaard, J. G., Slutter, R. G., & Fisher, J. W. (1971). Shear strength of stud connectors in lightweight and normal weight concrete, AISC Eng'g Jr., April 1971 (71-10).

Pavlović, M., & Veljković, M. (2017). FE validation of push-out tests. Steel Construction, 10(2), 135-144.

Porter, T. K. (2017). *The Fatigue Resistance of Headed Shear Stud Connectors in Steel-Precast Composite Girders*(Master's thesis, University of Waterloo).

Sjaarda, M., Porter, T., West, J. S., & Walbridge, S. (2017). Fatigue Behavior of Welded Shear Studs in Precast Composite Beams. Journal of Bridge Engineering, 22(11), 04017089.

Sjaarda, M., West, J. S., & Walbridge, S. (2018). Assessment of Shear Connections through Composite Beam Modelling, Transportation Research Board Annual Meeting, Washington, D.C., January 7 - 11, 2018.

Seracino, R., Oehlers, D. J., & Yeo, M. F. (2003). Behaviour of stud shear connectors subjected to bi-directional cyclic loading. *Advances in structural engineering*, *6*(1), 65-75.

Skorupa, M. (1998). Load interaction effects during fatigue crack growth under variable amplitude loading—a literature review. Part I: empirical trends. *Fatigue & Fracture of Engineering Materials & Structures*, *21*(8), 987-1006.'

Slutter, R. G., & Driscoll, G. C., Jr. (1965). FLEXURAL STRENGTH OF STEEL AND CONCRETE COMPOSITE BEAMS. Journal of the Structural Division, ASCE, Vol. 91, No. ST2, April 1965.

Slutter, R. G., & Fisher, J. W. (1966). *Fatigue strength of shear connectors*. Fritz Eng. Lab., Lehigh University.

Stone, W. C., & Breen, J. E. (1984). *Design of post-tensioned girder anchorage zones*. PCI Journal, 1984

Tadros, Maher K., and Mantu C. Baishya. Rapid replacement of bridge decks. Vol. 407. Transportation Research Board, 1998.

Thomann, M., & Lebet, J. P. (2008). A mechanical model for connections by adherence for steel–concrete composite beams. *Engineering Structures*, *30*(1), 163-173.

Toprac, A. A. (1965). FATIGUE STRENGTH OF 3/4-INCH STUD SHEAR CONNECTORS. Presented at the 44th Annual Meeting of the Highway Research Board, Washington, D. Co, January 1965.

Yu-Hang, W., Jian-Guo, N., & Jian-Jun, L. (2014). Study on fatigue property of steel–concrete composite beams and studs. *Journal of Constructional Steel Research*, *94*, 1-10.

Yura, J. A., Methvin, E. R., & Engelhardt, M. D. (2008). *Design of Composite Steel Beams for Bridges* (No. FHWA/TX-08/0-4811-1).